INFLUENCE OF HULL CONFIGURATION AND VESSEL PROPULSION SYSTEMS ON SEA TURTLE SHELL INJURIES

A Thesis
Presented to
The Academic Faculty

by

Chad M. Spurlock

In Partial Fulfillment
of the Requirements for the Degree
Doctor of Philosophy in the
School of Civil and Environmental Engineering

Georgia Institute of Technology
August 2012

INFLUENCE OF HULL CONFIGURATION AND VESSEL PROPULSION SYSTEMS ON SEA TURTLE SHELL INJURIES

Approved by:

Dr. David Scott, Advisor
School of Civil and Environmental Engineering
Georgia Institute of Technology

Dr. Seung-Kyum Choi
School of Mechanical Engineering
Georgia Institute of Technology

Dr. Paul Work
School of Civil and Environmental Engineering
Georgia Institute of Technology

Dr. Laurence Jacobs
School of Civil and Environmental Engineering
Georgia Institute of Technology

Dr. Kimberly Kurtis
School of Civil and Environmental Engineering
Georgia Institute of Technology

Date Approved: April 26, 2012

ACKNOWLEDGEMENTS

I would like to thank my advisor, Dr. David Scott, for his guidance, motivation, and patience on this project and throughout my graduate career. I would like to thank Dr. Paul Work for his numerous contributions and support. I would also like to thank Mark Dodd for contributing specimens, equipment, and expertise to this research. I would like to show my appreciation to the committee members, Dr. Seung-Kyum Choi, Dr. Laurence Jacobs, and Dr. Kimberly Kurtis, for reading this dissertation and providing their insights. I would also like to thank Adam MacKinnon, Ashley Raybould, Brian Stacy, Alex Costidis, DuBose Griffin, Shane Boylan, and the volunteers from the Georgia Sea Turtle Center for all their assistance and expertise during the field tests.

This project would not exist without the work and dedication of Justin Hodges and Adam Sapp. In addition, I would like to express my appreciation to Hector Olguin, Justin Lanier, Gabe Hoffman, Rebekah Sheffield, and Tyler Blount, whose efforts in the laboratory and field were invaluable in the completion of this research. I would also like to thank my fellow graduate students, Mesut Turel, Zafer Defne, Fahad Mohammed, and Chatchawin Srisuwan for their support and friendship.

TABLE OF CONTENTS

LIST OF TABLES

LIST OF FIGURES

LIST OF SYMBOLS AND ABBREVIATIONS

E_T	Elastic modulus of the composite material system
A_T	Total cross-sectional area of the composite material system
E_C	Elastic modulus of the foam core material
A_C	Cross-sectional area of the foam core
E_F	Elastic modulus of the face material
A_F	Cross-sectional area of the faces
$(EI)_{eq}$	Equivalent flexural rigidity of composite material system
b	Width
t	Face thickness
c	Core depth
d	Distance between centers of two faces
$(AG)_{eq}$	Equivalent shear rigidity of composite material system
G_C^*	Shear modulus of foam
E_S	Elastic modulus of solid polyurethane
ρ_C^*	Density of foam material
ρ_S	Density of solid polyurethane
δ	Total deflection in bending
δ_B	Deflection due to bending effects
δ_S	Deflection due to shear effects
P	Applied force
L	Span length
P_0	Maximum contact force
T	Twice pulse duration of impact

LIST OF TERMS

Bycatch	The unintentional catch of non-targeted species, such as turtles and bottom fishes during shrimp trawling
Cancellous bone	A spongy type of bone that is porous, weaker, and less stiff
Carapace	Dorsal osseous shell of the turtle
Carapace width	Straight-line or curved distance across the widest part of the carapace
CCL	Curved carapace length
Cold stun	Hypothermic reaction due prolonged exposure to cold water temperatures
Collagen	A protein that is the basis for bone and other fibrous tissues
Convergence zone	Location where two flows meet and interact
Cortical bone	A relatively dense type of bone forming the outer shell of most bones
Estuarine	Partly enclosed coastal waters with access to the open sea
Fontanels	Carapacial unossified areas between the peripheral and costal bones
Hydroxyapatite	Mineral form of calcium apatite that is the principal mineral component of bone
Keratin	Fibrous protein which forms tissues such as hair, nails, and scales
Neritic zone	Waters over the continental shelves with depths < 200 m
Oceanic zone	Waters beyond the edge of the continental shelf with depths > 200 m
Osteons	Fundamental unit of compact bone
pcf	Pounds per cubic foot
Phase I	Previous research of the mechanical properties of loggerhead carapace bone
Phase II	Previous field experiments investigating vessel speed, turtle depth in the water column, engine type, and propeller guards using a fiberglass carapace

Phase III	The current research of design, fabrication, and testing of an artificial carapace
Plastron	Ventral osseous shell of the turtle
Primary bone	First bone tissue
Ribs	Beneath the carapace there are eight pairs of dorsal ribs fused to the costal or pleural and to the neural plates.
SCL	Straight carapace length
Scutes	Horny shields covering the carapace and plastron. The shape and size do not correspond with the underlying bony plates.
Secondary bone	Second layer of bone tissue that replaces primary bone during bone remodeling
Stranding	Event in which a marine animal is found dead on shore or beach
TED	An acronym for “trawl efficiency device” or “turtle excluder device”
Total length	The straight-line distance between the snout and the rearmost part of the carapace
Trabeculae	Small beams or struts which compose cancellous bone
Vessel 1	5.4 m inboard jet propulsion vessel
Vessel 2	7.3 m 4-bladed outboard propeller-driven vessel

SUMMARY

This thesis presents results from the design, fabrication, and testing of an artificial loggerhead sea turtle carapace. This research was conducted to aid in developing management strategies to reduce the occurrence and lethality of sea turtle/vessel interactions. The objectives included the development of a synthetic material system to match loggerhead shell material properties, the design and fabrication of an artificial turtle, and field testing of both artificial and real sea turtles subjected to vessel impact to study the effects of hull shape, propulsion system, and location in the water column on the lethality of shell injuries. Finite element analysis was used to estimate the conditions which could produce a lethal injury from a vessel hull impact.

The current research is the third phase of a program to study recreational vessel strikes on sea turtles. In Phase I, coupons of loggerhead carapace were tested in tension to determine mechanical properties. In Phase II, fiberglass shells were used to study the effects of vessel speed, engine type, propeller guards, and animal position in the water column on the types and lethality of damage caused by vessel strikes. The desired mechanical properties of the artificial carapace were based on the results of Phase I, and data from previous field tests were used in the statistical analysis of the influence of hull shape on sea turtle injury.

A composite material system was developed to approximate pertinent material properties of the loggerhead carapace in tension and flexure. A sandwich composite with a polyurethane foam core and faces of polyester resin infused with glass microspheres was chosen as the material system. Artificial carapaces were produced with this material

system for field testing. The mechanical properties of both the constituent materials and the sandwich composite material were found for comparison to target properties and for use in the finite element analysis and design equations for composite materials.

Field tests were performed using full-scale models of a loggerhead sea turtle. Two vessels were used: one with an inboard jet propulsion system and one with an outboard four-bladed propeller engine. All tests were conducted at planing speed, about 40 km/h. Tests were performed with the turtle at three positions in the water column: at the surface, 48 cm, and 71 cm deep. An accelerometer was attached to the model turtles during testing. Deceased sea turtles were also tested to provide a comparison of injury severity and wound patterns from vessel strikes.

Statistical analysis of the field results indicated that hull shape and turtle position in the water column had little influence on the lethality or types of wounds sustained during vessel impact. The primary influence was engine type, with the jet propulsion vessel causing zero fatal wounds and the propeller engine causing fatal wounds when coming in contact with the turtle. Hull impact alone by either vessel did not result in fatal injuries to the artificial or real sea turtles.

A finite element analysis of the artificial carapace was performed in order to determine the contact force which would produce fracture from hull impact. The duration of impact and the contact forces were based on the accelerometer data from field tests, and an immersed boundary condition was used to simulate the turtle in the water. The material properties of the constituent materials of the carapace were found from experimental methods. The direction and area of the applied force were based on the results of a hull impact of the jet drive vessel. Stress distributions were analyzed to

determine failure of individual elements in the finite element model. The critical contact force was estimated to be 24 kN. Based on the vessels used in the field tests, this force would be generated by impact of a 1000 kg vessel traveling 110 km/h or a 7500 kg vessel traveling 40 km/h. The results of the finite element analysis suggest that hull impacts of common recreational jet-propulsion vessels under typical operating conditions are unlikely to cause lethal carapace fractures in loggerhead sea turtles.

This research program provides specific technical input to the Georgia Department of Natural Resources (GDNR) as it develops management strategies to protect sea turtle populations in Georgia's coastal waters. Based on the present work, the GDNR is considering a campaign to promote the use of jet drive recreational vessels over conventional outboard propellers by raising public awareness or through restrictions on future marina developments. The GDNR is also considering expanding restrictions on the use of recreational vessels along certain portions of Georgia's coast considered critical for sea turtle hatching and migration.

CHAPTER 1

INTRODUCTION

Loggerhead sea turtles (*Caretta caretta*) inhabit coastal estuarine and continental shelf waters in tropical and subtropical regions around the world. In the Atlantic Ocean, the primary population of loggerheads in the United States is located in the coastal region stretching from Florida to North Carolina, with smaller numbers in the Gulf of Mexico (National Marine Fisheries Service and U.S. Fish and Wildlife Service 2008). The loggerhead has been listed as a threatened species throughout its range under the Endangered Species Act of 1973 since 1978. In 1996, the International Union for Conservation of Nature and Natural Resources Red List included the loggerhead as an endangered species (Marine Turtle Specialist Group).

Major threats to sea turtles include habitat destruction and incidental capture in commercial and artisanal fisheries, but vessel strikes are an increasing cause of fatalities. In the United States, the number of recovered loggerhead carcasses showing propeller- or vessel-related injuries rose from about 10% in the 1980s to over 20% in 2004 (Conant et al. 2009). In US coastal waters, vessel strikes may account for 50-500 sea turtle deaths annually (Plotkin 1995). As development in the coastal areas of the southeastern US continues, the risk of vessel strikes from both commercial and noncommercial boats increases. Effective management strategies to reduce turtle mortality from vessel strikes require a better understanding of the influence of vessel type, speed, and propulsion systems on the lethality of turtle injuries from vessel strikes.

The injuries produced in previous field experiments were caused by both non-rotating (foot and skeg) and rotating (propeller) components of the outboard motor; the vessel hull itself did not appear to cause any damage (Sapp 2010; Work et al. 2010). A flat-bottomed skiff was used in these experiments, so other hull configurations with deeper drafts may produce blunt-force injuries. Previous experiments used a fiberglass carapace, which did not closely match the material properties, thickness, or sandwich composite construction of a loggerhead carapace. The current research program expands the field investigation to incorporate different hull configurations and propulsion systems of the vessels and includes an artificial turtle carapace which better simulates critical material parameters.

The purpose of this research was to determine the influence of vessel hull configurations and propulsion system type and operation on the incidence and lethality of wounds in loggerhead sea turtles. This research project supports several high priority actions of the Recovery Plan for the Northwest Atlantic Population of the Loggerhead Sea Turtle (National Marine Fisheries Service and U.S. Fish and Wildlife Service 2008) by collecting critical data for the development and implementation of strategies to reduce fatalities from vessel strikes. The primary objectives of this research were:

1. To identify critical material properties of natural loggerhead sea turtle carapace bone with respect to impact.
2. To develop a synthetic loggerhead carapace which matches material properties and behavior during impact.

3. To validate a methodology to develop composite material systems used in artificial bones with targeted mechanical properties based on the properties of the composite constituents.
4. To investigate the effects of common hull configurations on sea turtle shell injuries.
5. To investigate the effects of boat drive configuration on sea turtle shell injuries.
6. To determine which parameters influence the likelihood of fatal injury using statistical analysis of field test data.
7. To estimate the force at which hull impact would produce a fatal injury using finite element analysis.

CHAPTER 2

BACKGROUND AND LITERATURE REVIEW

In this chapter, some of the biological and behavioral characteristics of loggerhead sea turtles and threats, specifically those posed by vessel strikes, are reviewed. The turtle shell's two types of bone, dense cortical bone and spongy cancellous bone, and their sandwich structure are described. In order to construct a synthetic carapace for use in turtle/vessel interaction experiments, the behaviors of organic bone, synthetic bone, and sandwich composites are examined. The material behaviors of the two types of bone are explained, with an emphasis on those material parameters which are most important for impact loading scenarios. Commercially available synthetic bones are described with accounts of experimental investigations of their mechanical properties in comparison to organic specimens. The mechanical response, modes of failure, and impact resistance of sandwich composites are summarized. An overview of numerical methods used previously in the study of direct impact to skull bones is presented as a basis for the finite element modeling of the synthetic shell design. Finally, a review of the work accomplished in the two prior phases of the current research program is provided.

2.1 Loggerhead Biology and Habitat

Loggerhead sea turtles inhabit tropical and temperate regions of the Indian, Pacific, and Atlantic Oceans (Dodd 1988). Although difficult to determine exactly, the total population is estimated by monitoring the number of nesting females from year to year. The total number of nesting sites in the US ranges from 47,000 to 90,000 per year, with the majority (over 10,000) of nesting females in Florida and between 1000 and 9999

from Georgia to North Carolina (National Marine Fisheries Service and U.S. Fish and Wildlife Service 2008). Nesting occurs during spring and summer, with females laying an average of 110 eggs per clutch two to five times per season (Márquez M 1990).

The turtle's shell comprises two parts: the domed, dorsal carapace and the flat, ventral plastron (Scheyer 2007). Adult and juvenile loggerheads have a reddish-brown carapace and a light to medium yellow plastron, both of which are covered by non-overlapping epidermal keratin shields, or scutes. The heavily keratinized shell provides protection from the environment and against attack (Solomon et al. 1986). Areas of exposed skin (head and flippers) are dull brown dorsally and light to medium yellow laterally and ventrally. The average straight carapace length (SCL) of adults in the southeast US is 92 cm, with a corresponding mass of 116 kg (National Marine Fisheries Service and U.S. Fish and Wildlife Service 2008). The carapace width is 76 to 86% of its length, and the large, broad head is about 23 to 28% of carapace length (Márquez M 1990). A loggerhead sea turtle is shown in Figure 2.1.

Figure 2.1. Loggerhead sea turtle (*Caretta caretta*) (Strobilomyces 2006)

Loggerhead sea turtles are migratory and spend different life stages in different ocean habitats. Hatchlings emerge at night and move immediately to the surf, guided by natural light over the open ocean. They migrate offshore and spend weeks to months in areas along the continental shelf where surface waters form convergence zones. Loggerheads spend the next 7 to 11.5 years in the juvenile stage, which begins when they enter the oceanic zone. Turtles occupy the upper five meters of the water column for most of their time in the oceanic zone; at this stage, the curved carapace length (CCL) ranges from 8.5 to 64 cm (National Marine Fisheries Service and U.S. Fish and Wildlife Service 2008). At about 46 cm CCL, juveniles leave the oceanic habitat for continental shelf waters on the US eastern coast, Caribbean, and Gulf of Mexico. There, they mature to adulthood, which takes 13-20 years, until the CCL reaches approximately 87 cm (Conant et al. 2009). Juveniles in the neritic zone are more likely than adults to occupy relatively enclosed, shallow water estuarine habitats with limited ocean access. Loggerheads reach adult stage in the neritic zone and inhabit shallow waters with large expanses of open ocean access which provide year-round resident foraging areas for males and females. The adult stage and reproductive life of female loggerheads is estimated to be 25 years; less data are available for adult males. Although concentrated in warmer waters, the loggerheads' range extends throughout practically all the shelf waters along the Atlantic and Gulf of Mexico coastlines (National Marine Fisheries Service and U.S. Fish and Wildlife Service 2008).

Loggerhead sea turtles face threats at all life stages. Human activities detrimental to nesting habitats include coastal development and construction, artificial lighting, and sand extraction. Habitat destruction in the neritic and oceanic zones includes bottom

trawl and dredge fishing, channel dredging, and sand extraction. The most serious threat to the conservation and recovery of the loggerhead is incidental capture (bycatch) in commercial and artisanal fisheries (Conant et al. 2009). Fishing methods that capture and drown loggerheads include the use of gillnets, longlines, pots and traps, and trawl gear. Regulations exist to reduce the number of turtles killed by entanglement in marine debris and as bycatch. The effects of different hook types, baits, and fishing locations on sea turtle mortality have been studied (Gilman et al. 2007; Žydelis et al. 2009).

In addition to habitat destruction and incidental capture, propeller and collision injuries pose a serious threat to loggerheads and are becoming more common. The threat posed by vessel strikes is well-documented for many air-breathing marine vertebrates, such as manatees (Marmontel et al. 1997; Gerstein 2002; Nowacek et al. 2004; Haubold et al. 2006; Laist and Shaw 2006; Lightsey et al. 2006; Calleson and Frohlich 2007), dolphins (Wells and Scott 1997; Wilke et al. 2005), and whales (George et al. 1994; Knowlton and Kraus 2001; Laist et al. 2001; Nowacek et al. 2004; Panigada et al. 2006; Douglas et al. 2008). Fewer studies of the number of turtle strandings as a result of vessel strikes have been performed. In the summer of 1993, speedboats were responsible for eight turtle deaths in Laganas Bay, Greece (Venizelos 1993). From 1999 to 2002, injuries from vessel strikes killed at least 65 sea turtles annually on the Queensland coast of Australia (Hazel and Gyuris 2006). In the Canary Islands, 23% of the 93 sea turtles stranded from 1998 to 2001 died as a result of collisions with vessels (Orós et al. 2005), and in 2006, 9% of stranded turtles on Spain's Mediterranean coast showed evidence of vessel strikes (Tomás et al. 2008). From 1997 to 2005, 14.9% of all stranded loggerheads in the US Atlantic and Gulf of Mexico had sustained some type of propeller or collision

injuries, but it is unknown whether these wounds were post- or ante-mortem. The incidence of propeller wounds rose from approximately 10% in the 1980s to 20.5% in 2004. In some areas of Florida, as many as 60% of stranded loggerheads had evidence of propeller wounds (Conant et al. 2009). Obviously, not all turtles that are struck by vessels are discovered, which may mean the issue is more severe than estimated. A model developed using four years of turtle stranding data from North Carolina and oceanic drift bottle experiments predicted that as few as 20% of stranded turtles would reach the coast within two weeks of death (Hart et al. 2006).

Many commercial and noncommercial boating activities occur in sea turtles' foraging habitat in the nearshore environment, where turtles spend nearly all their time in the upper 5 m of the water column making short, shallow dives during the day and longer, deeper dives at night. The turtles rarely surface completely, however, making brief appearances to breathe with only the head visible for a few seconds. Their peak activity within one meter of the surface occurs at dawn and dusk, coinciding with increased fishing and recreational vessel operation and increasing the risk of turtle/ship interaction (Hazel et al. 2009). Hazel et al. (2007) conducted field experiments to assess the response of sea turtles to an approaching vessel in shallow water. As expected, an increase in vessel speed decreases the turtles' ability to avoid collision, with the majority of turtles failing to react to vessels traveling faster than 4 km/h, which is below idle speed for many vessels. As coastal development continues with a concomitant increase in the number of vessels, propeller and collision injuries are expected to rise (Conant et al. 2009).

2.2 Characteristics of Bone

2.2.1 General Morphology of Bone

Bone has two primary functions – to protect vital organs and to serve as levers for muscles to contract against – but it can also perform specialized functions such as the acoustic amplification of the ear bones (Turner 2006). Bones must be stiff in order to resist excessive deformation, yet remain flexible enough to absorb impact energy to avoid fracture, and stay lightweight to allow rapid movement (Seeman 2008). Unlike engineered materials, bone adapts its size, shape, density, and material composition to accommodate mechanical loads (Gibson 1985; Martin 1991; Turner 2006; Seeman 2008). For example, the increased areas at the ends of long bones reduce stress at joints (Turner 2006). The optimization of bone shape serves to minimize weight and distribute stresses evenly throughout the bone without sacrificing strength or rigidity (Currey 2002; Turner 2006).

Bone is a complex structure with component materials that can be grouped into three categories: minerals, organics, and liquid-filled pores (Piekarski 1973). The mineral phase is predominantly a calcium phosphate (hydroxyapatite), and collagen accounts for roughly 99% of the organic phase. The fluid phase includes blood vessels, marrow, and nerve tissue (Carter and Hayes 1977). Collagen is a protein that serves as a basic load-carrying material for both soft and hard biological materials, such as tendons, blood vessels, muscle, and bone (Meyers et al. 2008). Hydroxyapatite crystals are hexagonal platelets that fill the gaps between the ends of collagen fibrils (Piekarski 1973; Meyers et al. 2008). Bone tissue is composed of roughly 60% collagen and 30 to 40% hydroxyapatite by volume (Meyers et al. 2008).

Mechanically, bone is often considered to be a two-phase ceramic-polymer composite of hydroxyapatite crystals in a collagenous matrix (Piekarski 1973; Vincent 1990; Turner 2006; Meyers et al. 2008; Seeman 2008). Like other composite materials, mechanical properties are determined by the proportion, organization, and molecular structure of constituent materials (Turner 2006). The low elastic modulus collagen contributes toughness and ductility, and the high elastic modulus mineral phase contributes strength and stiffness. An increase in mineral content can increase stiffness but at the cost of ductility, resulting in a more brittle bone with reduced energy-absorption capability (Piekarski 1973; Turner 2006; Meyers et al. 2008). At low strain rates, liquids can flow freely through porous bone and do not affect the mechanical response (Piekarski 1973). If either the mineral or organic phase is dissolved, the other remains and is continuous (Piekarski 1973; Meyers et al. 2008).

Collagen is a stiff and hard protein that serves as a basic building block for both soft and hard biological materials. Collagen occurs as a triple helix with a diameter of approximately 1.5 nm (Meyers et al. 2008) with an elastic modulus from 1-1.5 GPa, an ultimate strength from 70-150 MPa, and a maximum strain of 10-20% (Meyers et al. 2008). The crystal structure of hydroxyapatite is composed of hexagonal platelets (Piekarski 1973). The elastic modulus of hydroxyapatite is approximately 130 GPa with a strength of 100 MPa (Meyers et al. 2008).

At the macrostructural level, bone is classified as either cortical (compact) or cancellous (trabecular) based on porosity and microstructure (Rho et al. 1998). Cancellous bone has a degree of porosity from 30 to 90% and cortical from 5 to 30% (Carter and Hayes 1977). Whole bones are often a combination of both types: cortical

bone surrounds a core of cancellous bone. The transition between the types of bone may be gradual or more distinct (Gibson 1985).

Cancellous bone consists of an interconnected network of rods and plates and may be either open-celled or close-celled. Open cells have interconnected voids formed by a network of rods; a network of plates produces closed cells. Orientation of trabeculae in cancellous bone depends on the direction of applied loads. For example, uniaxial loading in vertebrae results in trabeculae oriented as a vertically columnar structure. Both asymmetric and columnar structures can develop in open or closed cells. As a result, there are four basic types of cancellous bone: (1) asymmetric, open-cell rods; (2) asymmetric, closed-cell plates; (3) columnar, open-cell rods; and (4) columnar, closed-cell plates (Gibson 1985).

Martin and Burr (1989) distinguish four types of structures in cortical bone: primary osteonal, secondary osteonal, woven, and plexiform. The most common types are primary and secondary osteonal bone. Secondary osteonal bone is formed during the remodeling process and may be mechanically weaker than primary osteonal cortical bone (Martin and Burr 1989).

Forms of cortical bone that lack clearly patterned or distinguishable collagen fibers are called woven bone (Rho et al. 1998). Woven bone does not contain osteons and has a dissimilar structure from plexiform bone (Hollister 2011). Woven bone is found only in very young bone or at sites of bone trauma or disease and does not require existing bone or cartilage in order to form. Woven bone forms very rapidly with a disorganized structure of collagen fibers (Martin and Burr 1989).

Plexiform cortical bone is usually found in rapidly growing, large animals, such as cows, and is rarely seen in humans. Plexiform bone grows in a brick-like pattern on the outer bone surface, with each "brick" about 125 μm across (Martin and Burr 1989). Plexiform bone grows more rapidly than primary or secondary bone and can have greater stiffness, but its brick-like structure offers less crack propagation resistance (Hollister 2011).

2.2.2 Bone Mechanics

The mechanical properties of bone are determined by both compositional and organizational variables. Compositional factors include porosity, mineralization, and density; organizational factors include cancellous and cortical bone architecture (Martin 1991). The material properties of bone vary in different bones or in different locations in the same bone (Rho et al. 1998). Porosity, the fraction of bone volume occupied by voids, is a key determinant of mechanical properties of bone. The pores are filled with soft tissues, such as blood canals or marrow, which do not contribute to strength or stiffness, so an increase in porosity reduces bone strength and stiffness. The degree of mineralization (the ratio of mineral mass to bone mass) significantly affects the properties of bone. Stiffness increases rapidly with an increase in mineral content, but toughness and strain at failure tend to decrease. The density measurement of bone often refers to apparent density, which is the mass per unit volume of a region of bone tissue, including voids. The properties of cancellous bone are often studied with respect to apparent density, which affects stiffness, strength, shear modulus, and shear strength (Martin 1991).

Cancellous bone displays structural responses similar to other cellular materials, such as polymeric foams. In compression, cellular solids exhibit three distinct regions of behavior. Initially, the response is linear elastic. Eventually, the cell walls begin to fail by elastic buckling, plastic yielding, or brittle fracture. The material continues to collapse at a nearly constant load until the collapsed cells meet and touch, at which point the load increases sharply. Gibson (1985) idealizes the cellular structure to analyze the mechanisms of deformation. The mechanical response depends on three parameters: the type of cellular structure (open- or closed-cell), the apparent density, and the properties of the cell wall material. This approach can be extended to cancellous bone.

The marrow and fluids which fill the voids in bone are usually considered to have no effect on structural properties. During dynamic loading, there are three possible ways for marrow to contribute: hydraulic strengthening by developing a hydrostatic pressure in compression, viscous resistance to shear in cancellous bone, and viscous interaction between marrow and trabeculae. In a test of long bones subjected to non-destructive, axially-applied compressive loads, none of these methods occurs because the bones deform in such a way that there is minimal volumetric change. Thus, hydraulic strengthening cannot be generated. If no volume changes occur, interaction between marrow and trabeculae is unlikely. Finally, marrow is nearly liquid in the body and has negligible viscous resistance to shear deformation. It is possible that elevated strain rates during traumatic events could generate a response from marrow, but at normal loading regimes, any contribution is negligible (Bryant 1988).

Toughness is a measure of energy absorption before failure. Bone exhibits multiple methods to dissipate deformation energy and limit crack propagation, including

microcracking, crack deflection, and fiber bridging. Bone is an anisotropic material, and toughening mechanisms depend on orientation of bone tissue (Peterlik et al. 2005). Toughness is highly dependent on the degree of mineralization, decreasing with an increase in mineral content (Meyers et al. 2008). One measure of toughness is the area under a stress-strain curve, which quantifies the total energy, elastic and plastic, before bone fracture. This calculation yields a higher value for toughness than other commonly used methods, such as the critical stress intensity factor or fracture toughness, due to the contribution of plastic energy absorption (Yan and Mecholsky 2007).

Bone is viscoelastic, meaning its material properties are strain-rate dependent. At very high loading rates, values and curves from static tests may not be accurate (Currey 2002). The effect of strain rate in the normal range (0.01 to 0.1 per second) is small compared to other factors, such as apparent density, but it is nontrivial when comparing impact events and quasi-static loading (Carter and Hayes 1977; Linde et al. 1991; Turner and Burr 1993). In human bone, a thousand-fold increase in strain rate results in a 40-50% increase in stiffness and strength. Violent fractures may occur at strain rates from 0.3 to 1.0 per second, but direct impacts may be significantly higher (Currey 2002).

2.2.3 Synthetic Bone

Synthetic bone test specimens are often used for mechanical testing due to their availability and low variability in material properties (Cristofolini et al. 1996; Cristofolini and Viceconti 2000; Patel et al. 2008). Composite synthetic bones use polyurethane rigid foams and fiberglass/epoxy resins because their mechanical properties are similar to cancellous and cortical bone, respectively. Polyurethane foam is available as open-cell or

closed-cell as a substitute for cancellous bone (Johnson and Keller 2008; Patel et al. 2008).

Cristofolini and Viceconti (1996; 2000) compared the mechanical properties of synthetic bones to human specimens in different loading conditions. The whole bone composite models employed a polyurethane foam core with a shell of glass fiber reinforced epoxy. The composite femurs' response to axial, torsional, and bending loads was within the range of cadaveric specimens. The composite tibias were tested in torsion, axial compression, and bending in two directions. The bending stiffness was similar to cadaveric specimens, but the synthetic models had a higher torsional stiffness than biological samples. The variability of the composite synthetic models was much lower than the cadaveric specimens for both femurs and tibias.

Johnson and Keller (2008) examined the compressive properties of open cell rigid foams and synthetic vertebrae. The synthetic vertebrae consisted of open-cell foam enclosed by a fiberglass/resin cortex. Despite the similar porosity and morphology between the foam and the human vertebral cancellous bone, the foam's lower material density caused lower values for strength and modulus.

Patel et al. (2008) investigated the use of lower density polyurethane foams as a substitute model for osteoporotic bone. The elastic modulus, yield strength, and energy absorbed were measured from compression tests for foams at different densities. Patel found the 0.16 g/cm^3 polyurethane foam had a comparable fracture stress and stiffness, but not energy absorption, to osteoporotic bone.

Szivek et al. (1995) tested polyurethane foams with three different ratios of isocyanate to resin in compression. The stiffness, yield strength, and ultimate strength

were consistent among samples and were within the range of cancellous bone properties. The mechanical properties of biological bone specimens vary widely due to age, sex, preexisting conditions, and site of bone sample, but synthetic materials exhibit a much more consistent mechanical response and are an effective alternative.

2.2.4 Loggerhead Carapace

The loggerhead carapace has a composite sandwich structure, with an interior of cancellous bone between external and internal cortical bone layers. In the loggerhead, the external cortical bone is thicker than the internal cortical bone. The external compact bone layer has a high number of primary vascular canals and primary osteons. The cancellous bone is mainly primary trabeculae, and the center region is highly porous. The internal cortical bone has parallel fibers and is also highly vascularized (Scheyer 2007). The carapace and plastron are covered by epidermal keratinous plates, or scutes, which protect against attack and the environment and reduce drag. The keratin layer thickens and hardens with age (Solomon et al. 1986).

The bones that compose the shell ossify in the dermis, the deep layer of the skin. A row of central (neural) scutes cap the neural spines of the dorsal vertebrae, and a lateral row of costal scutes is directly connected with the dorsal ribs, as shown in Figure 2.2.

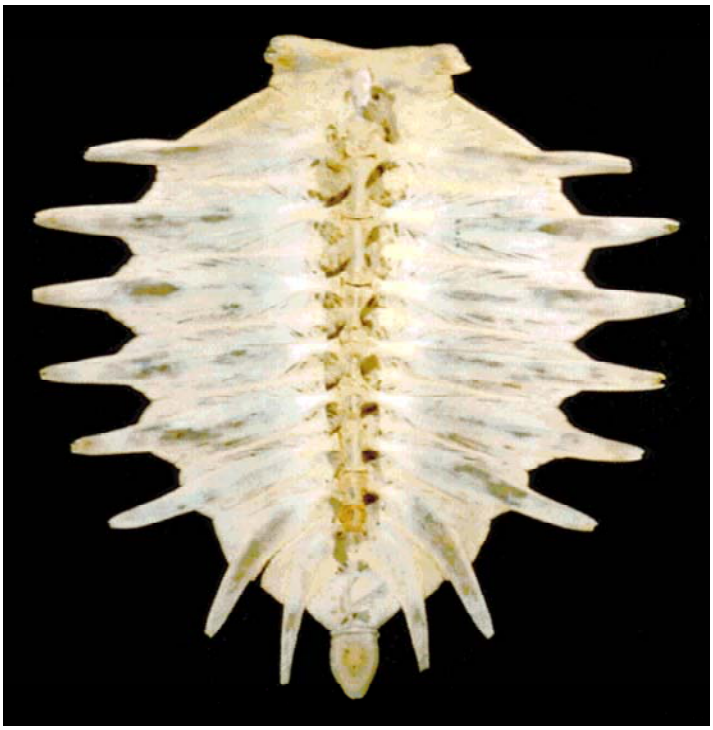

Figure 2.2. The carapace in ventral view, showing the close association of the ribs with the costal plates (Rieppel 2001)

A row of marginal (peripheral) scutes, an anterior nuchal bone, and one or two posterior pygal plate(s) complete the carapace (Dodd 1988; Rieppel 2001). In sea turtles, the costal and the peripheral bones of the carapace and plastron are separated by large fontanels (Scheyer 2007). The bones of the carapace are shown in Figure 2.3.

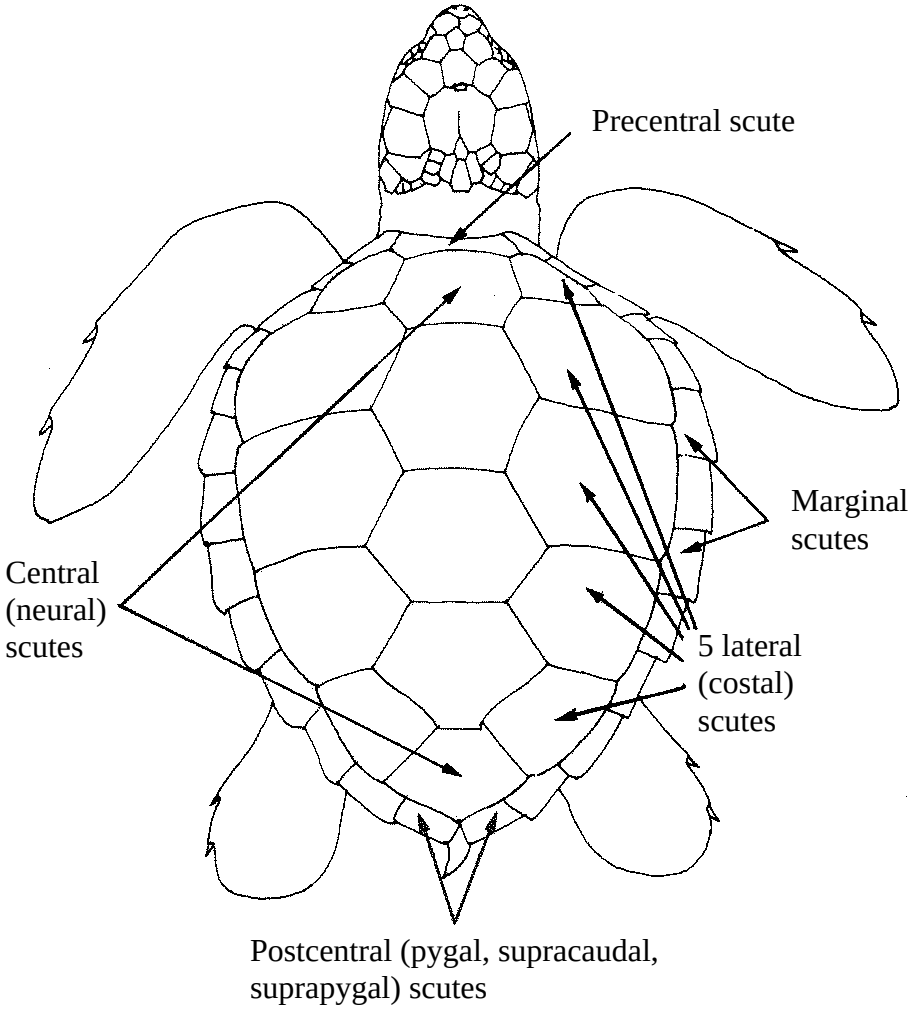

Figure 2.3. Loggerhead carapace bones (Márquez M 1990)

2.3 Sandwich Composites and Impact

Many bones, including the loggerhead carapace, have a structure of soft cancellous bone framed by cortical bone similar to sandwich composite materials. Sandwich structures consist of a thick, lightweight core material between two thin, stiff faces. In commercial applications, the core may be foam or honeycomb, and the faces may be fiber-reinforced composites or metal materials. The addition of the core produces a shell structure that is much stronger under transverse and bending loads with a small increase in weight (Aktay et al. 2005). The faces provide resistance to axial loads, and the

core transmits shear between the faces (Nemes and Simmonds 1992). Sandwich composites are often used in aerospace, marine, and automotive applications, making their behavior under impact conditions a primary concern (Aktay et al. 2005). These sandwich composite structures are liable to impacts from dropped tools, hail, birds, and runway debris (Anderson and Madenci 2000).

Sandwich structures are vulnerable to damage from low-velocity impacts (Schubel et al. 2005). Contact deformations of sandwich composites are dominated by deformation of the core rather than the faces, which offer little resistance to impact damage (Nemes and Simmonds 1992). Impact loading can cause localized internal damage in the face, in the core, or at their interface, resulting in a reduction in tensile, compressive, and bending strength. The critical failure modes of sandwich structures are core buckling, delamination of the impacted face sheet, core cracking, matrix cracking, fiber breakage in the faces, debonding between the face and core, and facesheet buckling (Jiang and Shu 2005; Schubel et al. 2005). No damage occurs if the elastic strain energy can absorb the impact energy of the projectile (Aktay et al. 2005).

The study of low-velocity impact can be categorized into three areas of concern: impact dynamics of the structural response, impact damage and failure modes, and residual properties (Abrate 1997). In the present study, the structural response of the carapace is most relevant, and damage is qualitatively judged as fatal or non-fatal. The investigation of mechanical properties after damage is not considered.

2.4 Finite Element Analysis of Bone

Finite element analysis (FEA) is used frequently in the study of the mechanical function of organisms (Dumont et al. 2009). A number of parameters can be measured,

such as stresses, strains, displacements, forces, accelerations, and velocities, with the goal of relating these factors to types and severity of injury (Horgan and Gilchrist 2003; Mackerle 2003). Unlike lumped parameter and continuum models of impact, finite element analysis allows for calculations of stresses and strains in a system of complex geometry, material properties, and boundary conditions (Sauren and Claessens 1993; Raul et al. 2008). Even then, finite element analysis should be validated with experiments whenever possible (Dumont et al. 2009). A lack of experimental data means that many finite element models yield qualitative rather than quantitative results (Voo et al. 1996). Experimental studies often use animals, cadavers, dummies, or other physical models (Voo et al. 1996; Horgan and Gilchrist 2003). The finite element modeling of biological materials and structures is often hindered by a lack of information regarding material properties, geometric detail, and experimental data for validation (Voo et al. 1996).

Although ship/turtle collision has not been studied using numerical models, human skull fracture due to direct impact has been modeled using FEA. The skull and shell have a similar domed shape and layers of cortical and cancellous bone. Horgan and Gilchrist (2003) generated three models of the human skull at varying mesh sizes. They constructed models using all brick (solid) elements, a composite shell (plate) element, and a combination of shell and brick elements for the cortical and cancellous bone, respectively. The composite shell increased the speed of calculation compared to solid element models. A finer mesh was required for more detailed investigations, but the coarse mesh yielded an acceptable pressure response. The bone material properties were elastic-plastic, isotropic, and homogeneous. The accurate thickness of the bone layers is important for predicting the pressure distribution.

Willinger et al. (2000) produced a skull fracture finite element model that accurately predicted fracture force, skull stiffness, and fracture pattern. The model used a composite shell element for the three-layer skull bone with a constant thickness of each layer, but the accurate modeling of skull thickness of each bone layer affects fracture force. The material properties were homogeneous, isotropic, and linear elastic. The simulation used the Tsai-Wu failure criterion for brittle materials, and a break-deletion element process was used to model failure propagation.

2.5 Current Research Program

The Georgia Department of Natural Resources (GDNR) prompted the current study of the detrimental effects of coastal development and marine traffic on sea turtle mortality. The goal was to develop a better understanding of the parameters that influence vessel strikes on sea turtles. The experimental program included determining the mechanical properties of the loggerhead carapace, identifying a suitable synthetic material, fabricating artificial carapaces, and performing field experiments to investigate a number of parameters. The research effort has been carried out in three primary phases. The current investigation is considered Phase III of the overall research program.

2.5.1 Phase I

The research conducted in Phase I (Hodges 2008) characterized the material properties of the loggerhead carapace. These results were from tensile tests of carapace samples based on ASTM D3039 (2008) and were used as target properties for the current study. Samples were harvested perpendicular to and parallel to the spine. No appreciable difference existed between tensile properties in the longitudinal and transverse directions.

In addition to material testing, the types and locations of vessel-related injuries of 110 sea turtles stranded in Georgia between 2001 and 2006 were classified based on photographs. The cause of damage was categorized as either from propeller, skeg, blunt object, or indeterminate injury. The regions of the carapace were categorized as front, middle, rear, and peripheral. The highest number of injuries were caused by skeg impact to the center region of the carapace.

2.5.2 Phase II

The work in Phase II (Sapp 2010; Work et al. 2010) produced synthetic shells to use in field testing to determine the influence of vessel speed, animal position in the water column, and vessel propulsion system on the lethality of vessel collisions on turtles. The speeds considered were idle (7 km/h), sub-planing (14 km/h), and planing (40 km/h). The two animal positions in the water column were at the water surface and at propeller depth. The engine types were a standard outboard motor with and without commercially available prop guards, and a jet-propulsion outboard motor. The artificial carapace design was constructed of two layers of fiberglass and polyester resin separated by a nonwoven fabric spacer. The presence of catastrophic injury was dependent on both vessel speed and propulsion type. The jet propulsion drive presented significantly lower risk of a fatal injury. The propeller guards shown in Figure 2.4 were ineffective at mitigating damage due to vessel strikes, and the position of the turtle in the water column did not directly affect the probability of injury.

Figure 2.4. Outboard propeller and guards used during Phase II field testing (Sapp 2010)

2.5.3 Phase III

The goals of the current phase of the research program included identifying critical material properties of the carapace with respect to impact, designing an artificial carapace material system with more accurate mechanical behavior, developing a body and attachment system for field tests, and investigating the effects of hull configuration on sea turtle injuries. Material test results from Phase I were used as target properties for the material system, and the design was based on examples of synthetic bone materials and the sandwich structure of the carapace. A program of field tests was developed to determine the effects of hull shape and engine type on the types and lethality of wounds inflicted by vessel strikes. Finite element analysis of the artificial turtle model was used to estimate the critical force that produced carapace fracture.

CHAPTER 3

DESIGN, FABRICATION, AND MATERIAL TESTING OF ARTIFICIAL CARAPACE

This chapter presents the methods and results of material characterization of the loggerhead carapace and the program to develop and manufacture artificial carapaces for field tests. A review of the previous work conducted by Hodges (2008) and Sapp (2010) is presented first, describing the target material properties and desired improvements to the field test specimens. The candidate materials' selection, fabrication, testing, and evaluation are explained, and the mechanical properties of the constituents of the composite material are determined. The fabrication processes of the carapaces and body of the artificial turtle are detailed, and a comparison between artificial and organic material properties is provided.

3.1 Previous Work

3.1.1 Phase I

In the first phase of this research program (Hodges 2008), the primary objective was to determine material properties of the loggerhead carapace using mechanical test methods. Rectangular samples from the carapaces were harvested in a manner designed to identify potential variations in properties due to coupon location and orientation. Samples were taken both parallel (longitudinal) and perpendicular (transverse) to the spine. Specialized tabs were developed to accommodate the samples' irregular geometry and minimize curvature-induced moments during tensile testing. The tabs were

constructed from 3.18 cm PVC cap and pipe with a steel hook inserted in the end, as shown in Figure 3.1. Samples were then embedded in epoxy, and the steel tabs were placed in the grips during testing. A carapace specimen is shown during testing and after fracture in Figure 3.2. A total of 31 samples were tested from a single loggerhead carapace.

The tensile testing program of the biological samples in Phase I investigated four material properties of interest: tensile strength, elastic modulus, strain at failure, and ultimate force per unit width. Stress is a quantitative measure of the intensity of a load over an area and is calculated by dividing the force by the cross-sectional area. The tensile strength is the maximum stress value. Strain is a dimensionless measure of deformation and is found by dividing the elongation of the sample by its original gauge length. Elastic modulus is the slope of the initial linear portion of the stress-strain curve. The strain at failure is the maximum strain value. The ultimate force-per-unit width is equal to maximum stress value times the sample thickness.

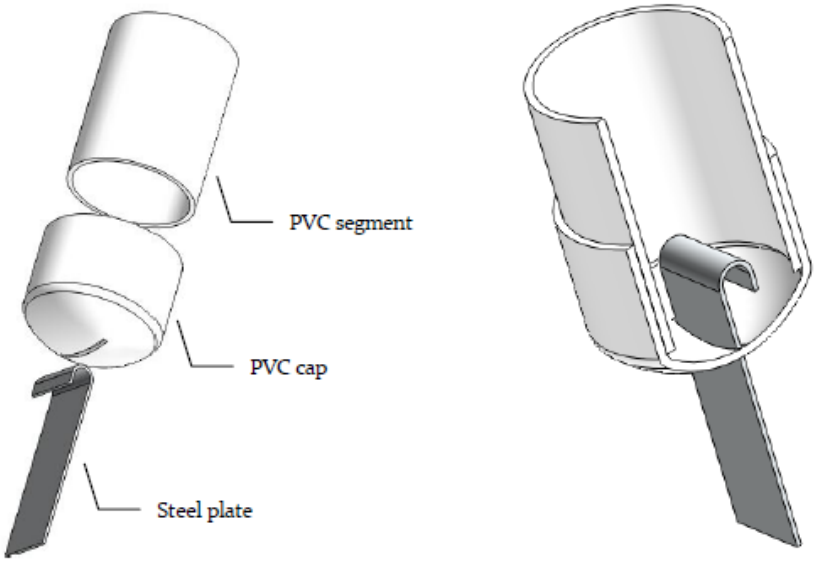

Figure 3.1. Schematics of tabs for tensile testing of carapace specimens

Figure 3.2. Organic specimen in tabs during testing and after failure

For an impact event, the ability to absorb energy without failing is the most critical material parameter (Wegst and Ashby 2004). Toughness is a measure of energy density, or energy absorbed per unit volume of a sample. The toughness values for the samples from Phase I were calculated as the area under the stress-strain curve and included as a fifth target property. The material properties from tensile testing in Phase I, shown in Table 3.1, were used as the target properties for the material systems developed in the current research. Hodges (2008) concluded that the values did not exhibit significant differences with respect to either location or direction of the samples .

Table 3.1. Results from Phase I tensile testing of loggerhead carapace

Orientation	Tensile Strength MPa	Modulus MPa	Strain at Failure %	Ult. Force / Width N/cm	Toughness kJ/m^3
Longitudinal	3.81	328	2.58	359	40.9
Transverse	4.34	295	2.91	457	64.5
Mean	4.08	312	2.74	408	52.7
Std. Dev.	1.24	161	0.0123	114	32.6
COV (%)	30%	51%	45%	28%	62%

3.1.2 Phase II

In this phase of the research program (Sapp 2010; Work et al. 2010), artificial carapaces were designed for use in field tests to determine the effects of animal position in the water column, vessel speed, and engine type on sea turtle mortality. The material design consisted of two layers of 229 g/m^2 fiberglass mat in polyester resin separated by a layer of 2 mm nonwoven polyester fabric spacer. The spacer was used to add flexural rigidity by increasing the distance between the stronger fiberglass mat layers, resulting in a higher moment of inertia. This design increased the rigidity of the synthetic carapace as a whole while keeping the force per unit width at failure close to the target value of 408 N/cm. An internal rib structure was also added to the layer on the underside of the carapace to improve its structural rigidity without modifying the tensile strength significantly. The fabrication process is shown in Figures 3.3 and 3.4. The fiberglass carapace was attached to a PVC frame with a series of plastic cable ties, as shown in Figure 3.5.

Figure 3.3. Phase II fiberglass shell manufacturing process (Sapp 2010)

Although the synthetic shell design used in Phase II of the current program approximated certain tensile properties of the loggerhead carapace reasonably well, the failure modes during field testing showed marked differences from actual vessel strike incidents. Namely, the impact of the skeg seems to crush the real turtle carapace, while the synthetic shells showed much more deformation and larger damaged areas, as shown in Figure 3.6. The propeller wounds observed during Phase II field tests showed a series of parallel slicing wounds as expected; however, tearing in the shell perpendicular to the line of impact of propeller blades also occurred, as noted on Figure 3.7.

Figure 3.4. Underside of Phase II fiberglass shell with rib layout (Sapp 2010)

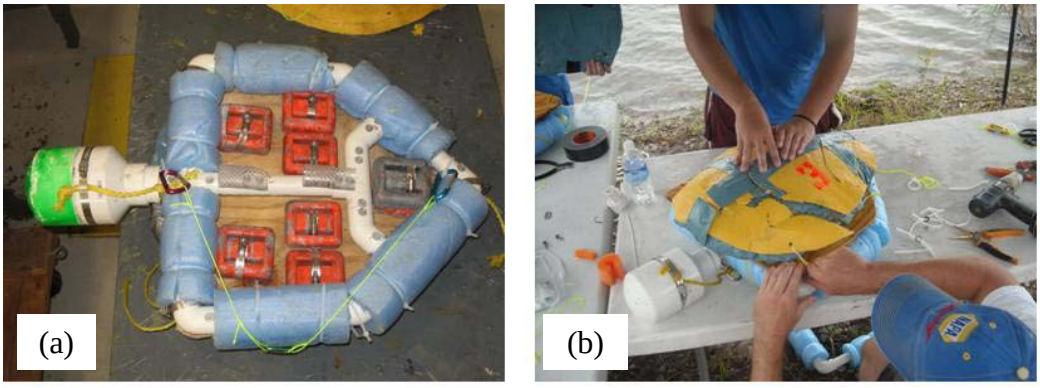

Figure 3.5. (a) Underside showing frame, weights, and flotation (b) Attachment of components with plastic cable ties for Phase II shell (Sapp 2010)

Figure 3.6. Damage to fiberglass shell from blunt impact of skeg from Phase II field tests (Sapp 2010)

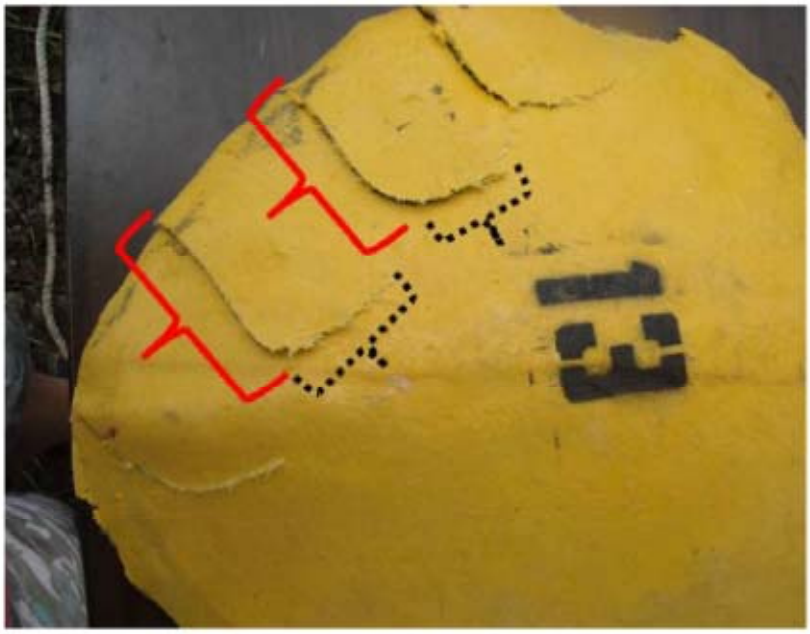

Figure 3.7. Fiberglass shell showing propeller wounds (marked with solid brackets) and tearing (marked with dashed brackets) from Phase II field tests (Sapp 2010)

Both these discrepancies may be due to the synthetic shell's higher overall flexibility, as well as the shell and frame assembly being less rigid than a live turtle. There also existed some energy dissipation during impact as the shell was allowed to move relative to the frame when the plastic tie attachments were broken. These mechanisms may have allowed a longer time of impact, affording the shell more time to

deform. Therefore, a stronger attachment between the shell and frame is necessary in addition to an improvement in the material system used for the synthetic carapace.

3.2 Material Testing for Current Investigation

3.2.1 Tensile and Flexural Testing of Organic Samples

Three loggerhead carapaces were obtained from the Georgia Department of Natural Resources (GDNR) in January 2011. The carapaces were from cold-stunned turtles and had been kept frozen in GDNR facilities. The carapaces were kept on ice when transferred from Brunswick, GA to Savannah, GA, and immediately transferred to a freezer at $-20℃$. Coupons were taken in March 2011 from one carapace for further tensile and flexural testing in comparison to the original target properties from Phase I. The carapace had a curved carapace length of 81 cm, width of 74 cm, and weight of 7.75 kg. First, the carapace was cut on either side of the spine, and then samples were taken from between the rib bones of the carapace in order to avoid the discontinuities the ribs posed. A total of twenty transverse (perpendicular to the spine) 2.5 cm wide samples were taken using a band saw and stored in freezer bags at $-20℃$. The coupons were numbered sequentially, from head to tail, for each half of the carapace. Six were tested in tension and six in flexure in accordance with ASTM D3039 (2008) and ASTM D790 (2010), respectively. The hydration of a bone specimen affects material properties such as elastic modulus, strength, and toughness. In order to approximate living bone, specimens are often thawed in saline solution and kept hydrated during testing (Reilly et al. 1974; Linde et al. 1991; Jonas et al. 1993; Turner and Burr 1993). The flexural samples were thawed in a 0.15 M saline solution prior to testing. Because the tensile samples were placed in the tabs with epoxy which took multiple days to harden, they were not thawed

in the saline solution. Prior to testing, the tensile samples were wrapped in saline-soaked gauze for thirty minutes. The results of the tensile testing are presented in Table 3.2 with a comparison to the values from Phase I. A typical stress-strain curve from tensile testing is shown in Figure 3.8.

Table 3.2. Tensile properties of loggerhead carapace with comparison to Phase I

	Tensile Strength MPa	Elastic Modulus MPa	Strain at Failure %	Ult. Force/ Unit Width N/cm	Tensile Toughness kJ/m^3
Mean	3.87	250	2.35	441	52.4
Std. Dev.	0.705	32.0	0.37	85.1	12.9
COV (%)	18.2%	12.8%	15.8%	19.3%	24.5%
Phase I	4.08	312	2.74	408	52.7
% Diff.	-5.25%	-19.7%	-16.2%	+8.04%	-0.61%

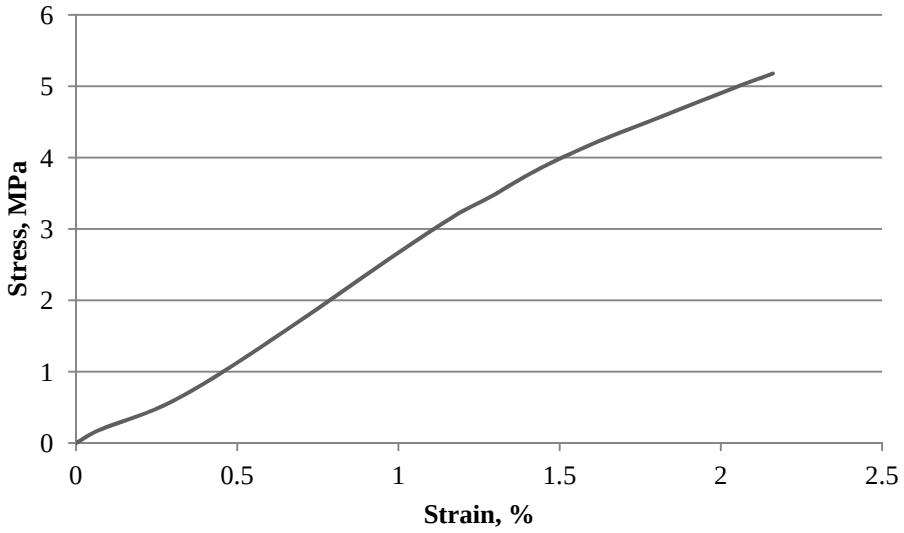

Figure 3.8. Stress-strain curve of organic sample L5

The flexural samples presented problems with their curvature and irregular shape over the supports, as shown in Figure 3.9. The curved samples deflected significantly at the beginning of the test as the ends compressed against the supports and the sample flattened under the initial load. Once the sample lay flat between the supports, its

resistance increased, and the slope of the load-deflection curve rose linearly, as shown in Figure 3.10.

Figure 3.9. Flexural testing of carapace specimen before application of load

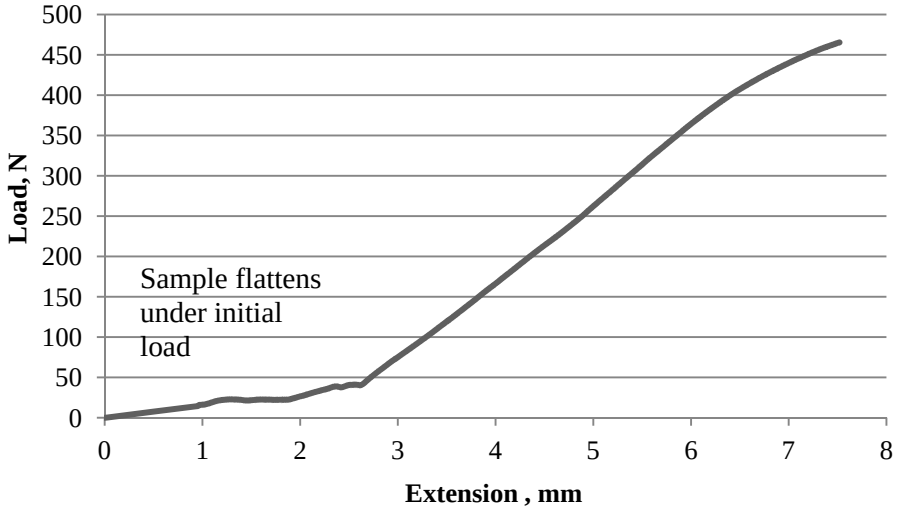

Figure 3.10. Load-deflection curve of organic specimen R5

Because the samples are composites of cancellous and cortical bone with unknown elastic moduli, *E*, the moment of inertia of the whole bone, *I*, cannot be estimated with any degree of accuracy. Therefore, the equivalent flexural rigidity, $(EI)_{eq}$, was estimated from the stiffness, P/δ, by using the well-known equation for displacement in three-point bending, $(EI)_{eq} = PL^3/48\delta$, where the stiffness is the slope of the linear portion of the graph. This calculation ignores shear effects in bending, but those should be minimal for the span-to-depth ratio of the samples. Flexural rigidity was used as a target property for synthetic samples. The flexural properties of the loggerhead carapace are shown in Table 3.3.

Table 3.3. Flexural properties of loggerhead carapace

	Stiffness N/mm	Flexural Energy N·mm	*EI* kN·mm^2
Mean	91.96	1336	5045
Std. Dev.	6.25	50.8	763
COV (%)	6.79%	3.80%	15.1%

The mechanical properties of bone vary considerably with age, anatomical location, time after death, presence of disease, specimen preservation, and test method (Turner and Burr 1993). A large number of specimens are required to determine mechanical properties with confidence. Variability in some tests has been up to 100% of the mean (Szivek et al. 1995; Cristofolini and Viceconti 2000). The target properties used in this investigation were from 31 tensile samples taken from a single loggerhead carapace and six samples in flexure from a second carapace. As the loggerhead is an endangered species, quantities of real shells available for testing were severely limited. Additionally, test shell collection was handled by GDNR personnel in order to ensure compliance with state and federal regulations regarding contact with the animals. This

extended the time between initial location of an animal for testing and the actual tests themselves. Based on results of human bone testing, the material properties of other loggerhead individuals likely vary widely and encompass a large range of values. Materials used in the manufacture of commercially available synthetic bone have significantly lower variability than organic specimens (Szivek et al. 1995; Cristofolini et al. 1996; Cristofolini and Viceconti 2000).

The results of the tensile testing closely matched those of Hodges (2008) with the exception of the elastic modulus, which differed by 20%. Many unknown factors may affect the bone's material properties, including turtle age, time after death, and storage conditions; it is therefore difficult to attribute this difference to a specific cause. The properties of the loggerhead carapaces were determined post-mortem, and some differences are expected compared to bones *in vivo* (i.e., in a live turtle). Furthermore, although the carapaces were harvested from cold-stunned turtles with no sign of disease or injury, the time after death was unknown. Based on the effects of strain rate on human bone, it is reasonable to assume that the material properties of the loggerhead carapace from the quasi-static tests underestimate the strength and stiffness during high strain rate events, such as impact loading. Further study of these parameters on the material properties of the loggerhead carapace is recommended.

3.2.2 Candidate Materials for Artificial Carapace

Because the turtle carapace consists of two layers of denser, stronger cortical bone with a middle layer of porous, weak cancellous bone, a sandwich structure design was chosen for the updated turtle shell design. Synthetic models of human bone have been created using a polyurethane foam to simulate cancellous bone and fiberglass epoxy resin

mixture for cortical bone, as described in Section 2.2.3. As such, this general material configuration was used as a starting point in developing a material system for the artificial carapace. The carapace samples tested previously yielded considerably lower strength values than human bone, so a number of combinations of various face materials with polyurethane foam cores were tested in an effort to match the target properties identified in Phase I. The candidate materials are listed below with their respective identification codes in parentheses. For example, the code for 256 kg/m^3 (16 pcf) foam with two faces of fiberglass mat in polyester resin is "16FPFG-2."

- Core Materials
    - 48 kg/m^3 (3 pcf) polyurethane foam (3F)
    - 256 kg/m^3 (16 pcf) polyurethane foam (16F)
- Resins (Matrix Materials)
    - Polyester resin (P)
    - Epoxy resin (E)
- Reinforcement and Filler Materials
    - 229 g/m^2 fiberglass mat (FG)
    - 6 mm fiberglass chopped strand (glass fibers) (GF)
    - 2 mm thick nonwoven polyester fabric (Coremat®) (C)
    - Glass microspheres (glass bubbles) (GB)
    - Phenolic microballoons (MB)

The fiberglass mat is a 229 g/m^2 mesh of non-oriented fiber, and the glass fibers are 6 mm fiberglass chopped strand. The amount of glass fibers used was half the weight per unit area of the fiberglass mat. The nonwoven polyester fabric is 2 mm thick and is

designed to be used as a spacer or backing material in composite layup. The hollow glass microspheres are approximately 20 μm in size, and the phenolic microballoons are hollow microspheres of phenol formaldehyde resin. The test matrix of candidate materials is shown in Table 3.4. Because the target mechanical properties are much lower than many traditional engineering materials, one-sided samples were also prepared.

Table 3.4. Candidate material systems combinations

Foam Core	**Face Materials**	
	Resin	**Reinforcement/Filler**
48 kg/m^3	None	None
	Polyester	Polyester Fabric
		Fiberglass mat
		Glass fibers
		Glass microspheres
		None
	Epoxy	Microballoons
		None
256 kg/m^3	None	None
	Polyester	Polyester Fabric
		Fiberglass mat
		Glass fibers
		Glass microspheres
		None
	Epoxy	Microballoons
		None

The urethane foam was prepared by combining two components in equal volume and mixing for forty-five seconds. The mixture was poured into a rectangular container and allowed to expand and harden. Rectangular coupons approximately 2.5 cm wide and 0.7 cm thick were prepared with a hand saw. The surface materials were then applied by hand, as shown in Figure 3.11.

Figure 3.11. Application of resin and glass fibers to foam coupons

Tensile testing was performed according to ASTM D3039 (2008) on a standard screw-type axial load machine. Samples which would have been crushed in the machine's grips, such as the 48 kg/m^3 foam with no face materials, were put in the specialized tabs developed by Hodges (2008). Five samples of each material system were tested. The results of tensile testing are summarized in Table 3.5 using nomenclature for each material.

Table 3.5. Results of tensile testing of candidate material systems

Material	Tensile Strength	Modulus	Strain at Failure	Ult. Force / Width	Toughness
	MPa	MPa	%	N/cm	kJ/m^3
Phase I	4.080	312	2.80	408	53
3F	0.197	4	8.57	15	11
3FP	0.941	77	2.57	66	15
3FE	0.392	5	22.56	34	63
3FPFG-1	10.263	496	4.51	739	254
3FPFG-2	17.298	667	4.60	1563	441
3FPGB-1	1.699	187	1.58	99	17
3FPGB-2	2.669	387	0.99	231	14
3FPC-1	0.945	143	3.26	64	15
3FPC-2	1.715	170	1.95	187	31
3FPGF-1	2.546	306	2.49	195	43
3FPGF-2	6.699	246	3.90	651	150
16F	2.615	116	3.48	184	54
16FP	2.128	198	1.55	171	19
16FE	2.097	92	3.72	164	48
16FPGB-1	3.809	313	1.64	241	35
16FPGB-2	4.910	137	5.55	477	153
16FPGB-2 (2)*	4.083	200	2.77	476	62
16FPC-1	3.687	244	2.60	291	57
16FPC-2	5.643	163	5.83	520	191
16FPGF-1	4.139	397	2.01	294	53
16FPGF-2	9.067	157	9.25	920	473

*thinner face thickness than 16FPGB-2

The 256 kg/m^3 foam core with faces of polyester resin infused with glass microspheres (16FPGB-2(2)), shown in Figure 3.12, was chosen as the material system. The choice was based on the material properties from tensile testing and other factors. The tensile properties were similar to those of the organic samples tested by Hodges (2008) with the exception of the elastic modulus; the target value was 312 MPa, and the material system's was 200 MPa. A typical stress-strain curve is shown in Figure 3.13. Organic materials have a large variability in material properties, however, and the target property was based on the testing of only one loggerhead carapace. Furthermore,

adjustments in the thicknesses of the core and/or faces could modify the ratio of the materials' cross-sectional areas and, consequently, the elastic modulus. This is clear from the difference in values between 16FPGB-2 and 16FPGB-2(2), which differed in the thickness of the faces and had substantially different modulus values. The ratio of resin to glass also affects the material properties and could easily be adjusted. The material system was also chosen for its ease of fabrication relative to other materials, particularly the glass fibers, which make it difficult to achieve a consistent thickness across a large surface such as the carapace. The polyester resin and glass microspheres face can also be applied in a spraying process, which reduces the fabrication time for each shell and provides better consistency of thickness and properties across all samples.

Figure 3.12. Application of polyester resin with glass microspheres to rectangular coupons

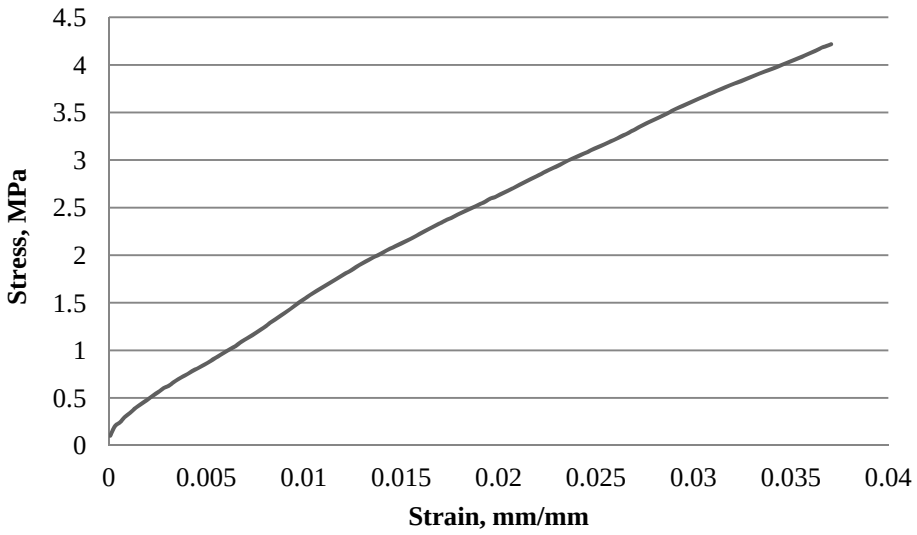

Figure 3.13. Stress-strain curve of 16FPGB(2) sample

3.2.3 Constituent Materials

After choosing the most promising candidate material system, further tests were performed to study the effect of layer thickness and the ratio of microspheres to resin on the material properties. Tests were also performed on the constituent materials; these values were used to estimate the combined material system's properties using equations of composite materials in tension and bending.

The foam is an expanding two-part, closed-cell, rigid polyurethane with a nominal density of 256 kg/m^3. The face coating, referred to as the "resin system," was a 1:1 mixture by volume of commercially available marine polyester resin and glass microspheres. The foam was tested in tension, bending, and compression and the resin system in tension only. The composite system was tested in both tension and flexure, and tests were performed on rectangular samples and coupons cut from artificial carapaces.

3.2.3.1 Polyurethane Foam

The polyurethane foam was poured into a large flat mold with acrylic glass sides, shown in Figure 3.14. The dimensions of the mold were 40 x 50 x 2.5 cm.

Figure 3.14. Mold for creating rectangular foam

Rectangular foam coupons 31 x 8.5 x 130 mm were cut and tested in tension in accordance with ASTM D3574 (2011) and in flexure according to ASTM D790 (2010). In the flexure tests, the crosshead displacement rate was adjusted for each sample depending on the depth and the span length. The maximum stress, σ_f, in bending is calculated as

$$\sigma_f = \frac{3PL}{2bd^2} \tag{3.1}$$

where P is the maximum load, L is the span length, b is the sample width, and d is the sample depth. The depth and width measurements were taken at the center of the span, i.e. at the point of applied load. The strain, ϵ_f, is calculated using

$$\epsilon_f = \frac{6Dd}{L^2} \tag{3.2}$$

where D is the maximum deflection. The modulus from bending, E_B, is found using

$$E_B = \frac{L^3 m}{4bd^3} \tag{3.3}$$

where m is the slope of the initial straight-line portion of the load-deflection curve, i.e. the bending stiffness. The toughness is the area under the stress-strain curve, and the total energy is the area under the load-deflection curve. The density was found by measuring the mass and volume of 25 mm cubes cut from the larger sheet of foam. The density, tensile, and flexural properties for the foam are shown in Tables 3.6 and 3.7.

Table 3.6. Tensile properties of 256 kg/m^3 PU foam

Density kg/m^3	Tensile Strength MPa	Modulus MPa	Strain at Failure %	Ult. Force / Width N/cm	Toughness kJ/m^3
331	4.24	153	5.43	360	149

Table 3.7. Flexural properties of 256 kg/m^3 PU foam

Total Energy N mm	Toughness kJ/m^3	Stiffness N/mm	Modulus MPa	*EI* kN·mm^2	Stress MPa	Strain %
813	204	5.47	173	274	6.52	0.0548

Compression tests were performed on the 256 kg/m^3 foam in accordance with ASTM D1621 (2010). The samples were poured in a 55 x 55 mm acrylic glass mold and allowed to expand vertically. Irregularities in geometry and noticeable voids in the foam were cut away from the top and bottom of each sample, making the height 37 mm. The

tests were performed at 3.7 mm/min on a hydraulic test frame between two steel platens in the direction of rise of the foam. The tests were stopped after cells collapsed and the load deflection curve began to increase after the plateau region of the stress-strain curve. Density was calculated using the overall dimensions of each compressive sample. A typical stress-strain curve is shown in Figure 3.15 , and the results for the samples are presented in Table 3.8.

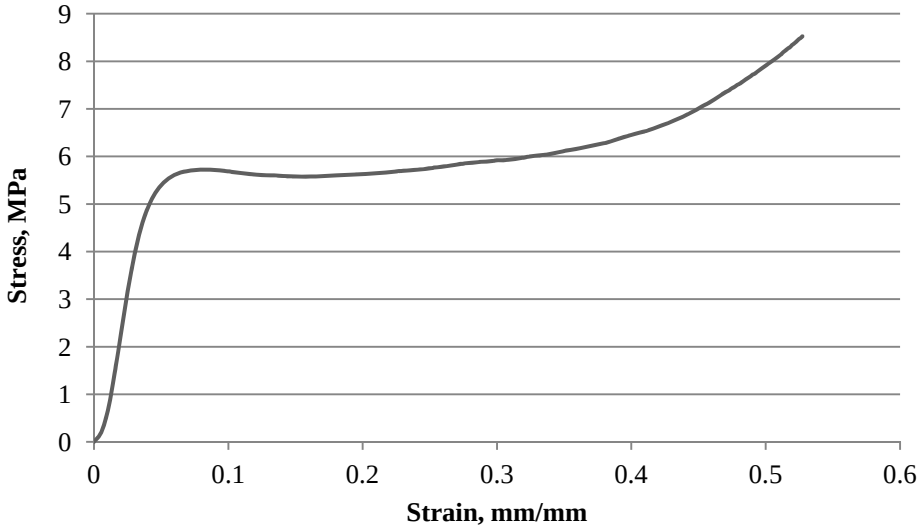

Figure 3.15. Stress-strain curve of 256 kg/m^3 PU foam in compression

Table 3.8. Compression properties of 256 kg/m^3 PU foam

Density kg/m^3	Modulus MPa	Yield Stress MPa	Yield Strain %
289	166	5.81	6.65

3.2.3.2 Resin with Glass Microspheres

The resin system was tested in tension at two different resin-to-glass ratios, 1:1 and 2:1. The resin and microspheres were measured to appropriate volumes and then stirred together by hand. A minimal loss of the glass spheres occurred during mixing. The

resin hardener, approximately 1% of the resin volume, was stirred in, and the mixture was poured on a piece of acrylic glass and allowed to harden. Six dogbone-shaped coupons with dimensions 12.8 x 2.8 x 58.7 mm were cut from each larger sheet and tested in accordance with ASTM D3039 (2008). As expected, an increase in the percentage of microspheres by volume reduced both tensile strength and modulus (Gupta and Nagorny 2006). The results of these tests are shown in Table 3.9.

Table 3.9. Material properties of resin infused with glass microspheres

Resin-to-Glass Ratio	Tensile Strength MPa	Elastic Modulus MPa	Strain at Failure %	Toughness kJ/m^3
1:1	15.7	964	3.22	338
2:1	20.3	1157	4.06	560

3.2.4 Composite Material System

Before production of the synthetic shells, flexural and tensile tests were performed on the foam/resin composite system. Rectangular coupons of foam were cut from a large rectangular sheet with a band saw, and then the resin system was applied by hand.

3.2.4.1 Flexural Testing

Flexural testing was performed on twelve samples using a universal testing machine with flexural loading head. The 3-point bending test procedure was performed in accordance with ASTM D790 (2010) . The results are shown in Table 3.10.

Table 3.10. Flexural properties of candidate composite material system

Stiffness N/mm	Flexural Energy N·mm	*EI* $kN·mm^2$
17.00	461.7	1205

3.2.4.2 Tensile Testing

Twelve rectangular samples were prepared for tensile testing. After the first two samples failed in the grips, the remaining samples were modified into dogbone-shaped samples. The reduced cross section was approximately 25 mm wide with a gauge length of 60 mm. The samples were tested on a hydraulic testing machine in accordance with ASTM D3039 (2008). Three of the remaining ten samples also failed in the grips of the test frame; these data are not included. The material properties are summarized in Table 3.11.

Table 3.11. Tensile properties of candidate composite material system

	Tensile Strength MPa	Elastic Modulus MPa	Strain at Failure %	Ult. Force/ Unit Width N/cm	Toughness kJ/m^3
Mean	4.44	122	4.21	440	102
Std Dev	0.586	10.9	0.700	57.8	27.8
COV (%)	13.2%	8.99%	16.9%	13.1%	27.4%

3.2.5 Discussion of Composite Material System Results

The elastic modulus of a composite material can be estimated by the equation

$$E_T = \frac{E_C A_C}{A_T} + \frac{E_F A_F}{A_T} \tag{3.4}$$

where E_T, E_c, and E_F are the elastic modulus values of the total composite, foam core, and faces, respectively, and A_T, A_C, and A_F are the cross-sectional area of the composite, core, and faces, respectively.

The values using the equation above were compared to the tensile testing results of three sets of data: a 1:1 resin mixture with a 14.5 mm thickness, a 1:1 resin mixture with a 10.7 mm thickness, and a 2:1 resin mixture with a 10.3 mm thickness. The cross-sectional area measurements were taken at the location of break after the sample failed.

The average tensile material properties for the foam and resin were used from Sections 3.2.3.1 and 3.2.3.2 . The results of the comparison are shown below in Table 3.12, where b is the width, t is the face thickness, c is the core thickness, and h is the total depth. The experimental and theoretical elastic modulus values show good agreement.

Table 3.12. Comparison of theoretical and experimental modulus values

Sample	Sample Dimensions (mm)				Modulus (MPa)		% Diff
	b	h	c	t	Theo.	Exp.	
1:1 - 1	26.09	14.60	13.48	0.56	215	194	10.9%
1:1 - 2	26.30	14.50	13.25	0.62	223	203	9.8%
1:1 - 3	26.85	14.27	13.05	0.61	222	200	11.2%
1:1 - 4	25.72	14.16	12.74	0.71	234	206	13.8%
1:1 - 5	26.85	14.44	12.98	0.73	235	190	23.7%
1:1 - 6	25.62	14.73	13.00	0.86	248	211	17.7%
1:1 - 7	26.51	10.71	9.61	0.55	236	271	12.8%
1:1 - 8	26.26	11.13	9.93	0.60	240	240	0.2%
1:1 - 9	25.82	10.30	8.96	0.67	259	249	3.8%
1:1 - 10	27.54	10.35	9.07	0.64	253	248	2.1%
1:1 - 11	26.17	10.77	9.53	0.62	246	249	1.1%
1:1 - 12	28.66	11.00	9.42	0.79	269	290	7.1%
2:1 - 1	26.81	10.04	9.11	0.46	246	230	7.0%
2:1 - 2	26.46	10.34	9.15	0.59	269	217	23.8%
2:1 - 3	27.60	10.70	9.61	0.54	255	239	6.8%
2:1 - 4	26.07	10.42	9.73	0.34	219	236	7.0%
2:1 - 5	27.65	10.17	9.34	0.41	235	230	2.1%
2:1 - 6	26.98	10.42	9.71	0.35	221	206	7.5%

The deflection of a flexural sample can be split into the contributions from bending and shear. The equivalent flexural rigidity of a composite material can be estimated using the equation

$$(EI)_{eq} = \frac{E_F b t^3}{6} + \frac{E_C b c^3}{12} + \frac{E_F b t d^2}{2} \tag{3.5}$$

and the equivalent shear rigidity by

$$(AG)_{eq} = \frac{bd^2 G_C^*}{c} \tag{3.6}$$

where d is the center-to-center distance between the faces, l is the span length, and G_C^* is the shear modulus. Cellular solids, including foam and cancellous bone, have material properties which are highly dependent on apparent density. For the foam core, the shear modulus can be estimated using the apparent density and solid material properties (E_S and ρ_S) of polyurethane using the following equation from Gibson and Ashby (1999):

$$G_C^* = C_2 E_S \left(\frac{\rho_C^*}{\rho_S}\right)^2 = 0.4 * 1.6 \left(\frac{331}{1200}\right)^2 = 0.049\ GPa \tag{3.7}$$

For a three-point bending test, the total deflection, δ, is calculated using the well-known equation:

$$\delta = \delta_B + \delta_S = \frac{PL^3}{48(EI)_{eq}} + \frac{PL}{4(AG)_{eq}} \tag{3.8}$$

Any value of the load, P, can be used to calculate the deflection, δ, and then the stiffness can be calculated as P/δ. The experimental stiffness value is calculated by measuring the slope of the linear portion of the load-deflection curve. A comparison of the expected and experimental values of stiffness is shown in Table 3.13. There is good agreement, with a 10% difference between the average values of the theoretical equation and experiment. The flexural stiffness of the composite material system can be predicted using the above equations and constituent material properties. The equations used to approximate the composite material properties do not take into account the porosity of the foam or other imperfections. It was assumed that at the scales used in the mechanical testing, the constituents could be treated as homogeneous materials. More exact approximation of the foam's behavior may be available, but for the purposes of this

study, the basic equations of composite materials were assumed to adequately represent the material's mechanical properties in tension and bending. Using the above approximations for elastic modulus and stiffness of the composite material system, thickness values of the foam core and faces can be calculated to better model the tensile and flexural properties of the organic carapace.

Table 3.13. Comparison of theoretical and experimental flexural stiffness values

Sample	Sample Dimensions (mm)						Stiffness (N/mm)		% Diff
	b	h	c	d	t	l	Theo.	Exp.	
1	28.61	10.09	8.50	9.29	0.79	150.43	15.85	18.50	14.3%
3	29.35	7.97	5.81	6.89	1.08	150.43	10.95	10.27	6.7%
5	29.87	10.02	8.15	9.08	0.93	150.43	17.79	18.88	5.8%
7	32.10	8.83	6.77	7.80	1.03	150.43	14.92	16.06	7.1%
9	32.68	9.96	8.43	9.19	0.76	150.43	17.20	19.35	11.1%
11	33.21	9.64	8.46	9.05	0.59	150.43	14.05	18.96	25.9%
13	33.02	9.07	7.73	8.40	0.67	150.43	12.93	14.30	9.5%
15	33.05	9.52	8.30	8.91	0.61	150.43	13.81	17.18	19.6%
17	32.76	10.01	8.06	9.03	0.97	150.43	19.91	17.98	10.8%
19	33.56	9.27	7.93	8.60	0.67	150.43	13.85	15.67	11.6%
21	32.58	8.46	6.82	7.64	0.82	150.43	12.08	13.18	8.3%
23	32.91	9.92	7.86	8.89	1.03	150.43	20.17	23.62	14.6%

3.3 Synthetic Shell Fabrication

3.3.1 Mold Construction

In order to form an artificial carapace in the correct shape, a mold was made of the same turtle carapace that was used as a basis for the synthetic shells produced by Sapp (2010). The mold making process is shown in Figure 3.16. The carapace was coated with automotive body filler on both sides, sanded smooth, and then coated with a urethane finish. The carapace was placed dorsal side down in a wooden box lined with plastic (Figure 3.16a) and then encased in a two-part liquid urethane mold rubber. The

shell was placed on a small wooden riser so that it would be completely surrounded by the mold rubber. The two parts were mixed equally by weight in a bucket and stirred with a paint mixer attachment on a power drill. The bucket was placed on a digital balance, and approximately 9 kg of one part of the mold rubber was poured; then an equal weight of the second part was added. The mixture was stirred for 60-90 seconds and then poured into the box. This process was repeated until the carapace was completely encased in mold rubber. The process was completed quickly to produce a continuous mold that did not separate into layers. The mold used approximately 115 L (122 kg) of mold rubber and was allowed to cure for five days before shell removal. The shell was removed by cutting around the perimeter of the carapace with a reciprocating saw (Figure 3.16b). Once the top (male part) of the mold was removed, plywood and handles were attached to the top of the mold to allow for placement during the shell casting process (Figure 3.16c). The plywood rested on the flat surface of the mold, leaving a void in which the foam carapace formed.

Figure 3.16. Mold construction process: (a) shell in wooden frame (b) cutting out shell from rubber mold (c) attaching lid to male part of mold (d) two halves of mold with shell removed.

3.3.2 Fabrication of Foam Carapace and Application of Resin

Before making a foam carapace, both halves of the mold were prepared with mold release spray (Figure 3.17a). For synthetic shell production, 0.95 L of each part of the 256 kg/m^3 foam were measured out and combined (Figure 3.17b). The mixture was stirred for forty-five seconds with a paddle mixer attached to a power drill (Figure 3.17c). The mixture was then poured into the bottom half (female) of the mold (Figure 3.17d). The lid with the attached top half (male) of the mold was quickly put in place and secured with three ratcheting tie downs to limit the rise of the foam. Small amounts of foam were

allowed to expand through two release holes located at the highest point of the carapace. The shell was left in the mold for 20-25 minutes before being removed. Excess foam and imperfections at the edges were chipped off, and the residue of the release spray was washed off using dish soap. After drying, the shell was sanded to reduce imperfections and to make the shell surface more receptive to the resin during the spraying process. The dorsal and ventral views of the foam carapace are shown in Figure 3.18. The foam shell has a mass of approximately 2.0 kg. A total of 60 foam shells were produced.

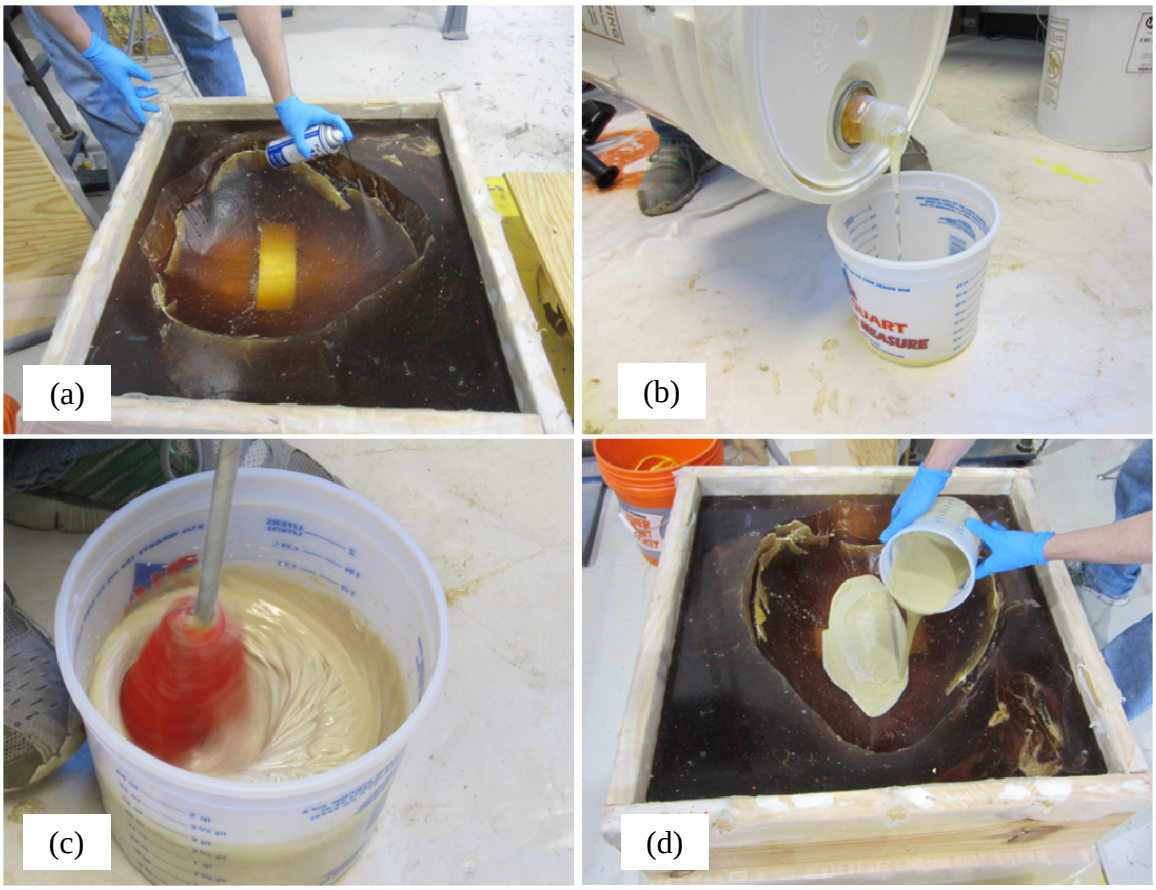

Figure 3.17. Fabrication of foam core of artificial carapace. (a) Spraying mold release. (b) Pouring one part of the foam. (c) Stirring the two parts together. (d) Pouring the mixture into the mold.

Figure 3.18. Foam carapaces after sanding

In preparation for coating with the resin system, the foam carapaces were washed and sanded. The polyester resin with glass microspheres mixture was applied using an air-powered spray gun with a 4.7 mm nozzle opening and an operating pressure of 0.5 MPa. The resin and microspheres were mixed in a 1:1 ratio by volume. The resin hardener, about 1% of the volume of resin, was added to the mixture immediately prior to spraying. The spraying process is shown in Figure 3.19. Three coats were applied to each side, 20-30 minutes apart. The spray gun's metal parts were cleaned with acetone between coats. After three coats had been applied to the inner surface, the shells were placed in a confined space and allowed to cure fully. The remaining side was then sprayed, typically the following day. A total of approximately 235 mL of the resin system was applied to each side of the carapace. The finished shells, shown in Figure 3.20, are white with a glossy finish and weigh 2.8 kg with a curved carapace length of 64 cm.

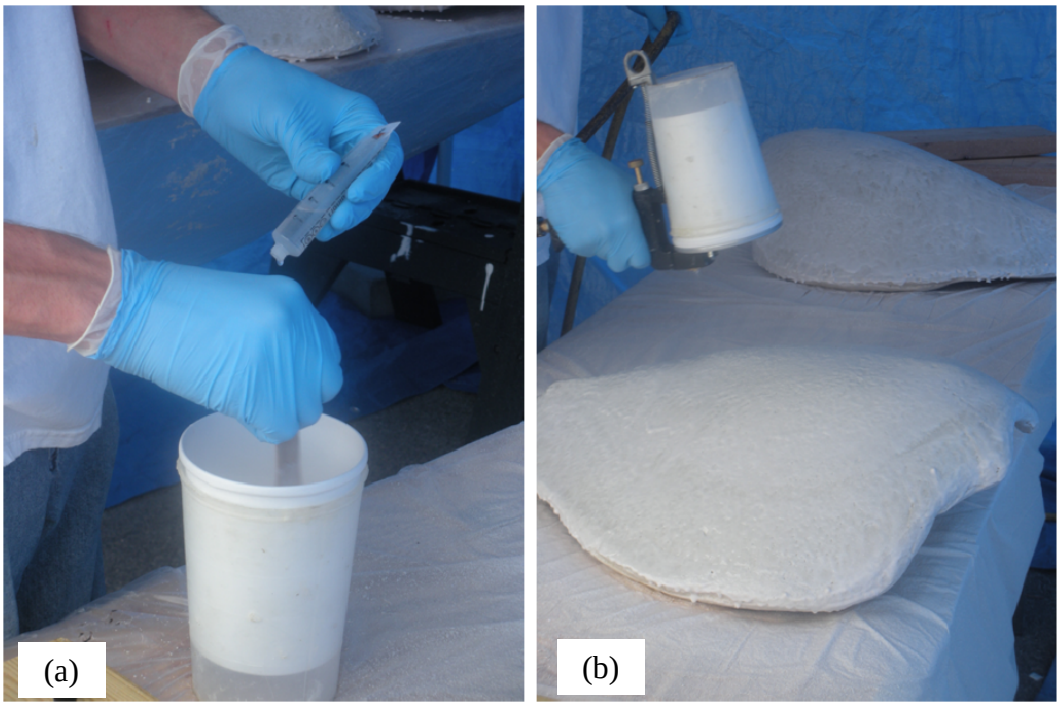

Figure 3.19. (a) Adding resin hardener to the resin and microspheres. (b) Applying resin infused with microspheres to artificial foam carapace with spray gun


Figure 3.20. Artificial carapaces with resin coating

3.3.3 Body Frame Design and Fabrication

In addition to the development of the artificial carapace, a body frame was designed to provide weight, buoyancy, and a method to attach the carapace. The frame also accommodated an accelerometer and ropes which held the turtle in the water. The body of the synthetic turtle was built from 1.2 cm thick medium-density fiberboard

(MDF), 2.5 cm diameter polyvinyl chloride (PVC) pipes and connecting pieces, and 24.5 kg of lead dive weights. The PVC frame was designed to provide support for the board, accommodate an accelerometer, and provide attachments for “head” and “tail” pieces used to better simulate a real turtle floating in the water. The PVC and weights were attached to the MDF with plastic cables ties. The accelerometer housing was glued to the MDF and attached to the PVC with cable ties. The frame assembly with the MDF, PVC, accelerometer case, and weights is shown in Figure 3.21.

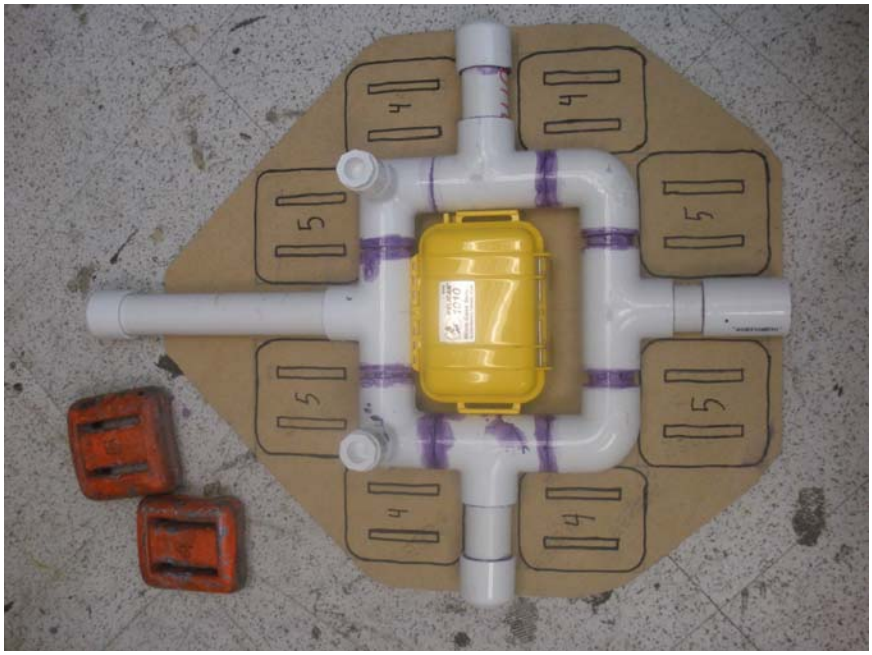

Figure 3.21. MDF with positions of weights drawn, PVC frame and accelerometer case

The board assembly was encased in 48 kg/m^3 polyurethane foam to provide buoyancy and prevent damage to the materials. Figure 3.22 shows the board, with weights, PVC, and accelerometer housing attached, placed on an uncoated shell inside the mold. The uncoated shell was sprayed thoroughly with mold release so that the body and carapace could be separated after removal from the mold. To completely surround

the board, the foam was poured multiple times, with care taken to avoid the accelerometer housing. The foam was allowed to expand freely, as shown in Figure 3.23.

After a sufficient amount of foam had been poured, the shell and body were removed from the mold and separated from each other. The excess foam was then cut flat on the bottom surface approximately 2.5 cm from the PVC and weights, and ends were modified to allow attachment of head and tail pieces. The body with the shell removed and the underside cut flat are shown in Figures 3.24 and 3.25.

Figure 3.22. Board, PVC frame, and weights resting on shell in mold prior to pouring the foam for the body

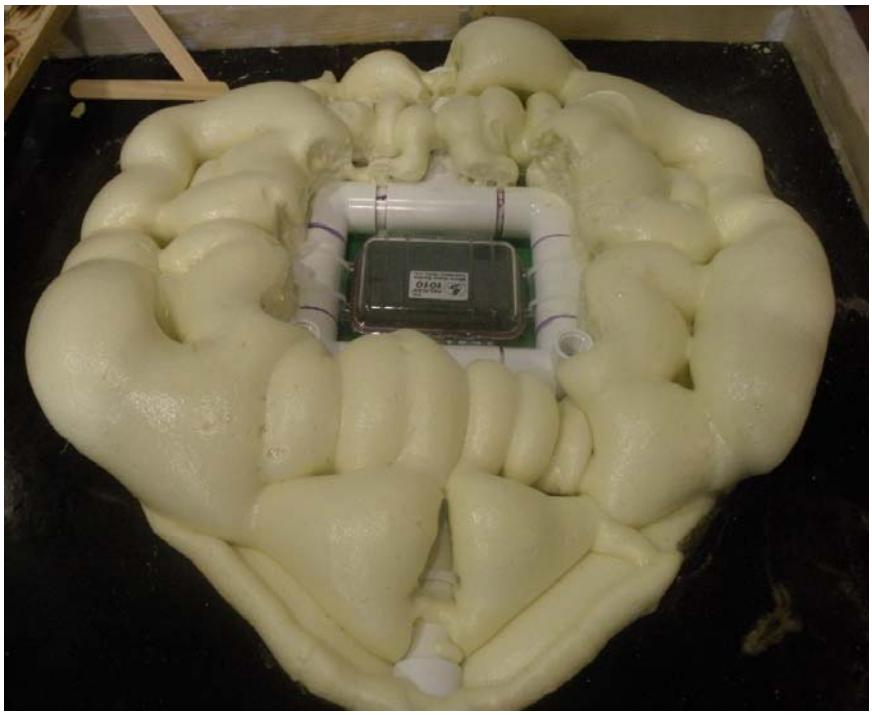

Figure 3.23. Board, PVC frame, and weights resting on shell in mold after pouring the foam for the body.

Figure 3.24. The body and foam carapace after separation

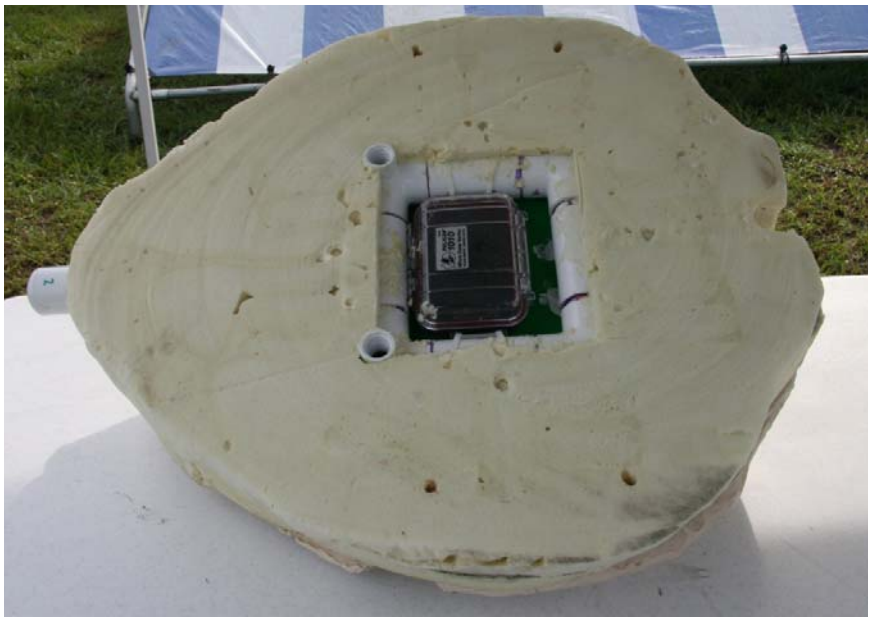

Figure 3.25. Underside of body after being cut flat showing accelerometer housing

3.3.4 Shell Attachment

A 1.9 cm thick piece of plywood on the underside of the artificial turtle, shown in Figure 3.26, served multiple purposes. Two holes near each edge aligned with holes in the carapaces for attachment with cable ties. Four eye hooks were screwed into the plywood for use in tethering the turtle to the shore with polypropylene ropes. The plywood also protected the accelerometer housing. The board was aligned by placing the two PVC protrusions through large holes in the board. This prevented movement of the board relative to the rest of the body during impact.

Figure 3.26. Plywood underside with four eye hooks and holes for attachment

The synthetic carapace was attached to the body at five locations using plastic cable ties – a method similar to the design used in previous field experiments (Sapp 2010; Work et al. 2010), There were two holes on each side of the turtle and one in the rear. The cable tie in the rear passed through the PVC frame, and the holes on the sides passed through the body and the plywood on the underside. This system allowed for the quick removal and attachment of shells between tests, and the body could be used for multiple shells during the course of testing. Figure 3.27 shows the process of attaching a carapace to a body. Five bodies were prepared for the first round of testing. A revised body design, described in Section 4.3.1.1 , was used in the second round of field tests.

Figure 3.27. Attachment of carapace to body using cable ties

3.4 Synthetic Shell Material Testing

Four synthetic shells were randomly selected for tensile and flexural coupon harvesting. The carapace was sectioned using a band saw. Five samples were taken from each half and numbered 1 to 5 from head to tail. For each shell, five samples were tested in tension and five in flexure. The tension samples were placed in the PVC tabs developed by Hodges (2008). The cross-sectional area of the tensile samples was measured at the location of failure after the test was completed. The area of the flexure samples was measured at the point of the applied load, and the span length was the distance between the supports, not the curved length of the sample.

The average thickness of the organic samples was 12 mm, while the average thickness of the synthetic coupons was 21 mm. The thicknesses of the samples during the testing of the candidate materials (Section 3.2.2) were designed to match those of the

organic specimens. The average thickness of the 16FPGB-2 material samples was 11.8 mm. The coating of automotive body filler on the carapace used for the mold making increased the thickness, and the foam exerts considerable lifting force on the lid of the mold during expansion, increasing the thickness further. The drastic increase in thickness raises the cross-sectional area and therefore lowers the stress values compared to the organic and candidate material specimens. The increased thickness also increases the second moment of area, I, resulting in higher flexural rigidity, EI, values in flexural testing. The increase in cross-sectional area of the foam, which is weaker than the resin system, considerably decreases the strength of the samples. The tensile testing results of the synthetic carapace coupons have been scaled in proportion to the thickness of the candidate materials; these values are reported in Table 3.14, and the flexural rigidity of the synthetic material system is shown in Table 3.15.

Table 3.14. Scaled tensile properties of synthetic shell with comparison to target value

	Stress	Elastic Modulus	Strain	Ult. Force/Unit Width	Toughness
	MPa	MPa	%	N/cm	kJ/m^3
Shell 1	4.436	253	3.18	312.3	83.1
Shell 2	4.258	265	2.48	290.6	53.6
Shell 3	5.013	235	3.63	381.6	100.9
Shell 4	3.700	232	2.54	257.0	48.6
Mean	4.317	247	2.92	306.6	70.0
Std. Dev.	0.713	29.0	0.780	73.5	36.4
COV (%)	16.5%	11.7%	26.7%	24.0%	52.0%
Organic	4.080	312	2.80	408.0	52.7
% Diff	+5.8%	-20.8%	+4.3%	-24.9%	+32.8%

Table 3.15. Flexural rigidity of synthetic shell with comparison to target values

	EI kN·mm^2
Shell 1	8414
Shell 2	7249
Shell 3	9218
Shell 4	8062
Mean	8171
Organic	5045
% Diff	+61.96%

The load-deflection curve of the samples in bending exhibited similar behavior to the organic specimens in Section 3.2.1. The curved sample flattened under the initial load, followed by a steep linear response until failure, from which the stiffness and *EI* values were computed. A characteristic curve is shown in Figure 3.28.

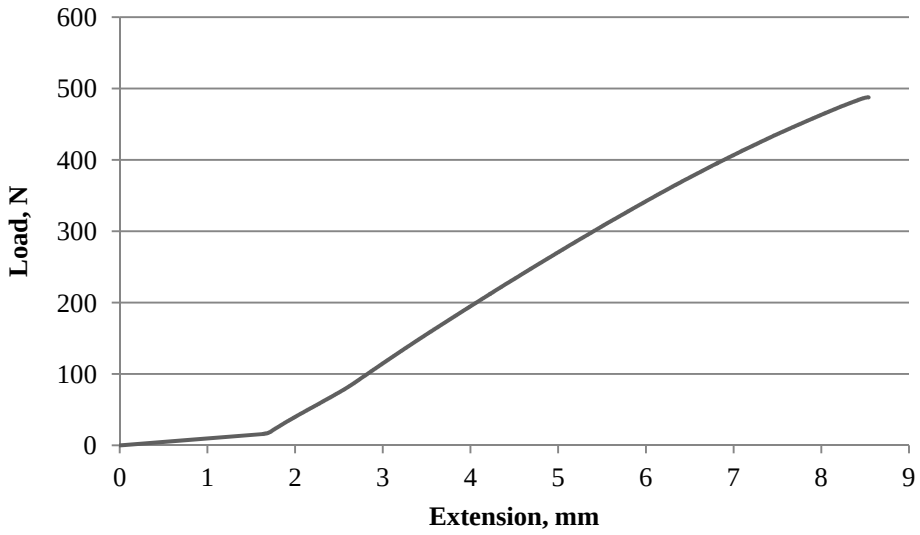

Figure 3.28. Load-deflection curve in bending of specimen R4 from Shell 3

3.4.1 Discussion

Overall, the synthetic shell reasonably approximated the material properties of the loggerhead carapace. The thickness, particularly of the foam core, affected the properties

of the material by decreasing ultimate strength and stiffness in tension and increasing equivalent flexural rigidity compared to the candidate materials. The toughness and flexural rigidity values of the synthetic material vary from those of the organic shell, but their higher values are conservative for the field tests. The target tensile and flexural properties are also based on only one carapace each, but the mechanical properties of bone can vary considerably among individuals (Currey 2002).

It is important to have consistent mechanical properties for all test specimens, and the synthetic material system exhibited consistent material properties across the four shells. The standard deviation and coefficient of variation values for the 20 synthetic coupons were lower than the 31 tensile tests performed in Phase I. The fabrication methods of the foam carapace and spraying process are capable of producing specimens with consistent dimensions and mechanical properties.

In addition to trying to match the mechanical properties of the loggerhead carapace, the synthetic samples needed to exhibit similar behavior and failure modes in testing. The tensile and flexural graphs of the loggerhead carapace in Figures 3.8 and 3.10and of the sandwich composite in Figures 3.13 and 3.28show that the response of both materials was similar. The tension samples did not exhibit large plastic region or nonlinear behavior. The flexural samples showed the same initial flattening under low loads, followed by a linear response until failure. ASTM D790 (2010) recommends using a span length-to-depth ratio greater than 16 to reduce shear effects in bending. For the synthetic samples, this depth-to-span ratio was not achievable due to the thickness of the samples.

Finding a balance between thicknesses of the foam core and faces is possible using Equations (3.4) and (3.5) and the constituents' material properties. In order to find thickness values of the core and faces which result in agreement with both the target modulus and flexural rigidity values, the equations for elastic modulus and equivalent flexural rigidity need to be solved simultaneously. The contribution of shear effects is considerably smaller than those of bending and are ignored in this process. Both equations can be written as functions of two variables: the thickness of the core, c, and the thickness of each face, t. The modified equations are shown below.

$$E_T = \frac{E_C c}{c + 2t} + \frac{2E_F t}{c + 2t} \tag{3.9}$$

$$(EI)_{eq} = \frac{E_F b t^3}{6} + \frac{E_C b c^3}{12} + \frac{E_F b t (c + t)^2}{2} \tag{3.10}$$

First, the function for elastic modulus is set equal to the target value of 312 MPa and solved for c in terms of t, which results in $c = 8.2t$. This is substituted into Equation (3.10) and solved for the target value of 5045 kN·mm^2. The dimensions which satisfy both target values simultaneously are $c = 13.2$ mm and $t = 1.6$ mm. By comparison, the average thickness of the organic samples was 12 mm. Using the constituent material properties, it is possible to design a synthetic carapace with similar mechanical properties and dimensions to an organic specimen.

CHAPTER 4

FIELD TESTING

The previous study on sea turtle injuries from vessel strikes (Work et al. 2010) indicated that an outboard propeller could cause serious damage to a turtle carapace at any speed. The previous field tests were conducted with a flat-bottomed skiff in order to limit the effects of hull impact. The current field experimental program was designed to investigate what effect, if any, hull shape has on the type and lethality of damage a turtle sustains from vessel strikes. The hypothesis under consideration is that vessels with deeper drafts and different hull geometry may cause a fatal blunt force injury with a hull collision only. Two vessels with deep-vee hulls were used in the field tests: one with an inboard jet propulsion system and one with an outboard propeller engine. In addition to the artificial turtles described in Section 3.3, deceased sea turtles were also subjected to vessel impacts. An accelerometer/datalogger was attached to each artificial specimen, and post-test assessments of injury patterns and lethality were measured and documented.

4.1 Description of Field Test Site

The field test site had to meet a number of criteria—including minimal marine traffic, little recreational activity, and limited wave and tidal action—which eliminated the use of coastal sites. The site also needed a boat ramp which could accommodate the vessels to be used. The site needed to be relatively shallow with a sandy bottom for easy deployment and retrieval of test specimens. There also needed to be space for preparation and assessment of specimens before and after testing. Many inland locations are privately owned and therefore difficult to obtain access. The testing site which met all of the

criteria was found on the Ogeechee River near Highway 204 south of Savannah, GA. A map of the location is shown in Figure 4.1.

Figure 4.1. Map of field test site (Google 2012)

4.2 Development of Field Test Program

Testing procedures were designed to investigate the effect of animal position in the water column, vessel propulsion system, and hull shape on the lethality of sea turtle injuries from vessel strikes. Two boats were used in the field experiments: a 5.4 m inboard jet propulsion vessel and a 7.3 m 4-bladed outboard propeller-driven vessel. Both have deep-vee hulls, which is defined as a hull deadrise angle greater than 20 degrees. A steep angle allows the hull to slice through water and waves. The two vessels are pictured in Figures 4.2 and 4.3. Hereafter, the jet boat will be referred to as “Vessel 1” and the propeller-driven boat as “Vessel 2.”

Figure 4.2. Vessel 1, 5.4 m inboard jet propulsion vessel

Figure 4.3. Vessel 2, 7.3 m 4-bladed outboard propeller-driven vessel

All tests were performed at planing speed, which is the speed at which a vessel skims across the surface with only a small portion of the hull in the water. For the vessels used, this speed was approximately 40 km/h. Initially two locations in the water column were selected: at the surface and at propeller depth (measured to the center of the hub with the boat at rest) of Vessel 2. After tests at propeller depth failed to produce any vessel strikes, an intermediate depth was added. The three depths for Vessel 2 were at

propeller depth (71 cm), at 48 cm, and at the surface (0 cm) . For Vessel 1, two depths in the water column were used: at the surface and at 48 cm.

Two rounds of tests were performed, the first on August 1, 2011, and the second on October 13, 2011. Between the two rounds of testing, a revised body design was developed with the carapace directly attached to the body, as described in Section 4.3.1.1 below. The tests performed during the first round of testing are summarized in Table 4.1. The second round also included trials using deceased sea turtles provided by GDNR. Investigation of the wounds in the real turtles was performed by biologists and scientists, whose results are forthcoming. The parameters of the second round of tests are shown in Tables 4.2 and 4.3.

Table 4.1. Test program for Round 1 (August 1, 2011)

Vessel #	Propulsion System	Depth (cm)	Number of Trials
1	Jet drive	48	5
1	Jet drive	0	6
2	Propeller	71	5
2	Propeller	48	5
2	Propeller	0	5

Table 4.2. Test program for synthetic shells, Round 2 (October 13, 2011)

Vessel #	Propulsion System	Depth (cm)	Number of Trials
1	Jet drive	0	5
2	Propeller	48	2
2	Propeller	0	8

Table 4.3. Test program for real turtles, Round 2 (October 13, 2011)

Vessel #	Propulsion System	Depth (cm)	Number of Trials
1	Jet drive	0	3
2	Propeller	48	5
2	Propeller	0	5

4.2.1 Instrumentation for Artificial Shell Field Tests

A plastic case on the underside of the body, shown in Figure 4.4, housed the accelerometer/datalogger. The three-axis digital accelerometer has a range of $\pm$15 g, an accuracy of $\pm$0.15 g, and a sampling rate up to 1600 Hz (MSR Electronics GmbH 2012). The datalogger can store up to two million measurements with installed memory and has a micro-SD slot for memory expansion. The plastic housing was used to prevent damage to the accelerometer from water and impact and provide a rigid base so the accelerometer would not move relative to the turtle during impact. The accelerometer/datalogger was attached to a removable rubber base with three screws and then placed in the plastic case. During testing the accelerometer was placed in a plastic bag for waterproofing. The accelerometer could easily be transferred between turtle bodies between tests. The accelerometer, rubber base, rubber lining, and plastic case are shown in Figure 4.5.

The accelerometer/datalogger was chosen because it offered monitoring and storage capabilities in a single small wireless unit that was easily incorporated in the test specimen. The battery life and storage were ample for use in multiple experiments during a day's testing without interruption for charging or downloading data, and the 1600 Hz sampling rate was sufficient for recording impact events. The ±15 g range was exceeded repeatedly during the field tests, meaning many initial impact accelerations were higher than reported, particularly in the case where the specimen was struck by the motor. However, the majority of the acceleration data recorded during a given field test were within the range of the device and could be used to describe the motion of the turtle after impact.

Figure 4.4. Underside of body showing accelerometer housing and PVC extensions

Figure 4.5. Accelerometer with rubber base, lining, and plastic housing

4.3 Field Test Procedures

The field tests required at least nine people to perform all the necessary tasks. Two people were in the boat: the boat operator and an observer in the bow of the boat to record the orientation of the specimen relative to the vessel at impact. During testing, two

people prepared the next turtle by attaching the carapace and readying the accelerometer. Two others worked on specimen deployment, retrieval, and positioning in the water. Two people took photographs and assessed the damaged specimens. One person was responsible for video recording.

4.3.1 Deployment of Artificial Shells

During field testing, the turtle was held in place using an anchor system. A 35 kg metal plate was dropped to the bottom of the river at a depth of approximately 3 m. A short piece of rope with a swiveling carabiner on its free end was attached to the anchor, as shown in Figure 4.6; the tether connecting the turtle to the shore ran through the carabiner. Flotation attached to the carabiner aided in finding it in the event the tether to shore was disconnected. The swiveling carabiner helped prevent ropes becoming tangled and twisted when pulling on the tether from shore.

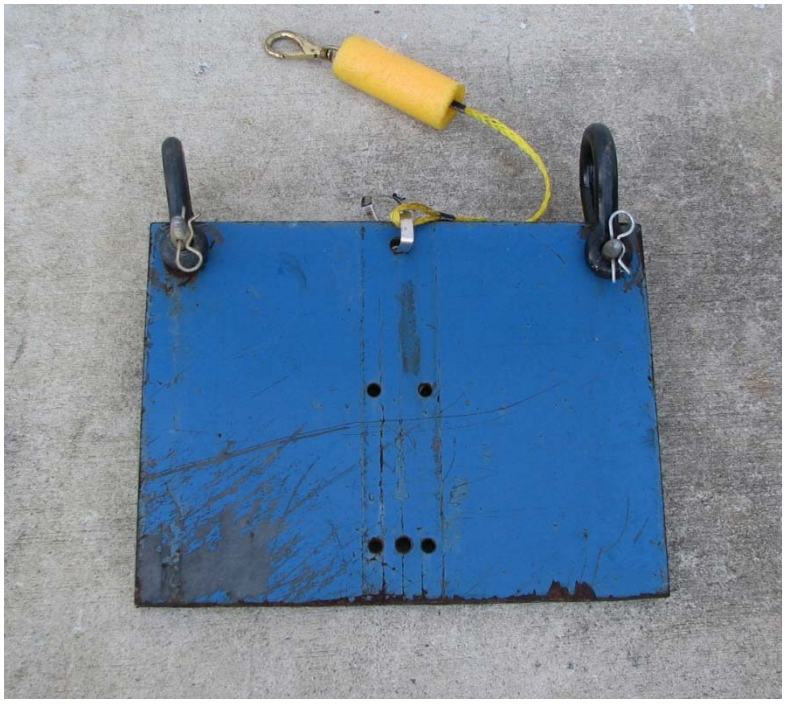

Figure 4.6. Metal anchor with rope and swiveling carabiner

Photographs of the deployment process are shown in Figure 4.7. To prepare a specimen for testing, the accelerometer was turned on to record continuously and then placed in its plastic housing (Figure 4.7a). The carapace and plywood were then attached to the body with plastic cable ties (Figure 4.7c). The carapace was also attached in the rear with a cable tie through the PVC frame. If the test was being performed below the surface, small floats were attached to the PVC head and tail pieces at the designated distance above the highest point on the carapace (Figure 4.7b). The floats also aided the vessel operator in seeing the target in the water. Four short ropes of equal length (0.5 m) were attached with carabiners to the eye hooks on the plywood underside, and the turtle was carried to the water's edge. The tether from the shore was then attached to the four ropes, and the turtle was placed in shallow water (Figure 4.7d). If the turtle was not level in the water, small adjustments were made to the length of one of the four ropes or water was allowed to fill the PVC frame to decrease buoyancy.

Figure 4.7. Preparation and deployment of artificial turtle showing (a) placement of accelerometer, (b) measurement and attachment of floats, (c) attachment of carapace to body with cable ties, (d) attachment of ropes and tether

The tether was used to position the turtle above the anchor. Lowering the turtle to the desired depth in the water column was achieved by maintaining tension on the rope. At surface depth, only the upper portion of the carapace was visible above the water, in accordance with biologists' description of typical turtle behavior at the surface. The turtle was kept level for all of the field tests to ensure a direct impact to the carapace, but its orientation in the water was not controlled. Live turtles may react to an approaching vessel by diving or some other avoidance method, resulting in a different attitude in the water than what was tested. The effects of turtle orientation or angle in the water were not investigated in these experiments but may change the angle of impact and consequently the mechanical response of the carapace. A schematic of the testing setup is shown in

Figure 4.8. Figures 4.9 and 4.10 show views of the test site with an approaching vessel and the line connecting the shore and turtle, which is visible in the water.

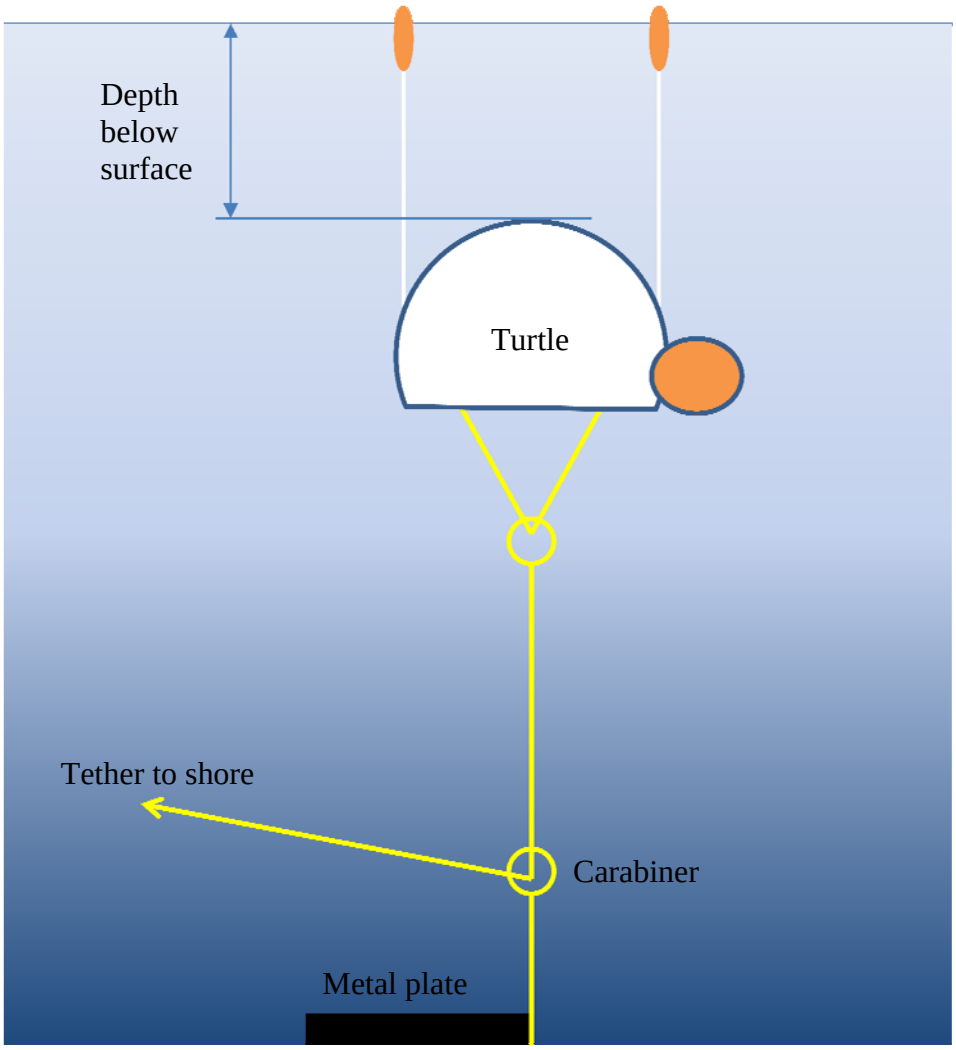

Figure 4.8. Schematic of field testing setup in the water

Figure 4.9. View of field test showing approaching vessel

Figure 4.10. View of field test showing turtle in water and tether from shore

4.3.1.1 Modification of Attachment of Shell and Body

After the first round of testing was complete, revisions were made to the attachment system based on the fracture patterns of the synthetic carapaces, which

seemed unrealistic compared to documented sea turtle injuries; carapaces showed long, continuous cracks that propagated from the impact site, as detailed in Section 4.4.1.1 . Test specimens also broke into numerous small pieces when struck by the propeller of Vessel 2. Rather than attach the shell at five discrete locations, a new method of attachment was developed in which the 48 kg/m^3 foam of the body was poured directly onto the shell's interior surface during fabrication. This was done to transfer more impact energy directly to the body and provide continuous support across the carapace. Even though the original system used a body molded to the interior shape of the shell, the attachment system of cable ties did not sufficiently transfer energy, with many shells exhibiting brittle fracture modes during testing. Other parts of the frame design, such as the layout of the PVC, weights, MDF, and accelerometer housing, remained the same. The plywood on the underside of the turtle was attached directly to the PVC frame with screws. A total of ten shells were prepared with the revised body for the second round of testing.

4.3.1.2 Deployment of Real Sea Turtles

The GDNR provided eleven deceased sea turtles for vessel strike testing. All the turtles were cold-stunned deaths that had been kept frozen at GDNR facilities. The sea turtles were thawed at the site before conducting the field experiments. Only one of the eleven was a loggerhead; the rest were green sea turtles. The real turtles were deployed in the water in a similar manner to the artificial turtles. Screws were placed directly in the plastron for attaching the tether. To provide buoyancy, flotation from life jackets was attached to the underside of some specimens, as shown in Figure 4.11. The shells were painted red to improve visibility in the water, as shown in Figure 4.12.

Figure 4.11. Attachment of flotation directly to a real turtle plastron

Figure 4.12. Real sea turtles prior to field testing with shells painted red

4.3.2 Field Testing Procedures

The turtle was held in place by keeping a slight tension on the tether but not enough to restrict the turtle's movement during impact. Typically, the vessel's impact

pushed the turtle down in the water column, lessening the tension on the line. During testing, the orientation of the turtle in the water immediately prior to impact was determined by an observer on the boat and corroborated with an observer on shore. This information was used to aid in correlating the direction of vessel travel with impact wounds during post-test inspection. The locations of the turtle were labeled in a manner similar to the face of a clock, with 12 at the head of the "animal," as shown in Figure 4.13. For example, if the boat approached the turtle's left side, the orientation was recorded as "9".

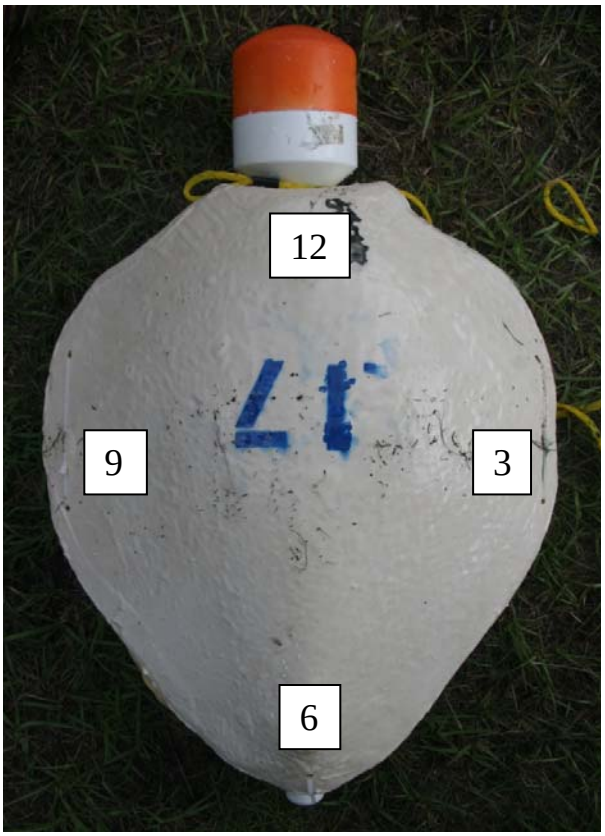

Figure 4.13. Orientation used to describe direction of boat at impact

The speed was monitored by the vessel operator, and video of the vessel impact was taken from shore. Debris from the impact was collected after each test. The time of

impact was recorded by the observer in the bow of the boat and by a person on shore. This was needed to identify which set of accelerometer data corresponded to which field test.

4.3.3 Assessment of Damage

After recovery of the turtle, photographs and measurements of the damage pattern, including depth and spacing of wounds, were taken. Measurements were made with a set of calipers, as shown in Figure 4.14. Metal discs of varying sizes were placed in the propeller wounds to estimate the diameter of the propeller size on the vessel, as shown in Figure 4.15.

Figure 4.14. Measurement of wound length and spacing after field testing

Figure 4.15. Measurement of propeller diameter from wound depth

The impact damage was classified as being caused by the hull, the skeg, or the propeller. Propeller wounds are a series of slicing wounds perpendicular to the vessel's direction of travel. Damage from skeg impact can occur as either large blunt trauma or as a singular slicing wound. Hull impact occurred as large, continuous cracks during Round 1. In the second round of tests, hull impact resulted in small indentations and scrapes. If the shell broke apart, the pieces were retrieved and reassembled on shore. The damaged carapaces were photographed individually and as group after a test series was completed. The damage was sketched and described on a data sheet; a typical data sheet is shown in Figure 4.16. The data sheets with the results from all tests may be found in Appendix B. Following guidance from GDNR biologists familiar with sea turtle biology and wounds, catastrophic (presumably fatal) injury was defined as damage that penetrated the carapace. Small cuts on the edges of the carapace that extended beyond the

body cavity were not classified as catastrophic. The location of injury was not relevant to the classification of injury as lethal or non-lethal, and any potential internal injuries from impact damage or accelerations were not considered.

A three-axis accelerometer/datalogger was used on most test specimens. Some tests omitted the accelerometer due to a higher risk of sustaining damage to the instrument. The accelerometer recorded at 1600 Hz and was activated prior to placing the specimen in the water. The accelerometer recording was stopped after retrieving the sample from the water. The accelerometer was not reset between tests which used the same shell multiple times. The individual tests were identified by the time of impact.

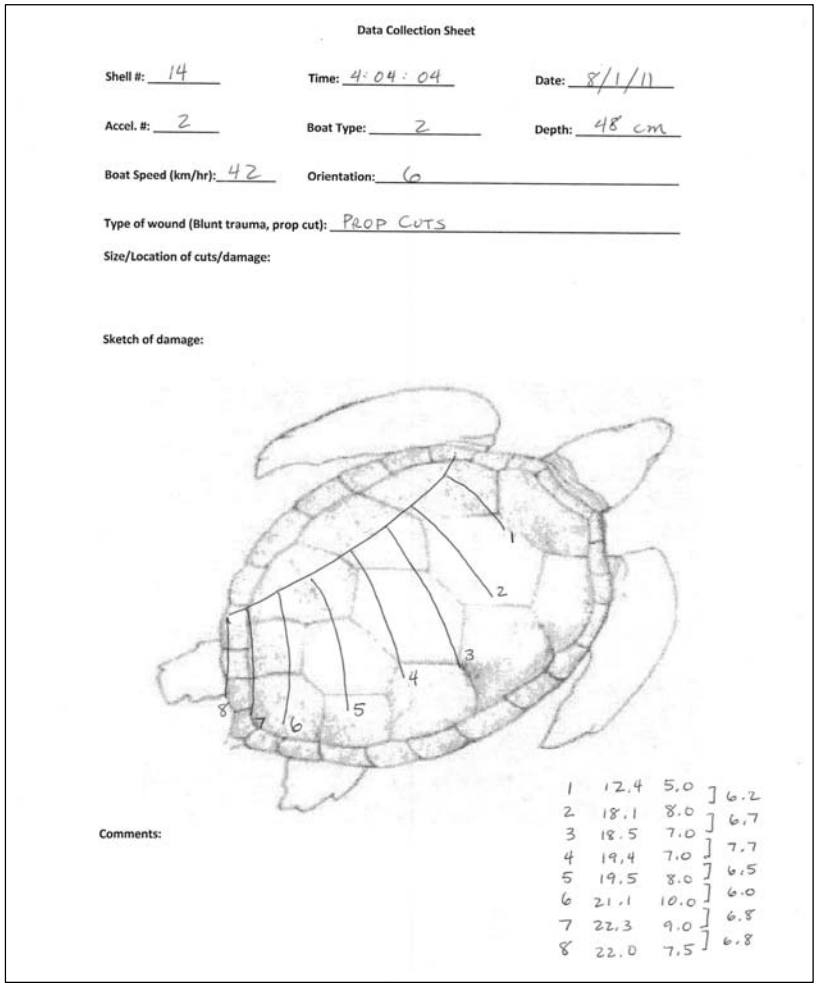
Data Collection Sheet

Shell #: 14 Time: 4:04:04 Date: 8/1/11

Accel. #: 2 Boat Type: 2 Depth: 48 cm

Boat Speed (km/hr): 42 Orientation: 6

Type of wound (Blunt trauma, prop cut): PROP CUTS

Size/Location of cuts/damage:

Sketch of damage:

Comments:

1	12.4	5.0	6.2
2	18.1	8.0	6.7
3	18.5	7.0	7.7
4	19.4	7.0	6.5
5	19.5	8.0	6.0
6	21.1	10.0	6.8
7	22.3	9.0	6.8
8	22.0	7.5	

Figure 4.16. Data collection sheet for assessment of damage patterns

4.4 Results of Field Testing

4.4.1 Characterization of Wounds

4.4.1.1 Artificial Turtles, Round 1 (August 1, 2011)

4.4.1.1.1 Vessel 1 (Jet Propulsion)

A total of eleven tests were performed using Vessel 1 in the first round of testing. None of the turtles at 48 cm deep was struck by the vessel. All five tests were performed with the same shell, Shell 1. Of the six tests at the surface, five shells experienced hull impact and broke. The one shell that did not break, Shell 7, experienced an indirect hit from the vessel. This was noted by the boat operator and confirmed by the accelerometer data, which showed a much lower peak acceleration value, 6.5 g, compared to the other tests. Therefore, a sixth shell was tested, Shell 7B, which broke upon impact. The test results are summarized in Tables 4.4 and 4.5. A photograph of the five damaged shells is shown in Figure 4.17.

Table 4.4. Test results for Vessel 1, Round 1 (August 1, 2011)

Test #	Shell #	Depth	Orientation	Speed (km/h)	Type of Wound	Peak Accel. (g)
1	1	48 cm	5	43	No impact	0.7
2	1	48 cm	9	42	No impact	0.5
3	1	48 cm	12	47	No impact	0.6
4	1	48 cm	1	42	No impact	0.7
5	1	48 cm	3	42	No impact	0.8
6	6	Surface	2 to 3	43	Blunt/Hull	24.3
7	7	Surface	10 to 11	43	None	6.5
8	8	Surface	10 to 11	45	Blunt/Hull	25.6
9	9	Surface	12 to 1	43	Blunt/Hull	24
10	10	Surface	1	42	Blunt/Hull	20.9
7B	2	Surface	11	45	Blunt/Hull	25

Table 4.5. Summary of results for Vessel 1, Round 1 (August 1, 2011)

Vessel	Depth	Hull Shape	Speed (km/h)	No. of trials	No. fatal injuries
1	48 cm	Deep-vee	40	5	0
1	Surface	Deep-vee	40	6	5

Figure 4.17. Results of test series at surface, Vessel 1, Round 1

4.4.1.1.2 Vessel 2 (Outboard Propeller)

A total of 15 tests were performed using the 4-bladed propeller-driven vessel, five at each depth. The shells at propeller depth (71 cm) did not experience any vessel impact. Of the other ten test shells, nine were considered to have experienced fatal wounds, with one experiencing a non-fatal hull impact. The tests conducted at the surface were not outfitted with accelerometers to avoid damage to the sensors. The tests results are summarized in Tables 4.6 and 4.7. Photographs for each test series are shown in Figures 4.18 and 4.19.

Table 4.6. Test results for Vessel 2, Round 1 (August 1, 2011)

Test #	Shell #	Depth	Orientation	Speed (km/h)	Type of Wound	Peak Accel. (g)
11A	11	71 cm	2	42	No impact	4.0
11B	11	71 cm	2	39	No impact	4.4
11C	11	71 cm	8	42	No impact	2.7
11D	11	71 cm	2	39	No impact	2.9
11E	11	71 cm	2	43	No impact	5.0
11F	11	48 cm	8	45	Massive blunt trauma	28.5
12	12	48 cm	11	45	Massive blunt trauma	28.4
13	13	48 cm	10	42	Prop cut	27.2
14	14	48 cm	6	42	Prop cut	28.5
15	15	48 cm	6	42	Prop cut	28.4
16	16	Surface	10	43	Prop and skeg	NA
17	17	Surface	3	39	Non-fatal blunt hull impact	NA
18	18	Surface	4	45	Blunt trauma	NA
19	19	Surface	10	43	Blunt trauma and prop cut	NA
20	20	Surface	1	40	Prop cut	NA

Table 4.7. Summary of results for Vessel 2, Round 1 (August 1, 2011)

Vessel	Depth	Hull Shape	Speed (km/h)	No. of trials	No. fatal injuries
2	71 cm	Deep-vee	40	5	0
2	48 cm	Deep-vee	40	5	5
2	Surface	Deep-vee	40	5	4

Figure 4.18. Results of test series at 48 cm, Vessel 2, Round 1

Figure 4.19. Results of test series at surface, Vessel 2, Round 1

Modifications to the test specimens were deemed necessary after comparison of the failure methods and patterns exhibited by the artificial carapaces in Round 1 to wounds sustained by real turtles. Vessel 1 (jet drive) caused large, continuous cracks, which were unlike reported injuries. Vessel 2 (propeller drive) caused the turtle carapace to be completely destroyed, resulting in large amounts of debris in the water, as shown in Figure 4.20. Modifications to the attachment system between carapace and body were made to increase the energy absorption capabilities and reduce the amount of debris. These modifications are outlined in Section 4.3.1.1 .

Figure 4.20. Debris in the water after impact of Vessel 2, Round 1

4.4.1.2 Artificial Turtles, Round 2 (October 13, 2011)

In the second round of tests, the revised body design described in Section 4.3.1.1 was used. The foam was poured directly onto the interior surface of the artificial carapace, creating a continuous connection with improved energy transfer between the

carapace and body. The tests were performed at the same site with the same vessels as Round 1. A total of 28 trials were performed: 15 artificial turtles and 13 real turtles.

4.4.1.2.1 Vessel 1 (Jet Propulsion)

Five shells were tested at the surface with the jet boat. None of the shells experienced damage which would be classified as a catastrophic injury. Small dents and cracks were noted at the location of impact in some cases, but the cracks did not propagate as they did in Round 1. The accelerometer readings indicate the shells experienced impact forces that were similar to the shells from Round 1. The drastic reduction in cracking illustrates the effect of the body revision and is a more realistic response. The results are summarized in Tables 4.8 and 4.9, and a photograph of the five shells is shown in Figure 4.21.

Table 4.8. Results for Vessel 1, Round 2 (October 13, 2011)

Shell #	Depth	Orientation	Speed (km/h)	Type of Wound	Size/Location of damage	Peak Accel. (g)
4	Surface	3	48	Blunt trauma, small area at impact site. Small cracks on surface that did not radiate out from site.	Damage dorsal in area of nuchal scutes	22.1
26	Surface	3	42	No true wound; pressure ding.	Dorsal area of 4th nuchal scute	20.9
22	Surface	3	42	Pressure ding with associated cracks; surface only. One crack radiates.	Dorsal area of 2nd nuchal scute	25.5
28	Surface	2	45	Pressure ding with associated cracks. One radiation crack near ding	Dorsal ~5th nuchal scute	23.7
39	Surface	4	47	Surface; pressure ding with associated cracks. Damage did not radiate from wound site.	Dorsal ~4th nuchal scute	26.1

Table 4.9. Summary of results for Vessel 1, Round 2 (October 13, 2011)

Vessel	Depth	Hull Shape	Speed (km/h)	No. of trials	No. fatal injuries
1	Surface	Deep-vee	40	5	0

Figure 4.21. Results of test series at surface, Vessel 1, Round 2

4.4.1.2.2 Vessel 2 (Outboard Propeller)

Ten tests were conducted using Vessel 2: eight at surface depth and two at 48 cm. Two carapaces, Shell 23 and Shell 24, were used for multiple trials at the surface. The first vessel strike did not cause any damage from hull impact, so the trials continued until catastrophic injury was caused. These repeated tests are given as 23B, 24B, and 24C in the tables. The two trials at 48 cm were conducted using undamaged shells from the tests using Vessel 1, Shells 4 and 26. These are noted as Shells 4P and 26P and were not instrumented with accelerometers. The test results are summarized in Tables 4.10 and

4.11. A photograph of the five shells used at surface depth is shown in Figure 4.22, and Shells 4P and 26P are shown in Figures 4.23 and 4.24.

Table 4.10. Results for Vessel 2, Round 2 (October 13, 2011)

Shell #	Depth	Orientation	Speed (km/h)	Type of Wound	Location of damage	Peak Accel. (g)
23	Surface	5	43	Hull impact, no damage		11.0
23B	Surface	11	43	Hull and motor impact. Blunt, prop, and skeg damage	Shell severely damaged.	28.3
24	Surface	12	45	None		24.7
24B	Surface	1-2	42	None		26.4
24C	Surface	3	37	Large pressure ding; radiating cracks in significant area cramal to pressure ding		28.5
27	Surface	7	43	Prop cut on left side.	Cut along edge of carapace and in foam.	28.3
37	Surface	7	42	Hull and motor impact. Blunt, prop, and skeg damage	Dorsal, nuchal scute area.	28.4
25	Surface	10	43	Blunt, prop, and skeg wound	Nuchal scutes dorsal	28.3
4P	48 cm	11	42	Blunt, prop, and skeg	Cut into carapace and foam.	NA
26P	48 cm	5	42	Blunt, prop, and skeg	Prop cuts in foam/ exposed to MDF board.	NA

Table 4.11. Summary of results for Vessel 2, Round 2 (October 13, 2011)

Vessel	Depth	Hull Shape	Speed (km/h)	No. of trials	No. fatal injuries
2	Surface	Deep-vee	40	8	5
2	48 cm	Deep-vee	40	2	2

Figure 4.22. Results of test series at surface, Vessel 2, Round 2

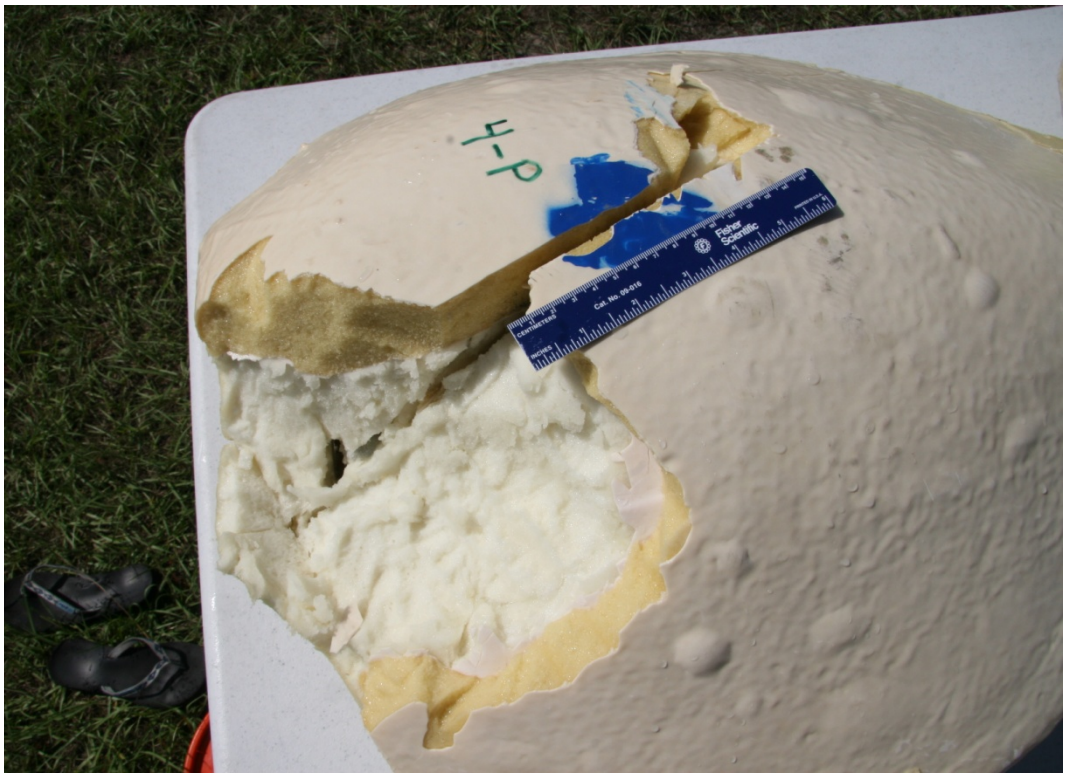

Figure 4.23. Shell 4P tested at 48 cm, Vessel 2, Round 2

Figure 4.24. Shell 26P tested at 48 cm, Vessel 2, Round 2

A summary of the types of impact sustained by the test specimens in Round 2 are shown in Table 4.12. A single test could produce more than one type of damage. At the surface, the greatest number of impacts were from the hull, but there is no evidence this resulted in serious damage. For the tests conducted with Vessel 2, propeller wounds were present in three tests and skeg wounds in five tests.

Table 4.12. Summary of injury types sustained during Round 2

Vessel	Depth	Propeller	Skeg	Hull
1	Surface	0	0	5
1	48 cm	0	0	0
2	Surface	2	3	4
2	48 cm	1	2	0
2	71 cm	0	0	0

4.4.1.3 Real turtles, Round 2 (October 13, 2011)

Preliminary results from testing of the real sea turtles are shown below. More detailed analysis was performed by scientists and biologists from Georgia Department of Natural Resources, South Carolina Department of Natural Resources, and the University of Florida who were present during field testing. Results from this round of testing are forthcoming. The turtles are numbered from R1 to R12. Only R1 was a loggerhead carcass.

4.4.1.3.1 Vessel 1 (Jet Propulsion)

Three tests were performed at surface depth with Vessel 1. None of the turtles sustained serious damage from the hull impact, with only small abrasions and cuts evident. The artificial carapaces from Round 2 and the real turtles showed similar types and degrees of injury when subjected to hull impact from the jet propulsion vessel. The results are summarized in Table 4.13 with a photograph of R3 in Figure 4.25.

Table 4.13. Results of Vessel 1 impact with sea turtles (October 13, 2011)

Shell #	Depth	Orientation	Speed (km/h)	Type of Wound	Size/Location of Cuts/Damage
R1	Surface	2	47	Blunt	Multiple scutes on dorsum; 1 cm area of carapace bone exposed on 1st vertebral.
R3	Surface	1	39	Blunt	Superficial abrasion across mid-back/ dorsal and left lateral carapace. White transfer on right lateral carapace
R4	Surface	3	47	Blunt;.	Poorly demarcated superficial abrasion on right 2nd costal. Sharp superficial abrasion (linear) and adjacent abrasion third vertebral. White paint on carapace (transverse orientation)

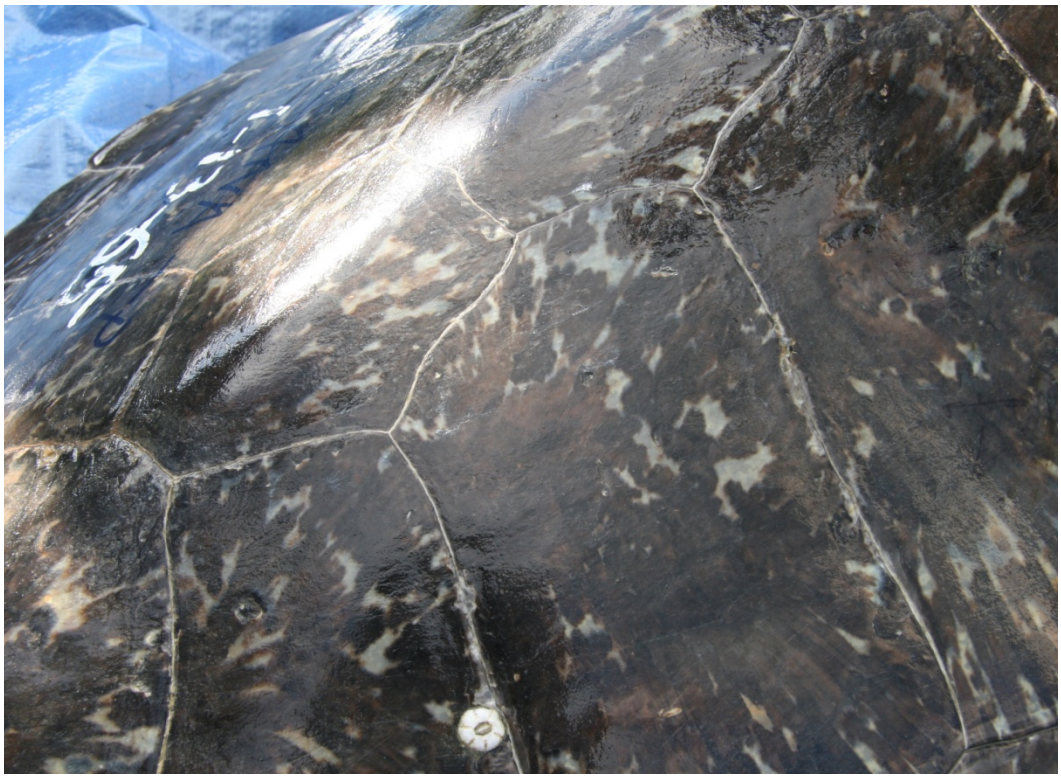

Figure 4.25. Abrasion on turtle R3 from hull impact of Vessel 1

4.4.1.3.2 Vessel 2 (Outboard Propeller)

Ten trials were performed using Vessel 2: five at surface depth and five at 48 cm. The turtles experienced severe damage from both the skeg and propeller. All ten

specimens were considered to suffer fatal injury. The results are summarized in Table 4.14.

Table 4.14. Results of Vessel 2 impacts with sea turtles (October 13, 2011)

Shell	Depth	Orientation	Speed (km/h)	Type of Wound	Size/Location of Cuts/Damage
R6	Surface	4-5	45	Prop cut; hull	5 prop cuts; left posterior lateral carapace
R7	Surface	3	43	Prop cut; hull	2 prop cuts posterior carapace; blunt injury to right posterior carapace; transverse direction
R8	Surface	2-3	45	Prop cut; hull	right dorsal and lateral mid-body carapace--linear wound. Fracture carapace under paint transfer. Right posterior carapace—prop
R9	Surface	2	45	Skeg; prop cut; hull	Linear skeg injury across right posterior carapace; 2 oblique prop wounds
R10	Surface	5	40	Skeg; prop cut; hull	Linear chop wound- posterior, dorsal midline- skeg. Oblique chop wound- posterior, dorsal midline- prop. Blunt fracture- mid-body, dorsal midline (paint transfer)
R1	48 cm		45	Skeg; prop cut	Cavity wound involving right lateral mid-body carapace, extensive exposure of cavity. 6 chop wounds and perpendicular line wound (skeg). Skeg damage to plastron
R3	48 cm	3	43	Skeg; prop cut	Massive blunt trauma to posterior half of carapace; 3 chop wounds visible.
R5	48 cm	3	34	Prop cut	3 prop wounds across anterior carapace, dorsal neck, shoulder (left)
R11	48 cm	3	43	Skeg	Skeg wound with fracture
R12	48 cm	4	39	Skeg	Extensive blunt trauma/ cavity wound. Prop cuts as well, but poorly discernible

Figure 4.26. Skeg and propeller wounds in turtle R1

Figure 4.27. Slicing skeg wound in turtle R8

4.4.2 Statistical Analysis of Injury Lethality

A statistical analysis of the field test data was performed to determine the influence of turtle depth in the water column, propulsion type, and hull shape on the likelihood of a catastrophic injury during a vessel strike. The first analysis used the current research data to investigate the effects of depth in the water and propulsion system on induced damage. A second analysis included data from Phase II to determine the influence of hull shape on damage. The data used are shown in Tables 4.15 and 4.16.

Table 4.15. Summary of fatal injuries from current research

Test Series	Propulsion System	Depth cm	Hull Shape	Speed km/h	No. of trials	No. fatal injuries
1	Jet Drive	48	Deep-vee	40	5	0
4	Outboard Propeller	48	Deep-vee	40	5	5
6	Jet Drive	0	Deep-vee	40	5	0
7	Outboard Propeller	0	Deep-vee	40	8	5

Table 4.16. Data included from Phase II (Sapp 2010)

Test Series	Propulsion System	Depth cm	Hull Shape	Speed km/h	No. of trials	No. fatal injuries
5	Outboard Propeller	0	Flat-bottomed	40	5	5
6	Outboard Propeller	56	Flat-bottomed	40	5	5
13	Jet Outboard	0	Flat-bottomed	40	5	0
14	Jet Outboard	56	Flat-bottomed	40	5	0

Multidimensional contingency tables are used to interpret data with respect to three or more variables. The multidimensional data can be used to test more than one hypothesis. The first analysis tests for mutual independence among all variables. In this case, the null hypothesis states that there are no interactions (either two-way or three-

way) among any of the variables. The null hypothesis is tested by computing degrees of freedom and the chi-squared value, a measure of the difference between the actual and expected frequencies of each entry, to find the *p*-value. A *p*-value less than 0.05 indicates the variables are not mutually independent, i.e. the null hypothesis should be rejected, and a value greater than 0.05 suggests the variables are mutually independent. If the null hypothesis is rejected, subsequent tests are performed to determine the dependencies and independencies between variables. These partial independence tests determine whether one of the variables is independent of the other two. By performing partial independence tests on each of the three variables with respect to the other two, the relationship of the variables may be determined (Zar 1999).

If one of the three variables is determined to have no influence, then the interaction between the two remaining variables is tested in a 2 x 2 contingency table. For the 2 x 2 analysis, the Fisher exact test (Fisher 1922) is used because it is more suitable for small sample sizes. This test calculates the probability of the contingency table as well as the probabilities of all possible tables with both the same row and column totals. The *p*-value is the sum of all the probabilities less than or equal to the probability of the original table (Lowry 2012). Sapp (2010) concluded that both vessel speed and propulsion type affect the likelihood of catastrophic injury, but depth in the water did not.

A three-dimensional contingency table, Table 4.17, of the data from the current research was constructed to test the mutual independence of the three variables: turtle depth in the water column, propulsion type, and occurrence of catastrophic injury. The test for mutual independence indicated that the variables were not independent of each other ($p = 0.00437$); therefore, tests for partial independence were performed for each

variable relative to the other two. Results showed that depth was independent of injury and propeller type (p = 0.448), but both injury and propulsion system were not independent (p = 0.00153) of the remaining two variables. The influence of propulsion system on the presence of fatal injury is directly tested using the Fisher exact test on a two-dimensional contingency table. In this test, p = 0.00036, so the variables are not independent. The results indicate that injury is dependent on propulsion system but not depth in the water column, which agrees with the conclusions of Work et al. (2010).

Table 4.17. Three-dimensional contingency table of Phase III field test data

	Jet Drive		Propeller	
	Surface	48 cm	Surface	48 cm
Lethal	0	0	5	5
Non-lethal	5	5	3	0

The statistical analysis of the influence of hull shape was performed with a combination of data from Phase II and the current research. The three variables were hull type (flat-bottomed or deep-vee), propulsion system (jet drive or propeller-driven), and fatal or non-fatal injury. Because tests on each set of data revealed no influence of depth, that variable was excluded. The current field tests were all performed with a vessel speed of 40 km/h, so speed was not a variable, and only test results from Phase II at planing speed are included. The data used are shown in Table 4.18.

Table 4.18. Three-dimensional contingency table of Phases II and III field test data

	Jet Drive		Propeller	
	Flat	Deep-vee	Flat	Deep-vee
Lethal	0	0	10	10
Non-lethal	10	10	0	3

Again, the test for mutual independence showed that the variables were not independent of each other (p = 9.36E-7). Using tests for partial independence, the results

show that hull shape is independent of injury and propulsion type (p = 0.423). The partial independence tests of presence of injury and propulsion system had p-values of 2.27E-7 and are therefore not considered to be independent. A comparison of only these two variables using the Fisher exact test returns a p-value of 2.32E-9; therefore, the propulsion system is the primary influence on catastrophic damage if the motor impacts the turtle. A summary of the tests and outcomes of all the statistical analyses performed is shown in Table 4.19. In conclusion, injury lethality is dependent on engine type but appears to be independent of turtle depth and hull shape.

Table 4.19. Summary of statistical analyses

Test for	Null Hypothesis	p-value	Outcome
Mutual Independence	Injury, depth, and engine type are all mutually independent	0.00437	Reject
Partial Independence	Injury is independent of depth and engine type	0.00153	Reject
Partial Independence	Depth is independent of injury and engine type	0.448	Accept
Partial Independence	Engine type is independent of depth and injury	0.00153	Reject
Fisher Exact Test	Injury is independent of engine type	0.000365	Reject
Mutual Independence	Injury, hull shape, and engine type are all mutually independent	9.36E-07	Reject
Partial Independence	Injury is independent of hull shape and engine type	2.27E-07	Reject
Partial Independence	Hull shape is independent of injury and engine type	0.423	Accept
Partial Independence	Engine type is independent of hull shape and injury	2.27E-07	Reject
Fisher Exact Test	Injury is independent of engine type	2.32E-09	Reject

4.4.3 Accelerometer Data

The artificial turtles were outfitted with a three-axis accelerometer/datalogger as described in Section 4.2.1. Accelerations were recorded at 1600 Hz. In the turtle's position in the water, a value of -1 g was recorded in the z-direction, so a value of 1 g was added to the values in the z-direction. During impact, the axes of the accelerometer move relative to the direction of gravity, so the addition of 1 g to only one axis is incorrect.

However, the impact takes place over a short time interval, about 0.05 s, leaving little time for large movements relative to the direction of gravity. The peak acceleration magnitude was calculated by finding the maximum value of the resultant acceleration, *i.e.* the square root of the sum of the squares of the three readings. The peak acceleration values are summarized in Table 4.20 for each field test performed using an accelerometer. A graph of peak acceleration values for each vessel in each round of testing is shown in Figure 4.28.

Table 4.20. Summary of peak acceleration values for vessel impacts

Test #	Vessel #	Round	Depth	Speed km/h	Peak Accel. g	Fatal Injury
6	1	1	Surface	43	24.3	x
7	1	1	Surface	43	6.5	
7B	1	1	Surface	45	25.0	x
8	1	1	Surface	43	25.6	x
9	1	1	Surface	42	24.0	x
10	1	1	Surface	45	20.9	x
4	1	2	Surface	48	22.1	
26	1	2	Surface	42	20.9	
22	1	2	Surface	42	25.5	
28	1	2	Surface	45	23.7	
39	1	2	Surface	47	26.1	
11F	2	1	48 cm	45	28.5	x
12	2	1	48 cm	45	28.4	x
13	2	1	48 cm	42	27.3	x
14	2	1	48 cm	42	28.5	x
15	2	1	48 cm	42	28.4	x
23	2	2	Surface	43	11.0	
23B	2	2	Surface	43	28.3	x
24	2	2	Surface	45	24.7	
24B	2	2	Surface	42	26.4	
24C	2	2	Surface	37	28.5	x
27	2	2	Surface	43	28.3	x
37	2	2	Surface	42	28.4	x
25	2	2	Surface	43	28.3	x

The average peak acceleration produced by Vessel 2 was higher than that for Vessel 1. This is expected because the propeller-driven boat is heavier and has more momentum during impact. Additionally, the impact of the motor, which is aluminum, may have a smaller contact area and higher stiffness than the hull, which would increase the force transmitted to the artificial turtle. Discounting the two outliers, Shells 7 and 23, the average peak accelerations were 23.8 g and 27.8 g for Vessel 1 and Vessel 2, respectively. Many of the readings during impact exceeded the range of the accelerometer, meaning the peak values may be higher than reported. A comparison of the peak values for non-lethal and lethal tests in Round 2 is shown in Figure 4.29. Five of the non-lethal values are from impact with Vessel 1, which typically produced lower values than Vessel 2.

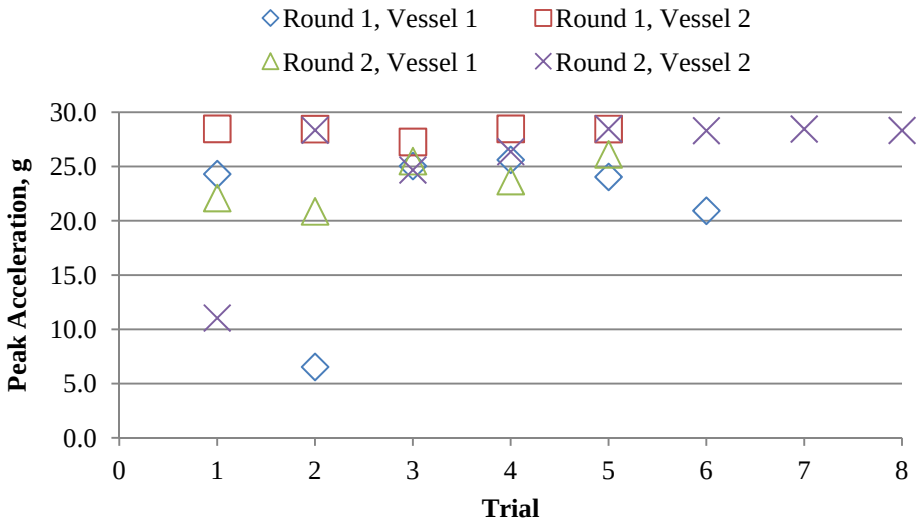

Figure 4.28. Peak acceleration values for all tests

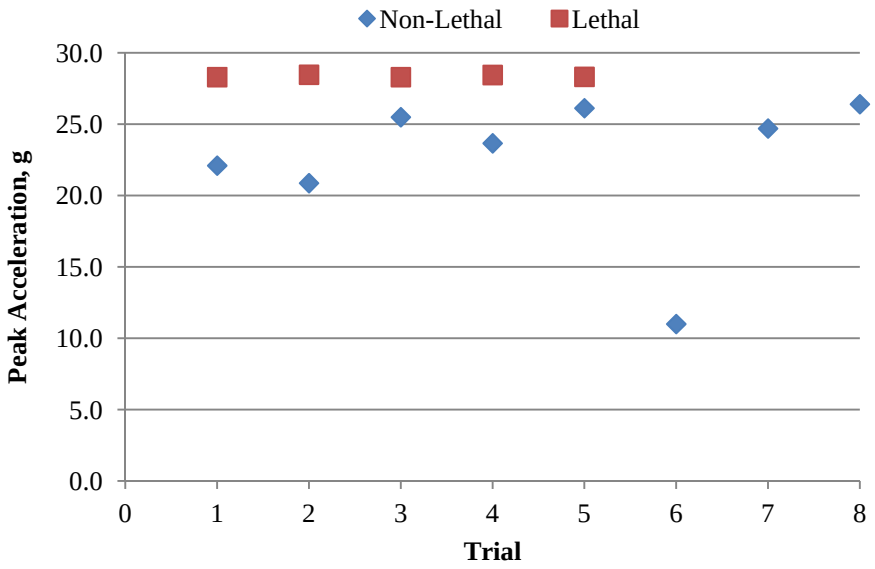

Figure 4.29. Peak acceleration values of lethal and non-lethal tests from Round 2

There was little difference among the acceleration values between Rounds 1 and 2 of the field tests. In the first round of tests, the average peak acceleration values for Vessels 1 and 2 were 24.0 g and 28.2 g, respectively; in the second set of tests, these values were 23.6 g and 27.6 g. The acceleration values remained nearly the same, yet the physical damage caused by Vessel 1 was dramatically different in the two rounds. This shows that the revised body design of Round 2 absorbed energy more efficiently than the first design. Acceleration is correlated to damage, as the two shells with abnormally low peak values, Shells 7 and 23, did not break. The threshold energy required to fracture a turtle carapace due to hull impact alone was not found in these tests. There are, however, a large variety of hull types, vessel sizes and speeds, so a combination that could cause a catastrophic injury is a possibility.

Many shells struck by Vessel 2 experienced an initial impact from the hull followed by an impact from the motor. The impacts were noted by the boat operator and are clearly evident in the accelerometer data. A sample acceleration record showing

double impact is shown in Figure 4.30. For shells which suffered fatal injury in a double impact, it is difficult to determine if the hull impact resulted in any damage, as the second impact by the motor usually resulted in lethal injury. The shells that had only hull impact in Round 2 did not suffer serious damage. In the eight field tests instrumented with accelerometers with Vessel 2, there were seven hull impacts and six motor impacts. The peak accelerations from hull impacts, including those from both vessels, and motor impacts are shown in Figure 4.31. The average peak for hull impact and motor impact are 22.1 g and 27.5 g, respectively. Two tests, Shells 37 and 25, had peak accelerations from hull impact that were higher than that caused by the motor. The hull impact produced accelerations of 28.4 and 28.3 g, while the motor caused peaks of 27.8 and 25.7 g, respectively.

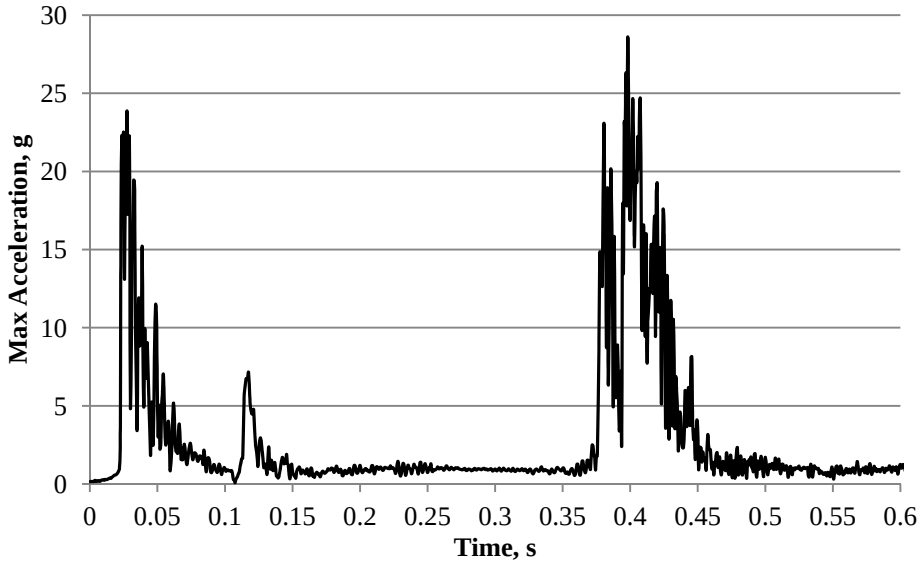

Figure 4.30. Double impact of hull and motor of Shell 23B, Vessel 2, Round 2

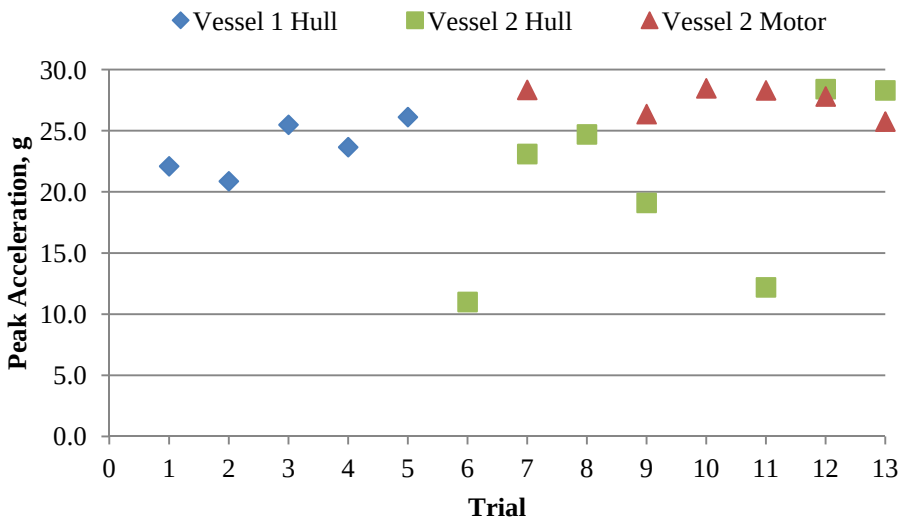

Figure 4.31. Peak accelerations for hull and motor impacts in Round 2

The accelerometer records for hull and motor impacts of Vessel 2 showed that hull impact had a shorter duration than motor impact. Typical graphs for motor and hull impacts are shown in Figures 4.32 and 4.33, respectively. The motor impacts had a longer time interval than hull impacts, as well as a less dominant peak acceleration. The average time for an impact event for the hull and motor are 0.05 and 0.10 s, respectively. The hull impact occurs as a single impact from which the carapace rebounds as a rigid body. The motor can impact the turtle in a number of ways: the motor foot, the skeg, or the propeller. Either the penetration of the skeg or foot or the multiple cuts from the propeller would increase the time of impact compared to the singular impact of the hull. Multiple propeller cuts result in acceleration values spread out over a longer time interval, as illustrated by the accelerations of Shell 15 in Figure 4.32.

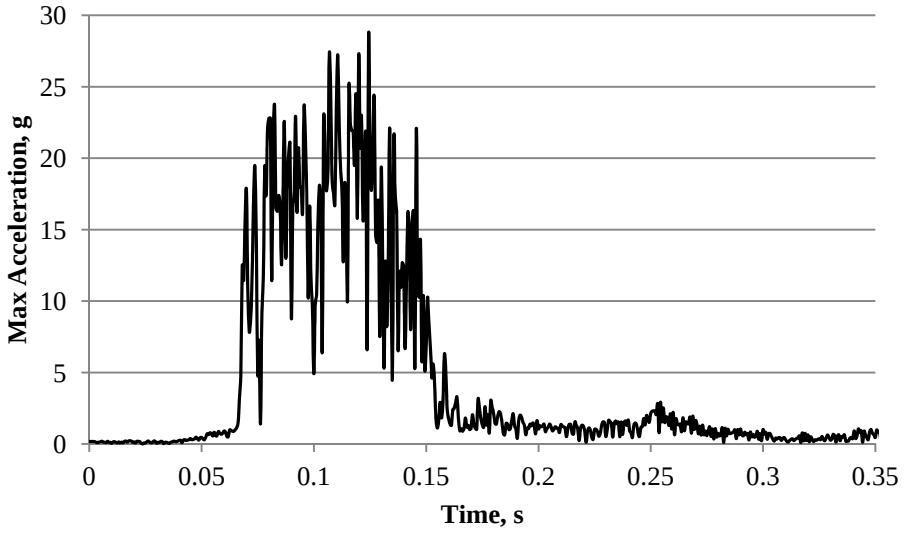

Figure 4.32. Resultant acceleration of Shell 15, motor impact only, Vessel 2, Round 1

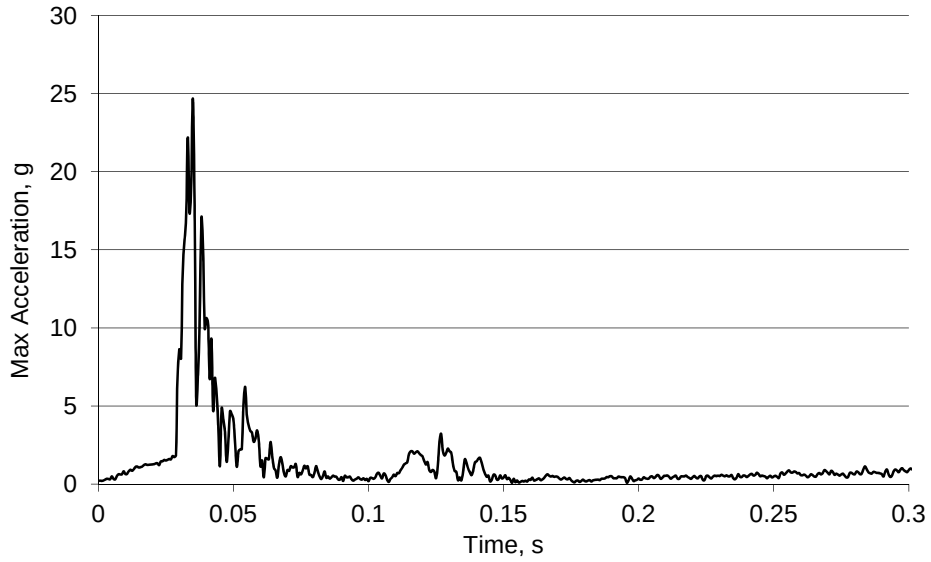

Figure 4.33. Resultant acceleration of Shell 24, hull impact only, Vessel 2, Round 2

The initial positions in the water column of the turtles in the field experiments were at the surface and at the depth of the center of the propeller, 71 cm, of Vessel 2. The tests at propeller-depth did not result in any vessel strikes, so an intermediate value, 48

cm, was used. At this depth, Vessel 1 did not strike any turtles. The peak acceleration values for these trials are summarized in Table 4.21.

Table 4.21. Summary of peak acceleration values from no contact trials

Test #	Vessel	Depth cm	Speed km/h	Peak Accel. g
1	1	48	43	0.7
2	1	48	42	0.5
3	1	48	47	0.6
4	1	48	42	0.7
5	1	48	42	0.8
11A	2	71	42	4.0
11B	2	71	39	4.4
11C	2	71	42	2.7
11D	2	71	39	2.9
11E	2	71	43	5.0

Vessel 1 passed over the submerged turtle with little effect, but the peak accelerations and displacements of Vessel 2 were substantially higher. The outcomes for Vessel 2 are also notably different from those during Phase II field testing, in which the outboard propeller caused damage to specimens at both the surface and at propeller depth. Those tests used a flat-bottomed skiff, however. Perhaps the bow wave of the deep-vee hulls in the current tests displaced the turtles in such a way as to avoid impact.

Hull impact alone by either vessel did not produce fractures in the real sea turtles or in the revised body system in Round 2. Vessel 1 did not produce any fractures in five tests in Round 2, with only small scrapes or indentations present. The damage caused by Vessel 2 was produced by either skeg or propeller impact, with Shells 23, 24, and 24B sustaining hull impacts with similar marks to those produced by Vessel 1. The peak acceleration of Shell 23 suggests an indirect hit, but the values for Shells 24 and 24B are comparable to tests that did fracture, indicating that the hull impact of Vessel 2 did not

cause any catastrophic injuries. The impact of either the skeg or propeller proved fatal in every instance, for both real and artificial turtles. The smaller draft of Vessel 1 also reduces the chance of striking a turtle below the water's surface, and the jet propulsion system does not cause fatal injury in the event of impact.

4.5 Discussion of Field Test Results

The analysis of field test data reveals that neither the position of the animal in the water nor hull type had significant influence on sea turtle mortality. The primary influences affecting mortality are speed of the vessel and propulsion type when the turtle is struck by the motor, with no fatal injuries caused by the jet propulsion vessels in this research or in the previous testing. The size and weight of the test specimen were chosen to match that used previously in Phase II. The 64 cm CCL and 35 kg specimen mass is representative of a juvenile loggerhead, while adults are in the range of 87 cm CCL and 116 kg (National Marine Fisheries Service and U.S. Fish and Wildlife Service 2008). The size of the specimen was selected based on guidance provided by GDNR. Personnel from GDNR had observed anecdotally that a majority of recovered turtles which exhibited vessel strike wounds were juveniles (Sapp 2010). A larger test specimen would likely reduce the acceleration experienced by the turtle during impact, and the effects of size or age on the carapace's material properties are currently unknown.

The revised body system used in the second round of tests made a significant difference in the carapace's behavior during impact, with no catastrophic injury caused by hull impact for either vessel. This behavior matches that of real turtles, which showed cuts and abrasions of hull impact but no serious damage. For Vessel 1, the acceleration values between the two rounds were nearly the same (24.0 and 23.6 g), but there were

zero fatal tests in Round 2 compared to five in Round 1. The real turtles were not outfitted with accelerometers which would have provided a comparison between peak values with the artificial turtles.

The peak acceleration in lethal tests was greater than those for non-lethal strikes in Round 2. The average values for lethal and non-lethal strikes were 28.4 and 22.5 g, respectively. However, the majority of the non-lethal strikes were from Vessel 1, which produced lower values than Vessel 2 on average. The average peaks for hull impact and motor impact were 22.1 g and 27.5 g, respectively. Two tests, Shells 37 and 25, experienced an initial impact from the hull that produced higher peak accelerations than the following impact of the motor. Any damage caused by the hull was, unfortunately, indistinguishable from the damage caused by the motor.

The tests at propeller depth (71 cm) of Vessel 2 failed to produce any impacts. These results differ from those of Phase II, which produced fatal wounds to turtles at all depths tested, including at propeller depth. Those tests used a flat-bottomed skiff, however, so the deep-vee hulls in the current tests displaced the turtles in such a way as to avoid impact. The results of the current investigation regarding the influence of hull type on the lethality of turtle injury cannot be considered conclusive. It is possible that larger vessels traveling at higher speeds may be capable of causing mortal wounds through hull impact alone. The force required to produce carapace fracture was investigated using finite element analysis, which is presented in the following chapter.

CHAPTER 5

FINITE ELEMENT ANALYSIS OF HULL IMPACT

In the field tests, only two recreational vessels were used, and neither produced fatal injuries from hull impact at planing speed. An impact from the motor caused fatal injuries to both artificial and real sea turtles, and the risk of lethal wounds from the propeller is less likely but still present at lower speeds (Work et al. 2010). In order to better inform the GDNR regarding management strategies related to jet propulsion vessels, it was necessary to estimate the force needed to cause a lethal injury to a turtle when struck by a boat hull. A finite element analysis (FEA) was performed to determine the critical force threshold for lethal injury from hull impact. This result was used to estimate the size and/or speed of a vessel which would cause carapace fracture in a turtle due to a collision with the hull.

The impact between the artificial carapace and a moving vessel was simulated using LS-DYNA® (Hallquist 2012), a commercial finite element analysis program specializing in dynamic problems. The numerical analysis allowed for the investigation of a range of parameters beyond those of the field investigation. The contact forces and duration of impact used in the computer model were estimated using accelerometer data from field tests, and an immersed boundary condition was used to simulate the turtle in the water. Pertinent mechanical properties of the constituent materials of the carapace were found via experimental methods, as described in Section 3.2.3. The stress distribution and acceleration records of the finite element model are compared to

experimental results to estimate the contact force and associated kinetic energy necessary to produce carapace fracture.

5.1 Geometry

The size and weight of the finite element model were based on the artificial turtles used in field testing. This is representative of a juvenile loggerhead, and the effects of weight, size, and carapace thickness on the FEA results were not investigated in this study. The geometry of the shell was acquired by measuring the vertical distance (z) to the shell from a reference plane with a digital point gauge with ±0.01 mm resolution. A board with a grid of evenly spaced (25.4 mm) holes was placed above the carapace, and a measurement was taken through each hole over half the carapace of both the dorsal and ventral surfaces. The carapace was modeled as symmetrical about the spine, and a total of 370 points were used for each surface. The thickness of the carapace was measured at a number of specific points to determine the offset between the two data sets. The points used to define the upper surface of the carapace are shown in Figure 5.1.

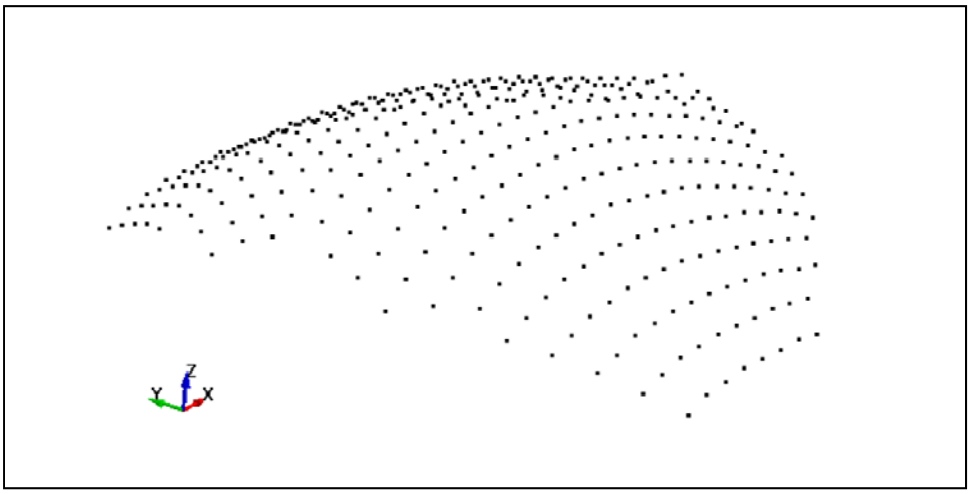

Figure 5.1. Nodes used to define dorsal surface of the carapace

The coordinates of the measurements were input into LS-PrePost ® (Hallquist 2011), a program for pre- and post-processing of LS-DYNA data. Surfaces were generated to fit the dorsal and ventral data sets. A third surface was defined as a flat plane at the lower surface of the turtle model, roughly 20 mm below the lowest point of the carapace. A curve, which was defined using the nodes on the perimeter of the dorsal surface, was used to trim the larger surface to the shape of the carapace. Figure 5.2 shows the three surfaces used to create the finite element model.

Shell (plane) elements were used to model the faces of polyester resin with glass microspheres, and solid (brick) elements were used for the foam core of the carapace and the foam turtle body. The dorsal surface mesh of shell elements was made using an auto meshing capability and generated a total of 1301 elements and 1347 nodes for the surface. The elements and nodes of the dorsal surface were projected vertically onto the ventral surface plane of the carapace and the flat lower surface. This created a total of three sets of shell elements which were aligned in the *z*-direction, as shown in Figure 5.3.

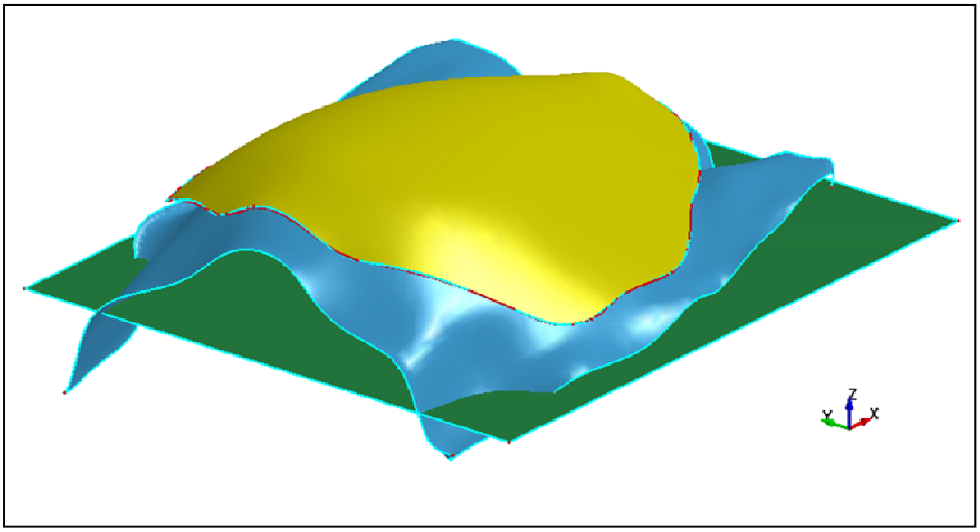

Figure 5.2. Three surfaces used to create finite element meshes

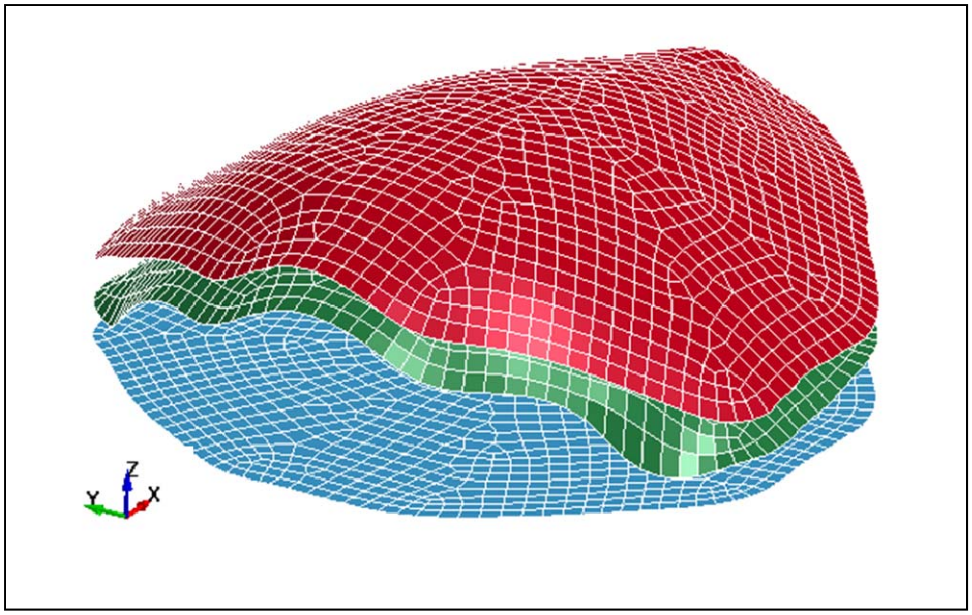

Figure 5.3. Three meshed surfaces of shell elements

The foam core of the carapace was generated by creating solid elements between two shell sets, the dorsal and ventral shell elements. The solid elements were four layers thick in the *z*-direction. A similar method was used to create the turtle body, using the shell sets of the ventral surface and flat, lower plane. After the solid elements for the body and core were generated, the shell elements were deleted. Shell elements 1 mm thick were used to model the face material of the carapace on the surface of the foam core. The total number of elements was 3090 shell elements for the faces of polyester resin infused glass microspheres, 5204 solid elements for the foam core, and 3903 solid elements for the turtle body. The complete turtle model is shown in Figure 5.4.

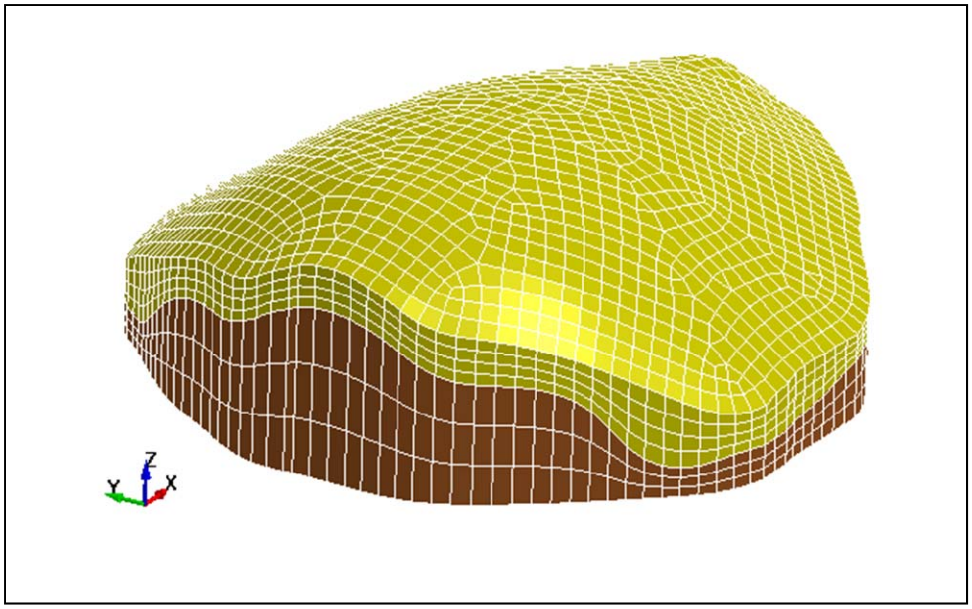

Figure 5.4. Turtle model showing solid elements of foam core and body

The water and air were modeled as solid elements which extended past the edges of the turtle model 200 mm in the *x*-direction and 245 mm in the *y*-direction. The water extended to a depth of 400 mm, and the air was defined up to 200 mm above the water's surface. The turtle model was positioned at a depth in the water similar to that during field testing, as shown in Figure 5.5. There were 4000 elements each for water and air.

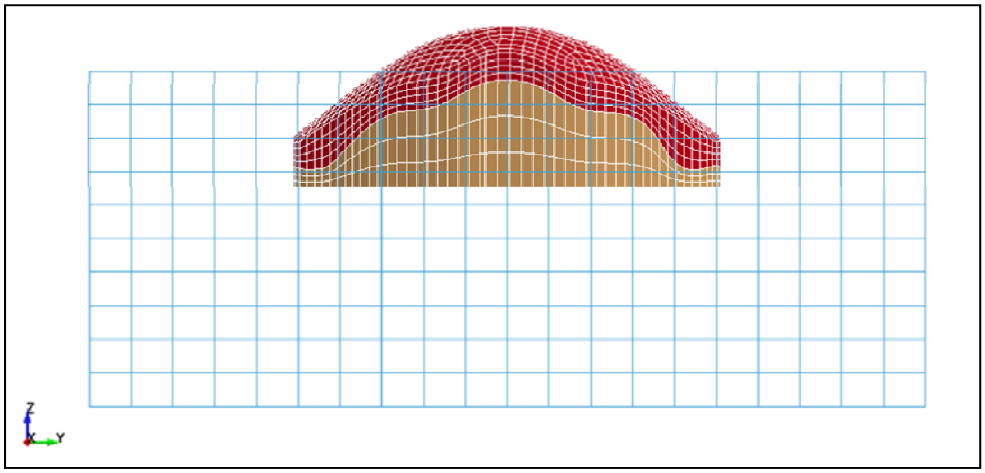

Figure 5.5. Turtle model and water elements

5.2 Material Properties

LS-DYNA has a large number of predefined material types. The material code used for the foam was MAT_SOIL_AND_FOAM, and the material used for the resin system was MAT_ELASTIC. A volume is defined around the turtle model as MAT_NULL with the properties of water to serve as the boundary conditions. The air was defined as a void with no material properties. The mechanical properties used for each material type are summarized in Tables 5.1 to 5.3. The density of the carapace core and face materials were measured directly, but the density of the foam body was set to provide mass to the finite element model to match the mass of the artificial turtles (34 kg) used in the field testing.

The material models used for the various layers of the carapace did not take into account the effects of strain rate and were considered homogeneous. The assumption that homogeneous, isotropic materials would suffice for the determination of a critical force value was based on the results of investigations which used FEA using elastic-plastic, isotropic, and homogeneous material models to find the fracture force of skulls (Willinger et al. 2000; Horgan and Gilchrist 2003). Voids and other imperfections in the foam or resin system were not included in the model. While these micro-level imperfections could potentially have some impact on the fracture of the shell, the general load-deformation response would not be significantly affected. As such, they were ignored in the present work.

Table 5.1. Material properties of foam

Material	Density kg/mm^3	Shear Modulus MPa	Bulk Modulus MPa	Tensile Strength MPa
Core	3.2E-7	49	63	4
Body	1.4E-6	2.4	0.56	2

Table 5.2. Material properties of polyester resin with glass microspheres

Density kg/mm^3	Elastic Modulus MPa	Poisson's Ratio	Thickness mm
1.4E-6	964	0.33	1.0

Table 5.3. Material properties of water

Density kg/mm^3	Cut-off Pressure GPa	Bulk Modulus GPa
1.0E-6	-1.0E11	2.2

The material code MAT_SOIL_AND_FOAM allows for different properties in tension and compression and also includes the ability to define up to ten data points to describe a stress-strain curve in compression. The curve is shown in Figure 5.6. Properties which were not directly measured, such as shear modulus of the foam materials, were estimated using equations from Gibson and Ashby (1999). The pressure cutoff is defined as the recommended value to allow for the material to cavitate (Hallquist 2009).

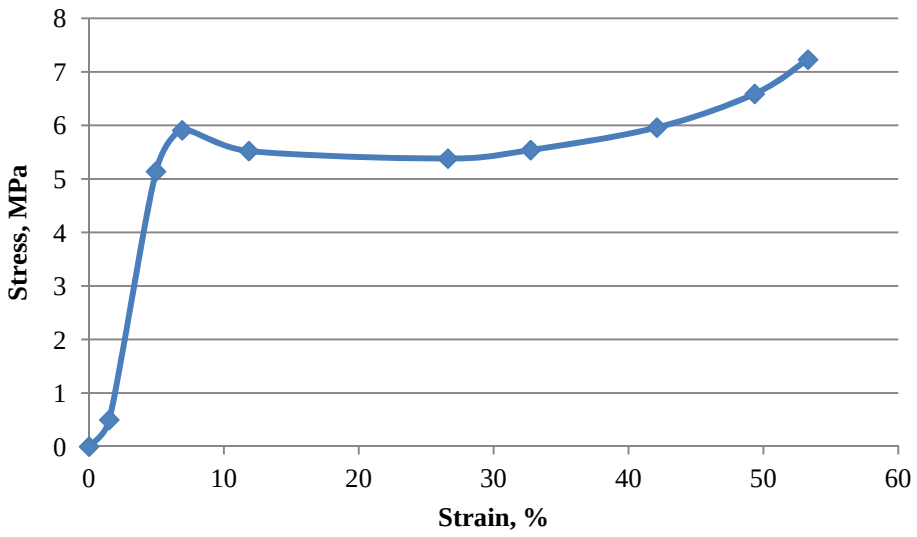

Figure 5.6. Stress-strain values used to define material properties of the foam core in the finite element model

5.3 Boundary Conditions

The model used Arbitrary Lagrangian Eulerian (ALE) solution methods to simulate the fluid-structure interaction (FSI) of the artificial turtle in the water. Solid (Lagrangian) and liquid (ALE) materials can be used in the same model, and the fluid-structure interaction is handled by a coupling algorithm. The water and air overlap the turtle model, and their nodes do not have to be shared. The turtle model can deform and move through the fluid mesh, which itself can deform. For FSI of solid and fluid materials, the coupling forces between the two materials are calculated and redistributed onto both materials at each time step. The CONSTRAINED_LAGRANGE_IN_SOLID command is used to define the master and slave parts of the FSI, to set the number of coupling points for use between the two types of materials, and to set the fluid-structure coupling method (Do and Day 2005). In the analysis, the depth of the turtle model simulated the placement during the field experiments, with the uppermost part of the carapace exposed above the water's surface. Because the FEA used a force applied directly to the nodes as opposed to the simulated impact of two objects, any effects of the boat immediately prior to impact, such as the bow wave's effect on the turtle's position or attitude in the water, were ignored.

5.4 Contact Force

The impact event can be described as a transfer of energy from the moving vessel to the relatively stationary turtle. The change in kinetic energy of the vessel during impact is absorbed in a number of ways: elastic strain energy, contact deformation, water resistance (drag), motion of the turtle, and fracture mechanisms. None of these was measurable in the field experiments, but the accelerometer gave a gross approximation of

the total force imparted to the model. Using the peak resultant acceleration to calculate the maximum contact force is a reasonable estimation, although this assumption ignores some mechanisms of energy loss.

The contact force and duration of impact were estimated using accelerometer data from the field tests. If the acceleration data exceeded the range of the accelerometer, the maximum value was used. The peak contact force was calculated using $F = ma$, where a is the peak resultant acceleration and m is the mass of the turtle model (35 kg). The area of contact from hull impact of Vessel 1 was found by measuring the marks on the turtle carapace after impact. For all these tests, the impact was from the side, with the orientation between 2 and 4, as described in Section 4.3.2. The peak acceleration ranged from 27.3 to 28.5 g. A summary of these values is presented in Table 5.4.

Table 5.4. Results of impacts from Vessel 1, Round 2

Shell #	Orientation	Peak Accel g	Peak Force kN	Contact Area mm^2
4	3	22.1	7.58	4550
26	3	20.9	7.16	1800
22	3	25.5	8.75	4600
28	2	23.7	8.12	1500
39	4	26.1	8.96	6600

Shell 22 was used as a basis for the numerical model. A location and area similar to that test was chosen for the application of the load in the numerical analysis. From analyzing the marks on the carapace after testing, the boat appeared to travel perpendicular to the spine and left a mark of 4600 mm^2 on the carapace. The contact force was applied across 32 nodes over an area of 4980 mm^2, which is shown in Figure 5.7. Based on the low-velocity impact of sandwich composites results of Schubel et al. (2005), a half sine curve was used to describe the contact force history:

$$f(t) = P_0 \sin\left(\frac{2\pi}{T} t\right) \tag{5.1}$$

where P_0 is the maximum force and T is twice the pulse duration. T was estimated from the acceleration data from the field tests and was kept constant at 40 ms in the finite element analysis. A graph of the force is shown in Figure 5.8. The peak force was scaled independently in the *y* and *z*-directions to produce acceleration values similar to those obtained during field tests for Shell 22.

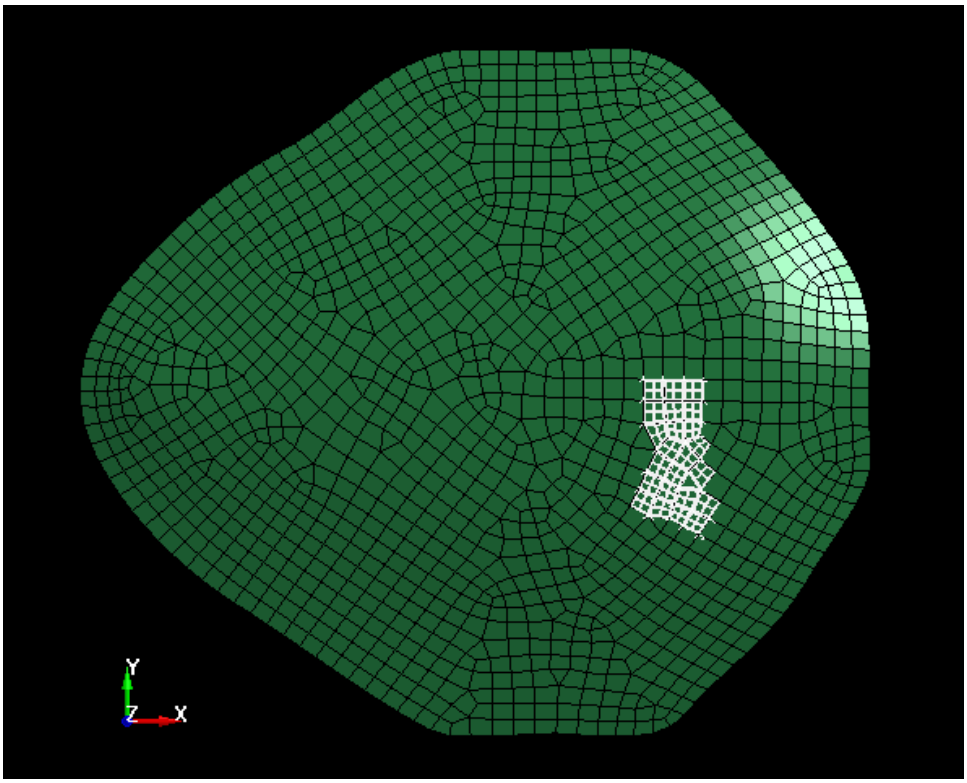

Figure 5.7. Area of applied force (shown in white) of finite element model

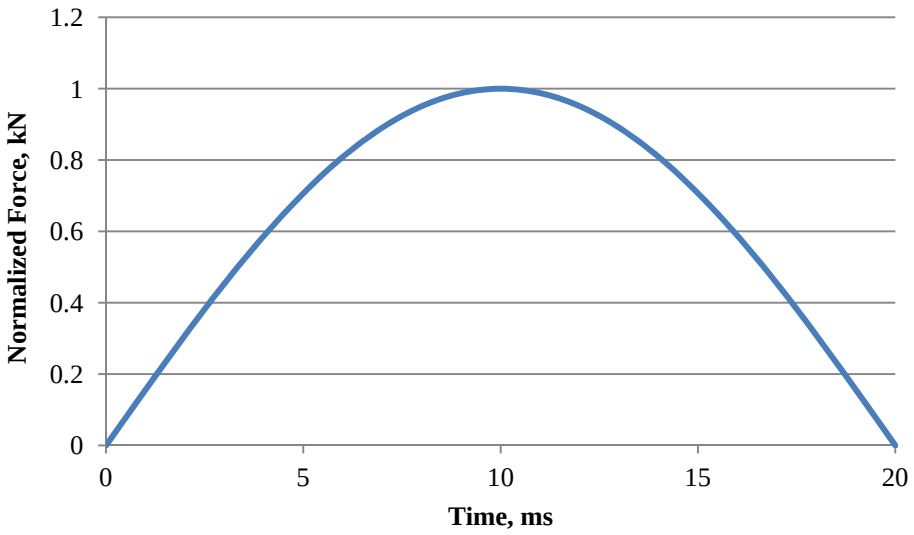

Figure 5.8. Load curve defined for finite element analysis

5.5 Effect of Impact Duration

The analysis described previously was based on the hull impact of one vessel at one speed. Vessels with different hull materials and shapes or sea turtles of different sizes would be expected to produce different impact conditions. The duration of contact between the hull and turtle during impact was investigated to determine its effect on the critical force, the force at which the carapace fractures. An increase in the duration of impact of the applied load (Equation (5.1)) in the finite element model resulted in lower stress values in the carapace. Therefore, as the time increased, the force required to produce a carapace fracture also increased. The critical forces and corresponding durations are shown in Figure 5.9.

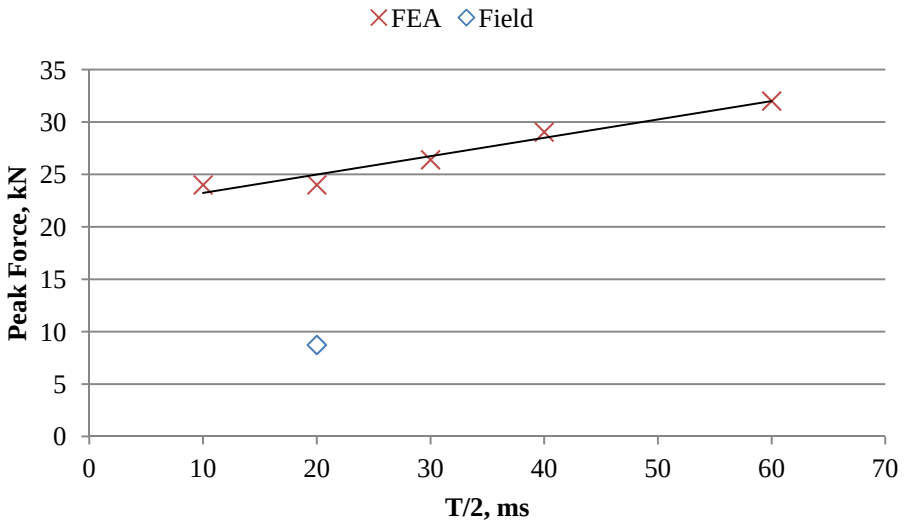

Figure 5.9. Relationship of critical force and impact duration in the FEA

5.6 Results

For the initial contact force of 8.75 kN, each of the 32 nodes was subjected to a 0.273 kN force. The *y* and *z*-components of the force were set to 0.9 and 0.4359, respectively, through an iterative process to produce a similar range of acceleration values to Shell 22. The duration of the impact was kept at 20 ms for all tests, and the analysis ran for 40 ms. The scale factor was gradually increased, and the accelerations and stresses of the carapace were recorded. The accelerations were recorded from node 2693 on the bottom surface of the turtle model, as shown in Figure 5.10. The accelerations for all three axes and the resultant were recorded for each test. The range of the accelerations is presented in Table 5.5. The applied force of 8.75 kN produced a peak resultant acceleration of 29.9 g compared to 25.5 g of Shell 22 in the field tests.

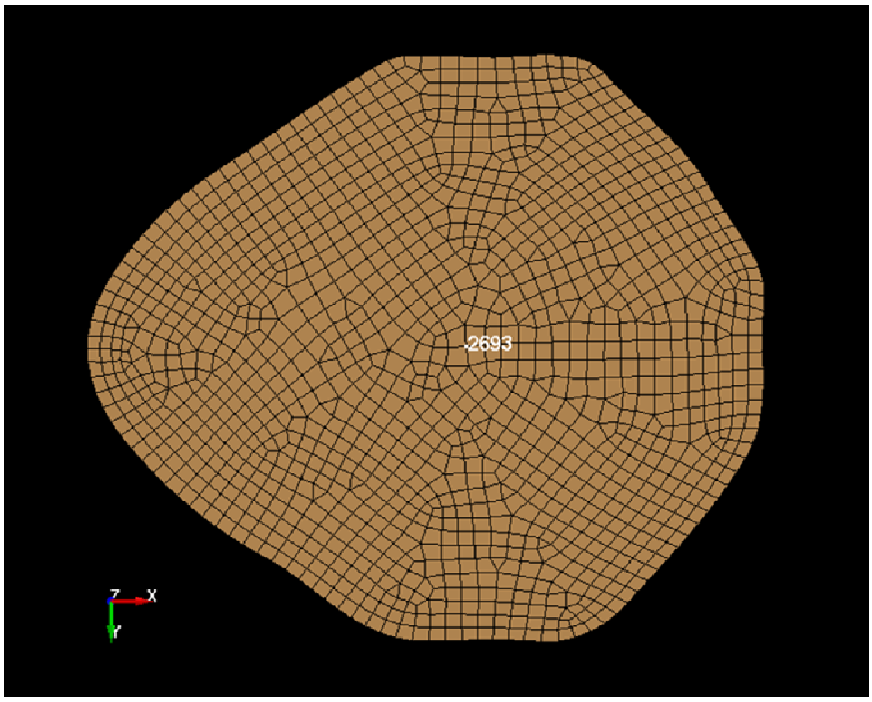

Figure 5.10. Location of node 2693

Table 5.5. Range of acceleration values from finite element analyses

Peak	*x*-axis		*y*-axis		*z*-axis		Resultant
Force	min	max	min	max	min	max	
8.75	-14.7	21.3	-21.3	21.1	-17.6	15.4	29.9
11.2	-14.5	18.4	-21.1	37.5	-19.9	36.2	39.2
14.4	-20.8	22.7	-29.6	60.3	-19.0	38.4	62.5
17.6	-28.1	48.6	-28.7	53.0	-31.1	50.2	63.1
20.8	-31.5	81.5	-23.0	47.4	-31.3	67.5	85.7
24	-76.4	75.1	-53.4	60.3	-44.8	65.6	97.5
Shell 22	-15.8	13.9	-15.7	4.8	-9.7	17.5	25.5

The acceleration data were used primarily to adjust the scale factor and direction of the applied force to find a response of the finite element model similar to the results of the field test. The stresses in the carapace were analyzed to determine the contact force at which fracture occurred. Schubel et al. (2005) noted that even when increasing the impact energy, the duration remained nearly constant, and the contact force history retained a sinusoidal shape. Therefore, only the contact force, and not duration, was modified

between tests. The equivalent tensile stress was used to determine failure of elements within the carapace. The face materials have a maximum strength of 16 MPa and the foam has strength values of 4.2 MPa and 5.8 MPa in tension and compression, respectively. Fracture was considered to have occurred when all four layers of the foam carapace had stress values beyond the material's limits.

The faces suffered a significant number of failed elements at 11.2 kN and above. At the baseline force of 8.75 kN, a small number (four) of the shell elements showed stress levels beyond the ultimate strength. This is quite similar to the results of many field tests, which showed small cracks at the contact area from the hull impact of the jet drive vessel, as shown in Figure 5.11.

The carapace showed initial signs of failure in a small number (six) of the solid foam elements at the 14.4 kN, but these were in the uppermost layer and were not considered evidence of serious injury, At the 24 kN force, stresses in all layers of the foam exceeded the strength of the material, and this was determined to be the critical force value. At the 20.8 kN force, the stresses occurred in only two of the four solid element layers. Contour plots of the effective stress in the foam carapace elements at 8.75 kN and 24 kN are shown in Figures 5.12 and 5.13, respectively.

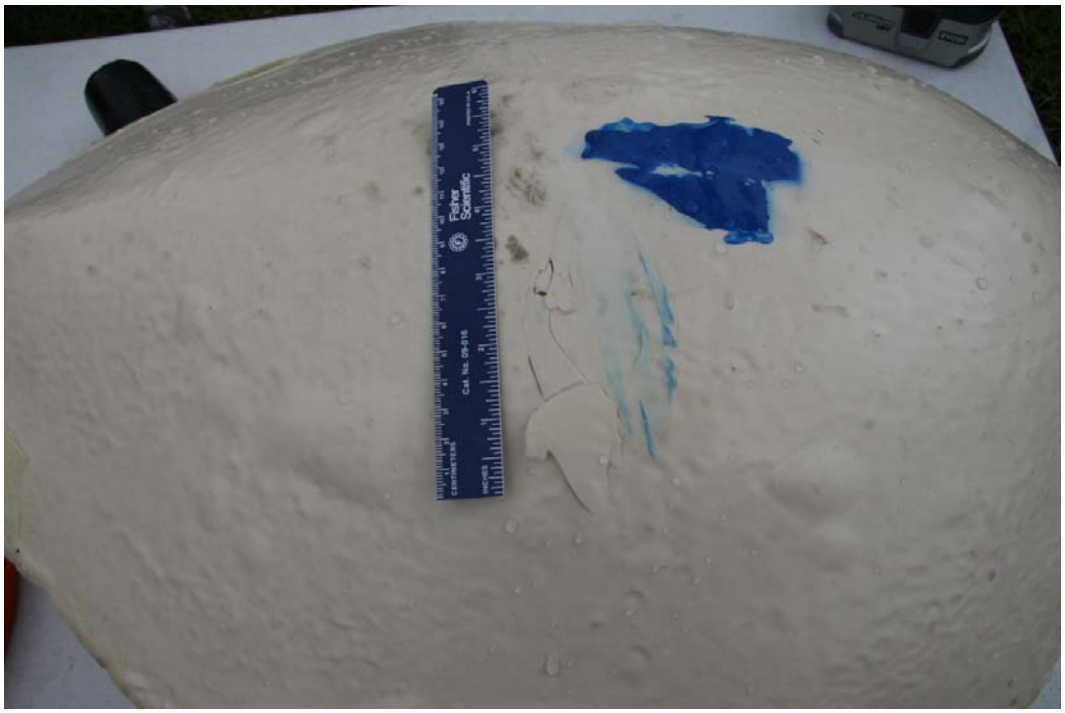

Figure 5.11. Surface cracks on Shell 4, Vessel 1, Round 2

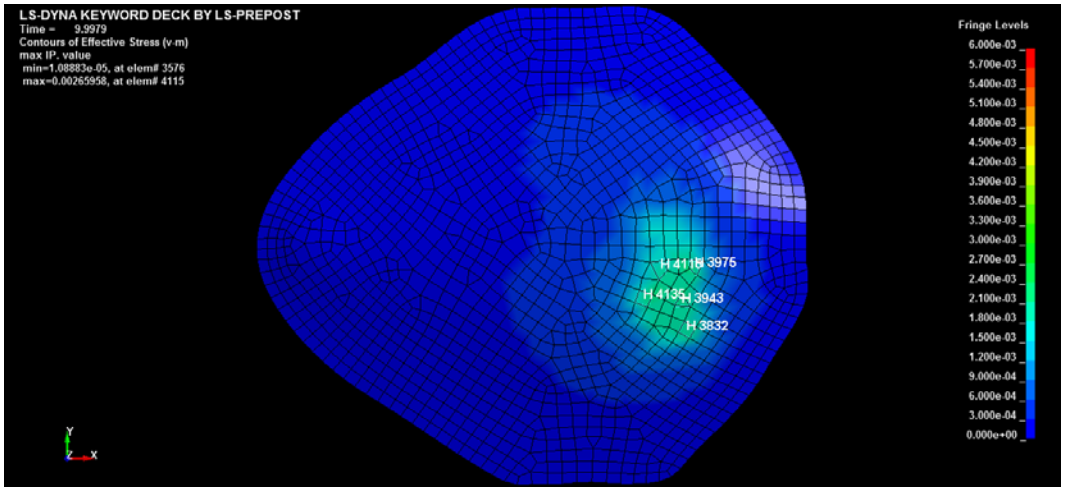

Figure 5.12. Contour plot of effective stress of solid elements at 8.75 kN

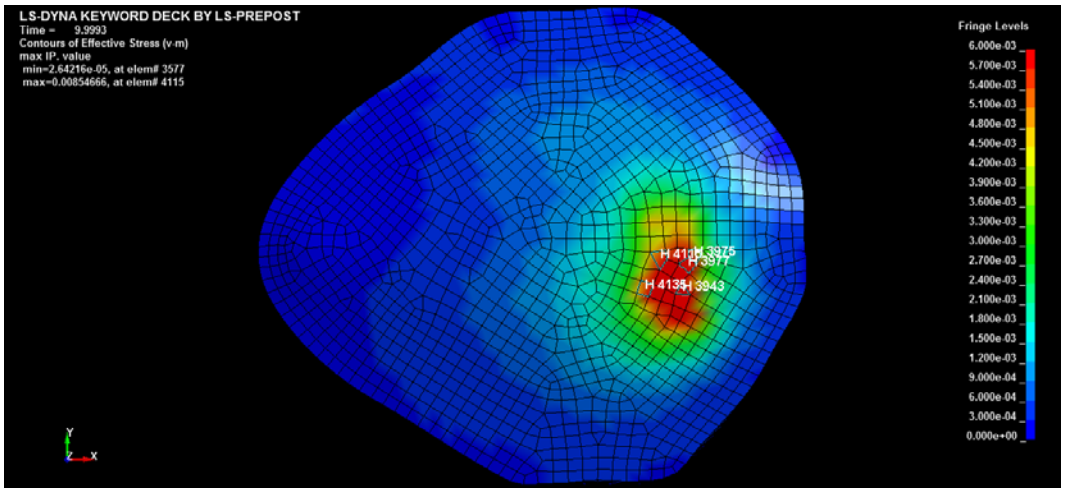

Figure 5.13. Contour plot of effective stress of solid elements at 24 kN

5.7 Conclusions

The maximum contact force can also be written as a function in terms of impact energy as

$$P_0 = \frac{2\pi}{T}\sqrt{2mE} \tag{5.2}$$

where E is the impact energy of a specific event (Schubel et al. 2005). Unlike laboratory impact tests in which the total energy of the impactor is absorbed by the test specimen, the turtle model in the field tests was subjected to a small proportion of the vessel's total kinetic energy. But assuming the turtle absorbed the same percentage of impact energy, the vessel would need to increase its kinetic energy by 650 % to produce a force of 24 kN. The jet propulsion vessel used in the field testing had a mass of approximately 1000 kg and a speed of 40 km/h. To generate the required force the same vessel would have to travel 110 km/h or have a mass of 7500 kg. The scenarios investigated were for one vessel size, speed, hull shape, and hull material. All of these parameters affect the contact force transmitted to the carapace, but for the vessel under consideration, carapace fracture from hull impact seems unlikely except at very high speeds.

Based on the results of experimental field test and finite element analysis, it is unlikely that a typical recreational vessel with a jet propulsion engine is capable of fatally injuring loggerhead sea turtles. The hull shape did not appear to influence the lethality of turtle injury, although only deep-vee hulls were used in the current research. The field tests in Phase II which used some flat-bottomed hulls with jet drive engines also produced no damage (Sapp 2010). Other hull shapes and materials may affect the duration of impact and contact force of a vessel strike. Figure 5.14 shows a graph with the dry weight and top speed of common jet drive boats and personal watercraft from Yamaha® and Sea-Doo® versus the energy required to fracture a carapace from hull impact, as determined from the finite element analysis (BoatTEST.com LLC 2012).

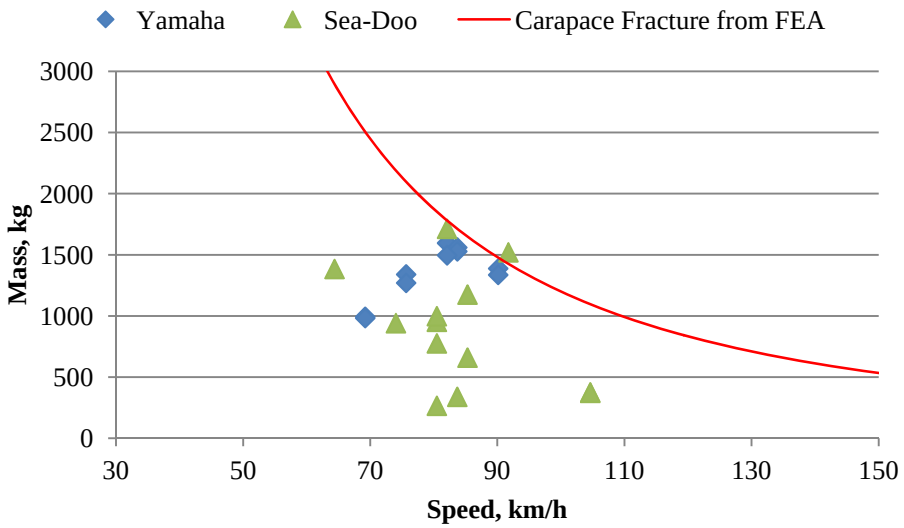

Figure 5.14. Plot of mass versus top speed for common recreational jet drive vessels with a comparison to the energy required to produce a carapace fracture from hull impact as calculated by the FEA

The mass of the vessels does not take into account the weight of the operator or passengers. Only one vessel exceeds the energy limit, and others are near this threshold, but under typical operating conditions vessels are not operated at top speed. Therefore, it

is unlikely that hull impacts of jet propulsion vessels present a serious threat to loggerhead sea turtles.

CHAPTER 6

CONCLUSIONS AND RECOMMENDATIONS FOR FUTURE STUDY

6.1 Conclusions

The goals of the current research were to develop a synthetic material system with mechanical properties similar to loggerhead carapace bone, fabricate full-scale test models, and investigate the effects of hull type and propulsion system on the lethality of sea turtle injuries through field testing, statistical analysis, and numerical simulation. Understanding the factors that affect sea turtle injuries will help in developing management strategies to reduce the number and lethality of vessel strikes in coastal waters.

A sandwich composite design was used in an effort to mimic the structure of the two bone types, cortical and cancellous, in the loggerhead carapace. Some commercially available synthetic bones use a polyurethane foam as a substitute for cancellous bone and a fiberglass/epoxy resin material for the cortical bone. Human bone, and subsequently human bone models, are significantly stronger than the loggerhead carapace, so systems with similar materials but with lower mechanical properties were developed. The selected material system employed a closed-cell polyurethane foam core with faces of polyester resin infused with glass microspheres. The sandwich composite material system reasonably approximated the desired mechanical properties of the loggerhead carapace. Because stress is a measure of force per unit area, the increased thickness of the artificial carapaces compared to the organic samples resulted in decreased strength and stiffness

properties in tension. The increased thickness also results in an increased moment of inertia and, therefore, higher flexural rigidity in bending. Synthetic bone specimens with the desired material properties and behavior compared to the organic material can be produced using the constituents' mechanical properties and design procedures of composite material systems.

Field tests were performed using full-scale models of a sea turtle with 64 cm curved carapace length and mass of 35 kg. Two vessels, both with deep-vee hulls, were used in testing. The 5.4 m inboard jet drive boat and a 7.3 m outboard propeller-driven vessel were designated Vessel 1 and Vessel 2, respectively. All tests were conducted at planing speed, about 40 km/h. Tests were performed with the turtle at three depths in the water column: at the surface, 48 cm, and 71 cm (propeller depth). An accelerometer recording at 1600 Hz was attached to the model turtles during testing. Deceased sea turtles were also tested.

A statistical analysis of the field test data was performed to investigate the influence of turtle depth in the water column, propulsion type, and hull shape on the likelihood of a fatal injury during a vessel strike. The analysis showed that depth of the turtle in the water column does not influence the lethality of injury, but the type of propulsion system does; the jet drive boat (Vessel 1) did not cause any fatal injuries during testing. Field test data from Phase II was incorporated to provide a basis for identifying the effects of hull type on the lethality of injury. Because statistical analysis from both Phases II and III determined that turtle depth in the water was not a factor, this variable was excluded from the combined data. All results used from Phase II were at planing speed (40 km/h), so the three variables were propulsion type, hull type, and

injury. Again, injury was shown to be dependent on propulsion type. Hull shape did not have an influence on the lethality of injury. However, in the tests conducted at propeller depth (71 cm) of Vessel 2, no impacts were recorded. The turtles were displaced out of the way of the approaching vessel, presumably by the bow wave. These results are quite different from the tests of Phase II, which used a flat-bottomed skiff. In those tests, fatal injuries occurred at all tested depths, including at propeller depth. The deep-vee hull may reduce the chances of turtle/ship interactions by reducing the depth in the water column at which impacts have a possibility of occurring. The jet propulsion vessel (Vessel 1) had a smaller draft than Vessel 2 (outboard motor propulsion), further reducing the chances of an impact.

After the body design was revised for use in the second round of testing, neither vessel caused lethal injuries to the carapace from hull impact only. This behavior was also demonstrated during the testing of the real turtles, in which only slight visible damage was observed after impacts by Vessel 1. In the field tests conducted with Vessel 2, impact from the motor, either the skeg or propeller, always resulted in fatal injuries to the turtles. Of the ten trials conducted in Round 2, three did not result in fatal injuries; however, all of these were hull impact only, with no impact of the motor. The revised body design used in Round 2 absorbed energy more efficiently than the first design. There was little change between the peak acceleration values between the rounds, but the resulting behavior and failure modes of the artificial carapaces changed dramatically, particularly those struck by Vessel 1. In the first round of tests, the average peak acceleration values for Vessels 1 and 2 were 24.0 g and 28.2 g, respectively; in the second set of tests, these values were 23.6 g and 27.6 g. Some test results imply a

correlation between peak acceleration and damage. For example, the two tests which produced the lowest values, Shells 7 and 23, did not break. The impact energy required to break the artificial carapace through hull impact alone was not determined from the current field tests, but it was estimated using numerical methods. It is reasonable to assume some combination of hull shape and material with vessel speed and size could cause carapace fracture and fatal injury.

The results of field testing show that vessels with jet propulsion systems pose significantly less risk to sea turtles, both in the effects of vessel strikes and the likelihood of the event occurring. In addition to propulsion type, speed was shown to influence sea turtle injury in the Phase II field tests. Although propeller wounds are possible at any speed, the risk was reduced at lower speeds. Modifying vessel propulsion types and speed would appear to reduce the incidence and severity of vessel strikes for sea turtles and other marine species, such as whales and manatees.

The finite element analysis of the hull impact of the artificial carapace determined the force at which the carapace would fracture. Using a contact force of 8.75 kN, which was found from the peak acceleration value of 25.5 g from Shell 22 in the field tests, the numerical simulation resulted in a peak resultant acceleration of 29.9 g. The contact force was increased incrementally until a value which produced failure through the thickness of the foam core was found. The foam core fractured at 24 kN, and the faces broke at 11.2 kN. The critical force was nearly three times higher than what was created during field testing. Compared to the contact force generated during field testing, the critical force determined from the simulation was nearly three times higher, and the corresponding energy was over seven times higher. For the vessel used in the field tests,

the increase in energy would require a seven-fold increase in mass or a tripling of the vessel speed. The finite element analysis suggests that for the jet propulsion vessel used, hull impact alone would not cause a fatal injury to sea turtles.

Finite element analysis was used to estimate the critical force threshold for carapace fracture from hull impact. A required level of kinetic energy for a vessel was calculated using FEA results, and this was compared to the mass and top speed of various jet propulsion vessels. The results suggest that vessel strikes of common recreational jet-boats under typical operating conditions are unlikely to cause lethal carapace fractures in loggerhead sea turtles. The impact duration in the FEA was modified to determine its effect on the critical force for carapace fracture. As the impact duration increased, the critical force increased as well. It is unknown how different hull shapes or materials affect the impact duration in a turtle/vessel interaction, which would affect the required mass and speed of a vessel to cause carapace fracture, but the effects of turtle size, hull shape, and vessel size and speed on the impact force and duration should be investigated in future field or laboratory experiments.

Results from the field experiments will help inform the GDNR's decision-making process to protect sea turtle populations in coastal and estuarine waters. As coastal development continues, the rise in vessel traffic will likely increase the number of turtle/vessel interactions. Speed limits in manatee habitats have proven to be effective in their conservation; however, unlike manatees, the sea turtle population is widely and randomly distributed in the near-shore environments, reducing the effectiveness of such a strategy (National Marine Fisheries Service and U.S. Fish and Wildlife Service 2008). Rather, the adoption of jet drive vessels could be encouraged by placing restrictions on

future marina/harbor developments. The construction of a marina requires permits which often tie the continued development of the project (which is constructed in stages) to its effects on marine life, specifically whales, manatees, and sea turtles. Future permits could stipulate that a certain percentage of docked vessels have jet drive engines. Additionally, increased public awareness of the benefits of jet propulsion systems compared to conventional outboard propellers might encourage the adoption of jet drive boats.

Field test results will also improve the interpretation and classification of wounds found in sea turtle strandings. This will help determine the number of sea turtle/vessel interactions more accurately, and photographic evidence from previous years can be re-examined as well. In addition to determining if a wound pattern is consistent with a vessel strike, the type and size of vessels may be estimated from the length and depth of wounds. The types of wounds present in stranded turtles can also inform the general interaction between turtles and boats, such as animal depth and vessel speed. If the turtles are being struck while below the water's surface, it is difficult for a boat operator to react quickly enough to avoid a collision. This can also be combined with temporal and spatial information of strandings to deduce which turtle behaviors increase the risk of vessel strikes.

6.2 Recommendations for Future Study

The artificial carapace design from the current research showed similar material properties in laboratory testing and behavior in field testing compared to loggerhead carapace bone. The target properties were found by testing coupons of whole bone from a loggerhead carapace. Mechanical testing of the cortical and cancellous bone that compose the shell would facilitate the design of a material system that could match the material

properties of each bone type in a sandwich composite construction. Typically, the mechanical properties of cortical and cancellous bone are found in tensile tests and compression tests, respectively. The determination of other properties, such as density, porosity, mineral content, and organic content would help in the formulation of equations relating material properties to these other parameters. These equations could be used to compare the carapace's properties to those in the literature. Investigation into the specific modes of failure occurring as a result of impact of the carapace would also provide insight into the mechanisms of energy absorption at work.

The most important improvement in the fabrication of the artificial carapace is thickness control of the foam. The increased thickness caused lower strength and modulus values and an increased bending stiffness. A combination of thickness control and adjustments to the properties of the resin infused with glass microspheres faces by modifying the ratio of resin to glass would provide the means to match the target properties of the loggerhead carapace more effectively. The effects of strain rate on the mechanical properties of the organic loggerhead carapace and the composite material system should be investigated as part of a complete material characterization.

Other possible refinements to the carapace design include the addition of a rib structure, fontanels, and a plastron. The ribs and spine are present as surface features in the current design but are not incorporated in a similar manner to the actual ribs and costal plates of a sea turtle carapace. A more accurate model would improve energy absorption and distribution throughout the carapace. The fontanels between scutes are soft areas which provide a path for energy dispersion away from the harder bone areas. They also provide a path for crack propagation through a relatively weak material. The

plastron on the underside of the turtle is attached to the carapace at their edges. This provides an enclosed, more rigid overall structure than a carapace alone. The incorporation of the plastron and carapace into a unified design would help a turtle behave as a whole rather than as a separate body and shell as in the current design. Even though the effects of vessel strikes are local, the overall rigidity affects the response.

During field testing, the propeller often broke the shell into numerous small pieces. The real turtles experienced similar damage patterns but without scattering shell pieces. This is because the carapace is attached with highly elastic muscles and ligaments, while the artificial foam body can be broken into discrete pieces. A layer of connective "tissue" in the artificial design would not provide strength but would connect continuously across the shell's interior surface.

The accelerometer used in field testing measured only axial accelerations but was not capable of recording any rotational data. An inertial measurement unit (IMU) with a three-axis accelerometer and three-axis gyroscope could record both types of data. This would provide a more complete picture of the response in the water before, during, and after impact. The IMU would also need a higher range for the accelerometer, as the range of ±15 g was exceeded repeatedly during testing.

Although Vessel 1 did not cause fracture in the turtle carapaces during Round 2, the acceleration values experienced by the turtles were comparable to those caused by Vessel 2. The average peak acceleration during impact was 23.8 g. The effects such an acceleration would have on the internal organs of a turtle are unknown at present, but the risks of damage caused by vessel strikes not studied in this research program are still

present. Future investigation of the potential damage to internal organs caused by vessel strikes is needed.

The accelerometers used in this research provided some measure of the turtle's behavior during impact. Underwater video of the vessel strike could provide useful information for describing the motion of the turtle before, during, and after impact. The water at the test sites used in Phases II and III was not clear enough to use underwater video, so it was not attempted. Finite element analysis could be expanded to include both the vessel and turtle in an impact simulation, rather than using an approximate force function.

APPENDIX A

MATERIAL PROPERTIES

The following tables and graphs are results from material testing and were used to find the material property values reported in Chapter 3. Tensile, flexural, and compressive data are presented. The properties are for the loggerhead carapace in tension and bending, the properties of the constituent materials (used to develop the finite element model), and those of the composite material system of the artificial carapace.

This section presents the tensile stress-strain graphs of the loggerhead carapace

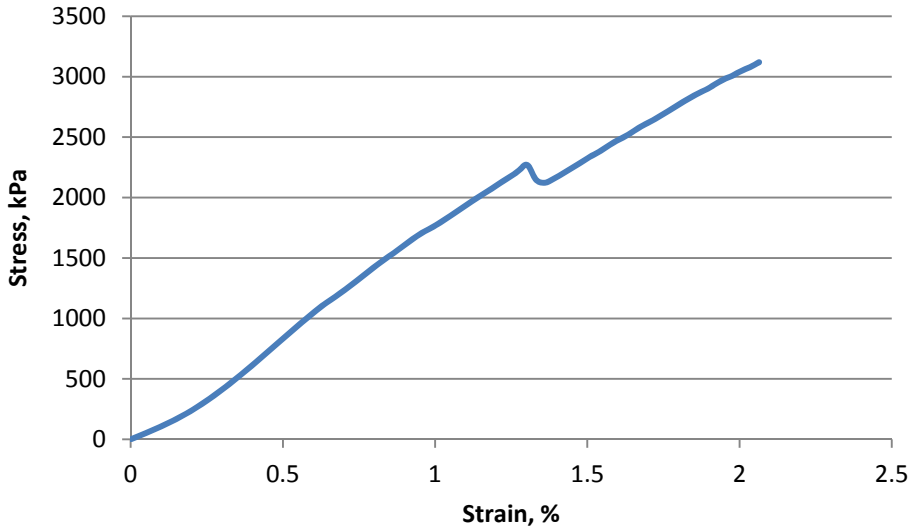

Figure A.1. Carapace 4 Sample L4

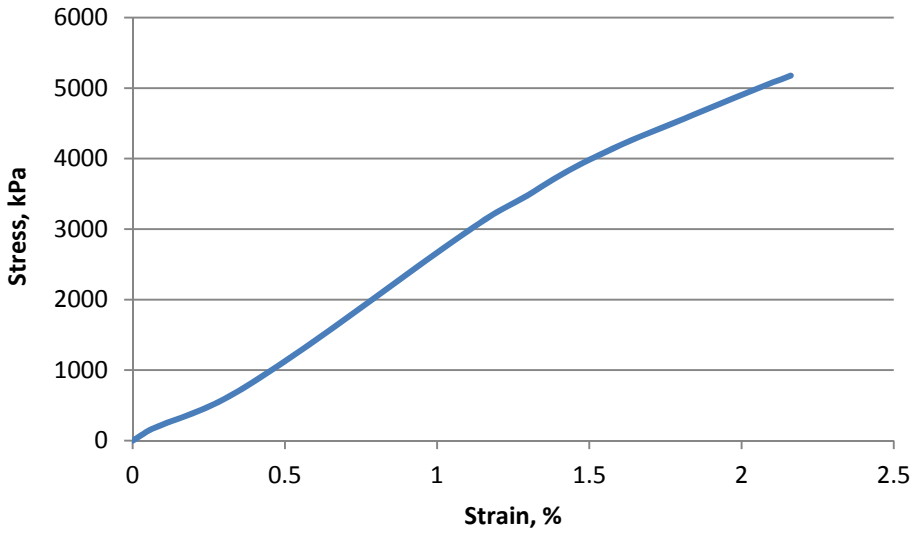

Figure A.2. Carapace 4 Sample L5

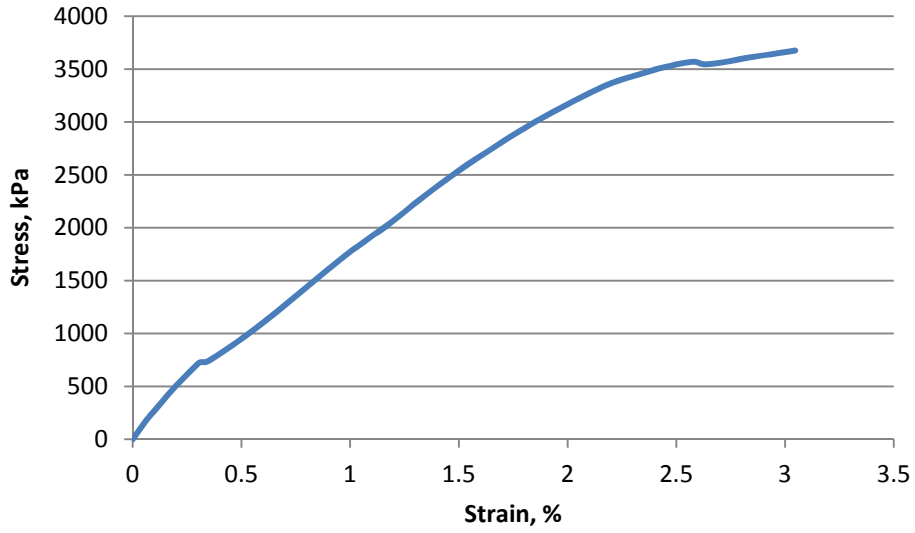

Figure A.3. Carapace 4 Sample L8

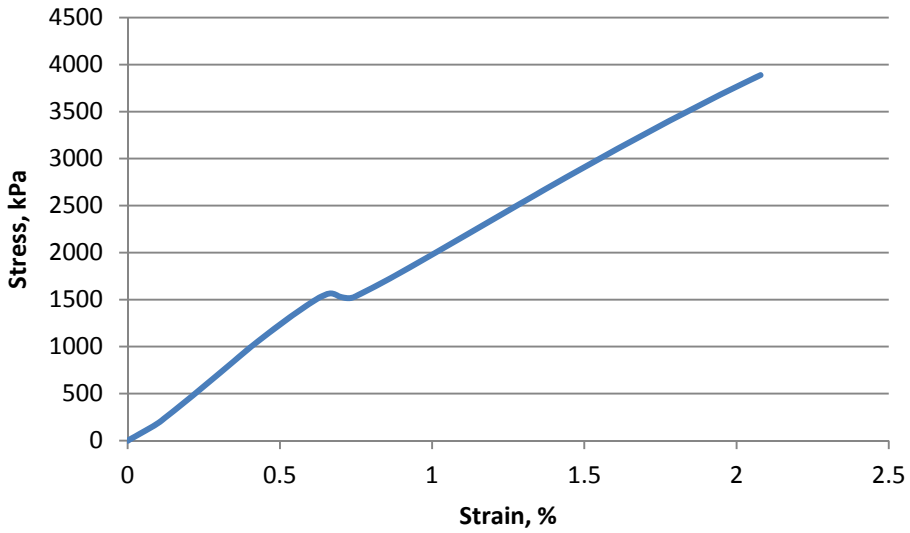

Figure A.4. Carapace 4 Sample R1

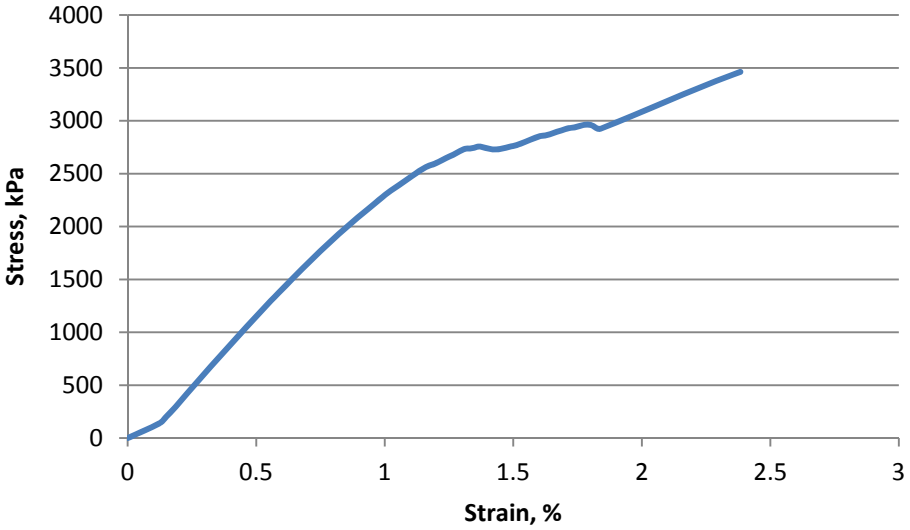

Figure A.5. Carapace 4 Sample R3

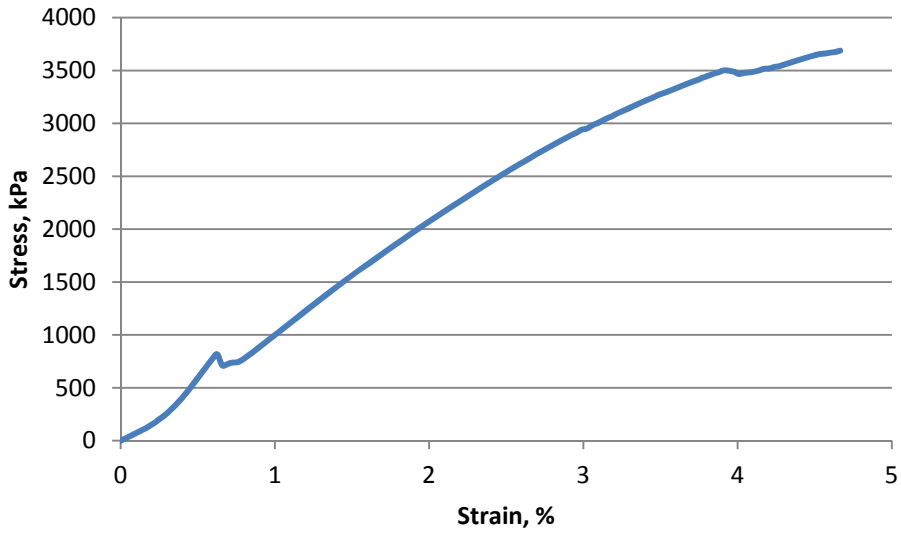

Figure A.6. Carapace 4 Sample R9

This section presents the flexural load-extension graphs of the PU foam

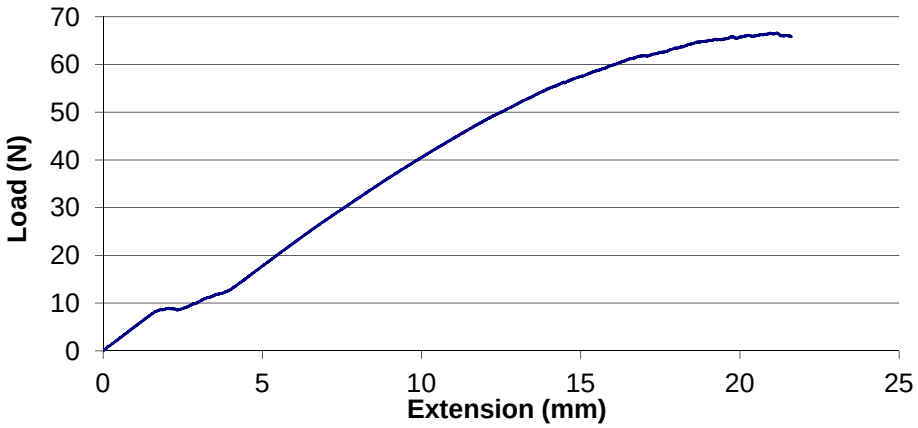

Figure A.7. Flexure Uncoated Sample 1

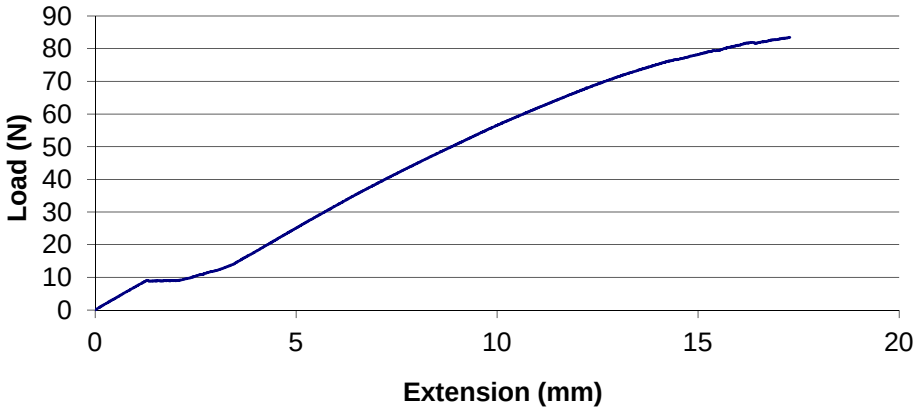

Figure A.8. Flexure Uncoated Sample 2

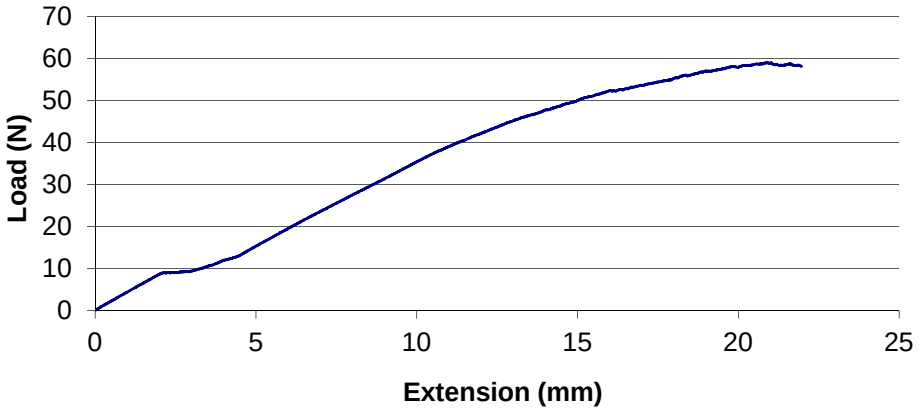

Figure A.9. Flexure Uncoated Sample 3

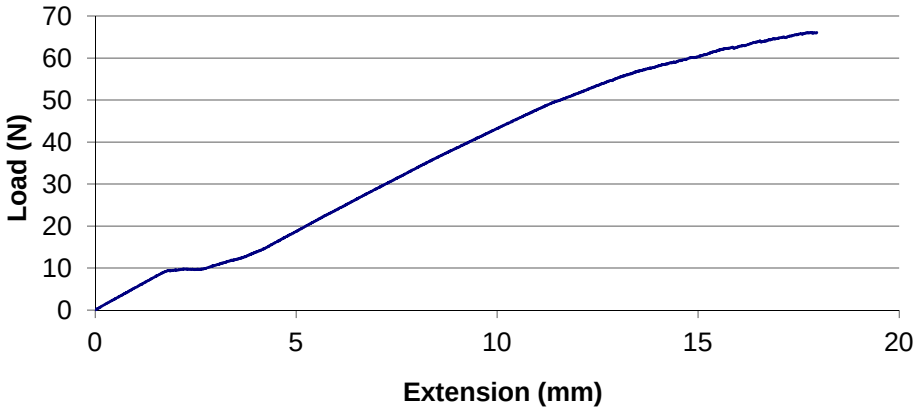

Figure A.10. Flexure Uncoated Sample 4

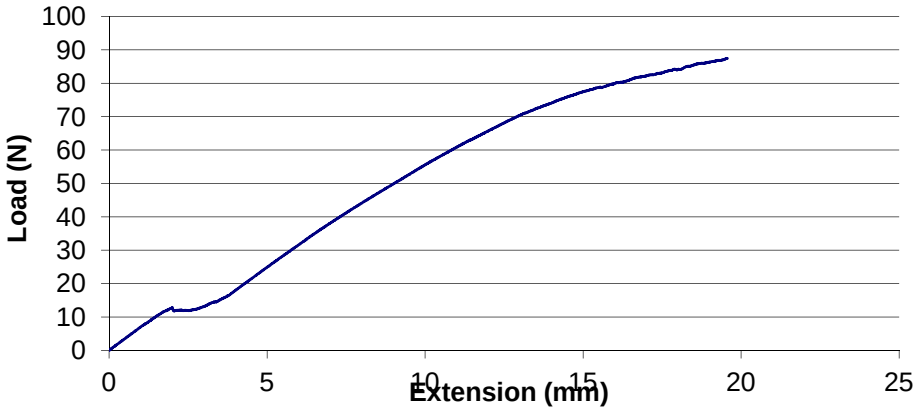

Figure A.11. Flexure Uncoated Sample5

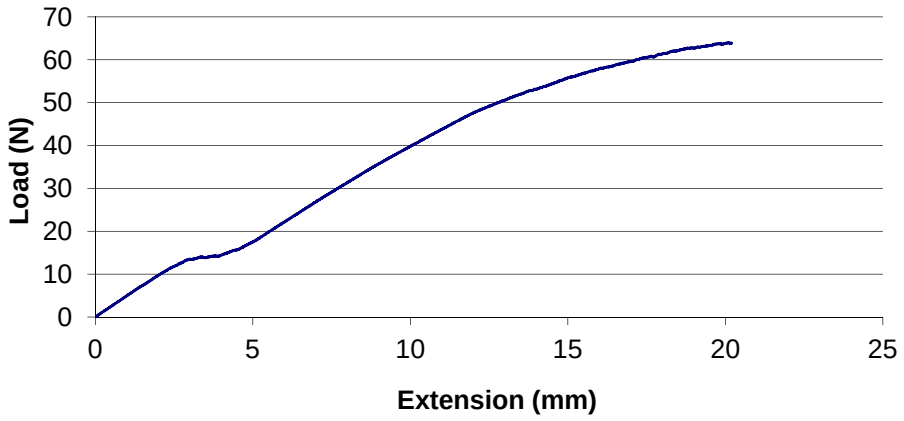

Figure A.12. Flexure Uncoated Sample 6

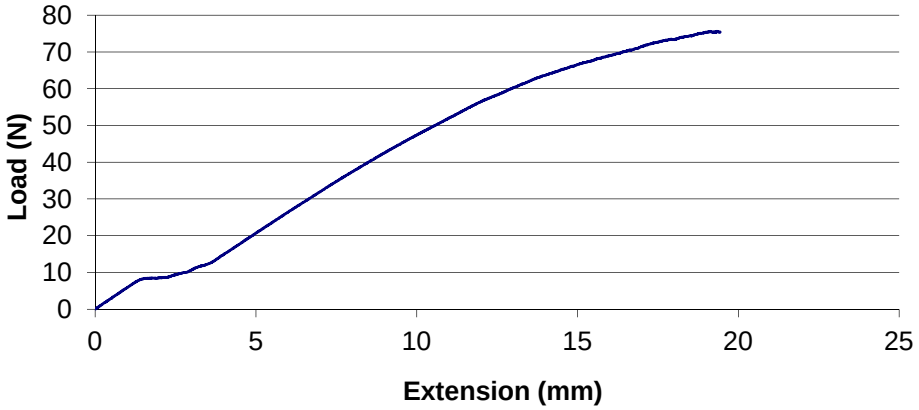

Figure A.13. Flexure Uncoated Sample 7

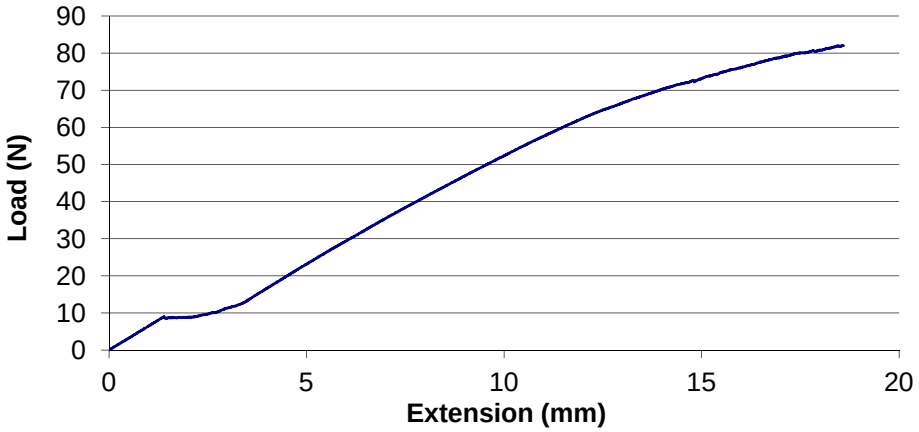

Figure A.14. Flexure Uncoated Sample 8

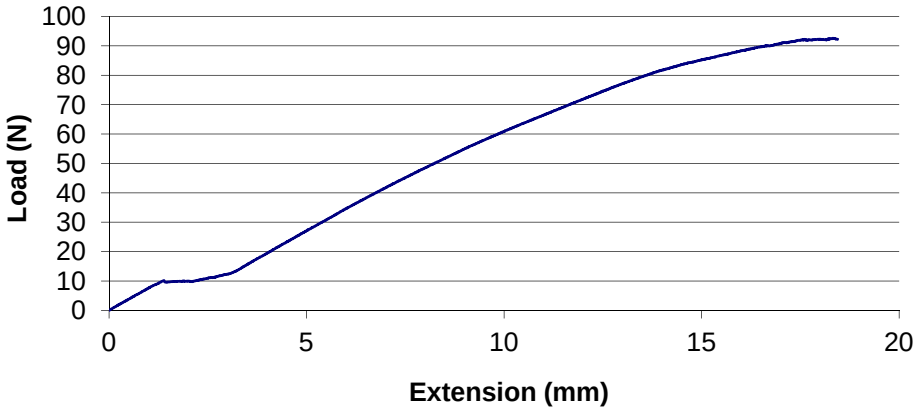

Figure A.15. Flexure Uncoated Sample 9

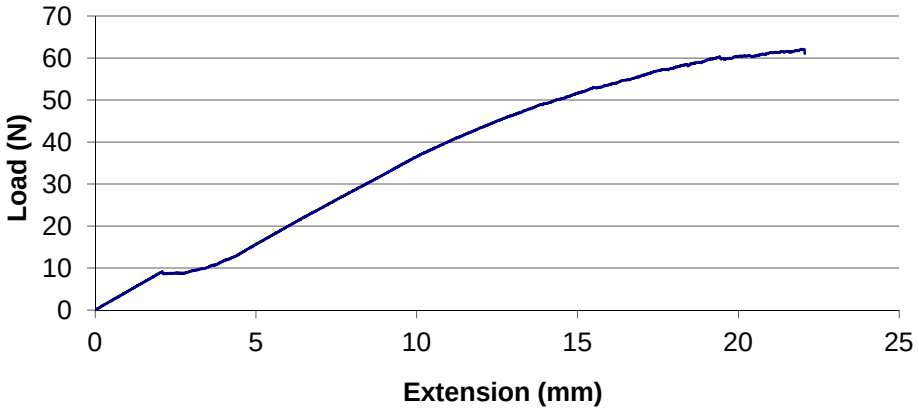

Figure A.16. Flexure Uncoated Sample 10

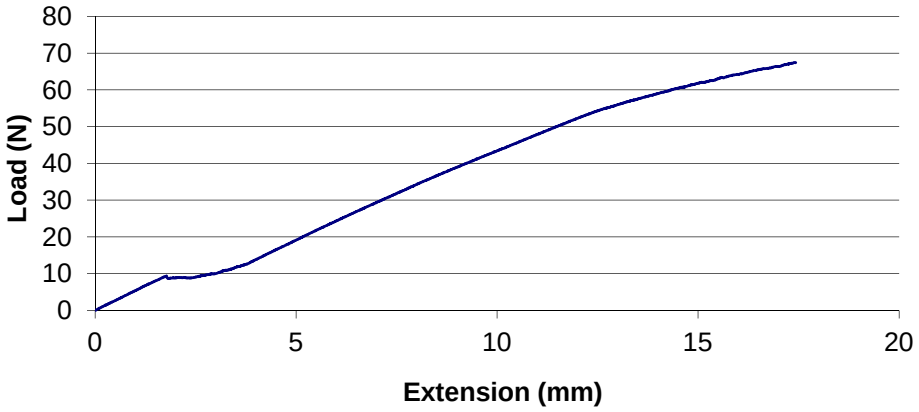

Figure A.17. Flexure Uncoated Sample 11

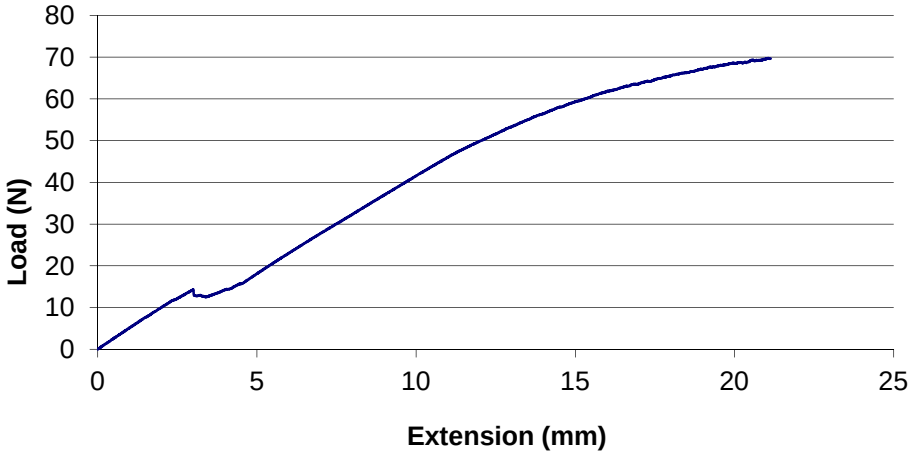

Figure A.18. Flexure Uncoated Sample 12

This section presents the compressive stress-strain graphs of the PU foam

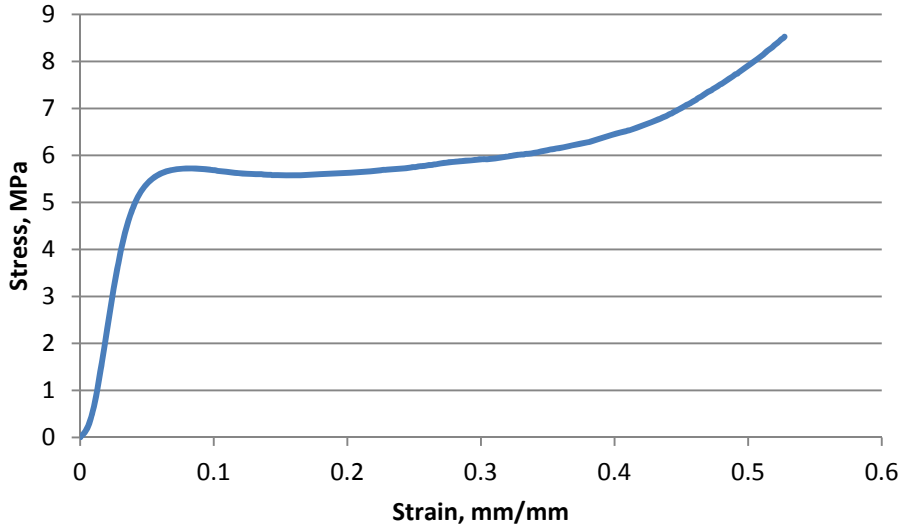

Figure A.19. Compression Block 1

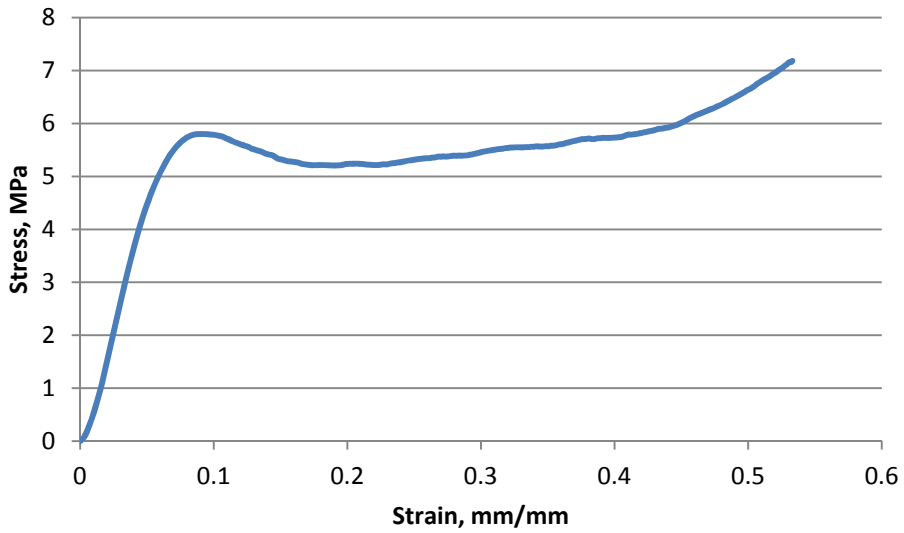

Figure A.20. Compression Block 2

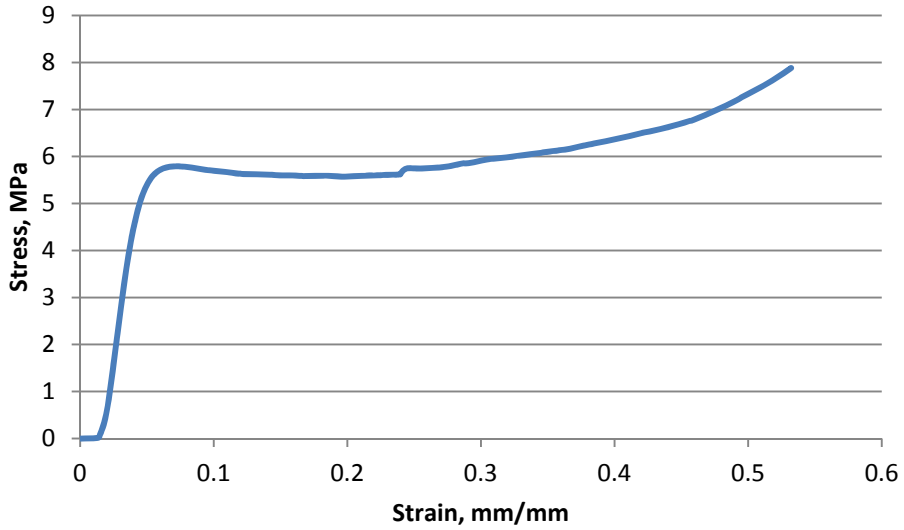

Figure A.21. Compression Block 3

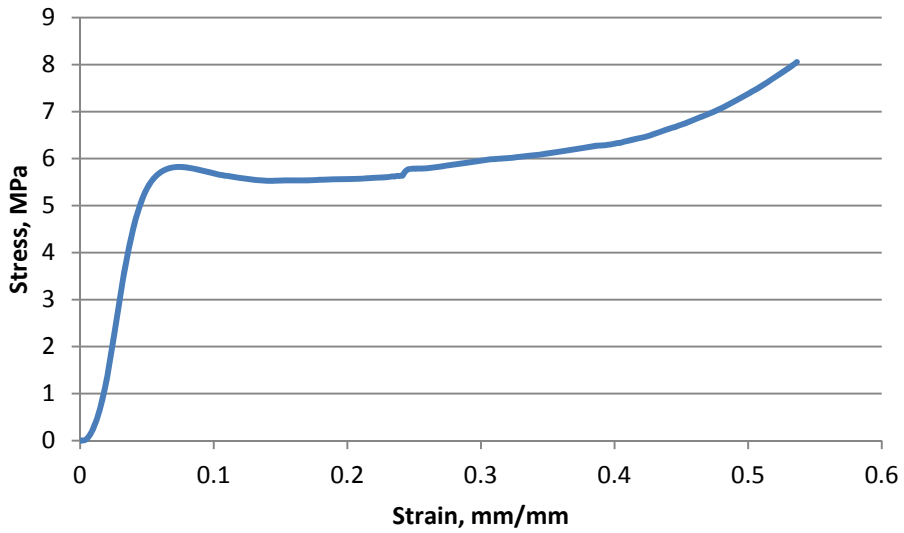

Figure A.22. Compression Block 4

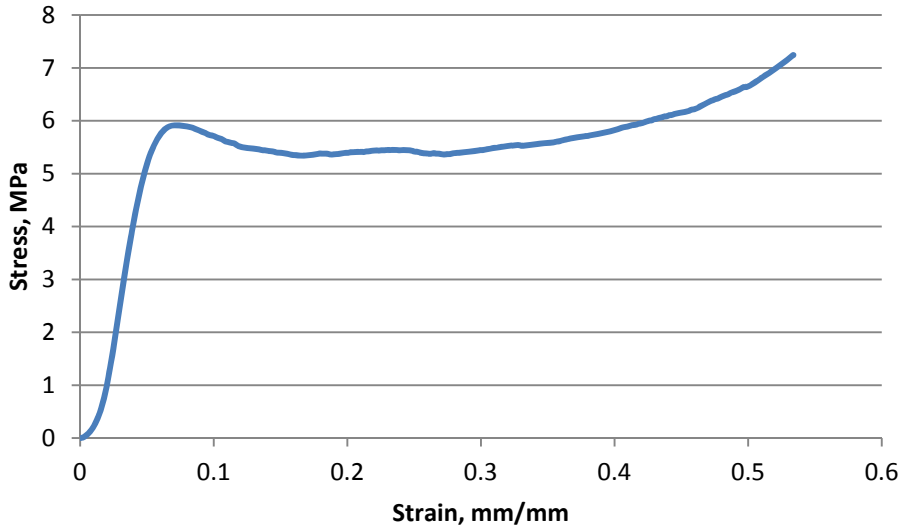

Figure A.23. Compression Block 5

This section presents the tensile stress-strain graphs of the PU foam

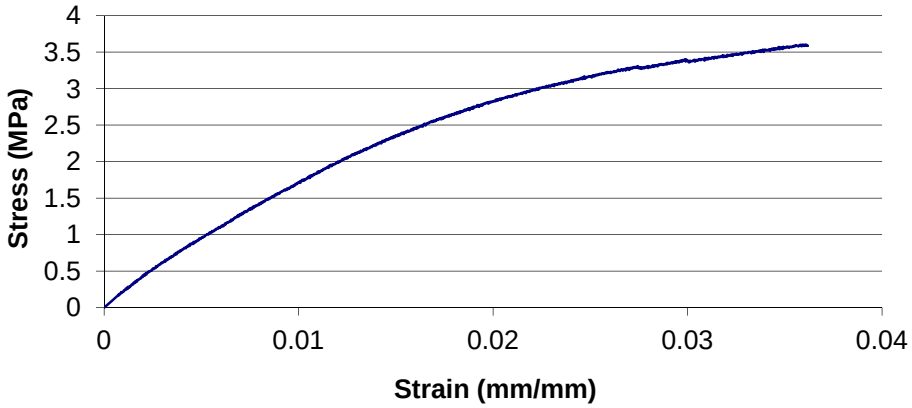

Figure A.24. Tensile Uncoated Sample 1

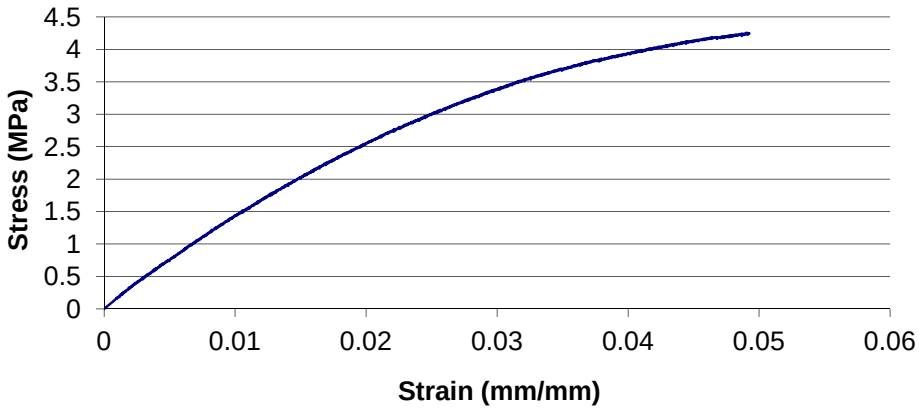

Figure A.25. Tensile Uncoated Sample 2

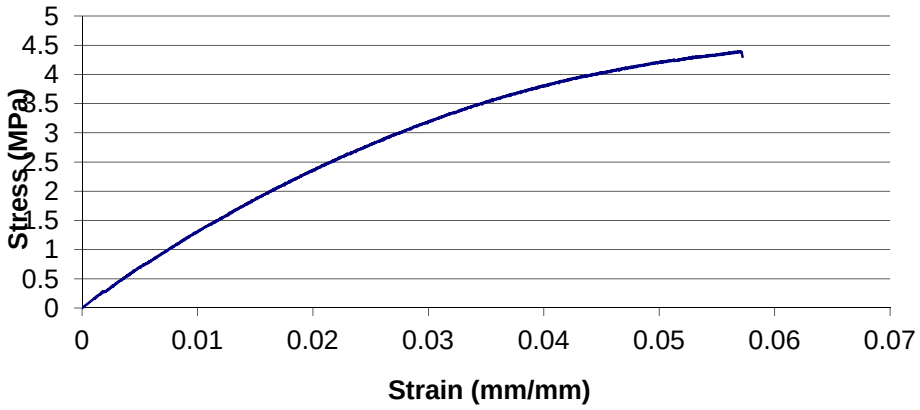

Figure A.26. Tensile Uncoated Sample 3

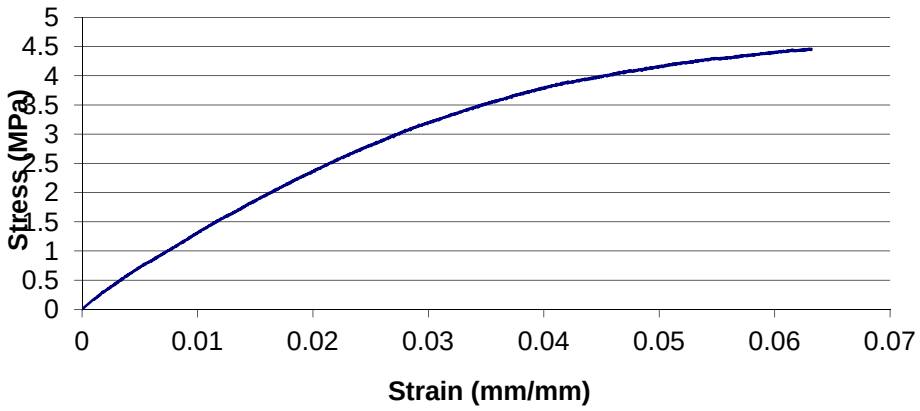

Figure A.27. Tensile Uncoated Sample 4

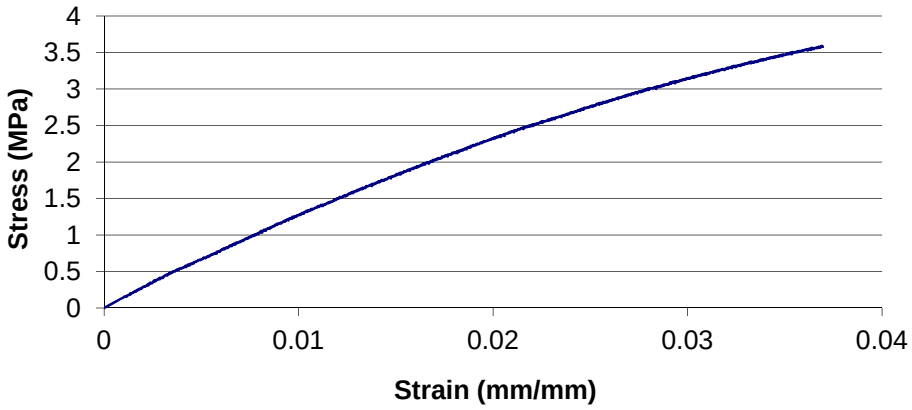

Figure A.28. Tensile Uncoated Sample 5

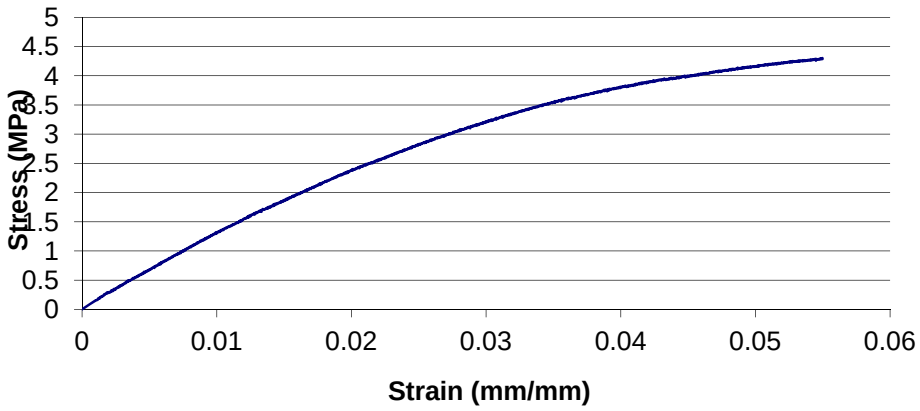

Figure A.29. Tensile Uncoated Sample 6

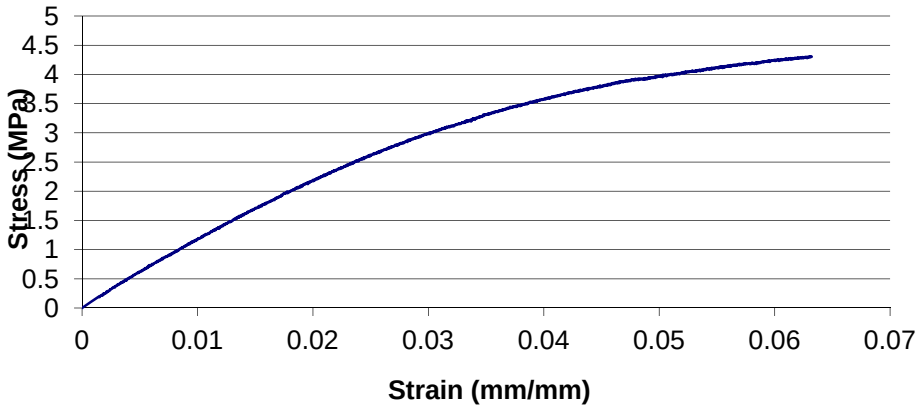

Figure A.30. Tensile Uncoated Sample 7

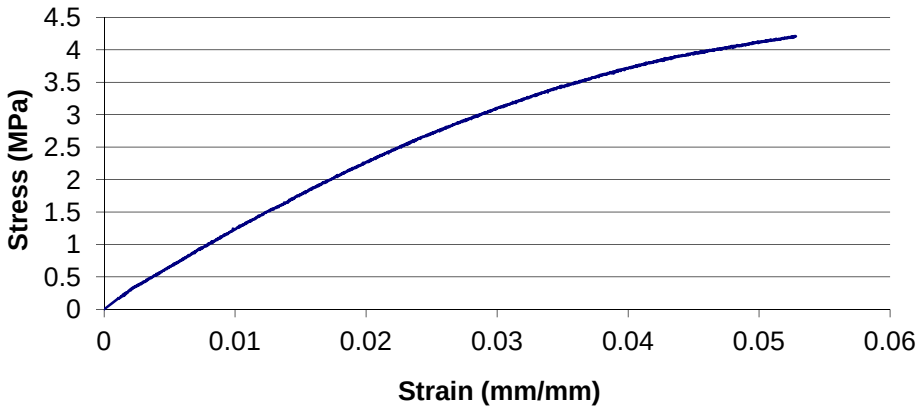

Figure A.31. Tensile Uncoated Sample 8

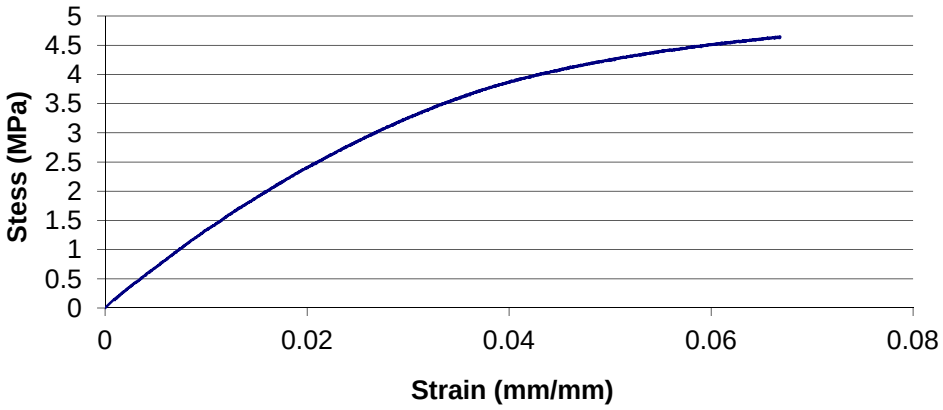

Figure A.32. Tensile Uncoated Sample 9

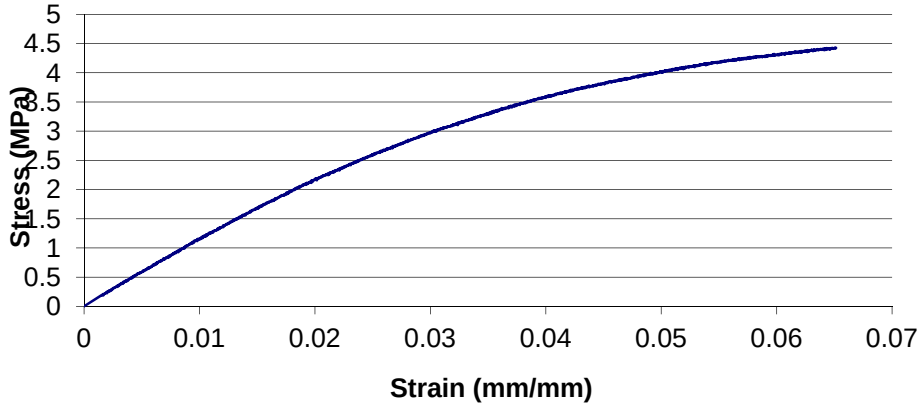

Figure A.33. Tensile Uncoated Sample 10

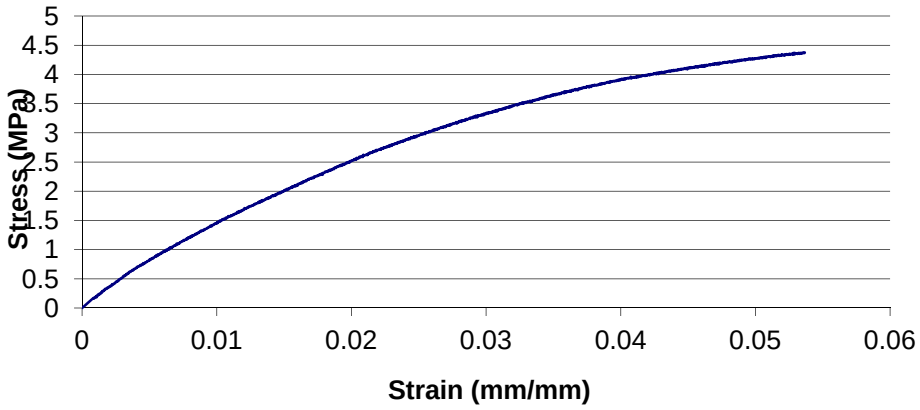

Figure A.34. Tensile Uncoated Sample 11

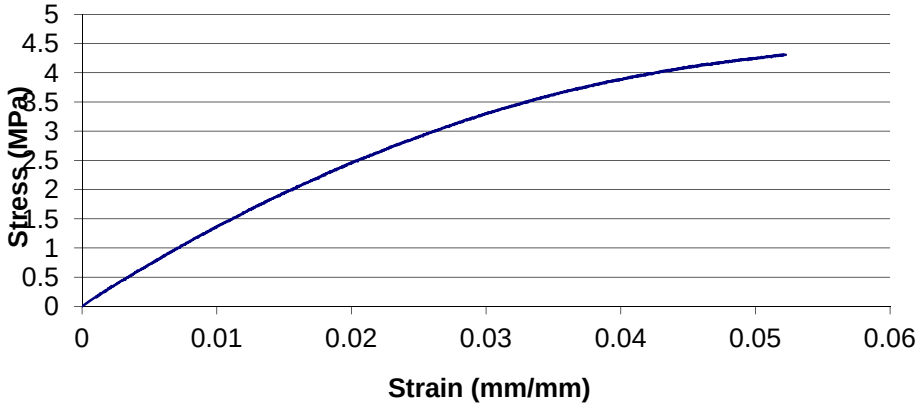

Figure A.35. Tensile Uncoated Sample 12

This section presents the flexural load-extension graphs of the loggerhead carapace

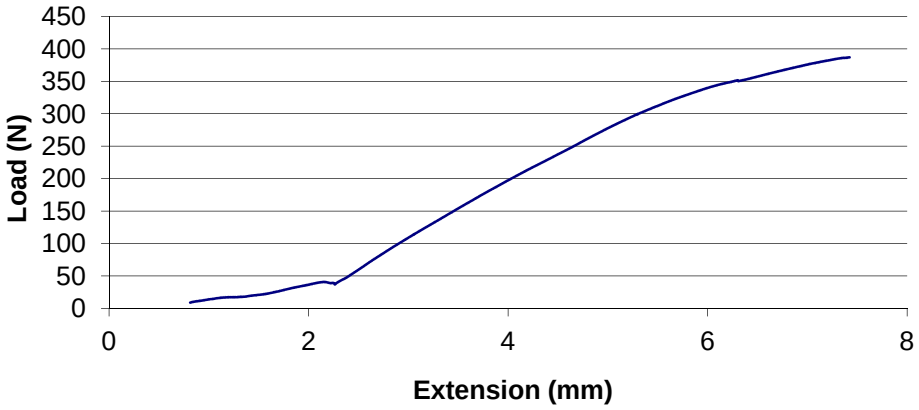

Figure A.36. Real Carapace Flexure Sample L1

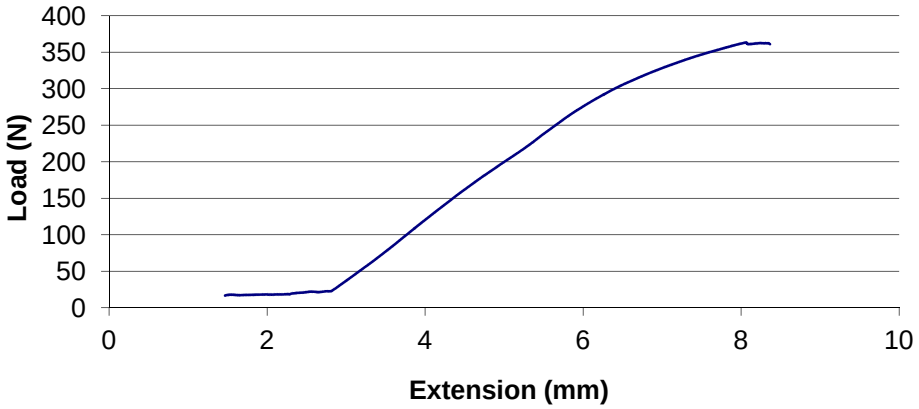

Figure A.37. Real Carapace Flexure Sample L7

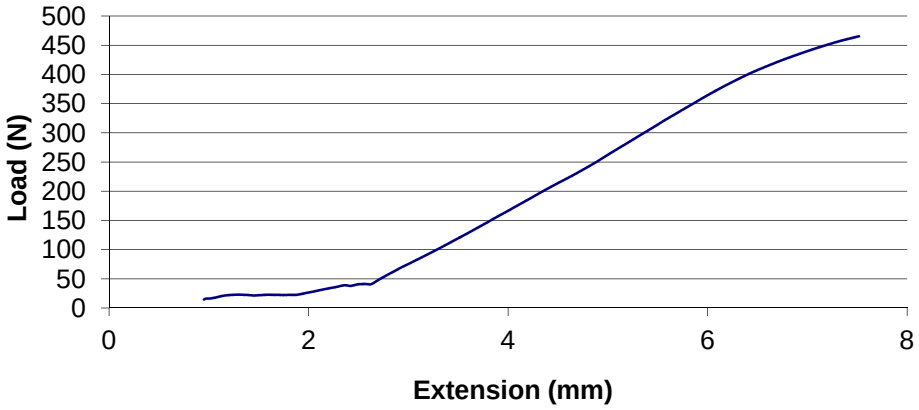

Figure A.38. Real Carapace Flexure Sample R5

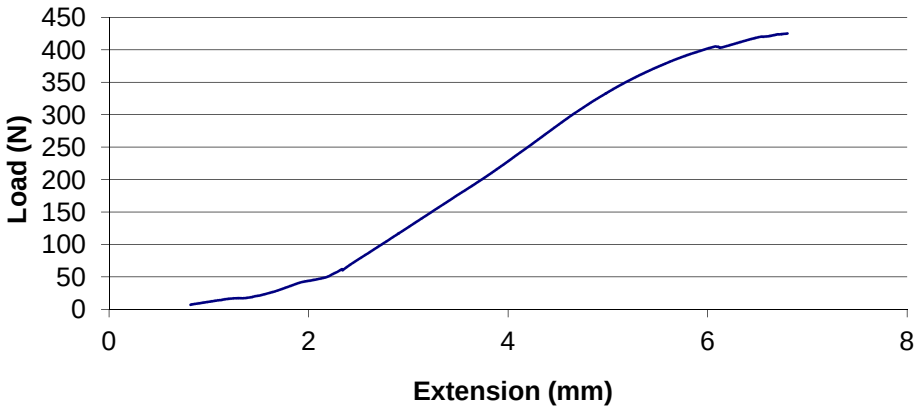

Figure A.39. Real Carapace Flexure Sample R6

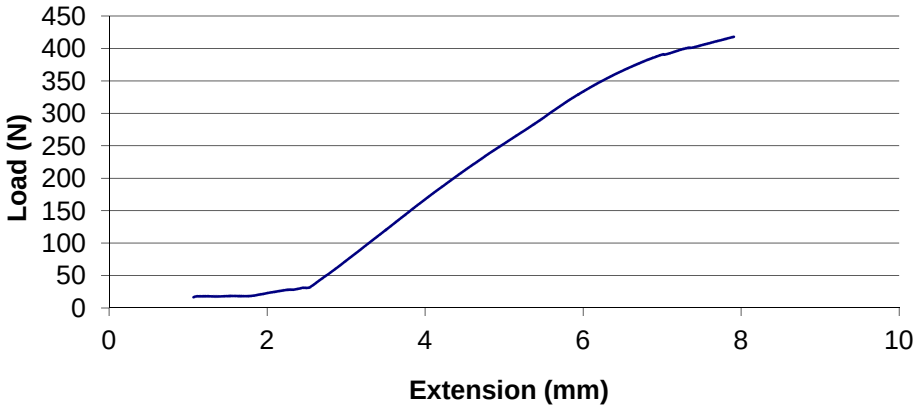

Figure A.40. Real Carapace Flexure Sample R7

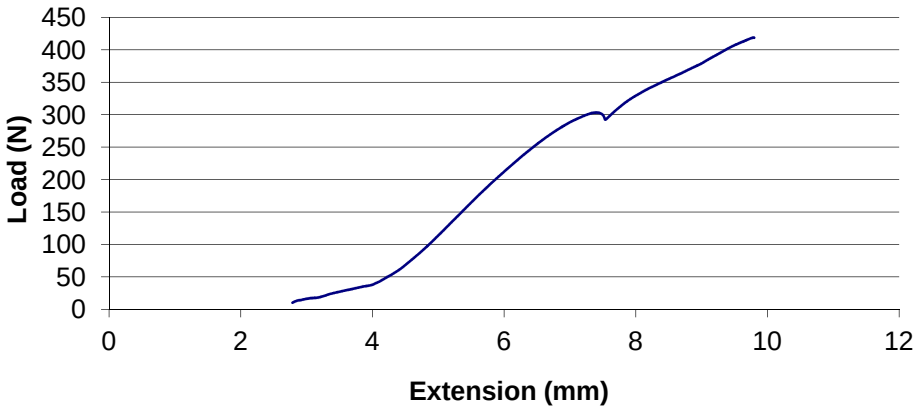

Figure A.41. Real Carapace Flexure Sample R8

This section presents the flexural load-extension graphs of rectangular coupons of the composite material system

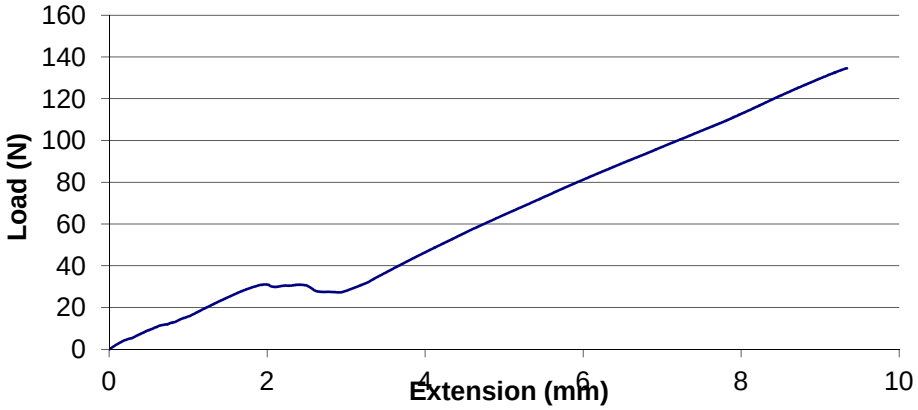

Figure A.42. Flexure Coated Foam Sample 1

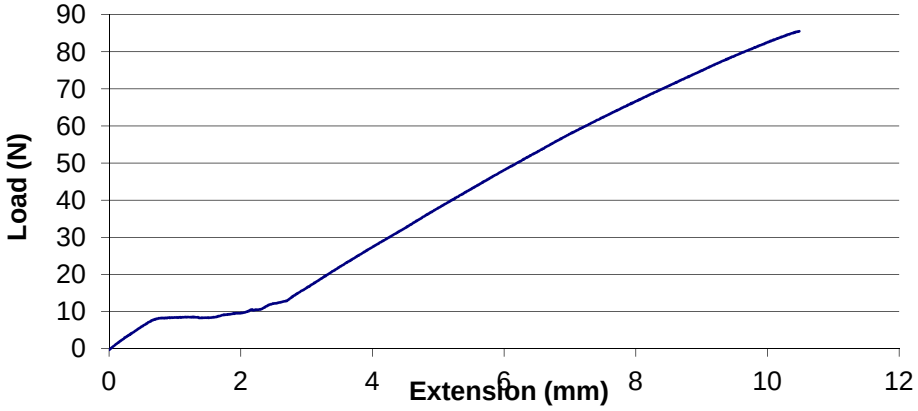

Figure A.43. Flexure Coated Foam Sample 2

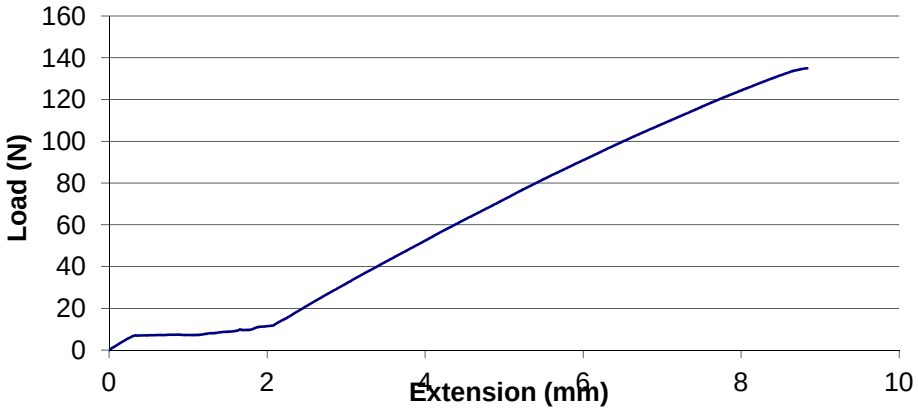

Figure A.44. Flexure Coated Foam Sample 3

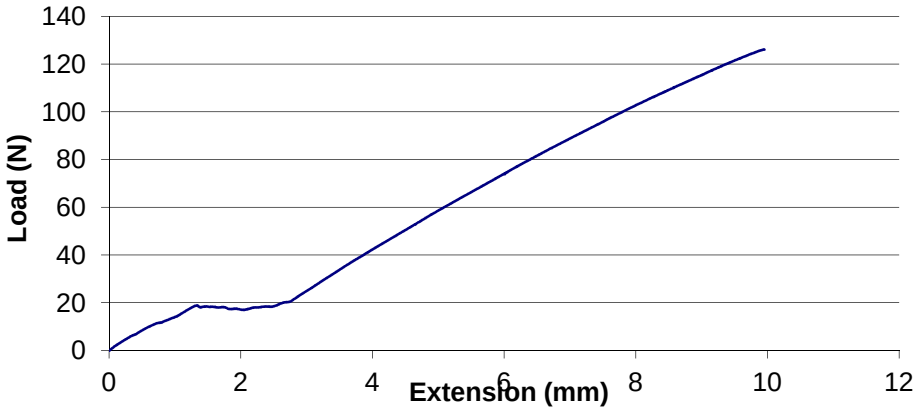

Figure A.45. Flexure Coated Foam Sample 4

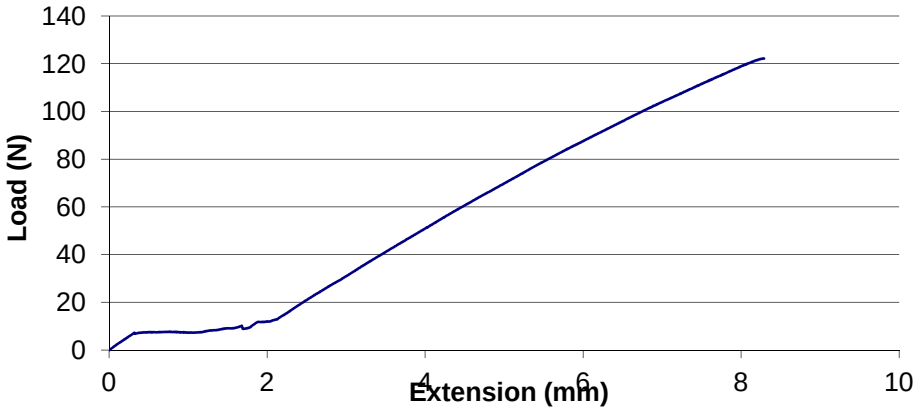

Figure A.46. Flexure Coated Foam Sample 5

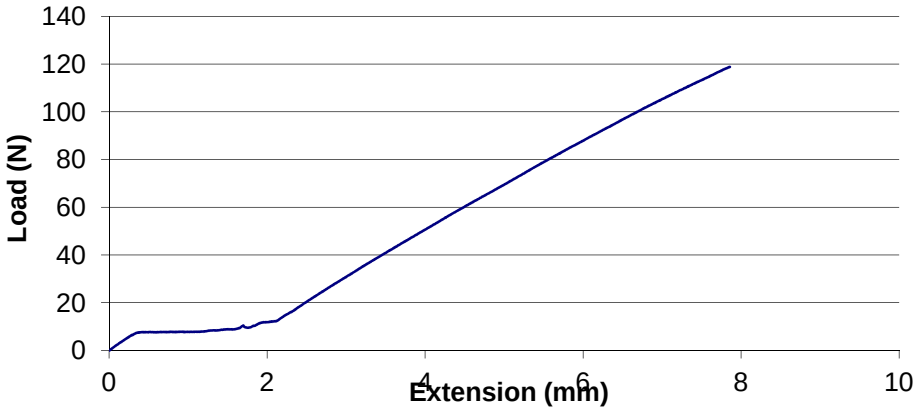

Figure A.47. Flexure Coated Foam Sample 6

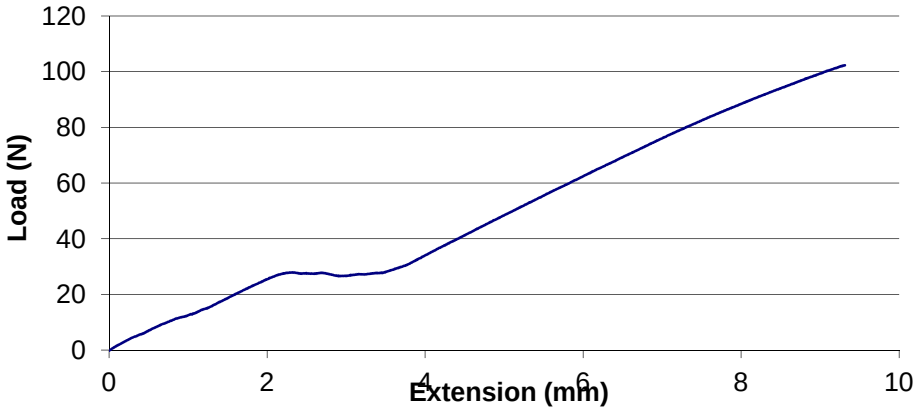

Figure A.48. Flexure Coated Foam Sample 7

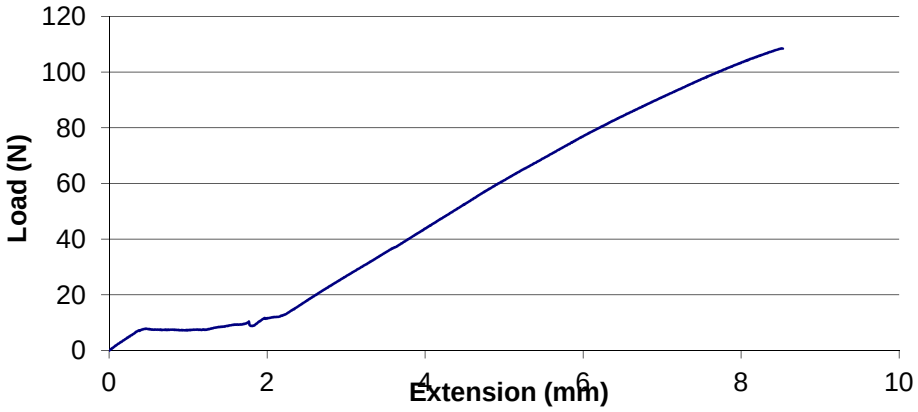

Figure A.49. Flexure Coated Foam Sample 8

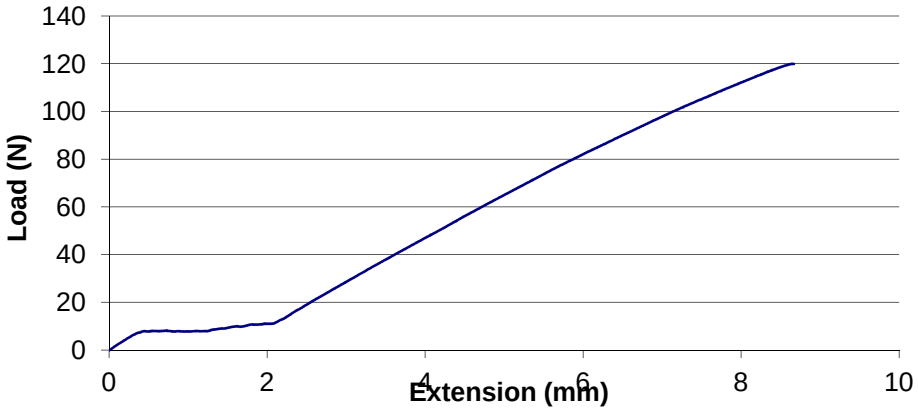

Figure A.50. Flexure Coated Foam Sample 9

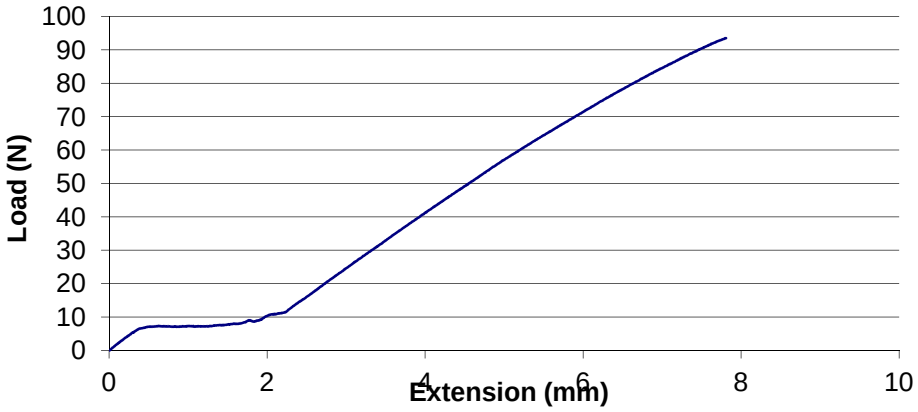

Figure A.51. Flexure Coated Foam Sample 10

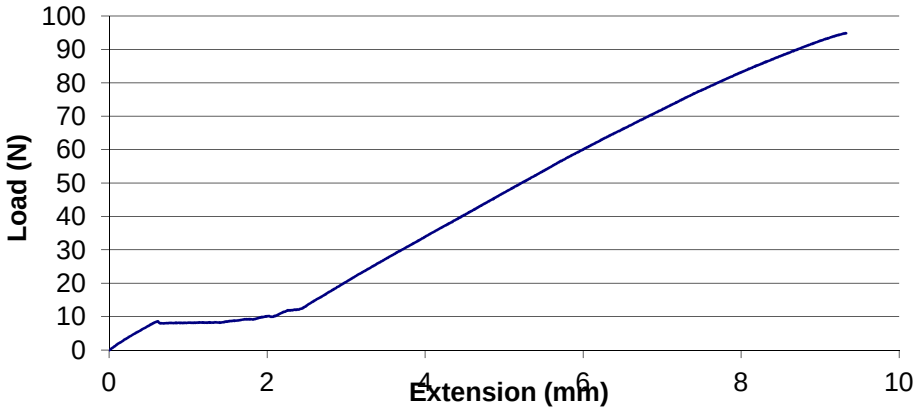

Figure A.52. Flexure Coated Foam Sample 11

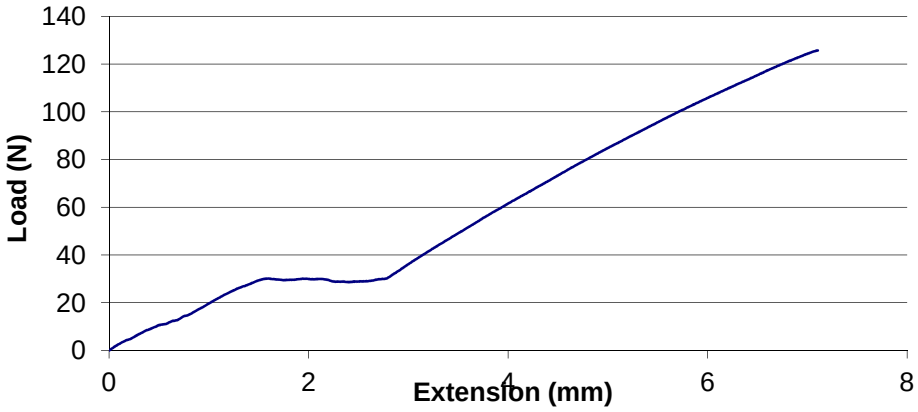

Figure A.53. Flexure Coated Foam Sample 12

This section presents the tensile stress-strain graphs of rectangular coupons of the composite material system

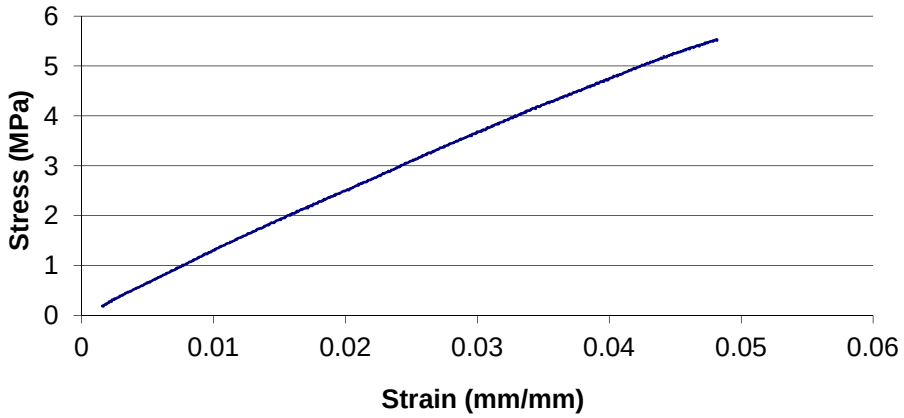

Figure A.54. Tensile Coated Foam Sample 6

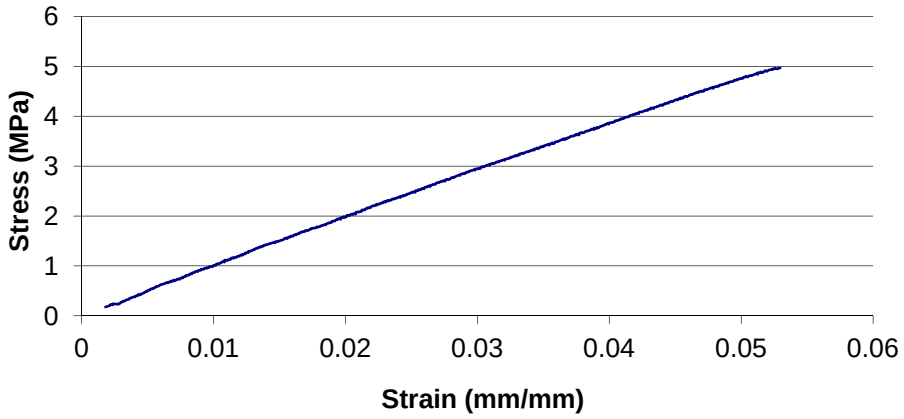

Figure A.55. Tensile Coated Foam Sample 8

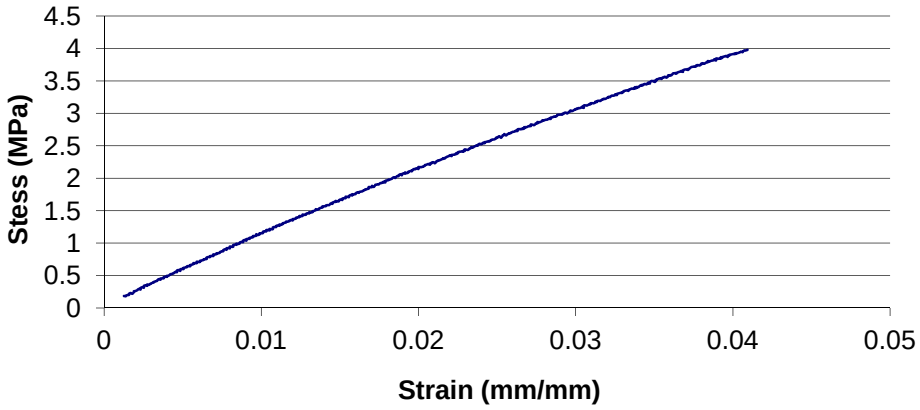

Figure A.56. Tensile Coated Foam Sample 10

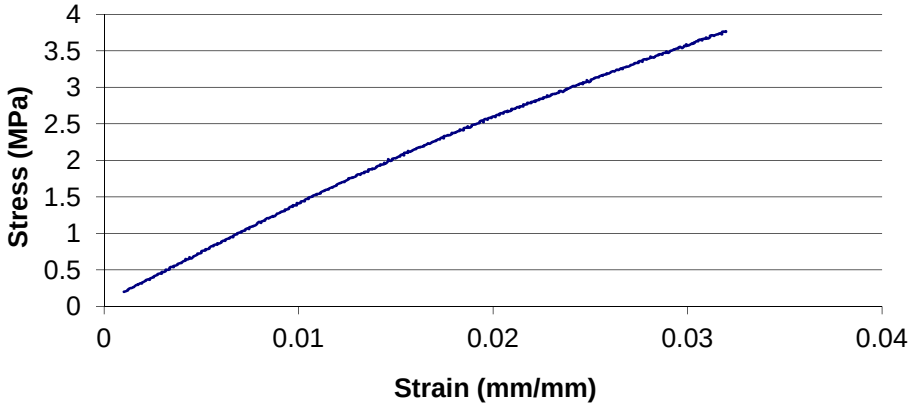

Figure A.57. Tensile Coated Foam Sample 12

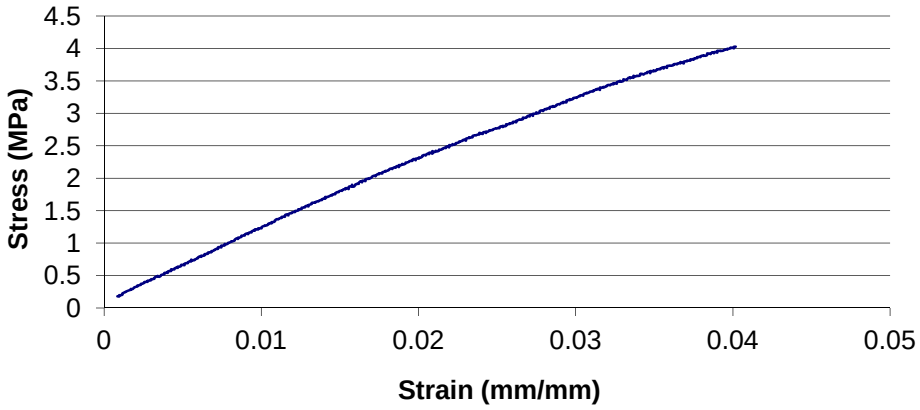

Figure A.58. Tensile Coated Foam Sample 14

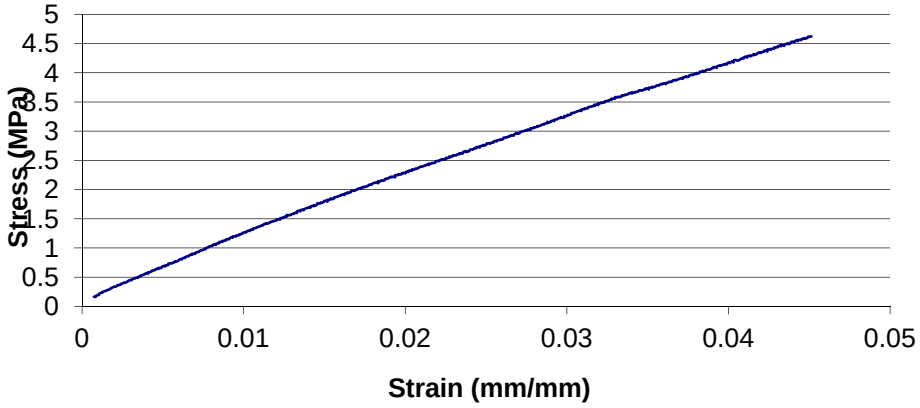

Figure A.59. Tensile Coated Foam Sample 20

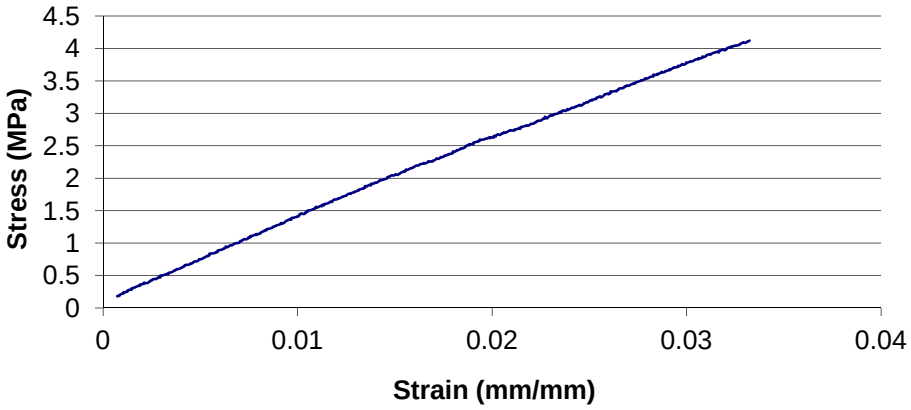

Figure A.60. Tensile Coated Foam Sample 22

This section presents the tensile stress-strain graphs of coupons of the composite material system from the artificial carapaces

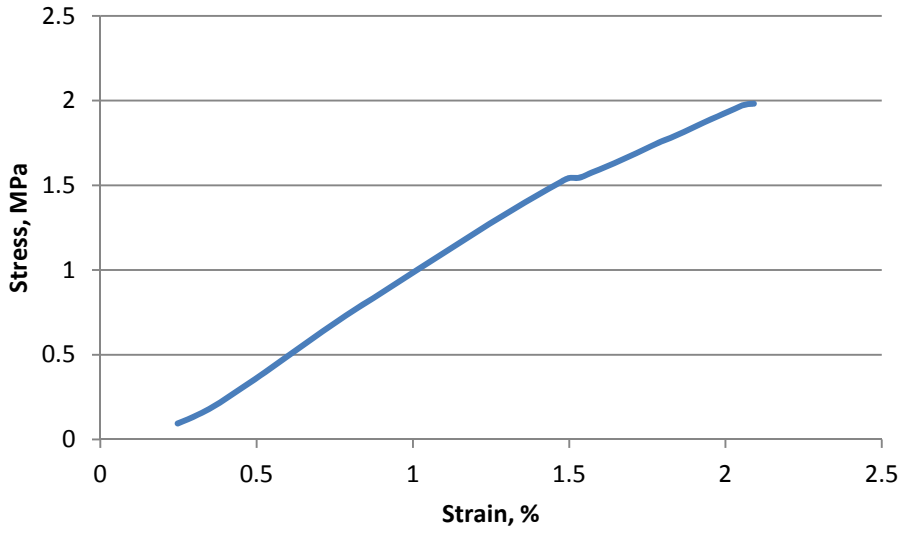

Figure A.61. Tensile Synthetic Final Sample L1-1

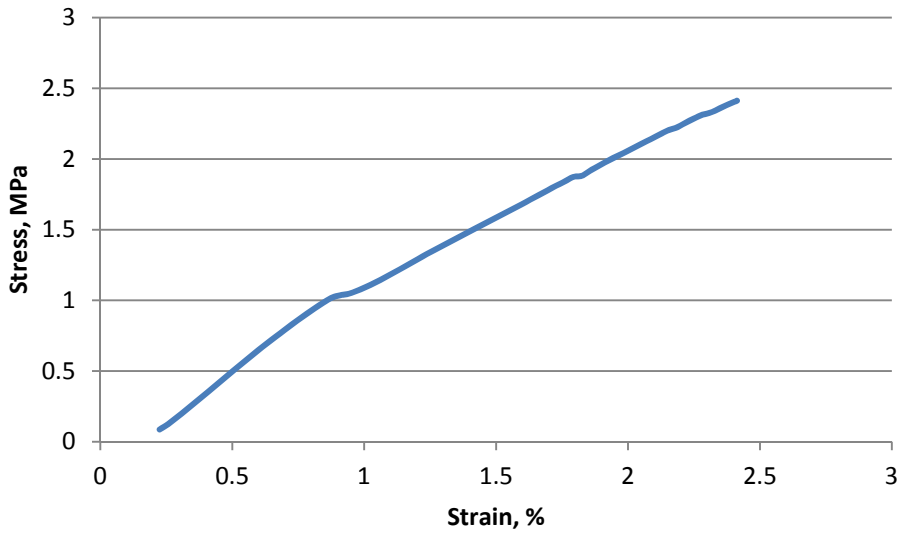

Figure A.62. Tensile Synthetic Final Sample L1-2

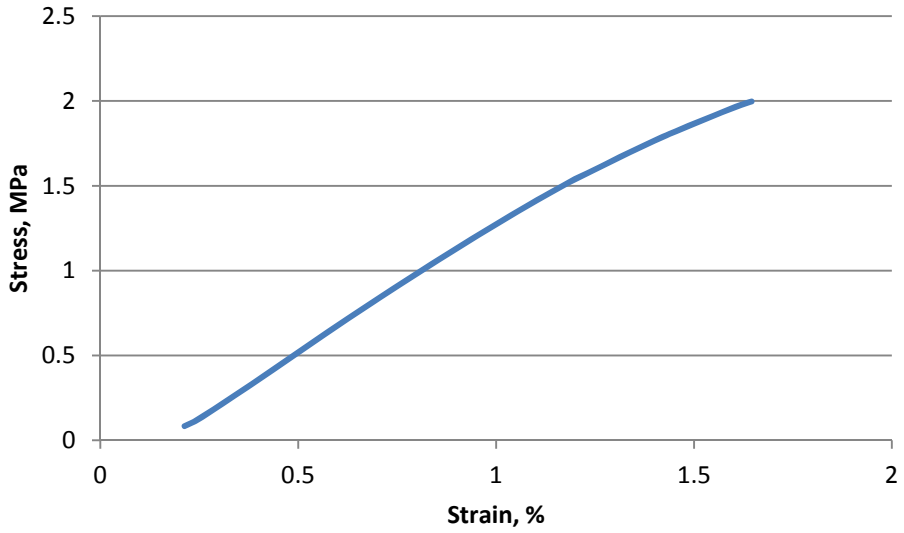

Figure A.63. Tensile Synthetic Final Sample L1-3

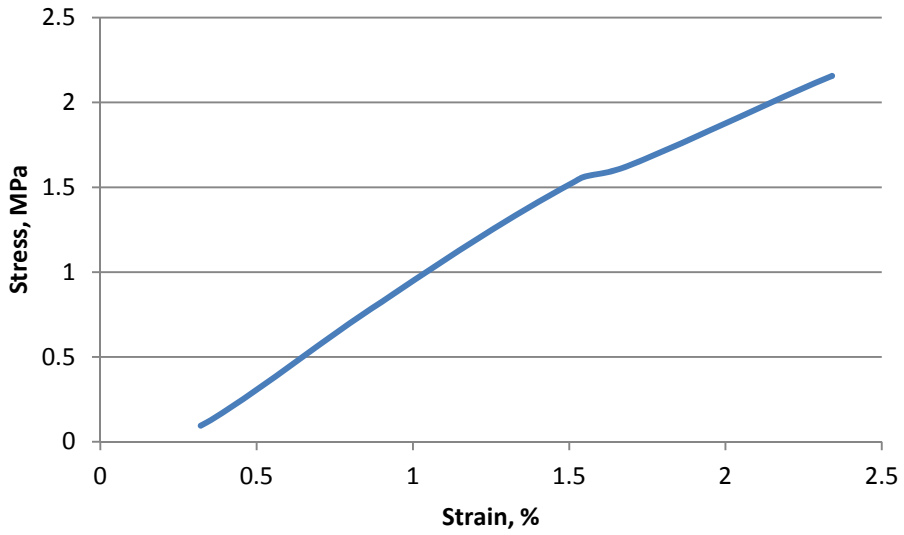

Figure A.64. Tensile Synthetic Final Sample L1-4

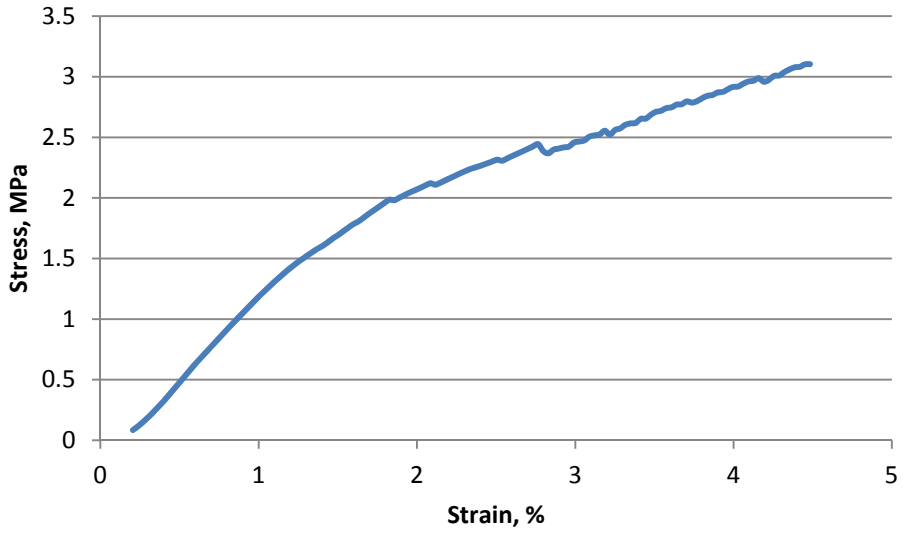

Figure A.65. Tensile Synthetic Final Sample L5-1

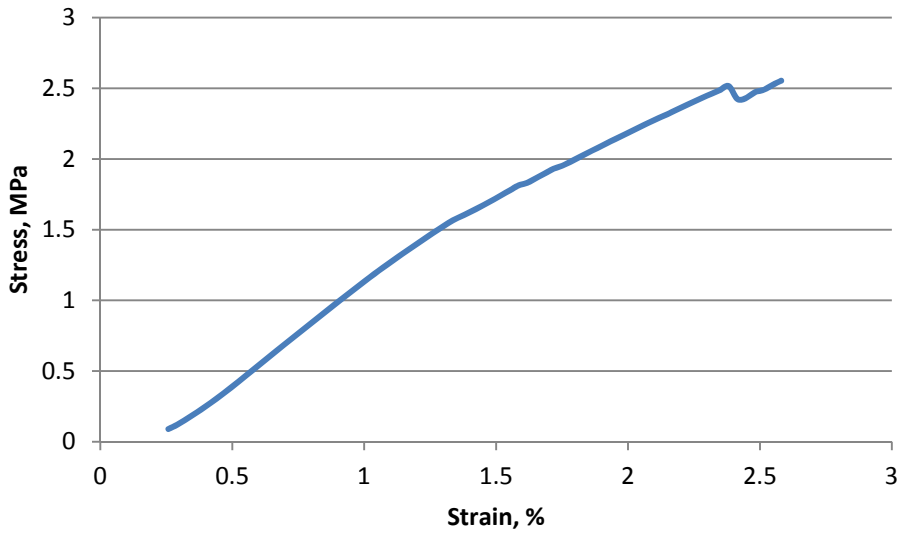

Figure A.66. Tensile Synthetic Final Sample L5-2

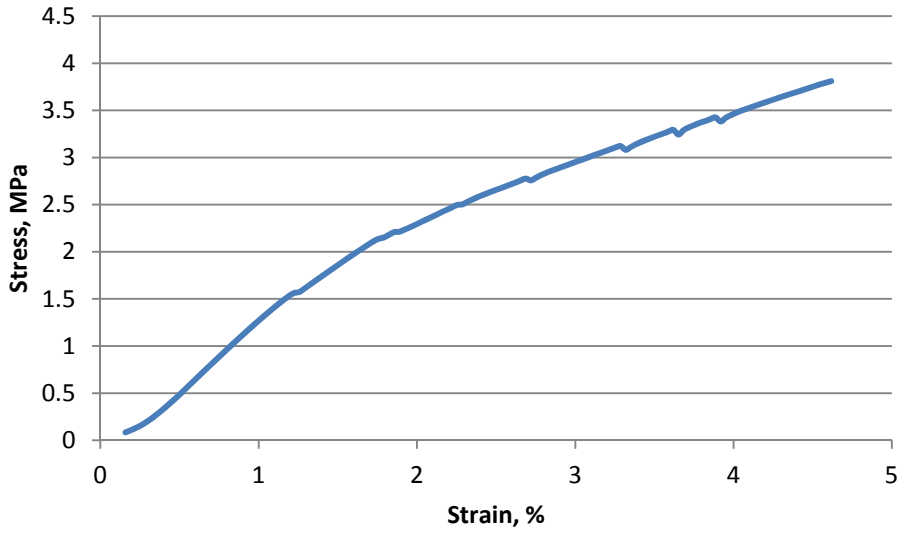

Figure A.67. Tensile Synthetic Final Sample L5-3

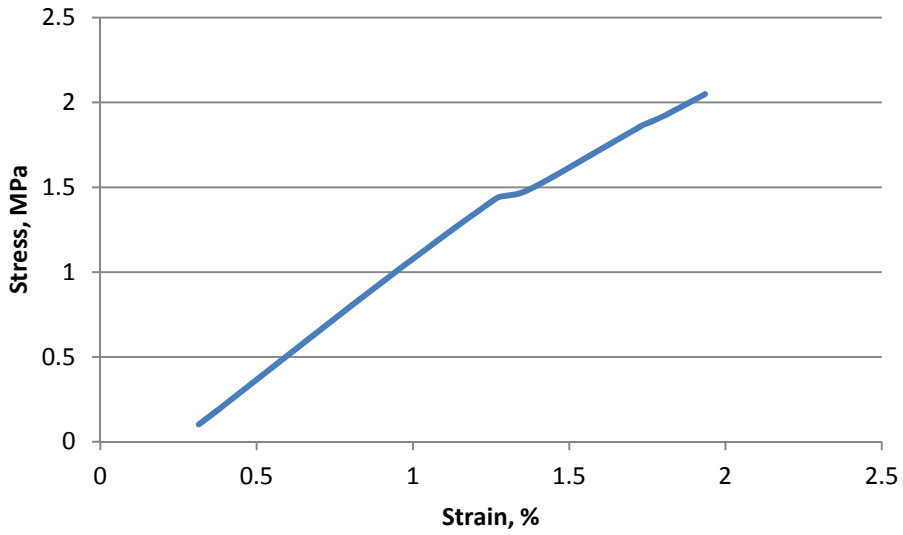

Figure A.68. Tensile Synthetic Final Sample L5-4

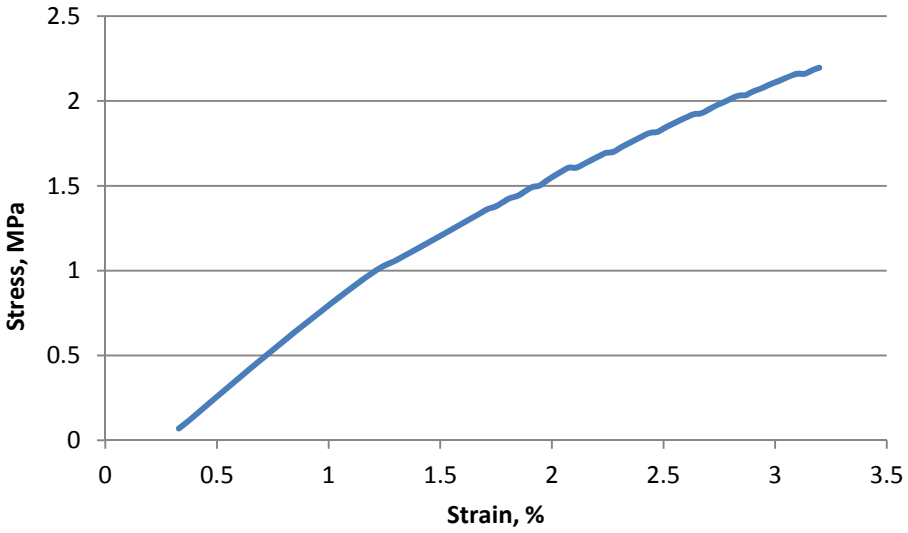

Figure A.69. Tensile Synthetic Final Sample R1-1

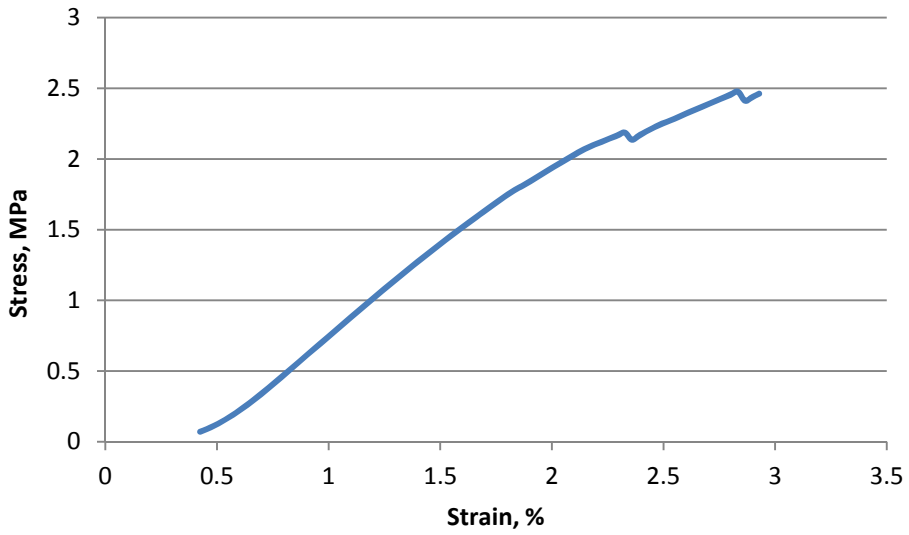

Figure A.70. Tensile Synthetic Final Sample R1-2

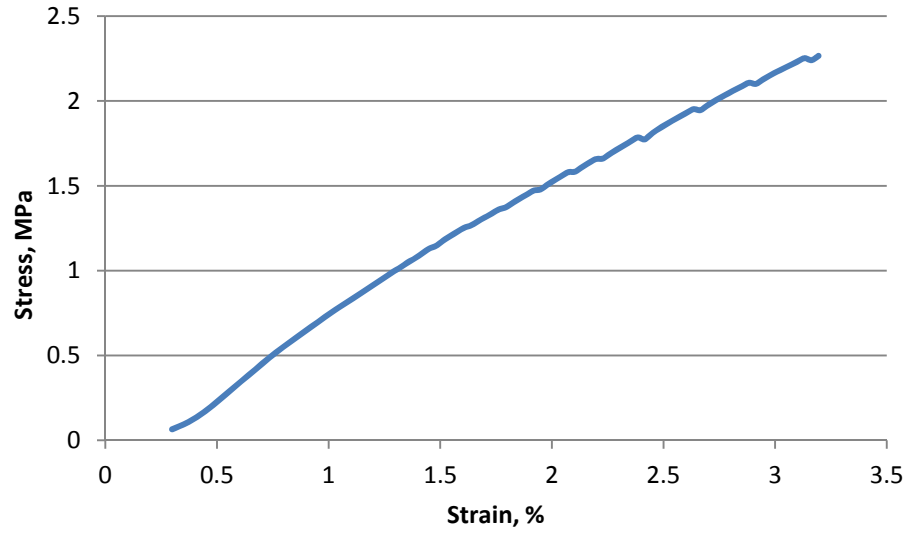

Figure A.71. Tensile Synthetic Final Sample R1-3

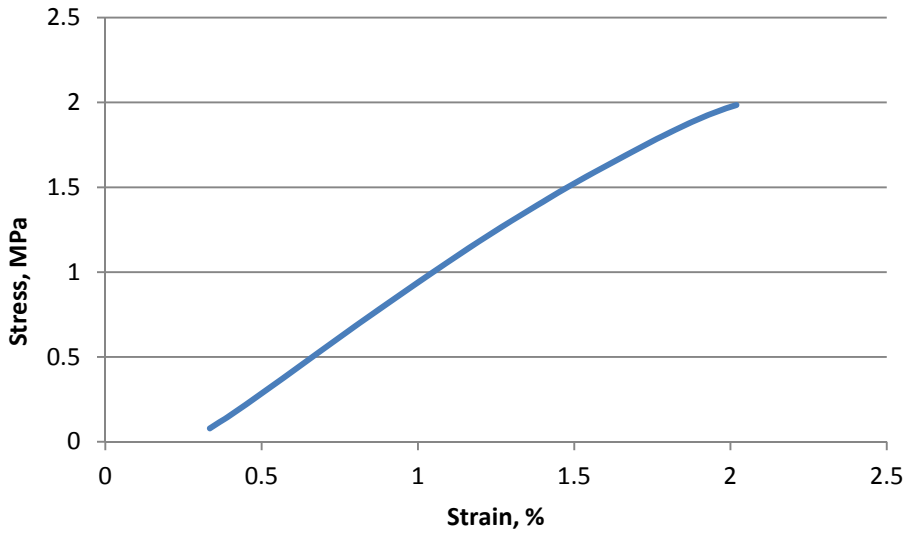

Figure A.72. Tensile Synthetic Final Sample R1-4

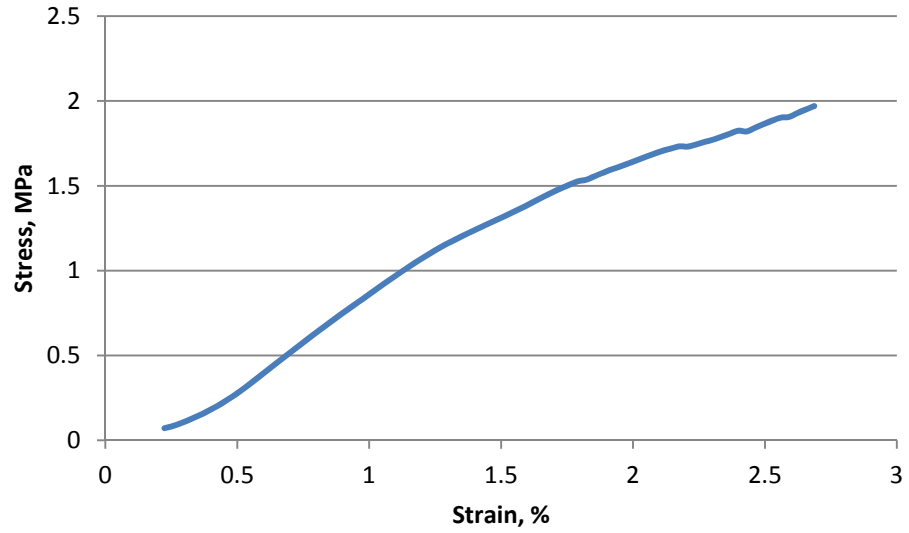

Figure A.73. Tensile Synthetic Final Sample R2-1

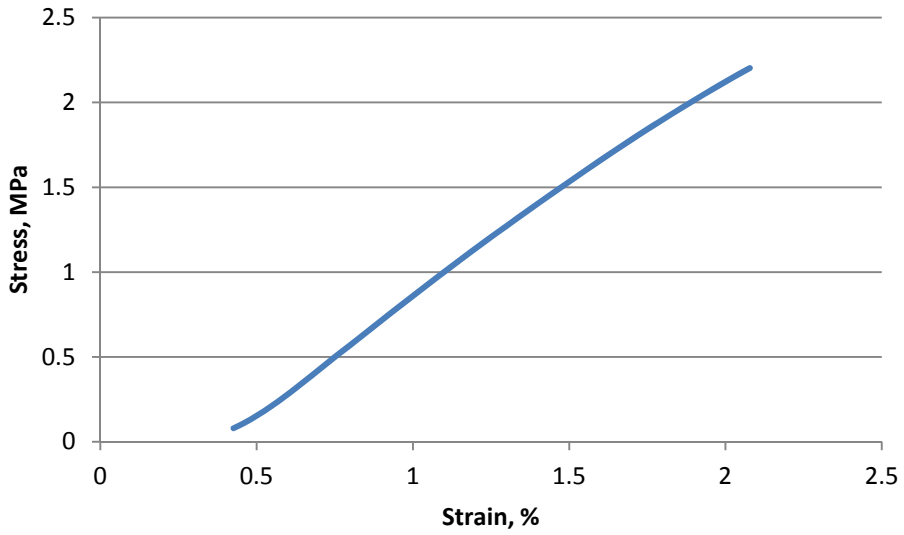

Figure A.74. Tensile Synthetic Final Sample R2-2

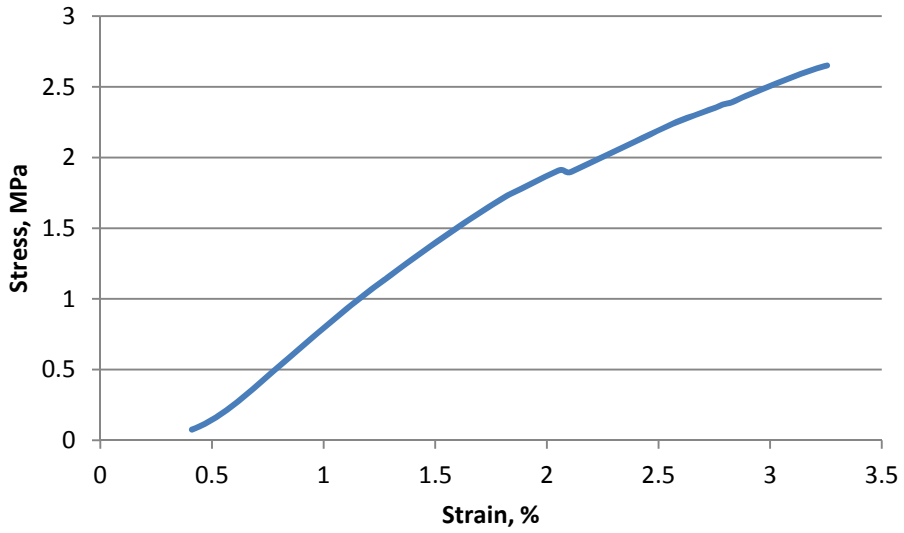

Figure A.75. Tensile Synthetic Final Sample R2-3

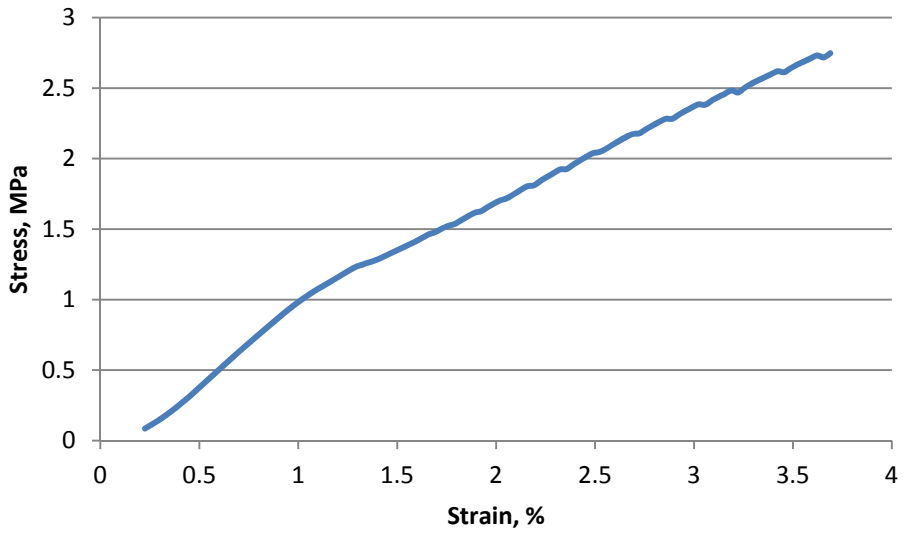

Figure A.76. Tensile Synthetic Final Sample R2-4

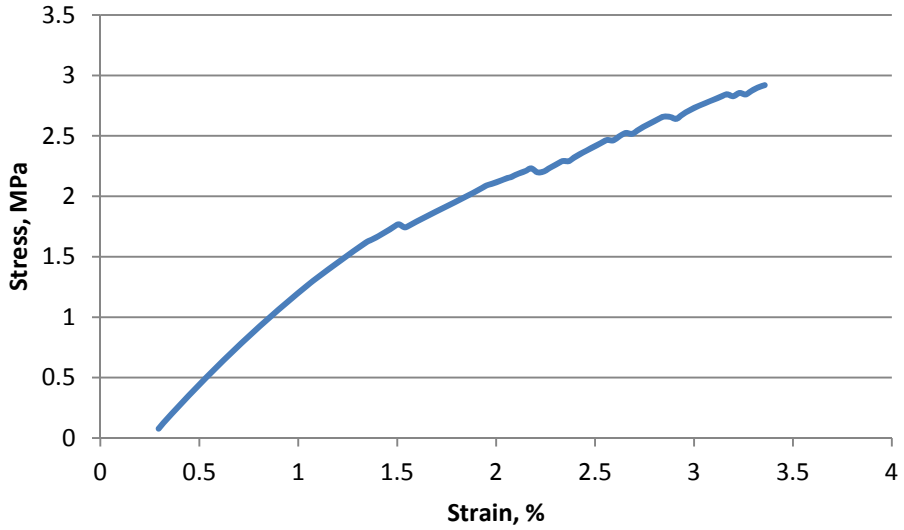

Figure A.77. Tensile Synthetic Final Sample R5-1

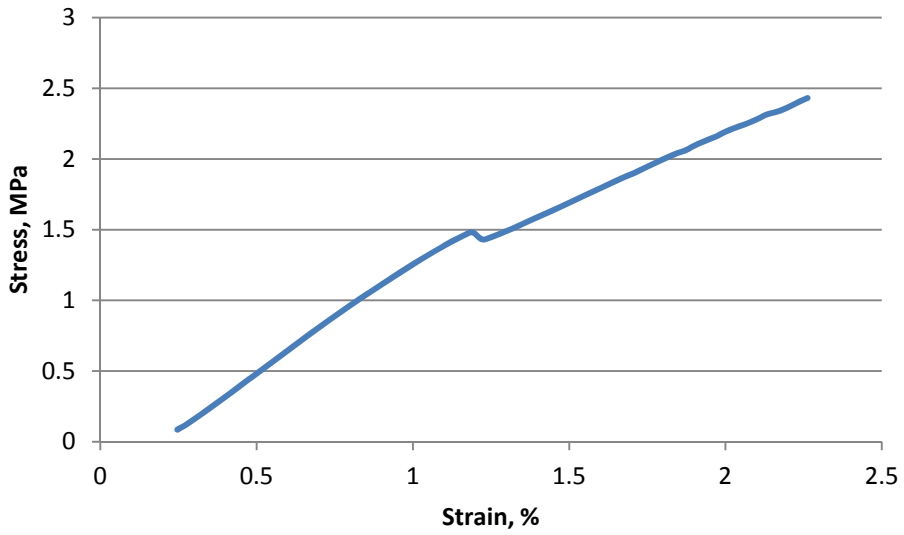

Figure A.78. Tensile Synthetic Final Sample R5-2

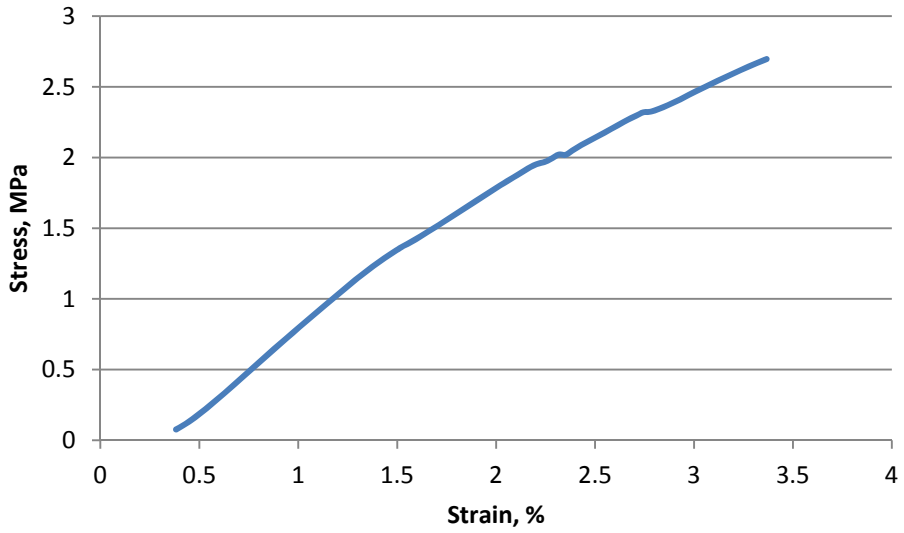

Figure A.79. Tensile Synthetic Final Sample R5-3

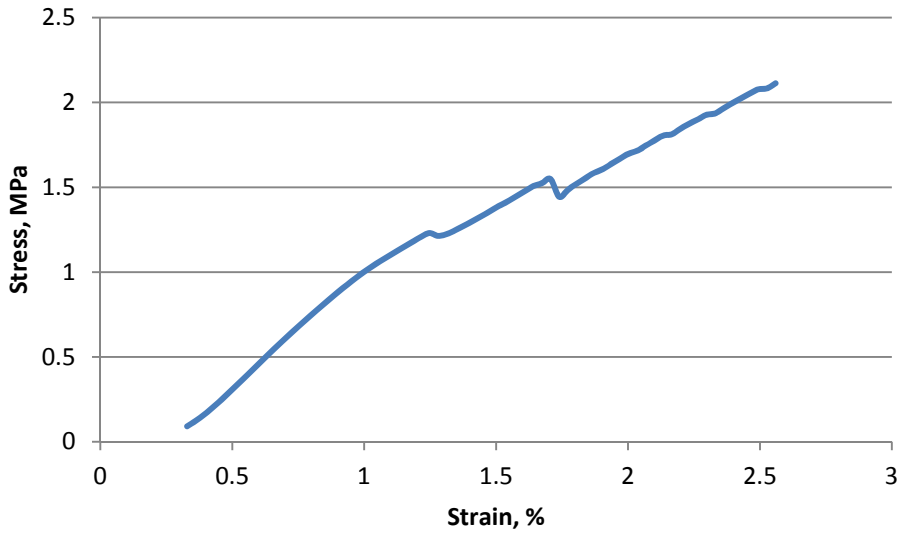

Figure A.80. Tensile Synthetic Final Sample R5-4

This section presents the flexural load-extension graphs of coupons of the composite material system from the artificial carapaces

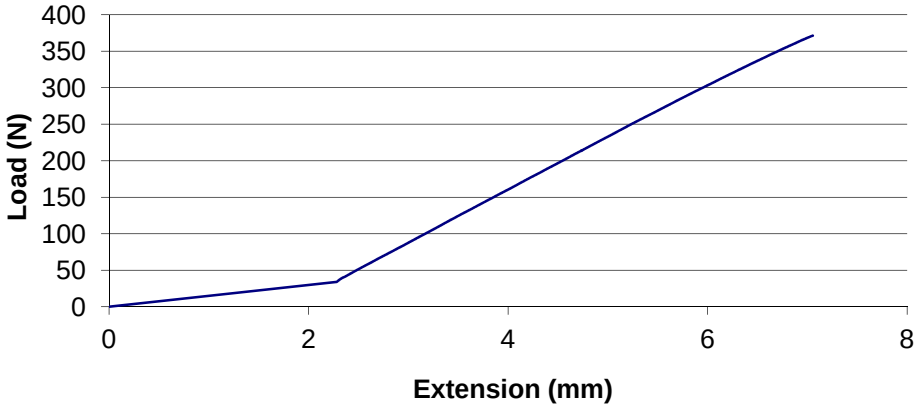

Figure A.81. Flexure Synthetic Final Sample L2-1

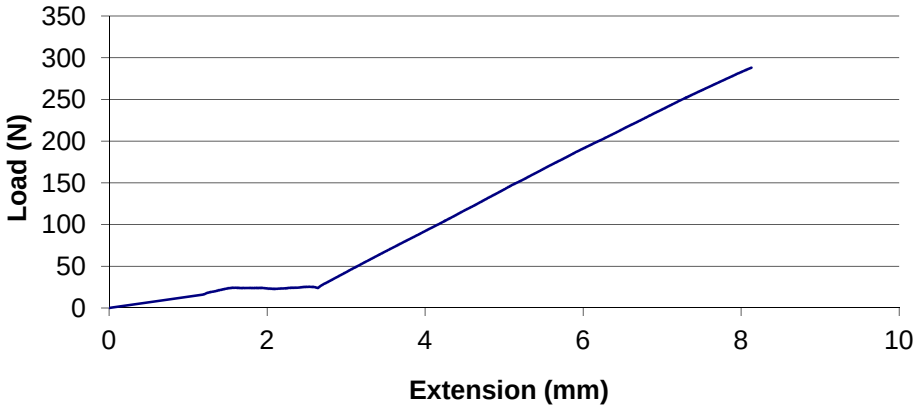

Figure A.82. Flexure Synthetic Final Sample L2-2

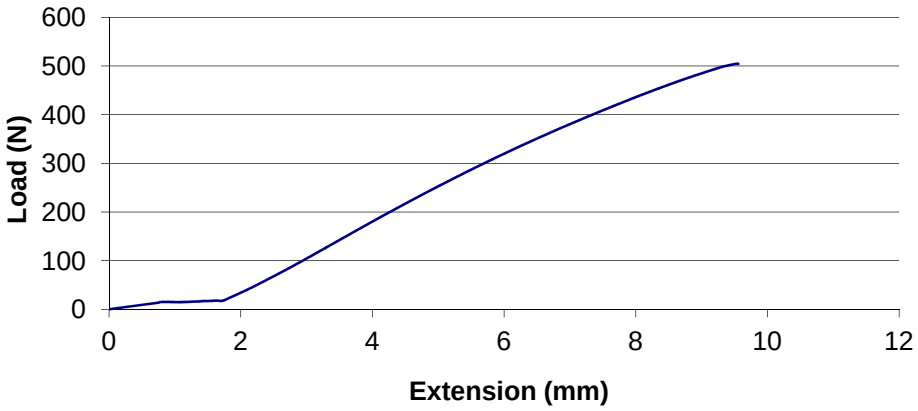

Figure A.83. Flexure Synthetic Final Sample L2-3

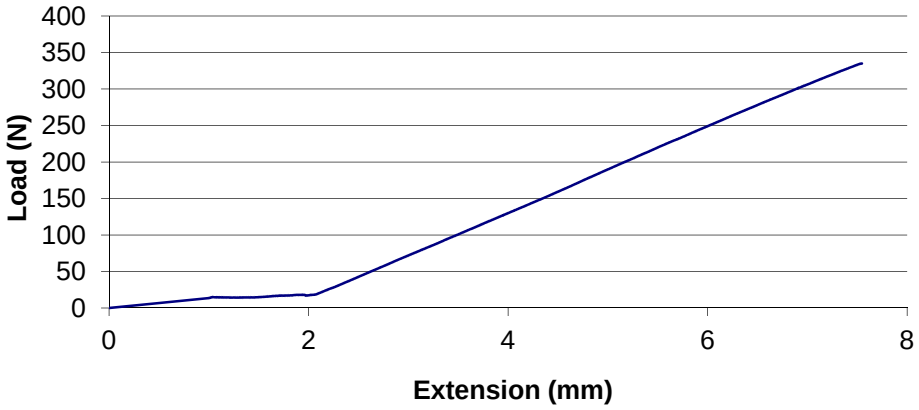

Figure A.84. Flexure Synthetic Final Sample L2-4

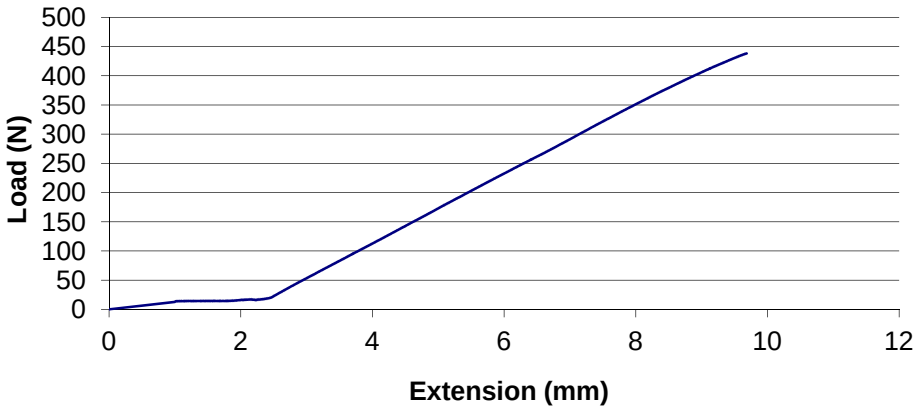

Figure A.85. Flexure Synthetic Final Sample L3-1

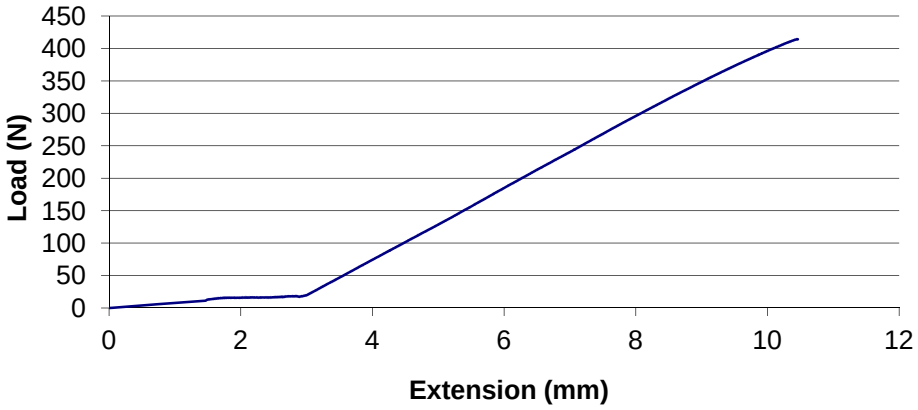

Figure A.86. Flexure Synthetic Final Sample L3-2

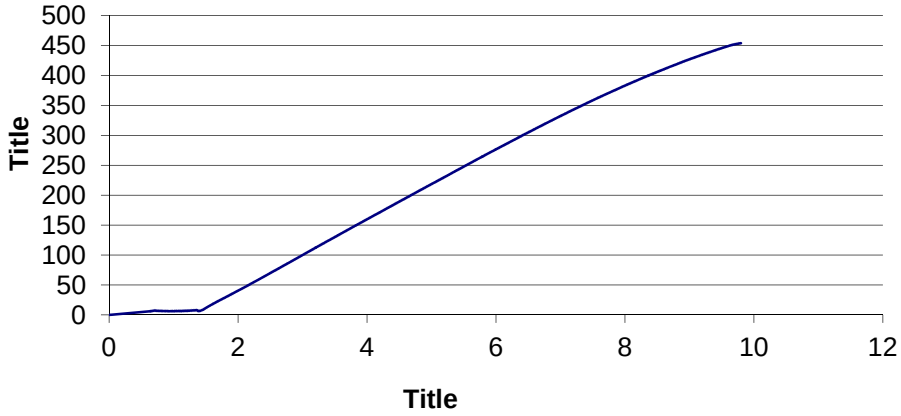

Figure A.87. Flexure Synthetic Final Sample L3-3

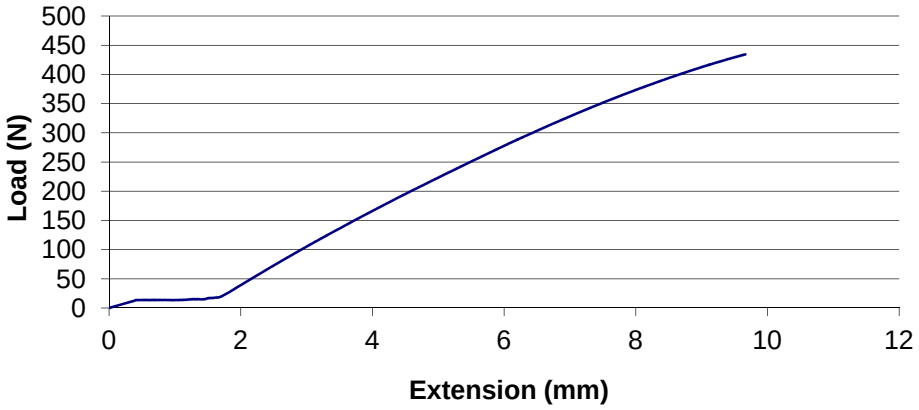

Figure A.88. Flexure Synthetic Final Sample L3-4

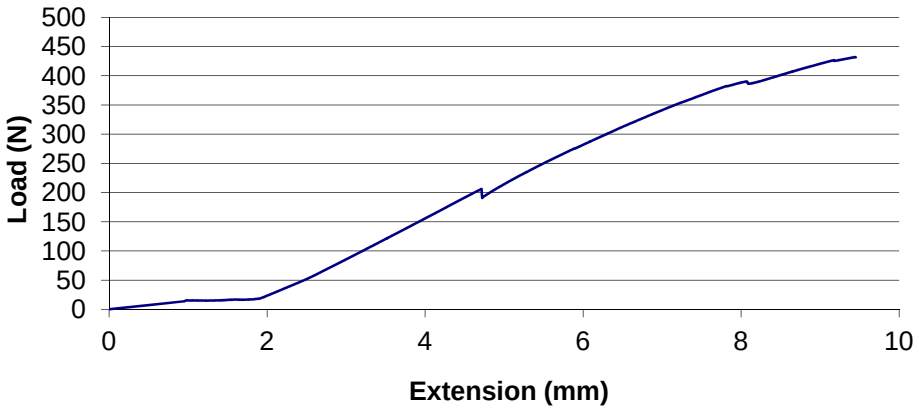

Figure A.89. Flexure Synthetic Final Sample L4-1

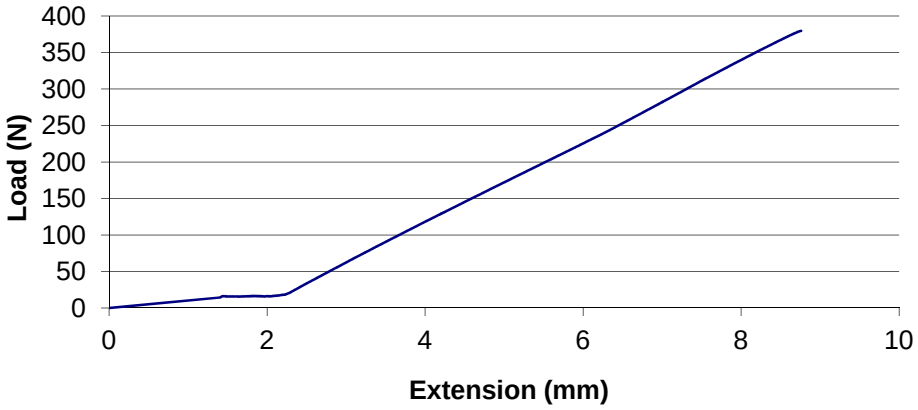

Figure A.90. Flexure Synthetic Final Sample L4-2

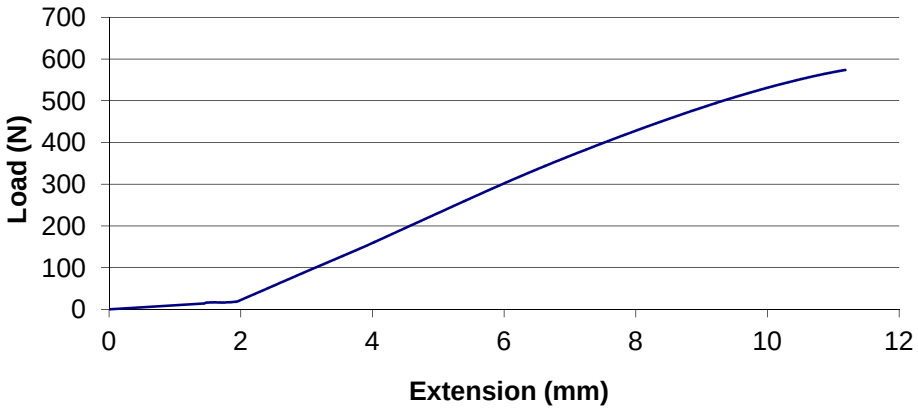

Figure A.91. Flexure Synthetic Final Sample L4-3

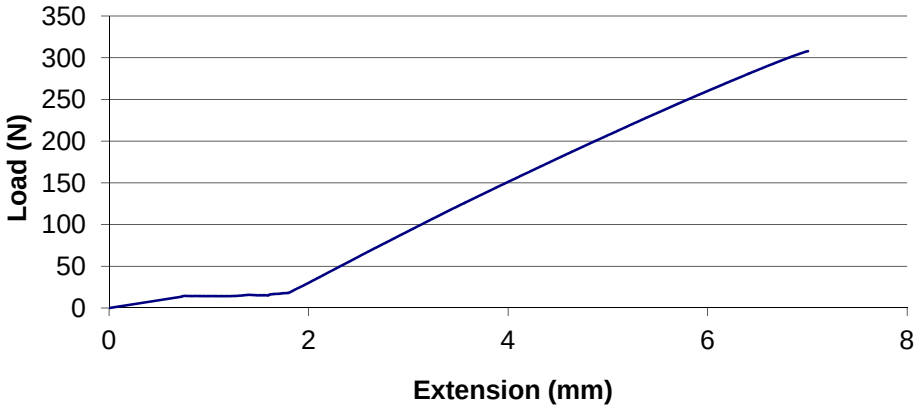

Figure A.92. Flexure Synthetic Final Sample L4-4

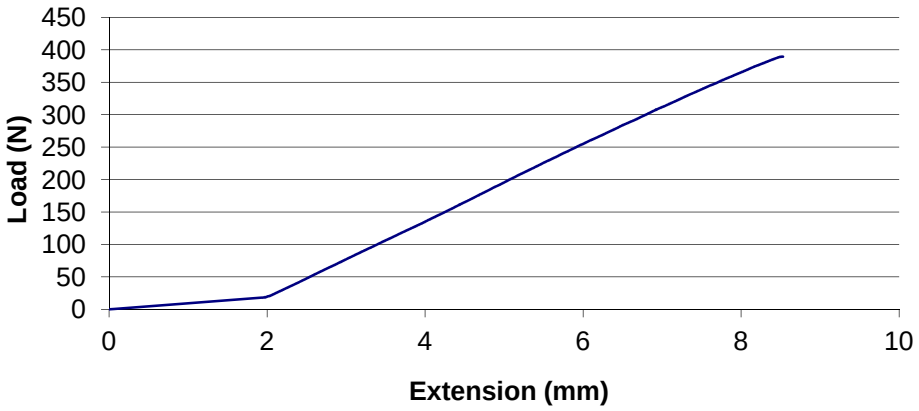

Figure A.93. Flexure Synthetic Final Sample R3-1

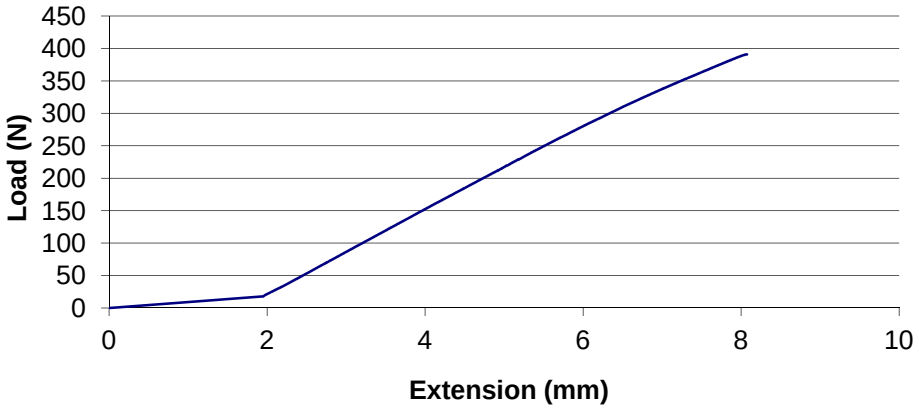

Figure A.94. Flexure Synthetic Final Sample R3-2

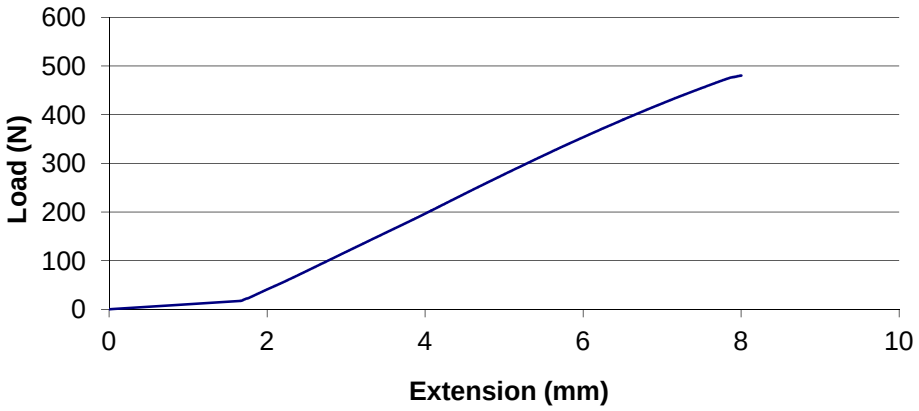

Figure A.95. Flexure Synthetic Final Sample R3-3

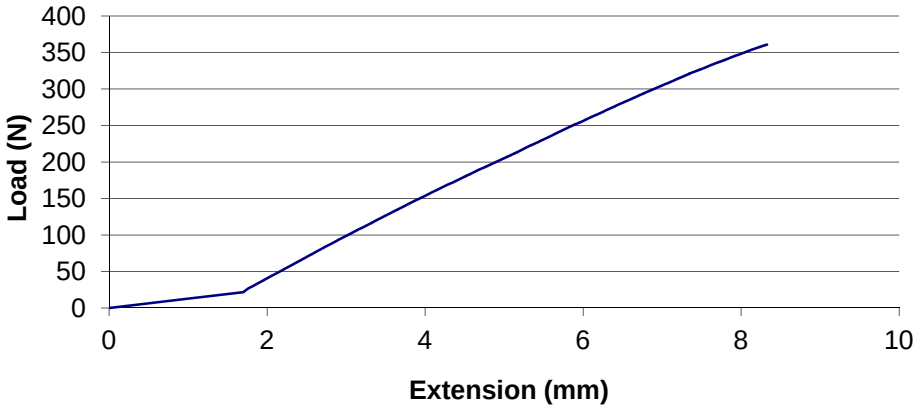

Figure A.96. Flexure Synthetic Final Sample R3-4

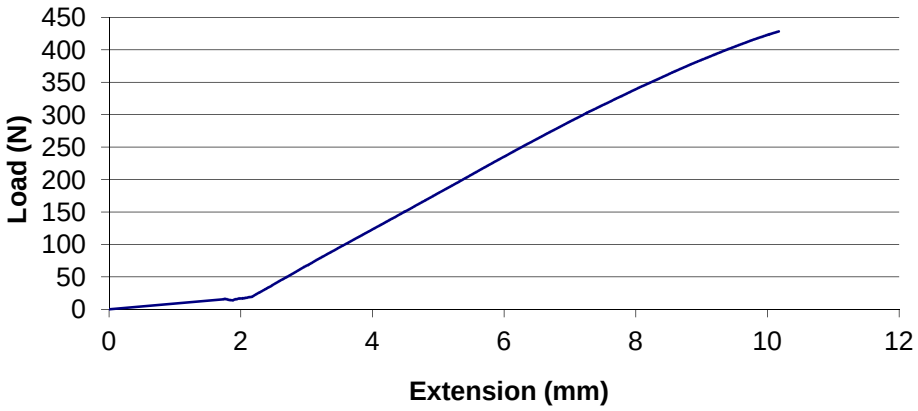

Figure A.97. Flexure Synthetic Final Sample R4-2

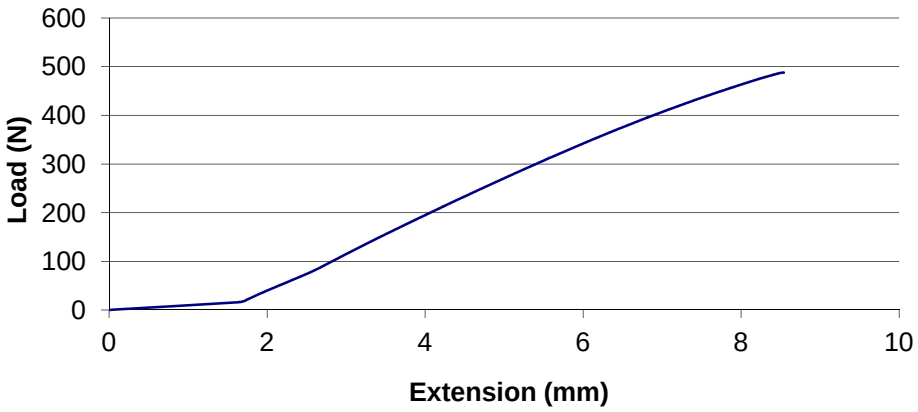

Figure A.98. Flexure Synthetic Final Sample R4-3

APPENDIX B

DATA SHEETS FROM FIELD TESTING

The data sheets from each field test are ordered chronologically and include the test number, vessel number, model depth in the water, and a description/sketch of the damage.

Data Collection Sheet

Shell #: 1 Time: 10:15:45 Date: 8/1/11

Accel. #: 1 Boat Type: JET Depth: PROP

Boat Speed (km/hr): 25 Orientation: 5:00

Type of wound (Blunt trauma, prop cut): _____

Size/Location of cuts/damage:

Sketch of damage:

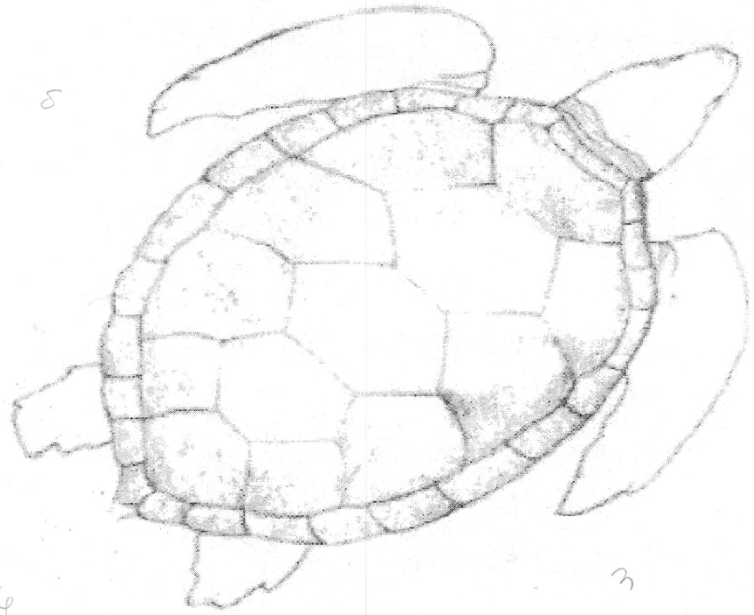

Comments:

Figure B.1. Data sheet for Shell 1

Data Collection Sheet

Shell #: 2 Time: 10:21:03 Date: 8/1/11

Accel. #: 1 Boat Type: JET Depth: PROP

Boat Speed (km/hr): 26 Orientation: 9:00

Type of wound (Blunt trauma, prop cut): _____

Size/Location of cuts/damage:

Sketch of damage:

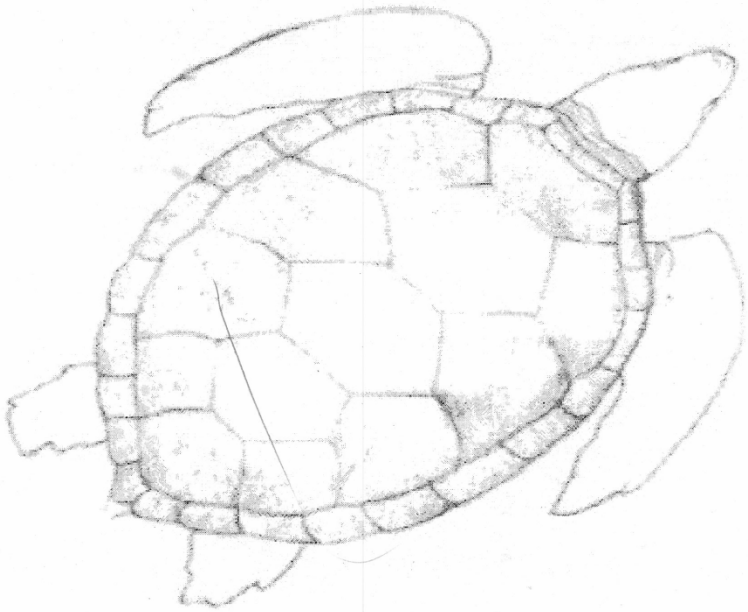

Comments:

Figure B.2. Data sheet for Shell 2

Data Collection Sheet

Shell #: 3 Time: 10:28:40 Date: 8/1/11

Accel. #: 1 Boat Type: JET Depth: PROP

Boat Speed (km/hr): 29 Orientation: 12:00

Type of wound (Blunt trauma, prop cut): _____

Size/Location of cuts/damage:

Sketch of damage:

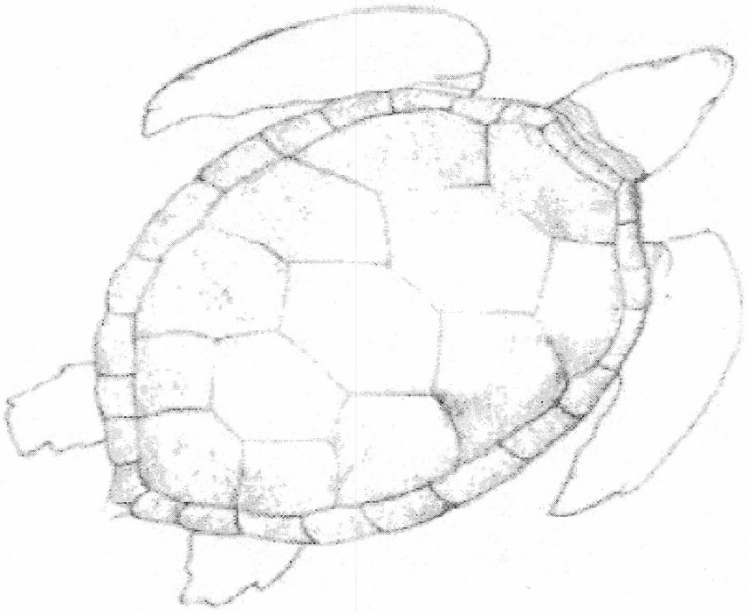

Comments:

Figure B.3. Data sheet for Shell 3

Data Collection Sheet

Shell #: 4 Time: 10:33:30 Date: 8/1/11

Accel. #: 1 Boat Type: JET Depth: PROP

Boat Speed (km/hr): 26 Orientation: 1:00

Type of wound (Blunt trauma, prop cut): _____

Size/Location of cuts/damage:

Sketch of damage:

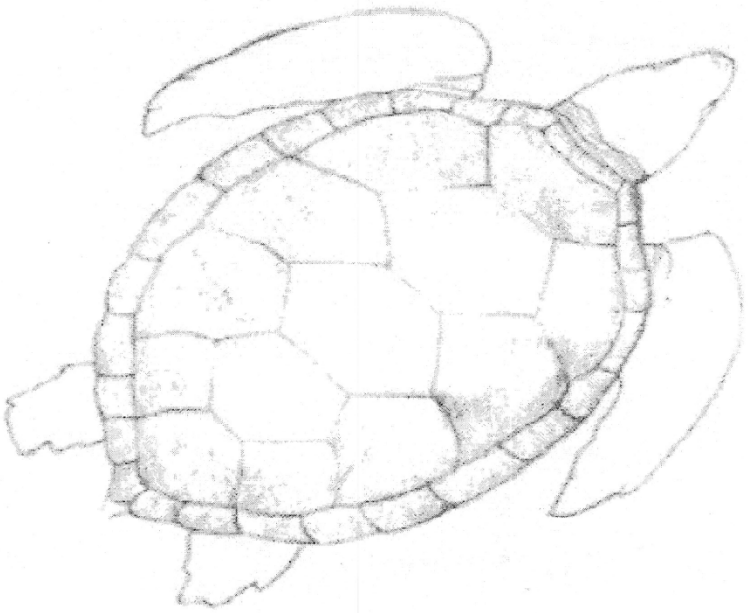

Comments:

Figure B.4. Data sheet for Shell 4

Aug 6th
1:3

Data Collection Sheet

Shell #: 5 Time: 10:38:20 Date: 8/1/2011

Accel. #: 1 Boat Type: JET Depth: PROP

Boat Speed (km/hr): 26 Orientation: 3:00

Type of wound (Blunt trauma, prop cut): _____

Size/Location of cuts/damage:

Sketch of damage:

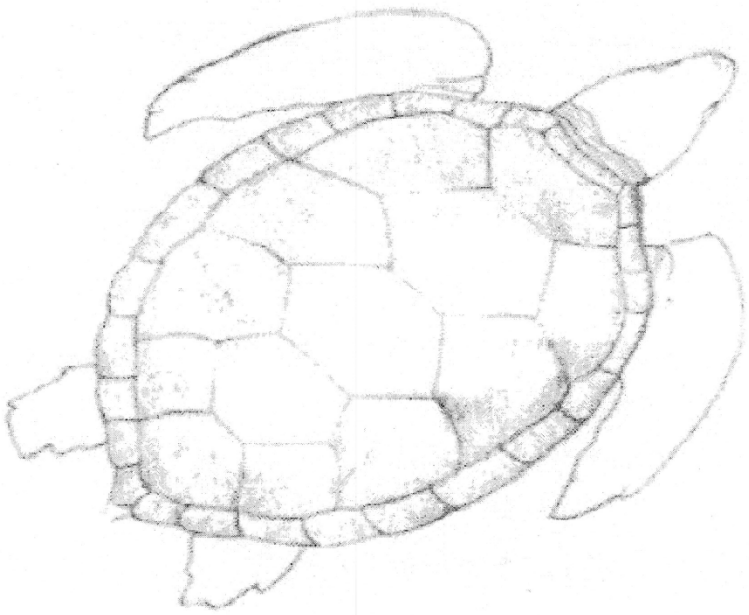

Comments:

Figure B.5. Data sheet for Shell 5

Data Collection Sheet

Shell #: 6 Time: 11:14:26 Date: 8/1/11

Accel. #: 1 Boat Type: JET Depth: SURFACE

Boat Speed (km/hr): 27 Orientation: 3:00

Type of wound (Blunt trauma, prop cut): BLUNT

Size/Location of cuts/damage:

Sketch of damage:

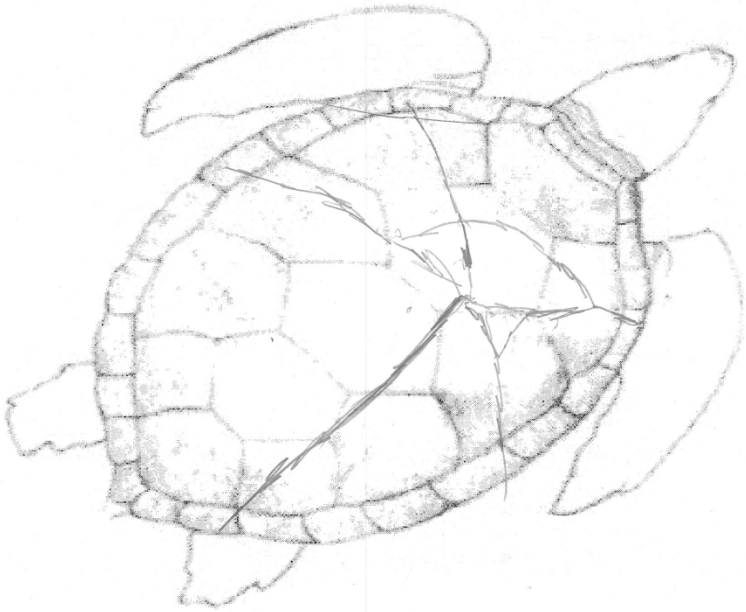

Comments:
PRE SHOT # 100-7686
100-7689
(DUBOSE)

Figure B.6. Data sheet for Shell 6

Data Collection Sheet

Shell #: 7 Time: 11:28:29 Date: 8/1

Accel. #: 1 Boat Type: JET Depth: SURFACE

Boat Speed (km/hr): 27 Orientation: 10:30

Type of wound (Blunt trauma, prop cut): NONE

Size/Location of cuts/damage:

Sketch of damage:

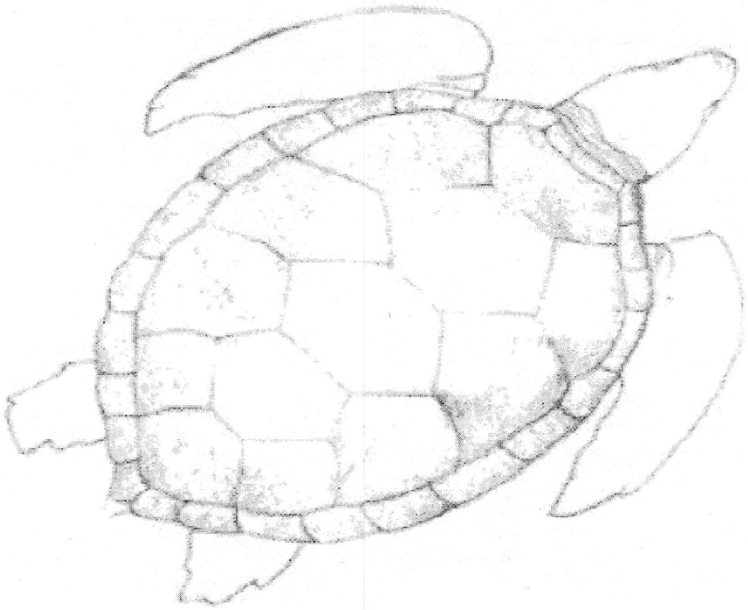

Comments:

HIT TARGET

Figure B.7. Data sheet for Shell 7

Data Collection Sheet

Shell #: 8 Time: 11:44:36 Date: 8/1

Accel. #: 1 Boat Type: JET Depth: SURFACE

Boat Speed (km/hr): 28 Orientation: 11:00

Type of wound (Blunt trauma, prop cut): BLUNT

Size/Location of cuts/damage:

Sketch of damage:

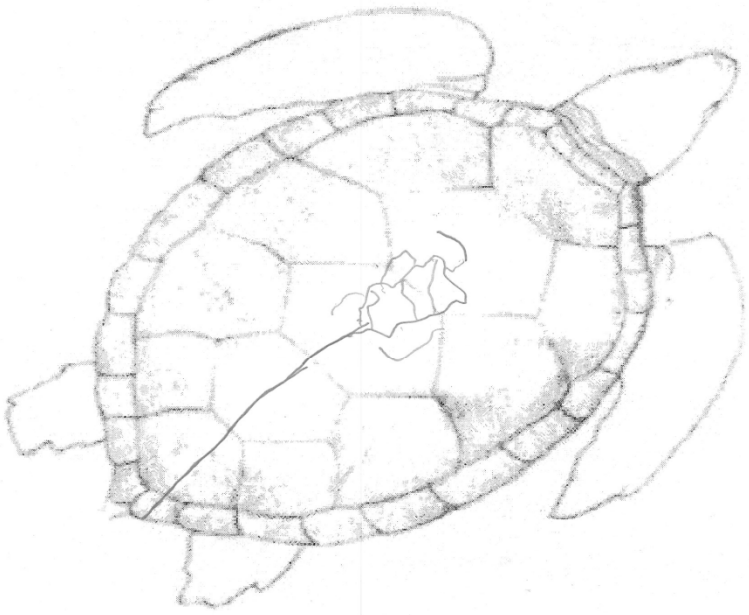

Comments:

Figure B.8. Data sheet for Shell 8

Data Collection Sheet

Shell #: 9 Time: 11:54:32 Date: 8/1/11

Accel. #: 1 Boat Type: JET Depth: SURFACE

Boat Speed (km/hr): 27 Orientation: 12:00

Type of wound (Blunt trauma, prop cut): BLUNT

Size/Location of cuts/damage:

Sketch of damage:

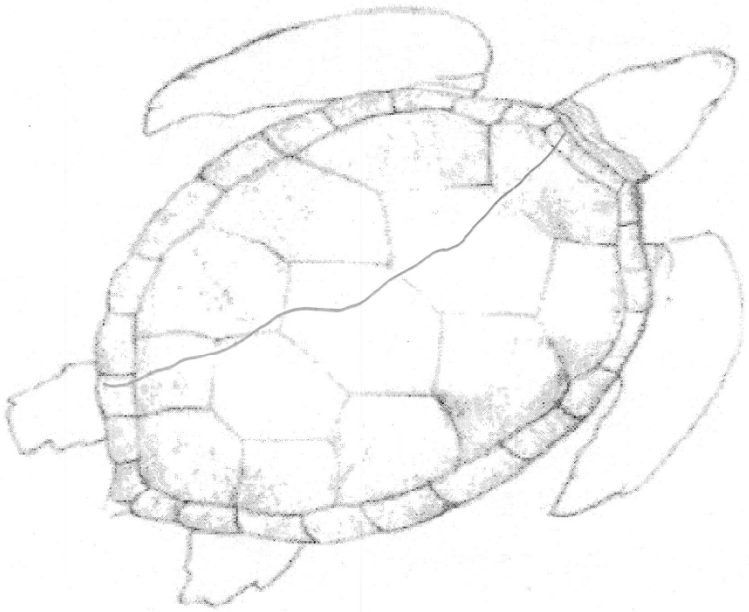

Comments:

HIT TARGET

Figure B.9. Data sheet for Shell 9

Data Collection Sheet

Shell #: 10 Time: 12:04:37 Date: 8/1/11

Accel. #: 1 Boat Type: SEJ Depth: SURFACE

Boat Speed (km/hr): 26 Orientation: 1:00

Type of wound (Blunt trauma, prop cut): _____

Size/Location of cuts/damage:

Sketch of damage:

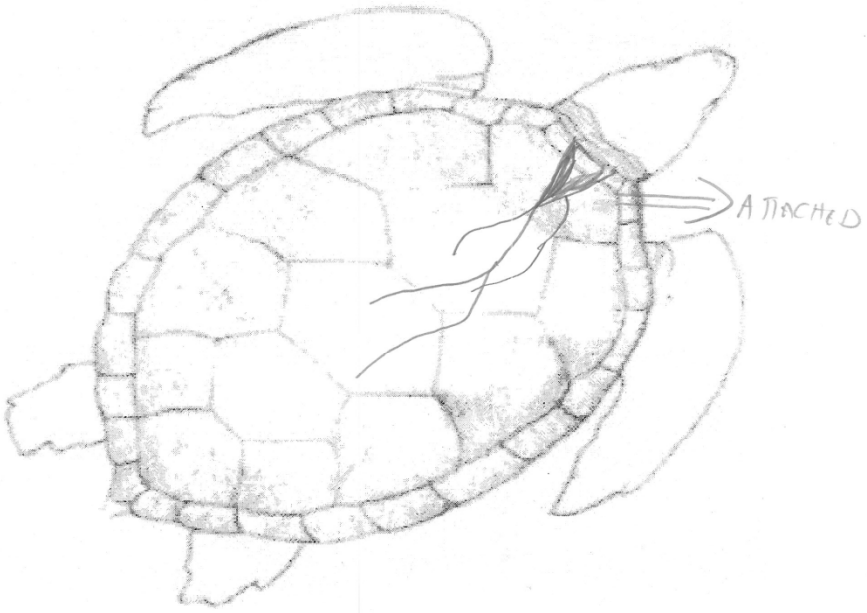

Comments:

Figure B.10. Data sheet for Shell 10

Data Collection Sheet

Shell #: 7B Time: 12:17:46 Date: 8/1/11

Accel. #: 1 Boat Type: JET Depth: SURFACE

Boat Speed (km/hr): 28 Orientation: 11:00

Type of wound (Blunt trauma, prop cut): _____

Size/Location of cuts/damage:

Sketch of damage:

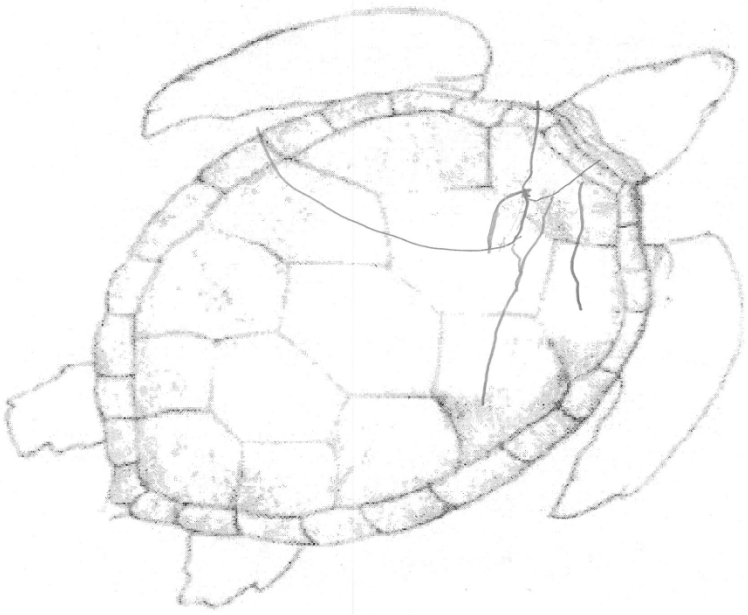

Comments:

Figure B.11. Data sheet for Shell 7B

Data Collection Sheet

Shell #: 11 Time: 01:53:01 Date: 8/1/2011

Accel. #: 2 Boat Type: DEEP V-4 PROP Depth: 28" - PROP DEPTH

Boat Speed (km/hr): PLANE Orientation: 10:00

Type of wound (Blunt trauma, prop cut): NONE

Size/Location of cuts/damage:

Sketch of damage:

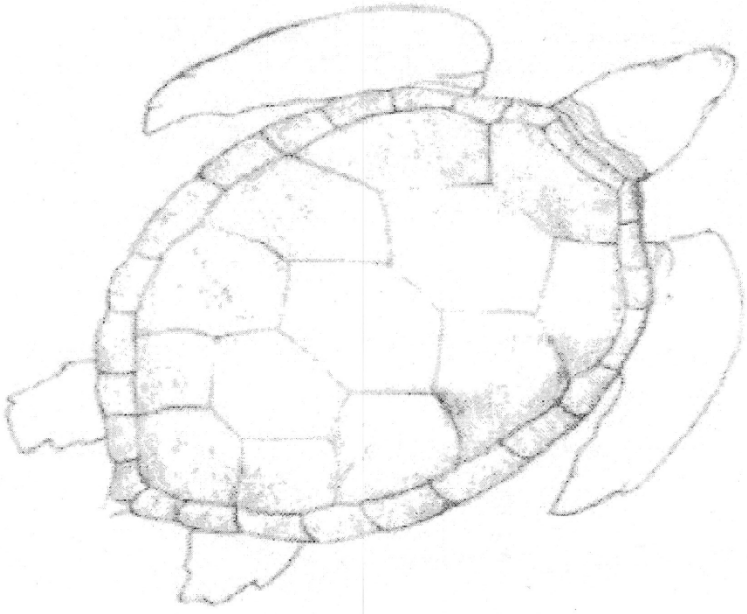

Comments:

PRESSURE WAVE DISPLACEMENT

Figure B.12. Data sheet for Shell 11

Data Collection Sheet

Shell #: 11C Time: 2:04:05 Date: 8/1/2011

Accel. #: 2 Boat Type: V-HULL 4 PROP Depth: 28" PROP DEPTH

Boat Speed (km/hr): PLANE Orientation: 8:00

Type of wound (Blunt trauma, prop cut): _____

Size/Location of cuts/damage:

Sketch of damage:

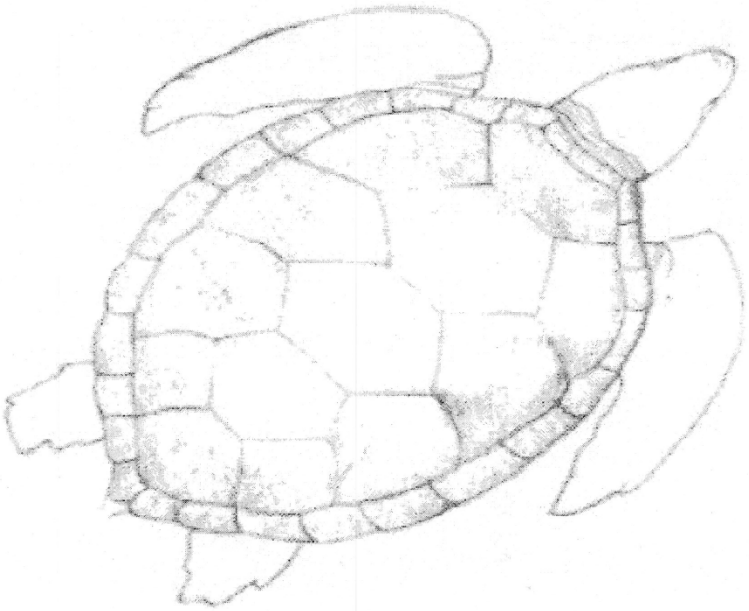

Comments:

P-WAVE DISPLACEMENT

Figure B.13. Data sheet for Shell 11C

Data Collection Sheet

Shell #: 11D Time: 2:07:33 Date: 8/1/2011

Accel. #: 2 Boat Type: V-HULL 4 PROP Depth: 28" PROP DEPTH

Boat Speed (km/hr): PLANE Orientation: 9:00

Type of wound (Blunt trauma, prop cut): _____

Size/Location of cuts/damage:

Sketch of damage:

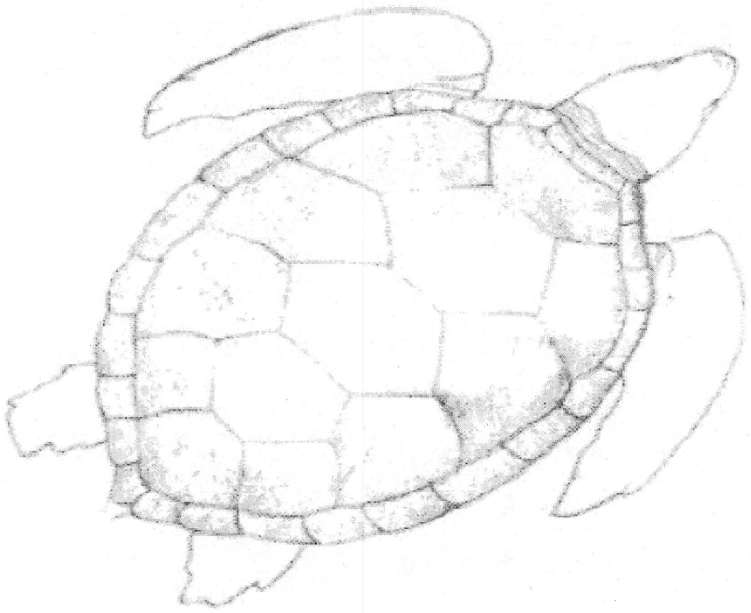

Comments:

NO DAMAGE (P_WAVE)

Figure B.14. Data sheet for Shell 11D

Data Collection Sheet

Shell #: 11E Time: 02:09:43 Date: 8/1/2011

Accel. #: 2 Boat Type: V-HULL 4 PROP Depth: 78" PROP

Boat Speed (km/hr): PLANE Orientation: 02:00

Type of wound (Blunt trauma, prop cut): _____

Size/Location of cuts/damage:

Sketch of damage:

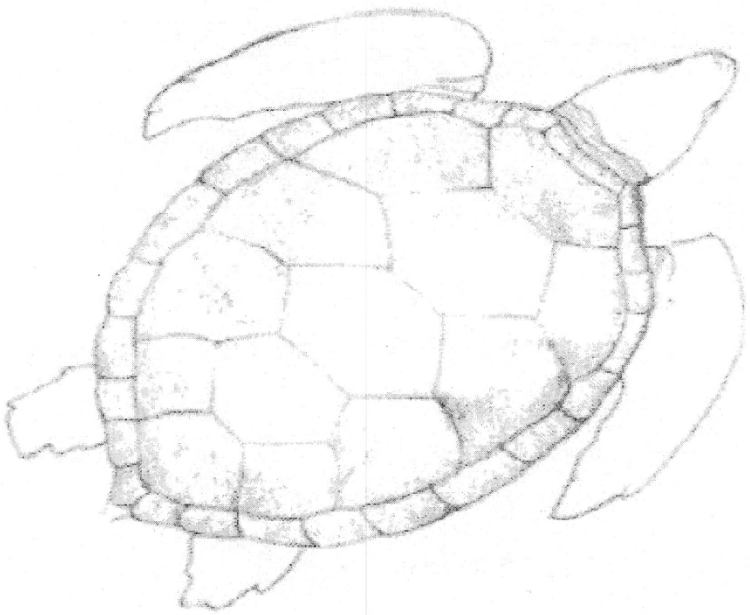

Comments:

Figure B.15. Data sheet for Shell 11E

Data Collection Sheet

Shell #: 11F Time: 02:20 ish Date: 8/1/2011

Accel. #: 2 Boat Type: V-Hull - 4 prop Depth: 19" prop

Boat Speed (km/hr): 24 Orientation: 2:00

Type of wound (Blunt trauma, prop cut): MASSIVE BLUNT TRAUMA

Size/Location of cuts/damage:

Sketch of damage:

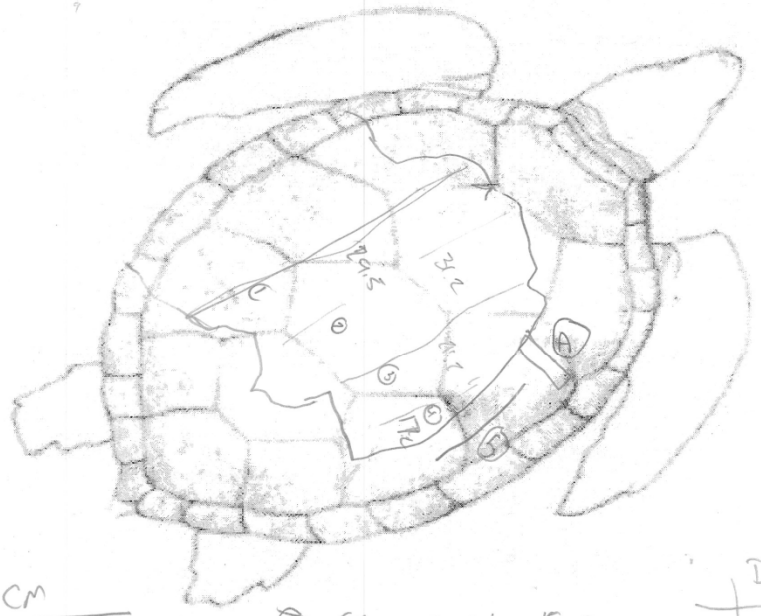

cm

Comments:

1	29.5	7.0
2	31.2	7.0
3	21.2	7.0
4	17.2	7.0
5	16.8	

(A) STEP DEPTH 15.0 cm

	DEPTH
1	8.0 cm
2	14.0 cm
3	12.5 cm
4	10.0 cm
5	4.5

Figure B.16. Data sheet for Shell 11F

Data Collection Sheet

Shell #: 12 Time: 3:00:30 Date: 8/1/11

Accel. #: 2 Boat Type: V-Hull 4 PROP Depth: 19" DEPTH

Boat Speed (km/hr): 28 Orientation: 11:00

Type of wound (Blunt trauma, prop cut): _____

Size/Location of cuts/damage:

Sketch of damage:

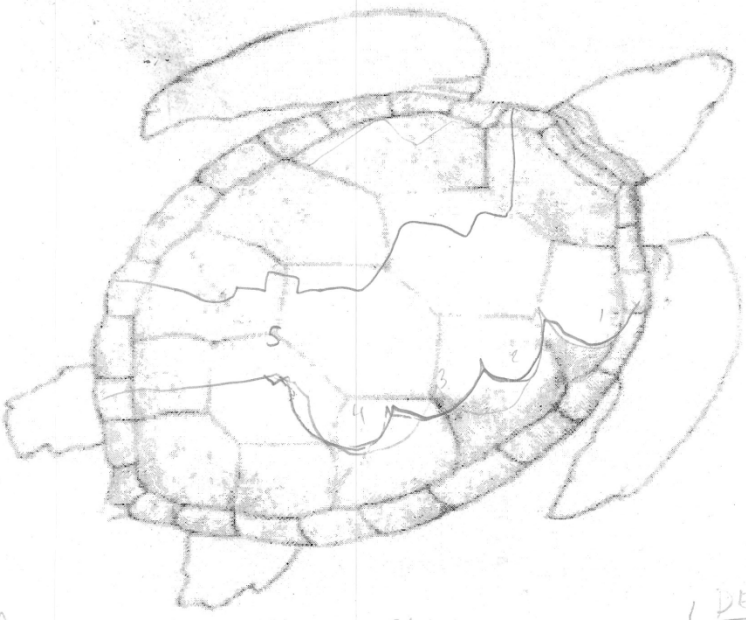

Comments:

	cm
1	—
2	—
3	27.4
4	23.2
5	16.5

SKEG
10,0 cm DEPTH
43.0 cm LENGTH

	DEPTH
1	—
2	7.5
3	6.5
4	5.5
5	3.0

Figure B.17. Data sheet for Shell 12

Data Collection Sheet

Shell #: 13 Time: 3:29:10 Date: 8/1/2011

Accel. #: 2 Boat Type: V-Hull 4 Prop Depth: 19"

Boat Speed (km/hr): 26 Orientation: 10:00

Type of wound (Blunt trauma, prop cut): PROP CUT

Size/Location of cuts/damage:

Sketch of damage:

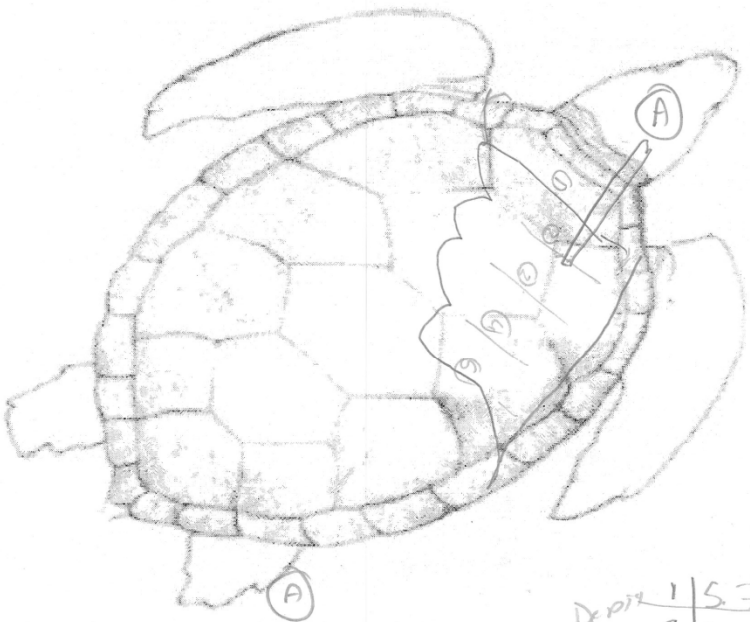

Comments:

1	24.5	7.2
2	20.3	6.8
3	20.5	6.2
4	18.6	6.3
5	15.5	

DEPTH	7.5
LENGTH	19.4

DEPTH 1	5.7
2	9.0
3	11.0
4	5.0
5	2.5

Figure B.18. Data sheet for Shell 13

Data Collection Sheet

Shell #: 14 Time: 16:04:04 (4:04:04) Date: 8/1/11

Accel. #: 2 Boat Type: Deep V 4 Prop Depth: 19"

Boat Speed (km/hr): 26mph Orientation: 6:00

Type of wound (Blunt trauma, prop cut):

Size/Location of cuts/damage:

Sketch of damage:

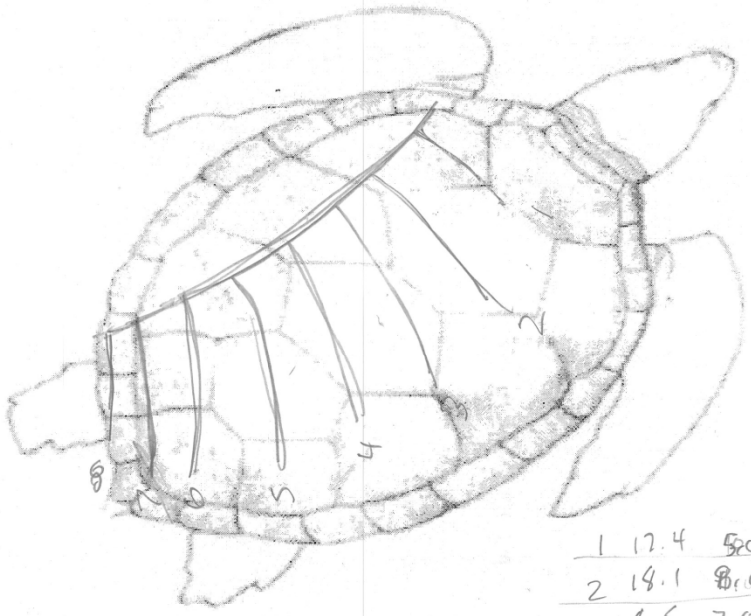

Comments:

1. 17.4
2. 18.1
3. 18.5
4. 19.4
5. 19.5
6. 21.1
7. 22.3
8. 22.0

1	17.4	5.0	6.2
2	18.1	8.0	6.7
3	18.5	7.0	7.7
4	19.4	7.0	6.5
5	19.5	8.0	6.0
6	21.1	10.0	6.8
7	22.3	9.0	6.8
8	22.0	7.5	

Figure B.19. Data sheet for Shell 14

Data Collection Sheet

Shell #: 15 Time: 16:26:46 Date: 8/1/11

Accel. #: 2 Boat Type: Deep V 4Prop Depth: 19"

Boat Speed (km/hr): 26 mph Orientation: 6:00

Type of wound (Blunt trauma, prop cut):

Size/Location of cuts/damage:

Sketch of damage:

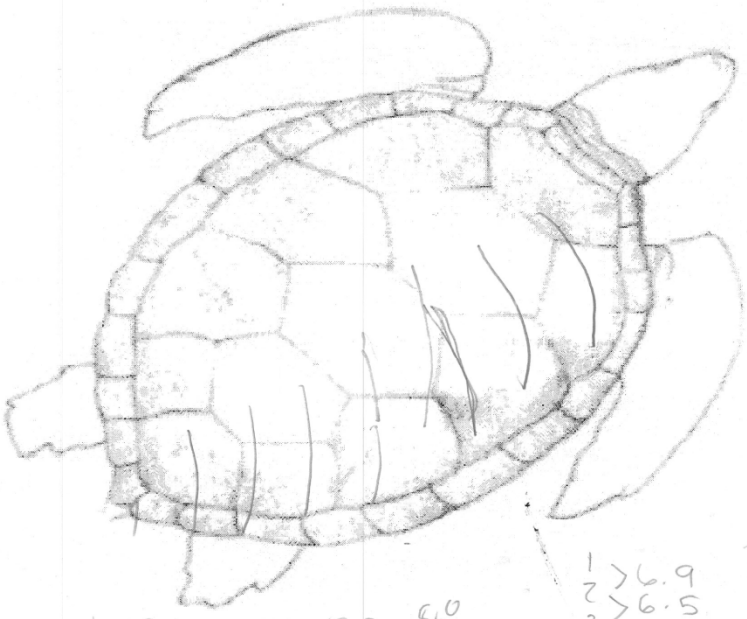

Comments:

LENGTH

1	13.4	3.5
2	18.6	8.0
3	19.7	9.0
4	20.1	10.5
5	20.0	4.5
7	20.8	8.5

7. 13.0 8.0

1 > 6.9
2 > 6.5
3 > 7.0
4 > 6.7
5 > 6.7
6 >
7 > 7.2

SKEG
8.4 DEEP
27.0 LENGTH

Figure B.20. Data sheet for Shell 15

Data Collection Sheet

Shell #: 16 Time: 5:36:16 Date: 8/1/11

Accel. #: X No accel. used Boat Type: Deep V 4bp Depth: surface

Boat Speed (~~km/hr~~ mph): 27 Orientation: 103:00

Type of wound (Blunt trauma, prop cut): _____

Size/Location of cuts/damage:

Span
1-2 = 7.2
2-3 = 7.9
3-4 = 7.1

Skeg
43.5cm length
depth 10cm

Sketch of damage:

	Cranial-caudal	Depth
1	15.5 cm	5.5
2	25.1	7.0
3	25.5	8.0
4	25.7	5.0

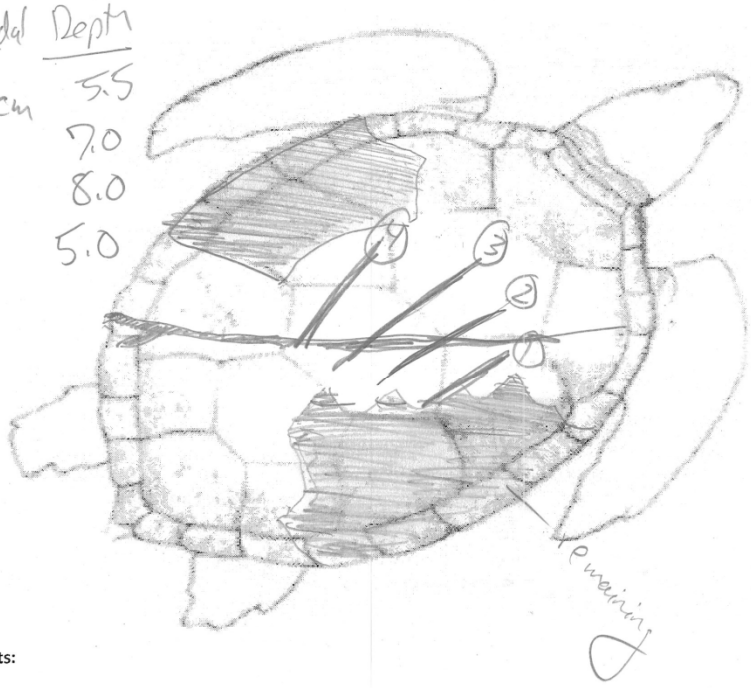

Comments:

Figure B.21. Data sheet for Shell 16

Data Collection Sheet

Shell #: 17 Time: 17:54:33 Date: 8/1/11

Accel. #: — Boat Type: DeepV 46p Depth: surface

Boat Speed (km/hr): 24 Orientation: 3:00

Type of wound (Blunt trauma, prop cut): Non-fatal blunt hull impact

Size/Location of cuts/damage:

Sketch of damage:

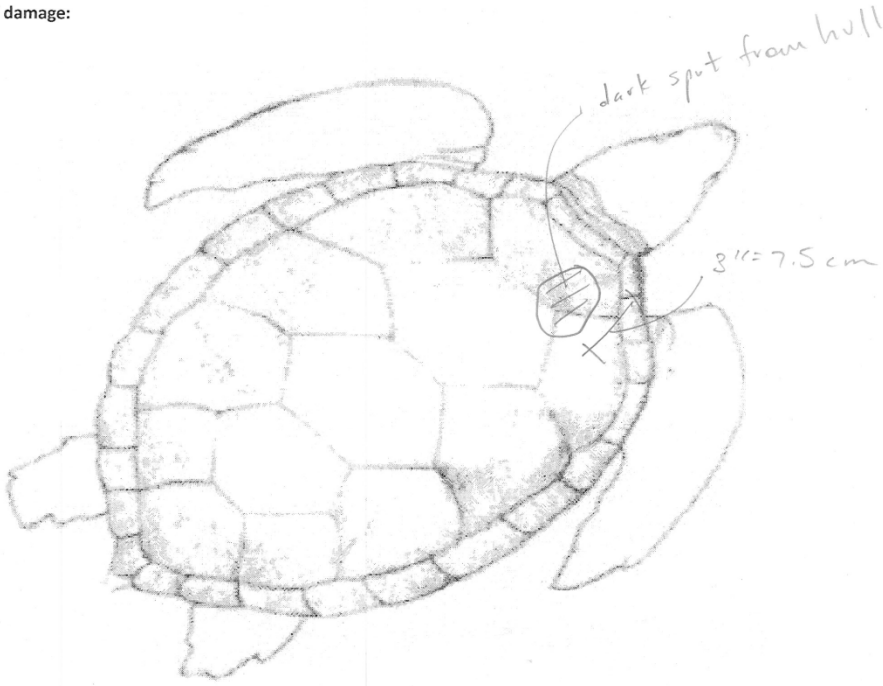

Comments:

Figure B.22. Data sheet for Shell 17

Data Collection Sheet

Shell #: 18 Time: 18:01:57 Date: 8/1

Accel. #: NA Boat Type: Deep V 4 Prop Depth: Surface

Boat Speed (km/hr): 28 Orientation: 10:00 - 4:00

Type of wound (Blunt trauma, prop cut): _____

Size/Location of cuts/damage:

Not reconstructed

Sketch of damage:

Comments:

Figure B.23. Data sheet for Shell 18

Data Collection Sheet

Shell #: 18 Time: 18:01 Date: 8/1

Accel. #: _____ Boat Type: Deep V 4 amp Depth: Surface

Boat Speed (km/hr): 28 Orientation: 4:00

Type of wound (Blunt trauma, prop cut): _____

Size/Location of cuts/damage:

Reconstructed

Sketch of damage:

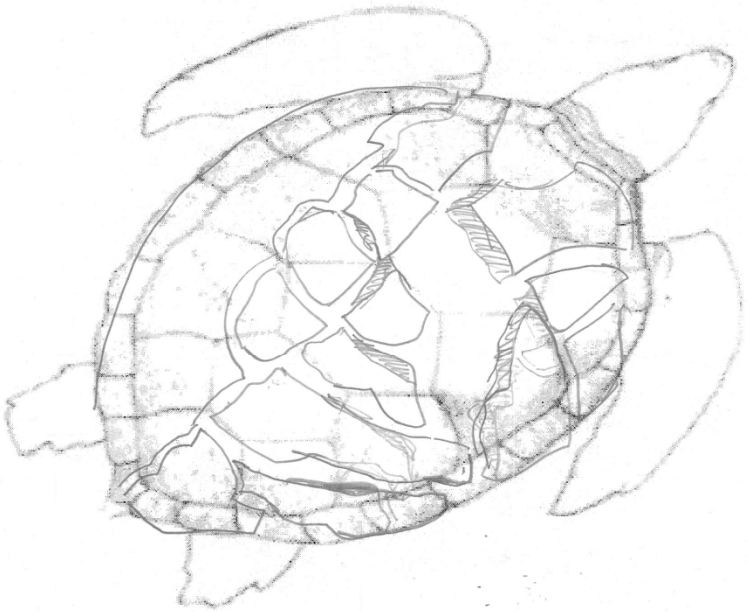

Comments:

Figure B.24. Data sheet for Shell 18

Data Collection Sheet

Shell #: 19 Time: 6:17 Date: 8/1

Accel. #: _____ Boat Type: Deep V 4prop Depth: Surface

Boat Speed (km/hr): 27 Orientation: 10 O'clock

Type of wound (Blunt trauma, prop cut): _____

Size/Location of cuts/damage:

1-2 8.5 * cut spans actual measurements difficult. 7cm estimate for missing foam
2-3 6
3-4 8
4-5: 8.7

Sketch of damage:

Prop cuts

	Length	Depth
1	14.0	5
2	25.5	4
3	26.1	8
4	26	9
5	16.1	8cm

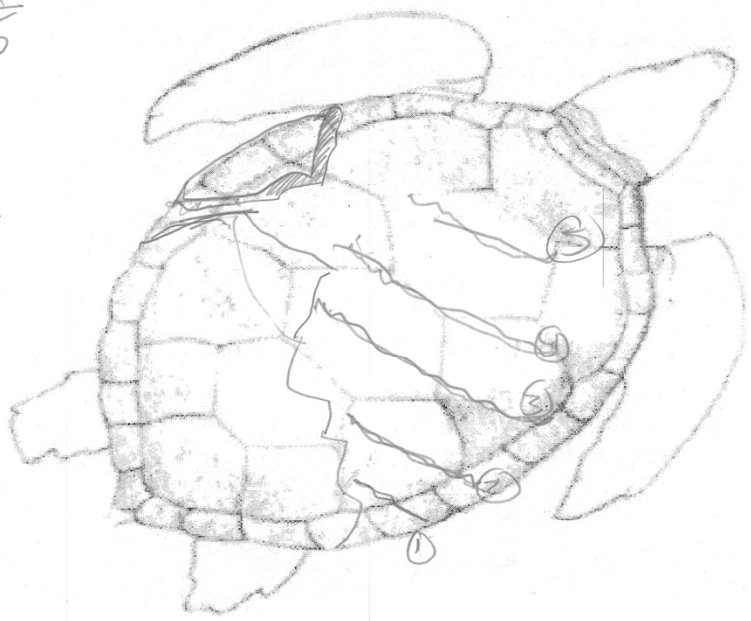

Comments:

Figure B.25. Data sheet for Shell 19

Data Collection Sheet

Shell #: R-1 Time: 903 Date: 10/13/11

Accel. #: _____ Boat Type: Jet Depth: Surface

Boat Speed (~~km~~/hr): 8.29 Orientation: 2 o'clock

Type of wound (Blunt trauma, prop cut): blunt

Size/Location of cuts/damage:

Multiple scutes on dorsum; 1cm area of carapace bone exposed on 1st vertebral

Sketch of damage:

SLN-T 70.8cm

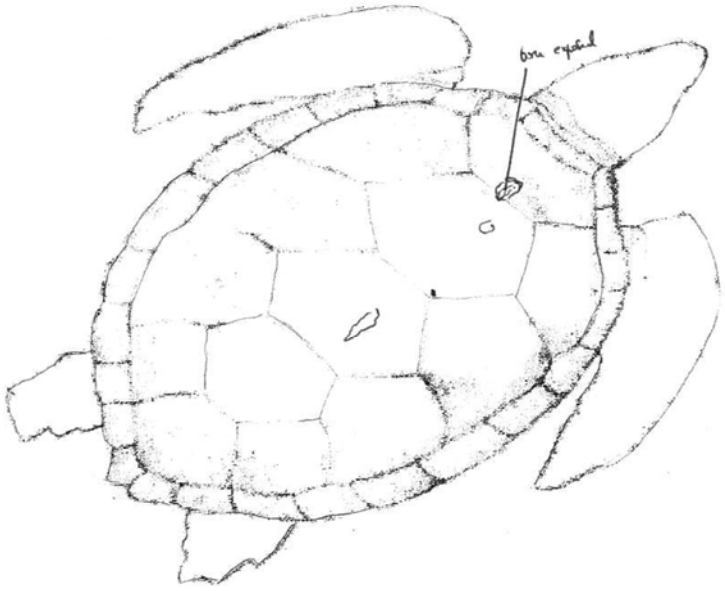

Comments:

Scutes flaked off of dorsum; pre-collision photo not taken

Loggerhead

Figure B.26. Data sheet for Shell R1

Data Collection Sheet

Shell #: 4 Time: 9:26 Date: 10/13/2011

Accel. #: 1 Boat Type: Jet Depth: Surface

Boat Speed (~~km/hr~~ mph): 30 Orientation: 3:00

Type of wound (Blunt trauma, prop cut): BLUNT TRAMA, SMALL AREA AT IMPACT SITE, DID NOT RADIATE OUT FROM SITE.

Size/Location of cuts/damage: DAMAGE DORSAL IN AREA OF NUCHAL SCUTES

Sketch of damage:

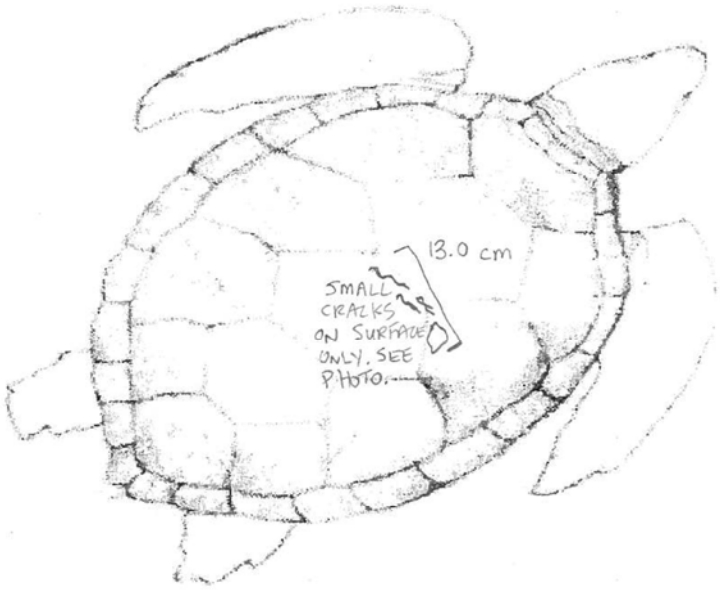

Comments: BOAT MADE IMPACT THAT YOU COULD HEAR.

Figure B.27. Data sheet for Shell 4

Data Collection Sheet

Shell #: 26 Time: 9:38 Date: 10/13/2011

Accel. #: 2 Boat Type: JET Depth: SURFACE

Boat Speed (km/hr): 26 Orientation: 3:00

Type of wound (Blunt trauma, prop cut): NO TRUE WOUND; PRESSURE DING

Size/Location of cuts/damage:

DORSAL AREA OF 4th NUCHAL SCUTE

Sketch of damage:

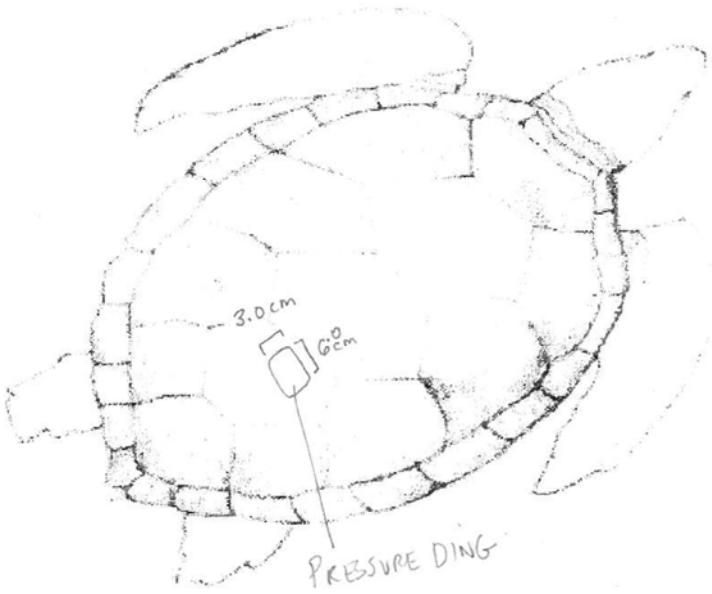

Comments:

COULD HEAR IMPACT OF BOAT

Figure B.28. Data sheet for Shell 26

Data Collection Sheet

Shell #: 22 Time: 9:44 Date: 10/13/2011

Accel. #: 1 Boat Type: JET Depth: SURFACE

Boat Speed (km/hr): 26 Orientation: 3:00

Type of wound (Blunt trauma, prop cut): PRESSURE DING W/ ASSOCIATED CRACKS; SURFACE ONLY. ONE CRACK RADIATES.

Size/Location of cuts/damage:

DORSAL WOUND 2 2ND NUCHAL SCUTE

Sketch of damage:

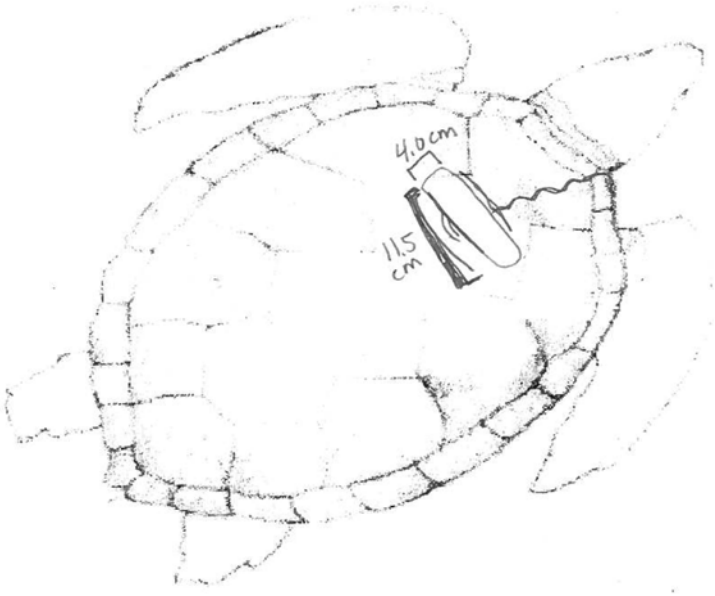

Comments:

COULD HEAR IMPACT OF BOAT. HEAD CAME OFF.

Figure B.29. Data sheet for Shell 22

Data Collection Sheet

Shell #: 28 Time: 9:50 Date: 10/13/2011

Accel. #: 2 Boat Type: JET Depth: SURFACE

Boat Speed (km/hr): 28 Orientation: 2:00

Type of wound (Blunt trauma, prop cut): PRESSURE DING W/ ASSOCIATED CRACKS. ONE RADIATING CRACK CAUDAL TO DING.

Size/Location of cuts/damage:

DORSAL ~5th NUCHAL SCUTE.

Sketch of damage:

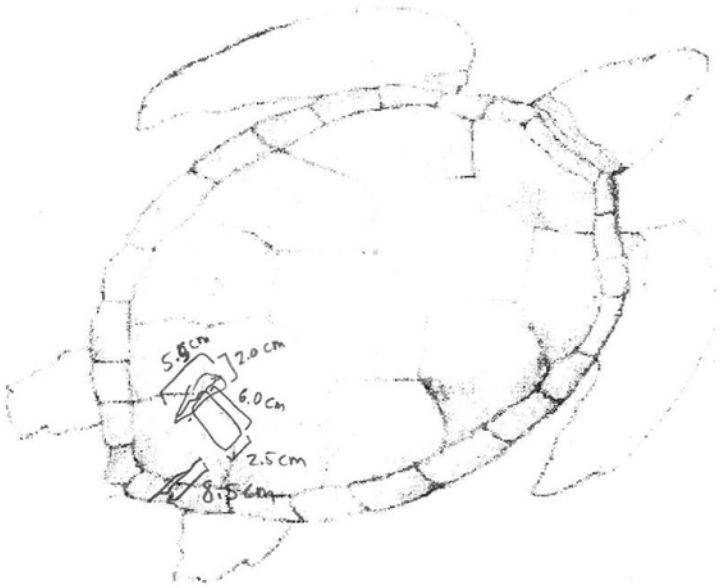

Comments:

HEAD CAME OFF; COULD HEAR IMPACT.

Figure B.30. Data sheet for Shell 28

Data Collection Sheet

Shell #: 39 Time: 9:56 Date: 10/13/2011

Accel. #: 1 Boat Type: JET Depth: SURFACE

Boat Speed (km/hr): 29 Orientation: 4:00

Type of wound (Blunt trauma, prop cut): SURFACE; PRESSURE DING W/ ASSOCIATED CRACKS. DAMAGE DID NOT RADIATE FROM WOUND SITE.

Size/Location of cuts/damage: DORSAL ~4th NUCHAL SCUTE

Sketch of damage:

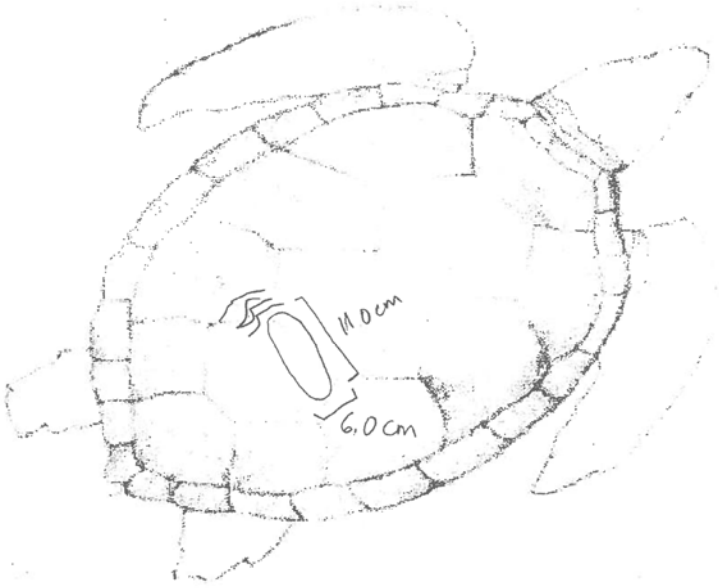

Comments:

COULD HEAR IMPACT. HEAD REMAINED INTACT

Figure B.31. Data sheet for Shell 39

Data Collection Sheet

Shell #: R-3 Time: 10:18 Date: 10/13/11

Accel. #: - Boat Type: Jet Depth: Surface

Boat Speed (km/hr): 24 mph Orientation: 1:00

Type of wound (Blunt trauma, prop cut): blunt

Size/Location of cuts/damage:

- Superficial abrasion across mid-body dorsal and left lateral carapace
- White transfer on right lateral carapace (Check to evaluate pre-photos for pre-existing)

Sketch of damage:

SL N-T 68.8cm

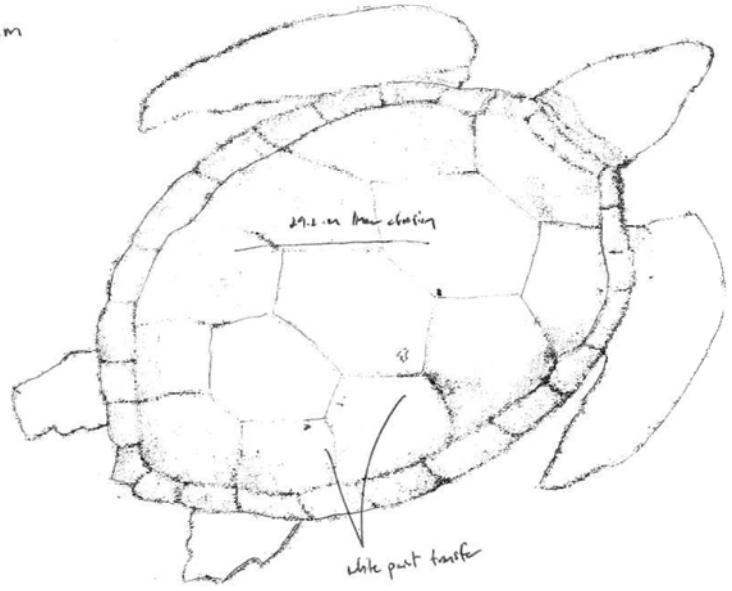

Comments:

Green

Figure B.32. Data sheet for Shell R3

Data Collection Sheet

Shell #: R-4 Time: 10:29 Date: 10/13/11

Accel. #: - Boat Type: Jet Depth: Surface

Boat Speed (km/hr): 29 Orientation: 3:00

Type of wound (Blunt trauma, prop cut): Blunt; grossly demarcated superficial abrasions (scrape)

Size/Location of cuts/damage: on right (2nd) costal. Sharp superficial abrasion (linear) and adjacent abrasion thread vertebral. White paint on posterolateral carapace (transverse orientation) - need to evaluate pre-collision photos.

Sketch of damage:

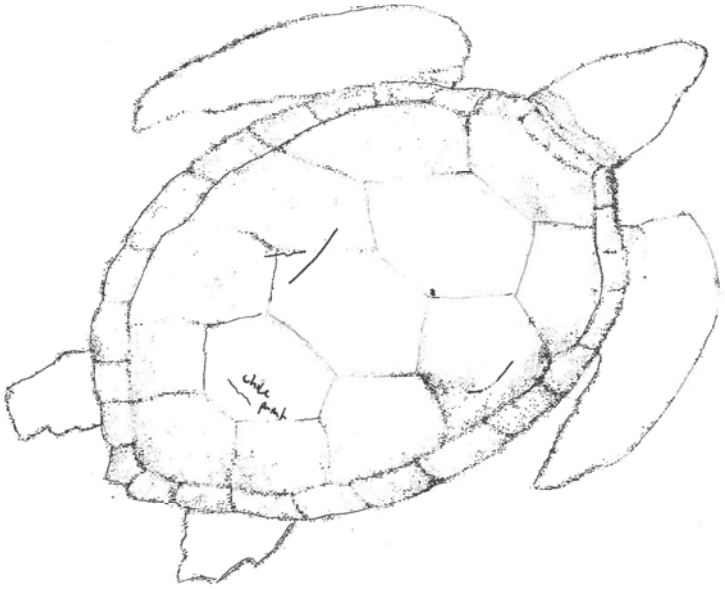

Comments: Paint marking (pre-collision) scuffed away

Green

Figure B.33. Data sheet for Shell R4

Data Collection Sheet

Shell #: 23 Time: 10:38 Date: 10/13/11

Accel. #: 1 Boat Type: Deep V 4-prop Depth: Surface

Boat Speed (km/hr): 27 Orientation: 5:00

Type of wound (Blunt trauma, prop cut): NO WOUND

Size/Location of cuts/damage:

Sketch of damage:

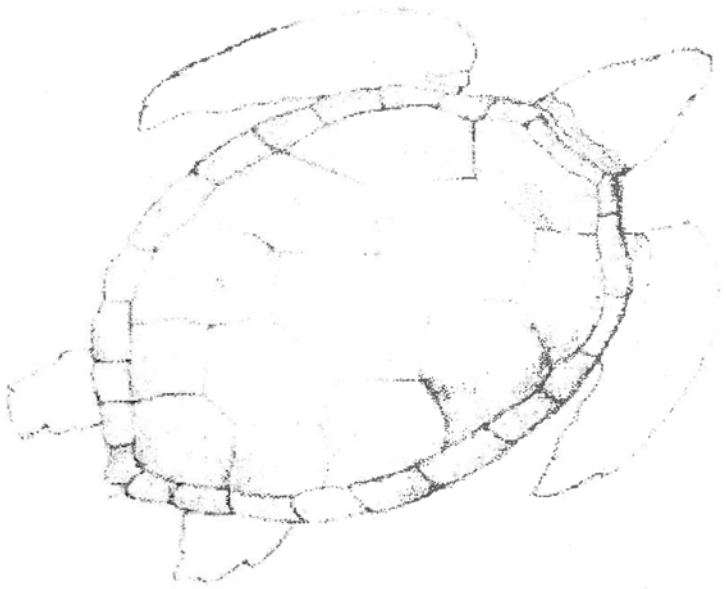

Comments:

SHELL WAS HIT BY HULL ONLY. SHELL RE-USED AS 23-B. PHOTO TAKEN. NO DAMAGE.

Figure B.34. Data sheet for Shell 23

Data Collection Sheet

Shell #: 23-B Time: 10:41 Date: 10/13/2011

Accel. #: 1 Boat Type: DEEP-V PROP Depth: SURFACE

Boat Speed (km/hr): 27 Orientation: 11:00

Type of wound (Blunt trauma, prop cut): BLUNT (X), PROP AND SKEG

Size/Location of cuts/damage:

SHELL SEVERELY DAMAGED.

Sketch of damage:

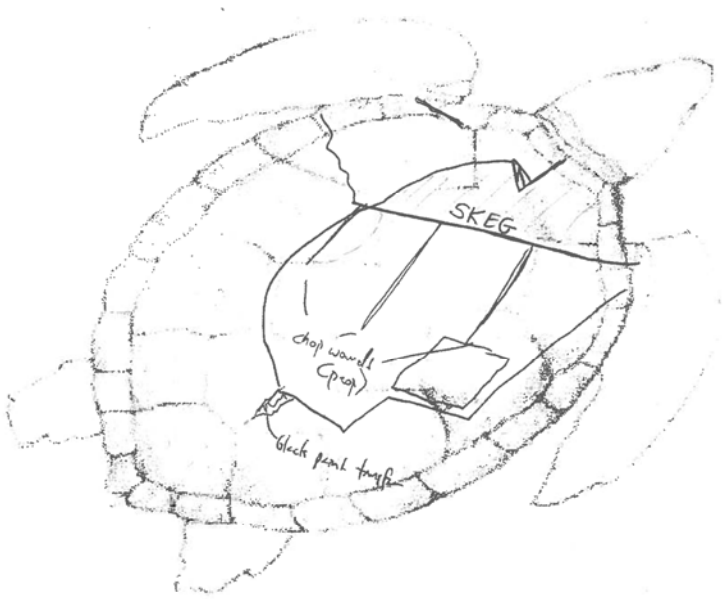

Comments:

THIS WAS USED PREVIOUSLY FOR 23.

Figure B.35. Data sheet for Shell 23B

Data Collection Sheet

Shell #: 24 Time: 10:47 Date: 10/13/2011

Accel. #: 2 Boat Type: DEEP V-PROP Depth: SURFACE

Boat Speed (km/hr): 28 Orientation: 12:00

Type of wound (Blunt trauma, prop cut): NONE

Size/Location of cuts/damage:

Sketch of damage:

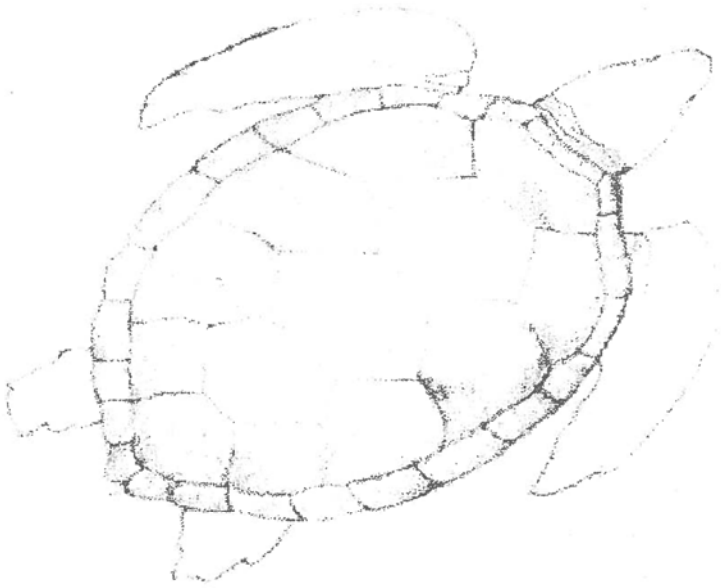

Comments:

REUSED FOR 24-B

Figure B.36. Data sheet for Shell 24

Data Collection Sheet

Shell #: 24-B Time: 10:52 Date: 10/13/2011

Accel. #: 2 Boat Type: DEEP V-PROP Depth: SURFACE

Boat Speed (km/hr): 26 Orientation: 1:30

Type of wound (Blunt trauma, prop cut): NONE

Size/Location of cuts/damage:

Sketch of damage:

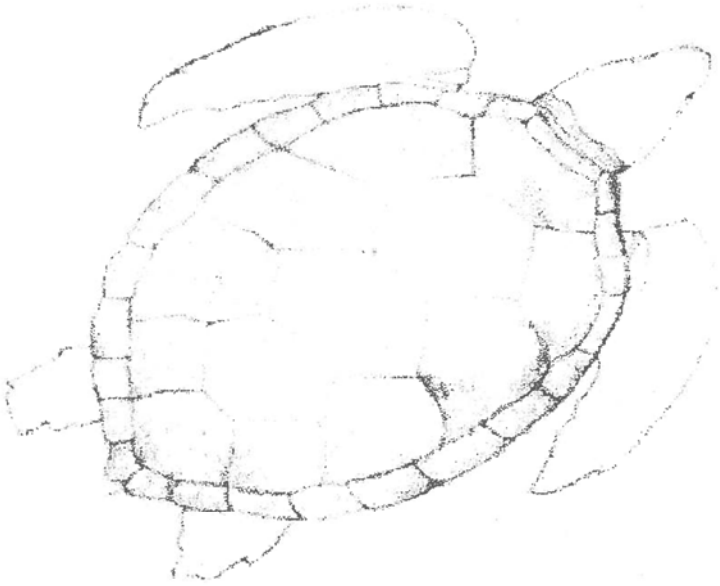

Comments:

PREVIOUSLY USED FOR 24.

Figure B.37. Data sheet for Shell 24B

Data Collection Sheet

Shell #: 24-C Time: 10:58 Date: 10-13-2011

Accel. #: 2 Boat Type: DEEP-V-PROP Depth: SURFACE

Boat Speed (km/hr): 23 Orientation: 3:00

Type of wound (Blunt trauma, prop cut): LARGE PRESSURE DING; RADIATING

Size/Location of cuts/damage: CRACKS IN SIGNIFICANT AREA CRANIAL TO PRESSURE DING

Sketch of damage:

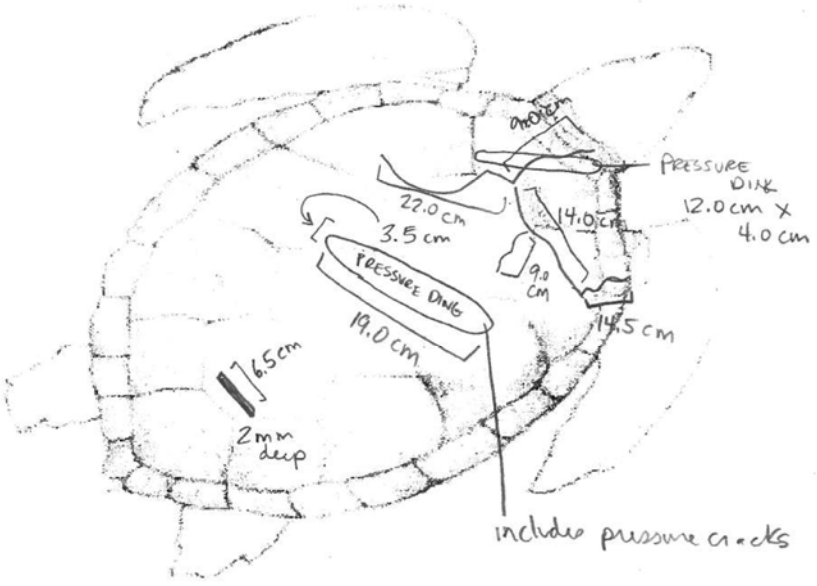

Comments:

PREVIOUSLY USED FOR 24, & 24-B.

Figure B.38. Data sheet for Shell 24C

Data Collection Sheet

Shell #: 27 Time: 11:05 Date: 10/13/2011

Accel. #: 1 Boat Type: V-HULL PROP Depth: SURFACE

Boat Speed (km/hr): 27 Orientation: 7:00

Type of wound (Blunt trauma, prop cut): PROP CUT ON LEFT SIDE.

Size/Location of cuts/damage:

CUT ALONG EDGE OF CARAPACE AND IN STYROFOAM

Sketch of damage:

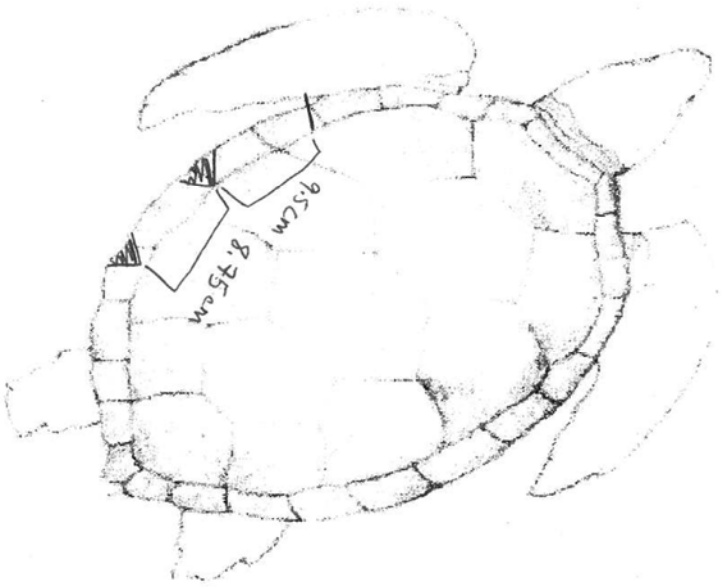

Comments:

Figure B.39. Data sheet for Shell 27

Data Collection Sheet

Shell #: 37 Time: 11:10 Date: 10/13/2011

Accel. #: 2 Boat Type: V-HULL PROP Depth: SURFACE

Boat Speed (km/hr): 26 Orientation: 7:00 - 2 impacts

Type of wound (Blunt trauma, prop cut): BLUNT, PROP, & SKEG

Size/Location of cuts/damage:

DORSAL, NUCHAL SCUTE AREA

Sketch of damage:

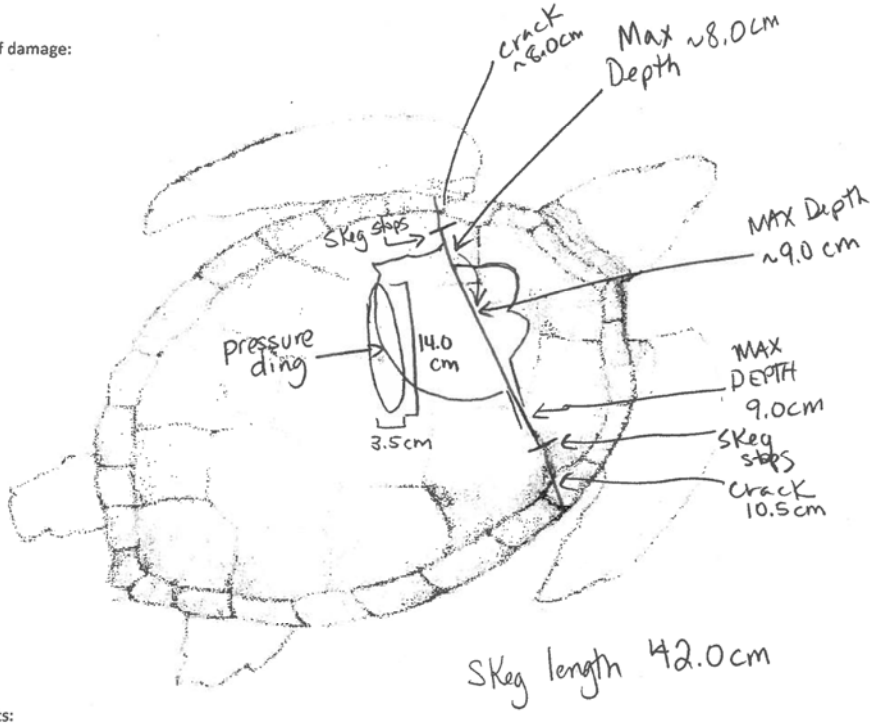

Comments:

Figure B.40. Data sheet for Shell 37

Data Collection Sheet

Shell #: 25 Time: 11:17 Date: 10|13|2011

Accel. #: 1 Boat Type: V-HULL PROP Depth: SURFACE

Boat Speed (km/hr): 27 Orientation: 10:00

Type of wound (Blunt trauma, prop cut): BLUNT, PROP, SKEG WOUND

Size/Location of cuts/damage: NUCHAL SCUTES DORSAL

Sketch of damage:

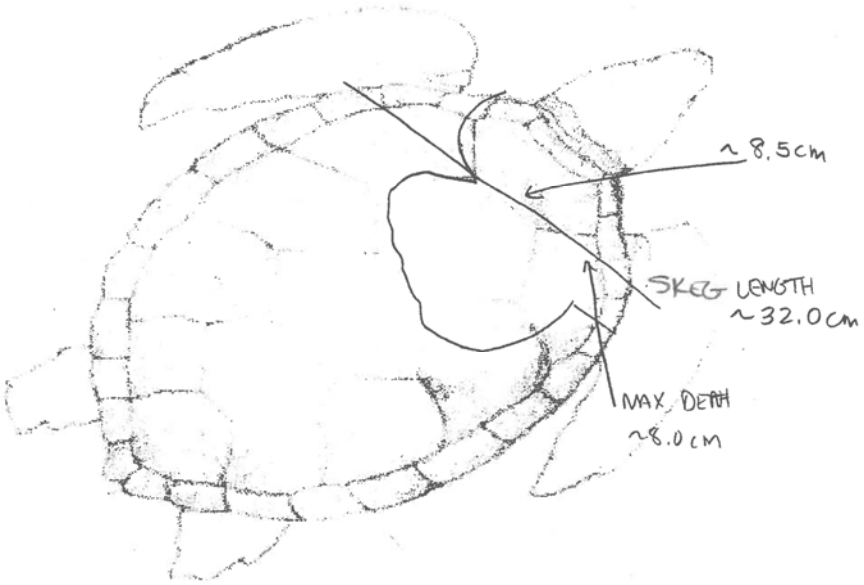

Comments:

Figure B.41. Data sheet for Shell 25

Data Collection Sheet

Shell #: R-6 Time: 11:53 Date: 10/13/11

Accel. #: _____ Boat Type: Deep V-Prop Depth: Surface

Boat Speed (km/hr): 28 Orientation: ~~1:30~~ 4:30 - double impact

Type of wound (Blunt trauma, prop cut): chop/prop cut

Size/Location of cuts/damage:

5 prop cuts ; left pattrolateral carapace

Sketch of damage:

SL-N-T ~ 71.5cm

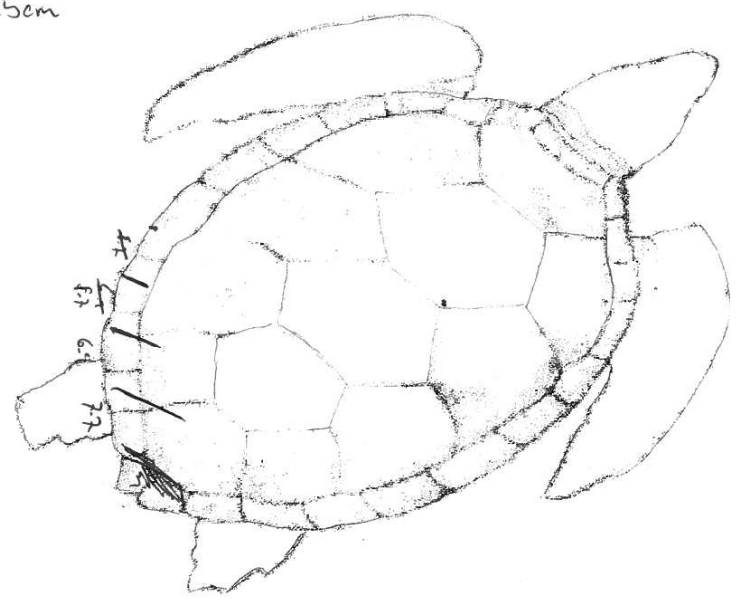

Comments:

Figure B.42. Data sheet for Shell R6

Data Collection Sheet

Shell #: R-7 Time: 11:59 Date: 10/13/11

Accel. #: _____ Boat Type: DeepV-Prop Depth: Surface

Boat Speed (km/hr): 27 Orientation: 3:00 - double strike

Type of wound (Blunt trauma, prop cut): prop cut; blunt

Size/Location of cuts/damage:

2 prop cuts posterior carapace; blunt injury to right posterolateral carapace; transverse abrasion

Sketch of damage:

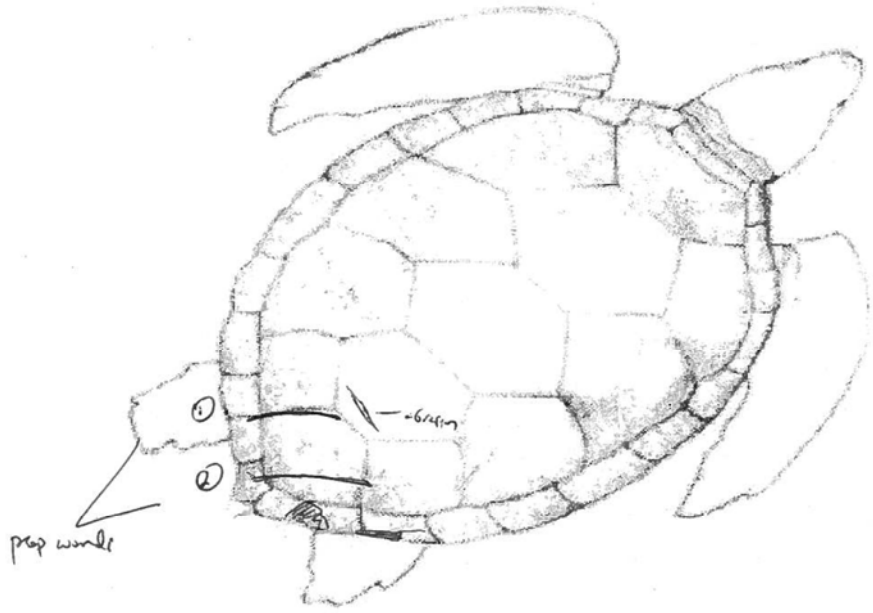

Comments:

	chord depth	chord length	span
wound 1	1.2 cm	18.4 cm	6.7 cm
2	4.0 cm	19.5 cm	

SCL = 69.0 cm

Figure B.43. Data sheet for Shell R7

Data Collection Sheet

Shell #: R-8 Time: 12:06 Date: 10/13/11

Accel. #: _____ Boat Type: DeepV-Prop Depth: Surface

Boat Speed (km/hr): 28 Orientation: ~~3:00~~ 2:30 - double impact

Type of wound (Blunt trauma, prop cut): blunt (claw) + prop

Size/Location of cuts/damage:

right dorsal + lateral mid-body carapace – linear wound fracture anterior dorsal carapace under point force

right posterolateral carapace – prop

Sketch of damage:

SCL- N-T 67.9cm

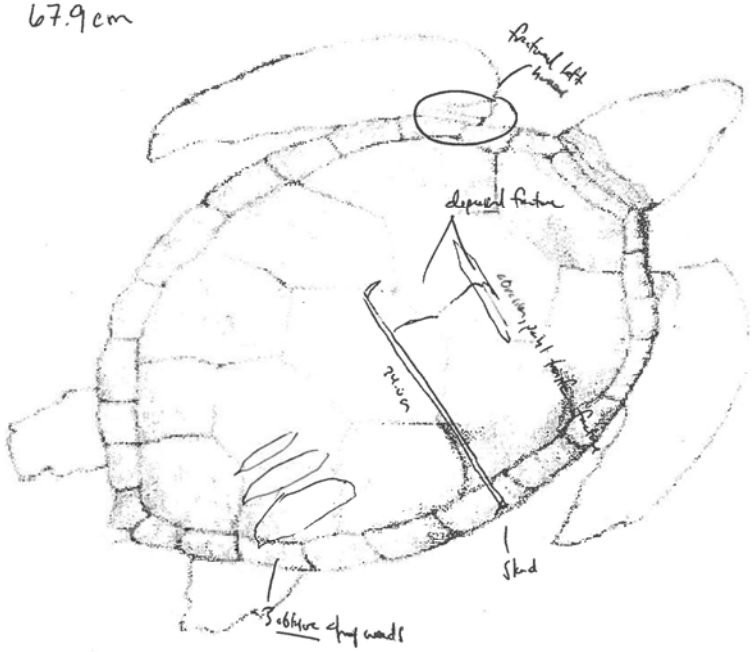

Comments:

Figure B.44. Data sheet for Shell R8

Data Collection Sheet

Shell #: R-9 Time: 12:15 Date: 10/13/11

Accel. #: _____ Boat Type: Deep V-Prop Depth: Surface

Boat Speed (km/hr): 28 Orientation: 2:00

Type of wound (Blunt trauma, prop cut): Inner Blunt (skeg); 2 prop (oblique); depressed fracture (skull)

Size/Location of cuts/damage:

Inner blunt injury across right posterior carapace; 2 oblique prop wounds

Sketch of damage:

SCL N-T 74.5cm

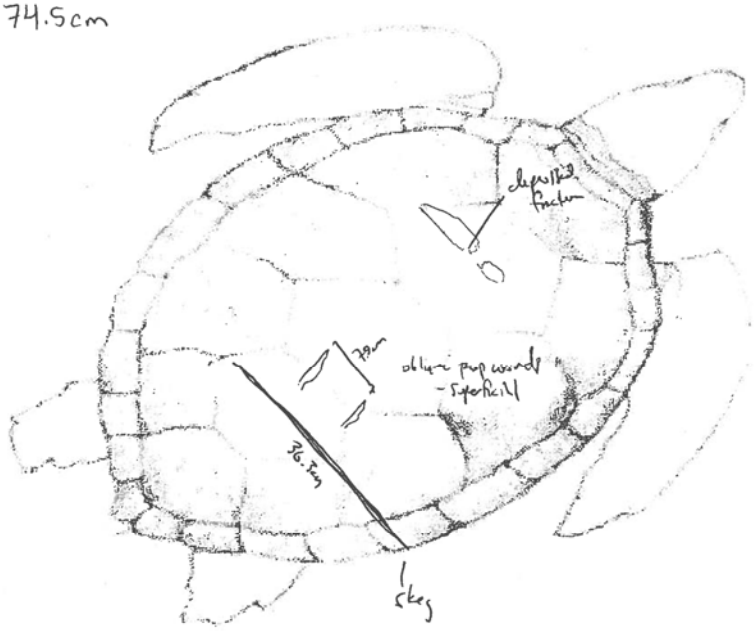

Comments:

Figure B.45. Data sheet for Shell R9

Data Collection Sheet

Shell #: R-10 Time: 12:24 Date: 10/13/10

Accel. #: _____ Boat Type: DeepV-Prop Depth: Surface

Boat Speed (km/hr): 25 Orientation: 5:00

Type of wound (Blunt trauma, prop cut): Inner wound (chop/blunt) ; single prop ; blunt

Size/Location of cuts/damage:

Inner chop wound - posterior, dorsal midline - skeg

oblique scrape chop wound - posterior, dorsal midline - prop

Sketch of damage: blunt fracture - mid-body, dorsal midline w/ penetration

SCL N-T:

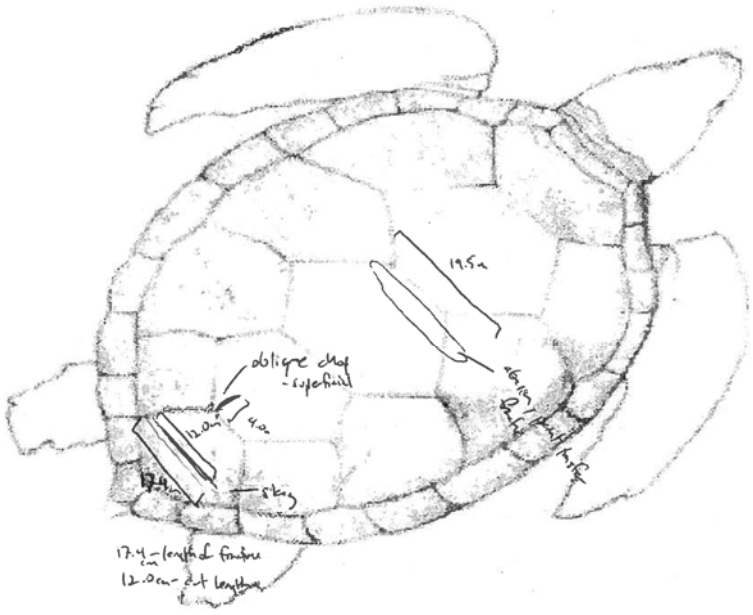

Comments:

Figure B.46. Data sheet for Shell R10

Data Collection Sheet

Shell #: 4-P Time: 12:36 Date: 10-13-11

Accel. #: NA Boat Type: Deep V 46 J-14" prop Depth: 19" (prop)

Boat Speed ~~(km/hr)~~: 26 mph Orientation: 12

Type of wound (Blunt trauma, prop cut): BLUNT, PROP, SKEG

Size/Location of cuts/damage:

CUT INTO CARAPACE & STYROFOAM

Sketch of damage:

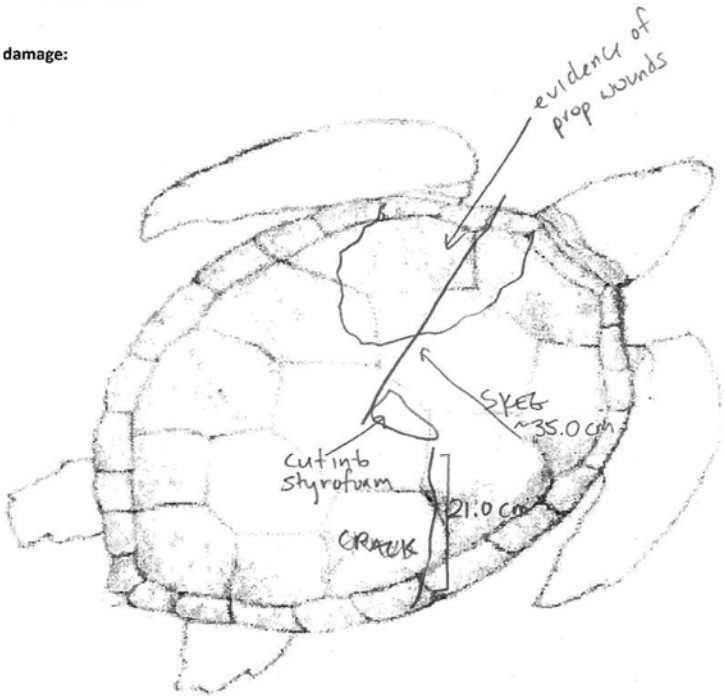

Comments:

PREVIOUSLY USED AS #4

Figure B.47. Data sheet for Shell 4P

Data Collection Sheet

Shell #: 26-P Time: 12:44 Date: 10/13/2011

Accel. #: NA Boat Type: V-HULL PROP Depth: 19" (prop)

Boat Speed (km/hr): 26 Orientation: 5:00

Type of wound (Blunt trauma, prop cut): BLUNT, PROP, SKEG

Size/Location of cuts/damage:

Sketch of damage:

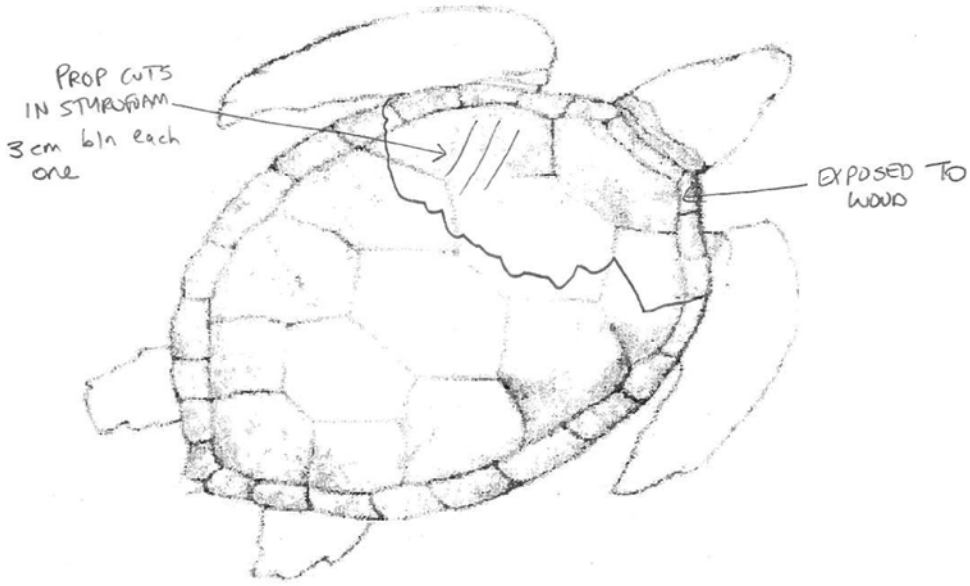

Comments:

Figure B.48. Data sheet for Shell 26P

Data Collection Sheet

Shell #: R-1 Time: 1:10 Date: 10/13/11

Accel. #: _____ Boat Type: DeepV Prop Depth: Prop Depth

Boat Speed (km/hr): 28 Orientation: 3:00

Type of wound (Blunt trauma, prop cut): prop cut + blunt

Size/Location of cuts/damage:

- Cavity wound involving right lateral mid-body carapace, extensive exposure of coelomic cavity
- 6 chop wounds + superficial linear wound (skeg)

Sketch of damage:

SCL - N-T: 70.8 cm

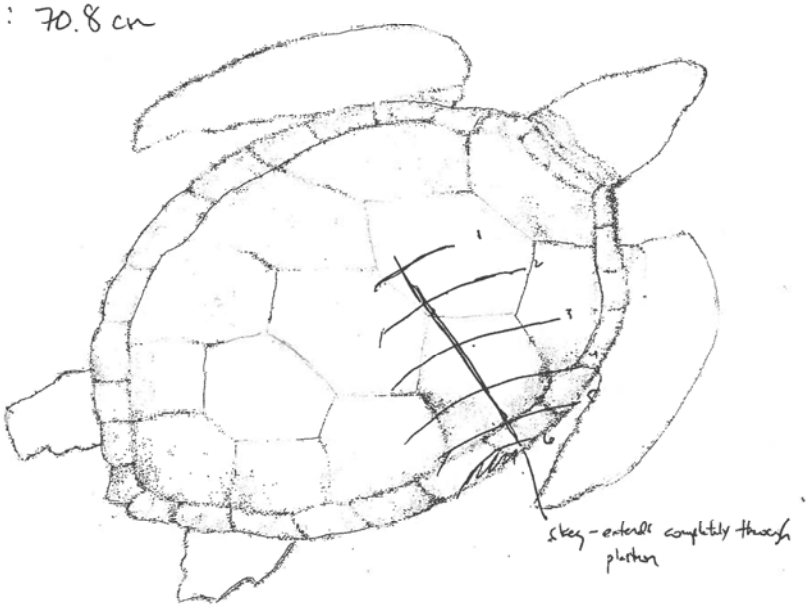

Comments:

	chord length
1.	27.7
2	/
3	/
4	/
5	/
6	/

	cut skeg
1-2	8.9 cm
2-3	7.3 cm
3-4	7.3 cm
4-5	6.4 cm

Figure B.49. Data sheet for Shell R1

Data Collection Sheet

Shell #: R-3 Time: 1:54 Date: 10/13/11

Accel. #: _____ Boat Type: Deep V Prop Depth: Prop Depth

Boat Speed (km/hr): 27 Orientation: 3:00 Caudal left floating

Type of wound (Blunt trauma, prop cut): blunt and prop

Size/Location of cuts/damage:

- Massive blunt trauma to posterior half of carapace + extensive depressed fracture
- 3 chop wounds visible

Sketch of damage:

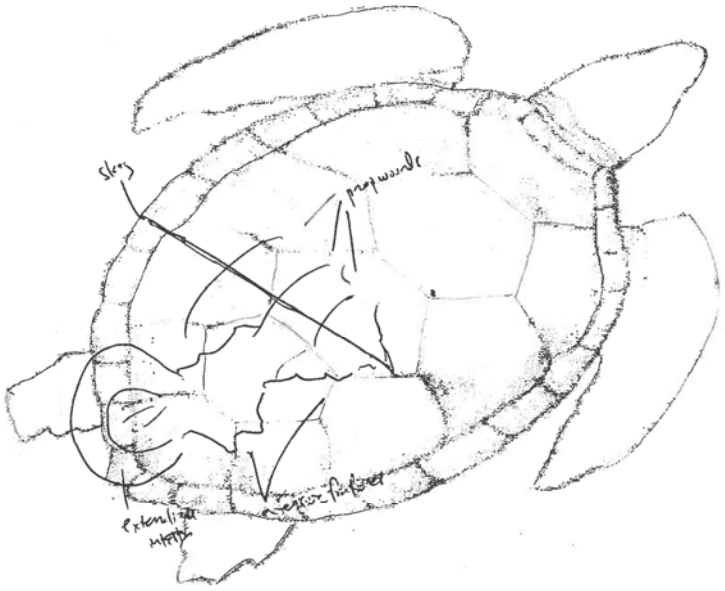

Comments:

SCL: 69.2 cm

Figure B.50. Data sheet for Shell R3

Data Collection Sheet

Shell #: R-5 Time: 2:20 Date: 10/13/11

Accel. #: _____ Boat Type: Deep V Prop Depth: Prop Depth

Boat Speed (km/hr): 21 Orientation: 3:00

Type of wound (Blunt trauma, prop cut): prop wounds + blunt

Size/Location of cuts/damage:

3 prop wounds across anterior carapace, distal neck, shoulder cleft

Sketch of damage:

SCL N-T: 72.2 cm

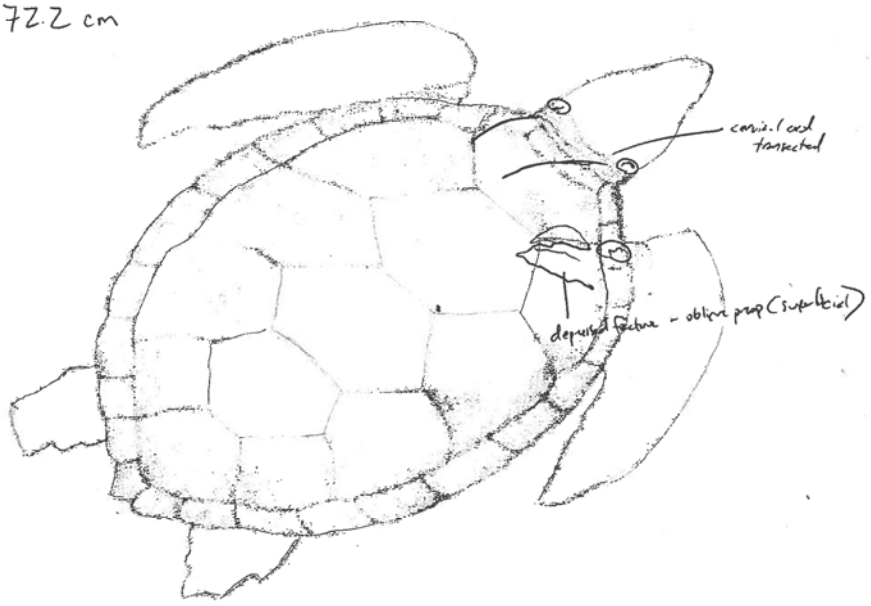

Comments:

cut sp	cut span
1-2	7.9cm
2-3	11.1cm

	chord length	max depth	chord depth
1	11.6 cm	1.0cm	0.6cm
2	16.2 cm	~~2.9cm~~	2.9 cm
3	/		

Figure B.51. Data sheet for Shell R5

Data Collection Sheet

Shell #: R-11 Time: 2:33 Date: 10/13/11

Accel. #: _____ Boat Type: Deep V Prop Depth: Prop Depth

Boat Speed (km/hr): 27 Orientation: 3:00

Type of wound (Blunt trauma, prop cut): _____

Size/Location of cuts/damage:

Sketch of damage:

SCL N-T: 68.6cm

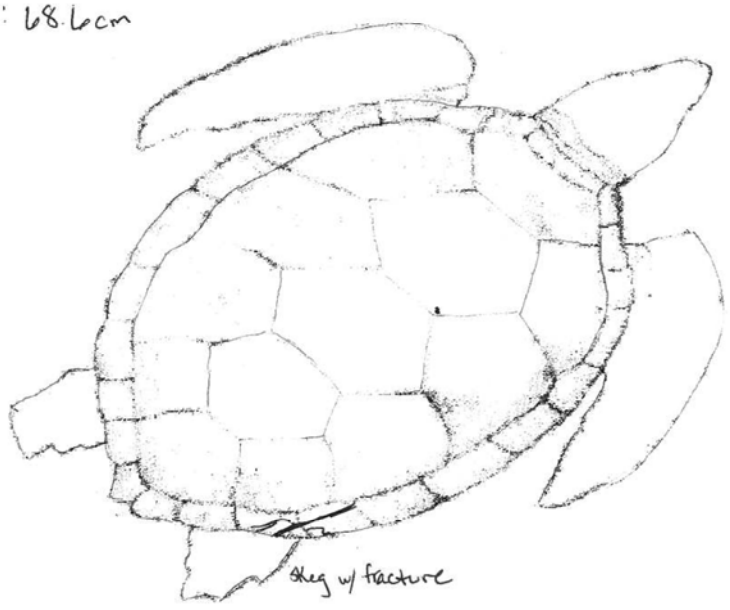

Comments:

Figure B.52. Data sheet for Shell R11

Data Collection Sheet

Shell #: R-12 Time: 2:44 Date: 10/13/11

Accel. #: _____ Boat Type: Deep V Prop Depth: Prop Depth

Boat Speed (km/hr): 24 Orientation: 4:00

Type of wound (Blunt trauma, prop cut): Blunt

Size/Location of cuts/damage:

Extensive blunt trauma/cavity wound
- prop cuts on well/part partly discarded

Sketch of damage:

SCL N-T: 74.8cm

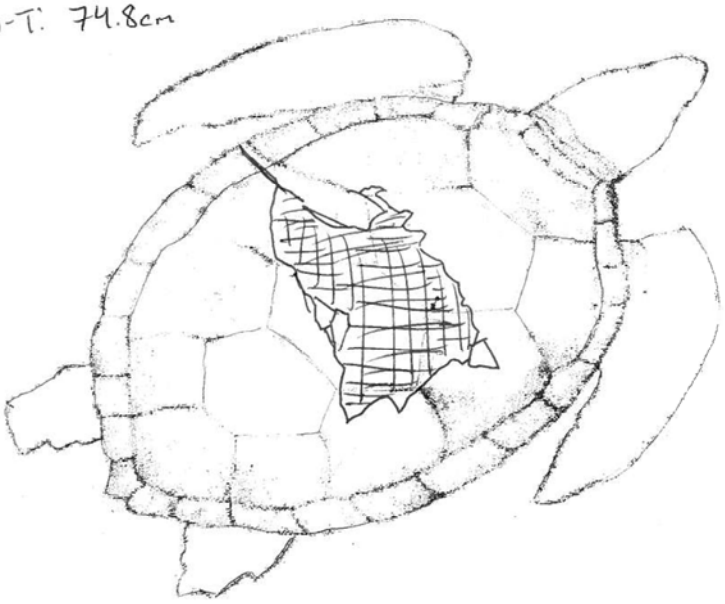

Comments:

Figure B.53. Data sheet for Shell R12

APPENDIX C

ACCELEROMETER DATA

The following graphs of the resultant acceleration for each field test were used to find the peak accelerations reported in Chapter 4. The test number, vessel number, and model depth in the water are noted in each caption.

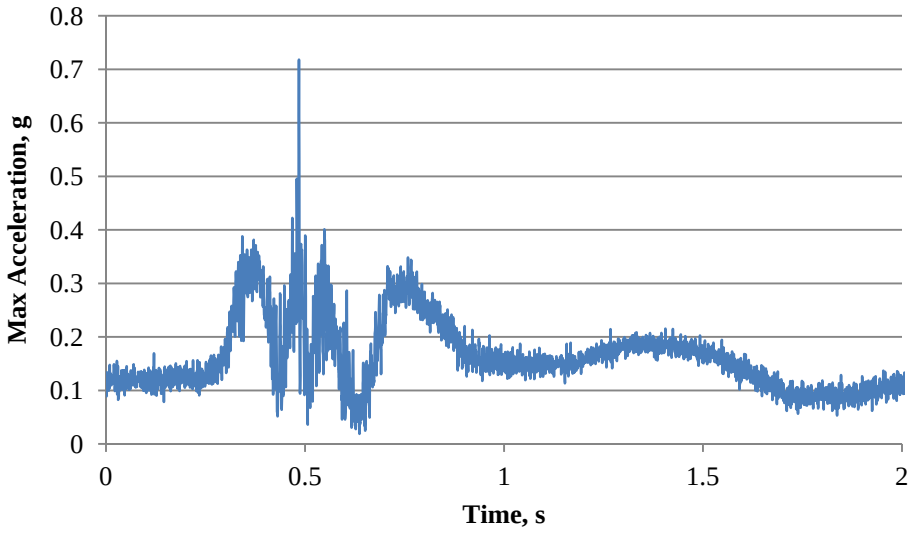

Figure C.1. Maximum acceleration record for Shell 1, Vessel 1, 48 cm

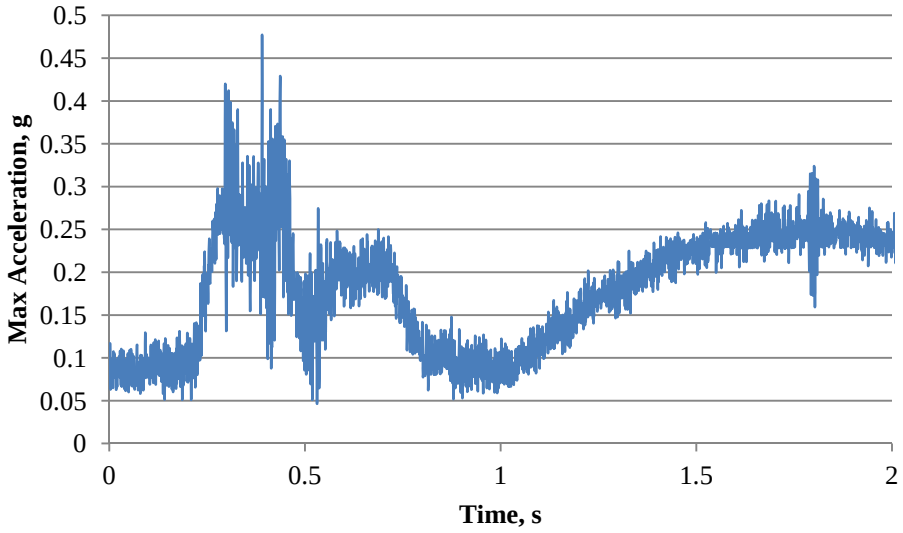

Figure C.2. Maximum acceleration record for Shell 2, Vessel 1, 48 cm

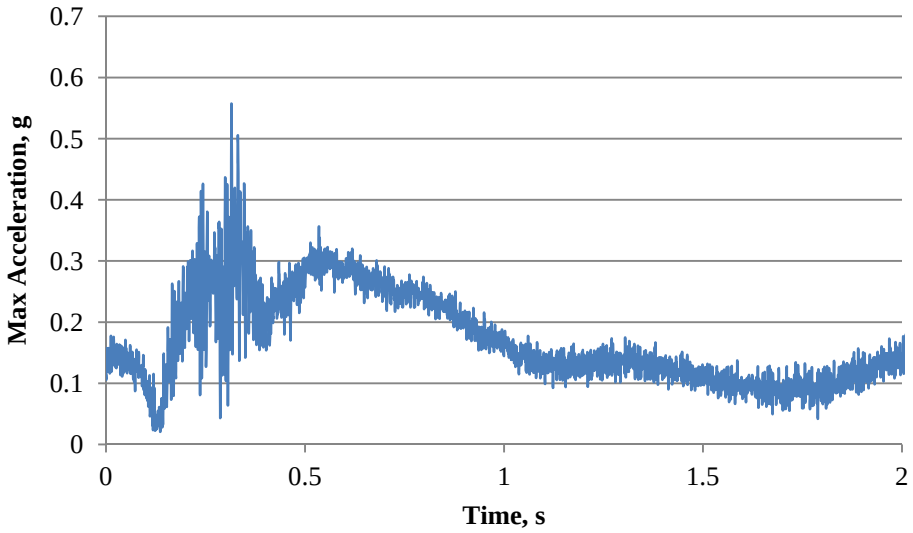

Figure C.3. Maximum acceleration record for Shell 3, Vessel 1, 48 cm

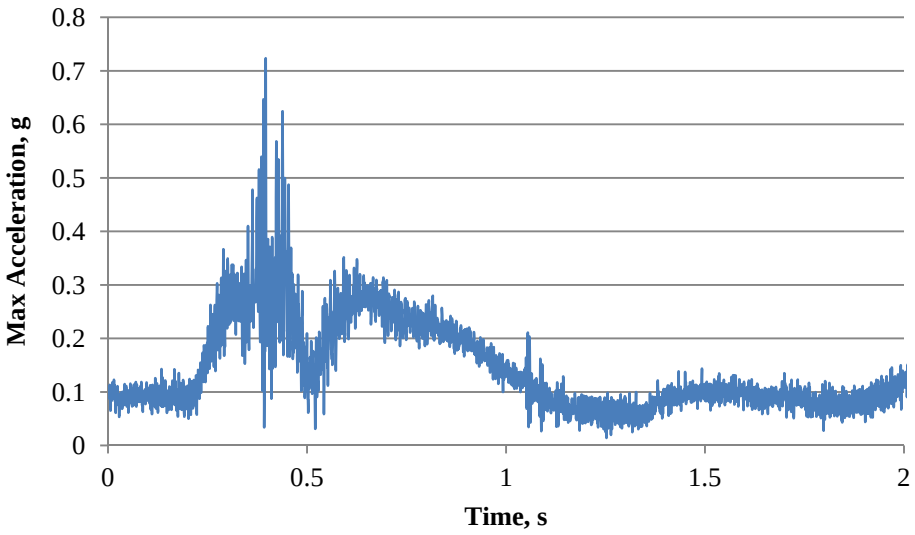

Figure C.4. Maximum acceleration record for Shell 4, Vessel 1, 48 cm

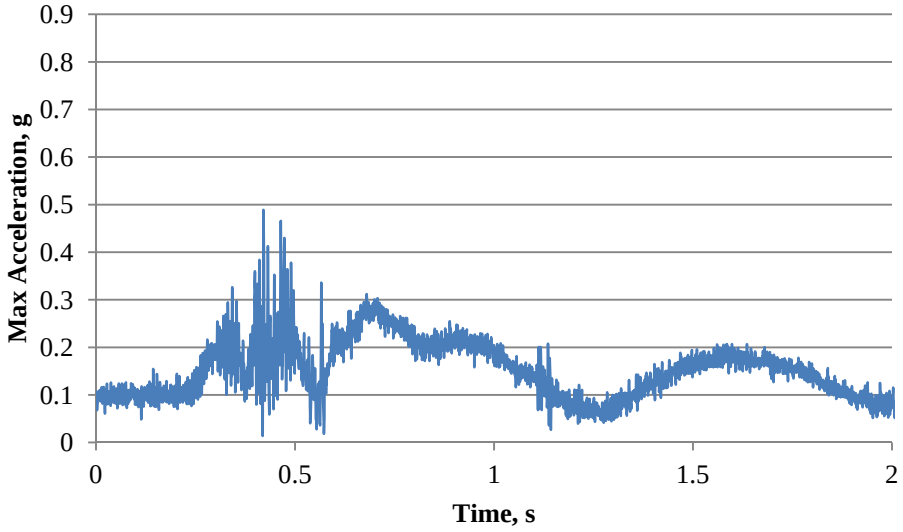

Figure C.5. Maximum acceleration record for Shell 5, Vessel 1, 48 cm

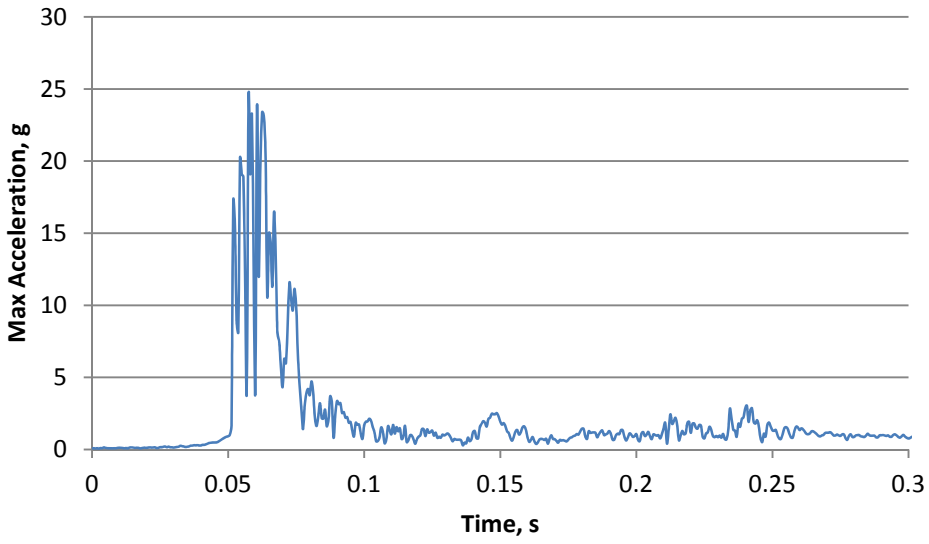

Figure C.6. Maximum acceleration record for Shell 6, Vessel 1, Surface

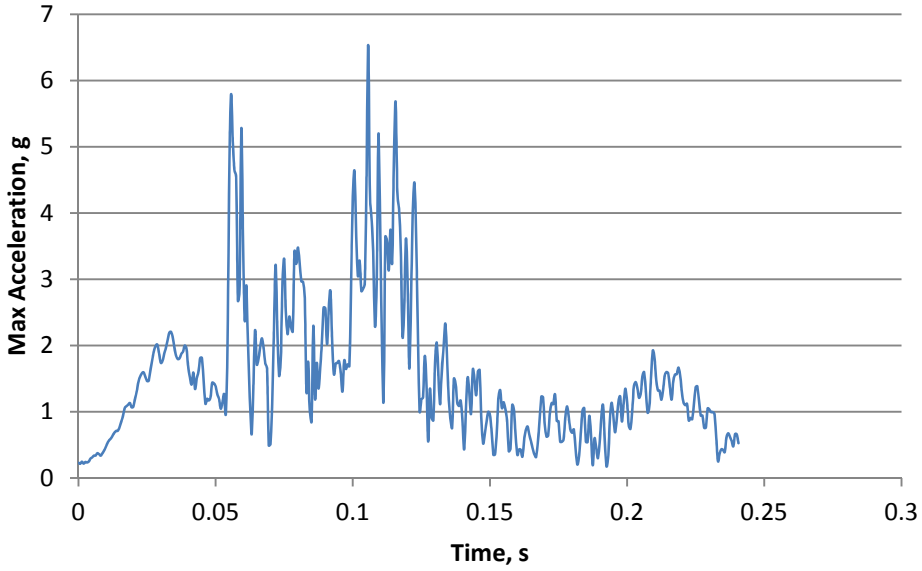

Figure C.7. Maximum acceleration record for Shell 7, Vessel 1, Surface

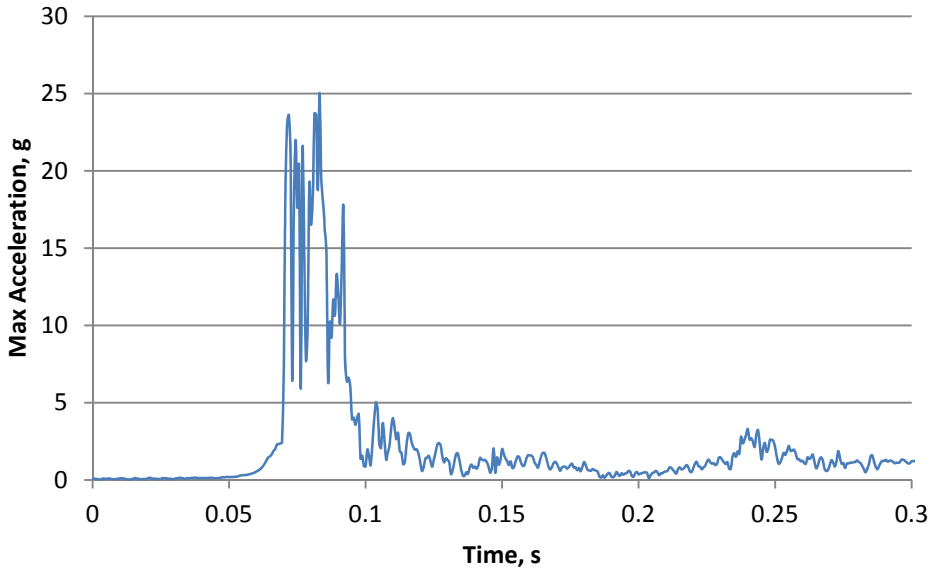

Figure C.8. Maximum acceleration record for Shell 7B, Vessel 1, Surface

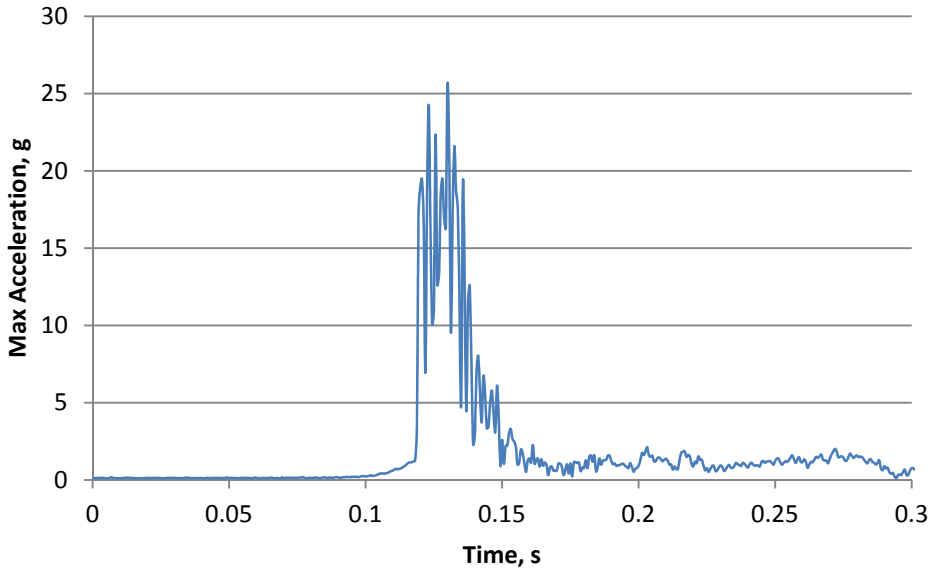

Figure C.9. Maximum acceleration record for Shell 8, Vessel 1, Surface

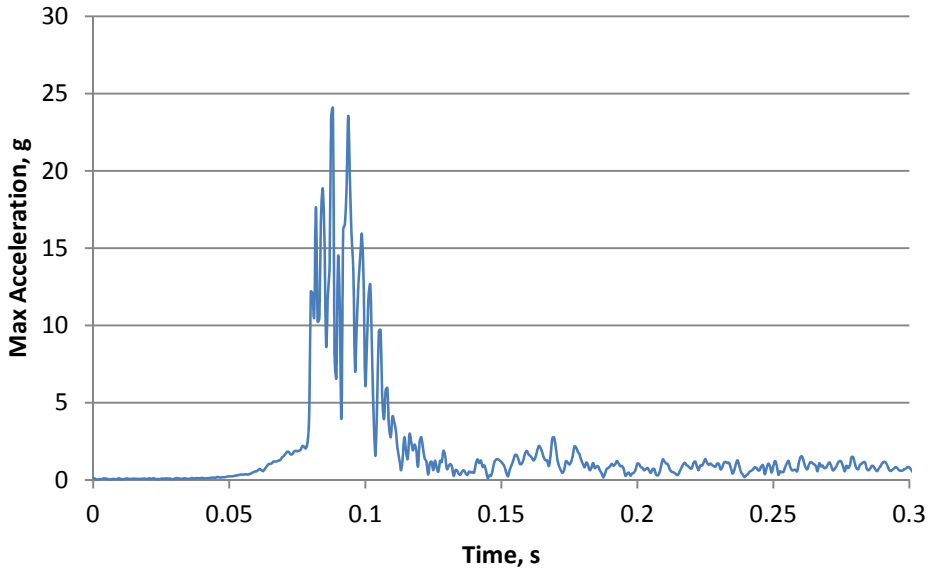

Figure C.10. Maximum acceleration record for Shell 9, Vessel 1, Surface

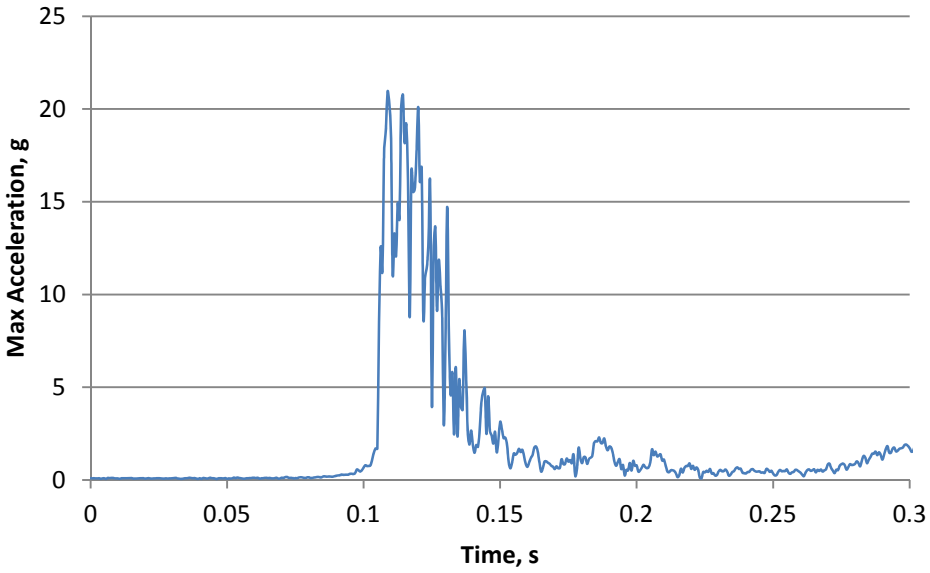

Figure C.11. Maximum acceleration record for Shell 10, Vessel 1, Surface

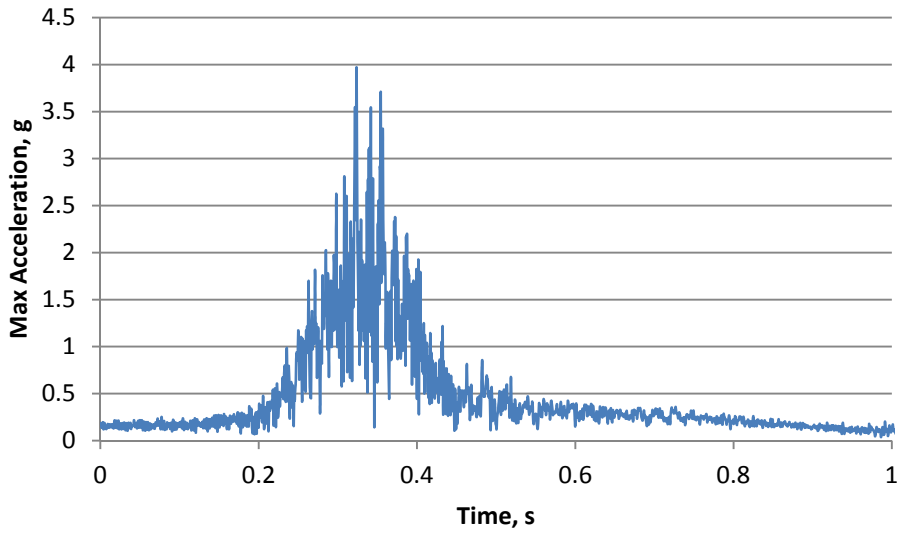

Figure C.12. Maximum acceleration record for 11A, Vessel 2, 71 cm

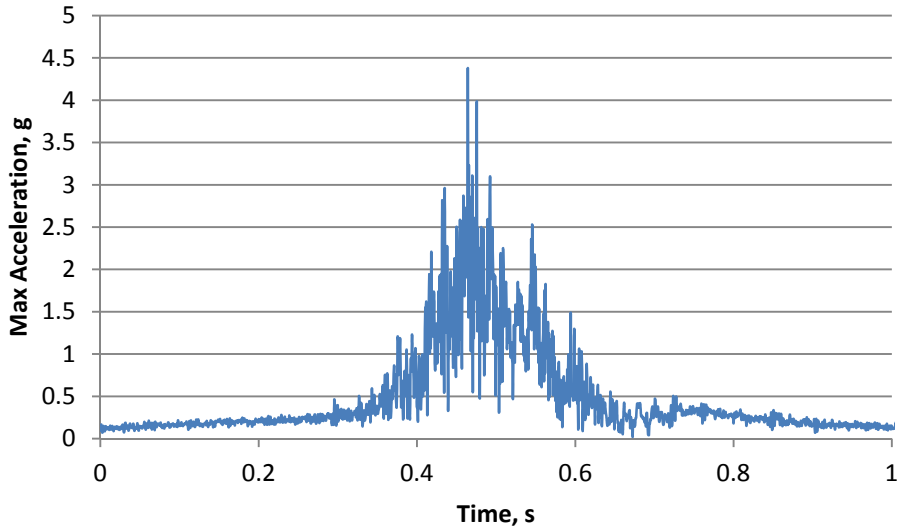

Figure C.13. Maximum acceleration record for 11B, Vessel 2, 71 cm

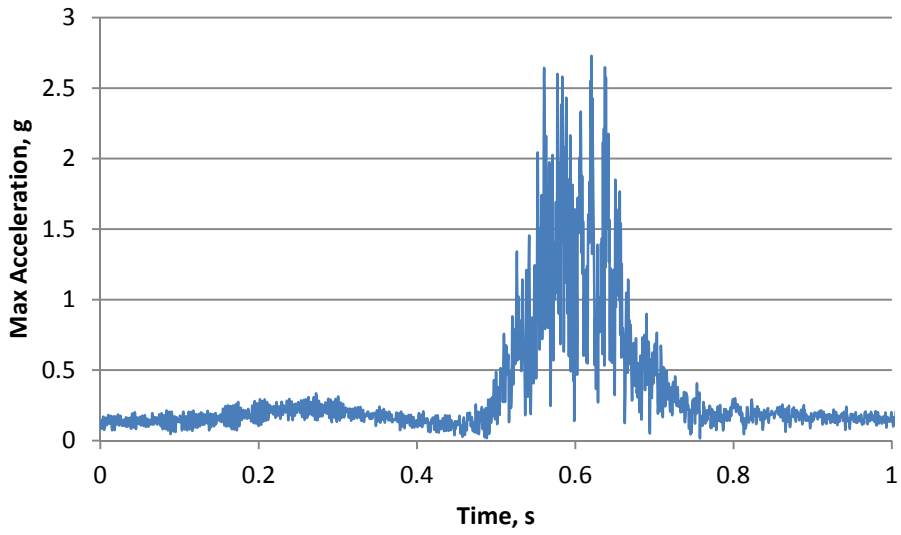

Figure C.14. Maximum acceleration record for 11C, Vessel 2, 71 cm

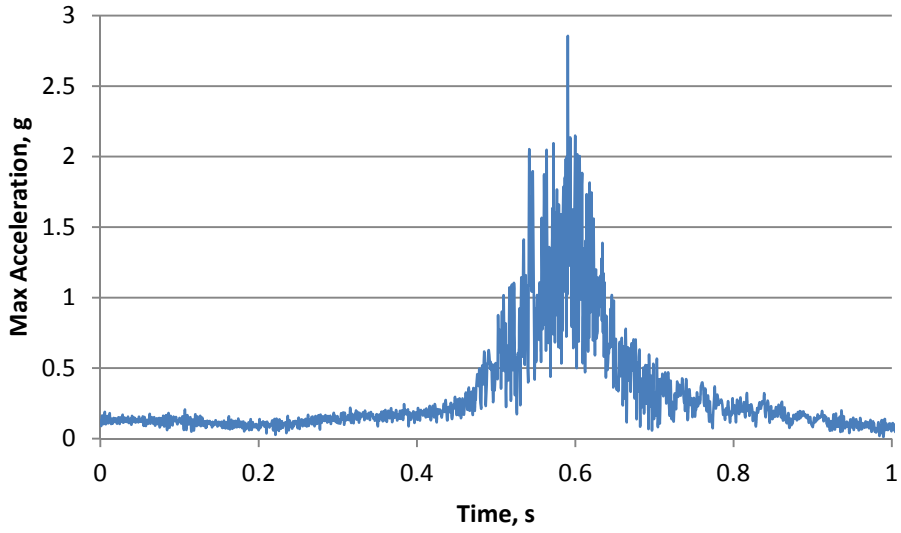

Figure C.15. Maximum acceleration record for 11D, Vessel 2, 71 cm

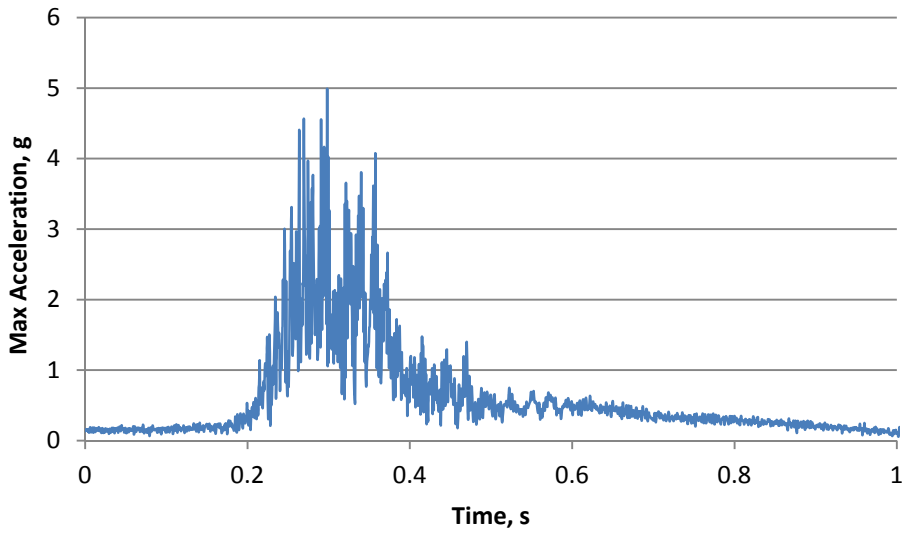

Figure C.16. Maximum acceleration record for 11E, Vessel 2, 71 cm

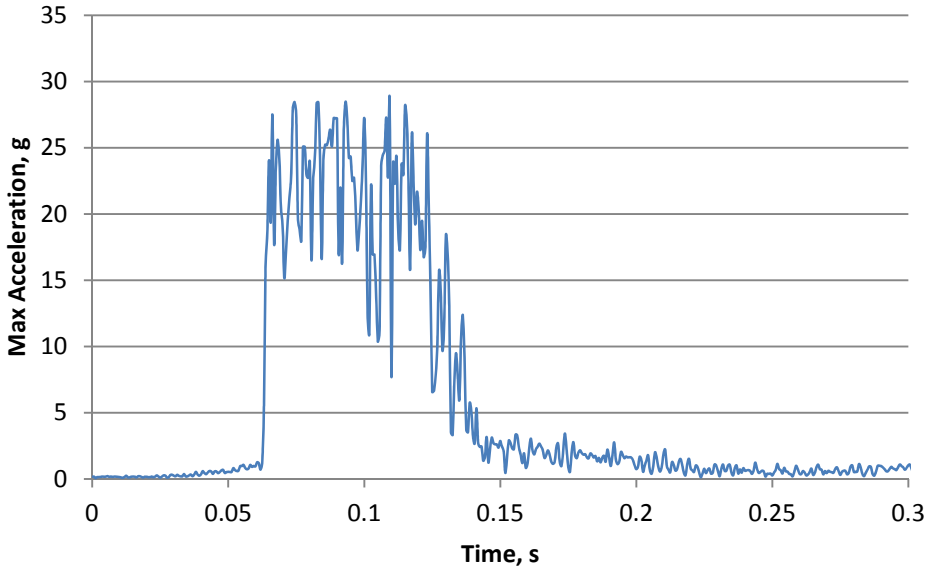

Figure C.17. Maximum acceleration record for Shell 11F, Vessel 2, 48 cm

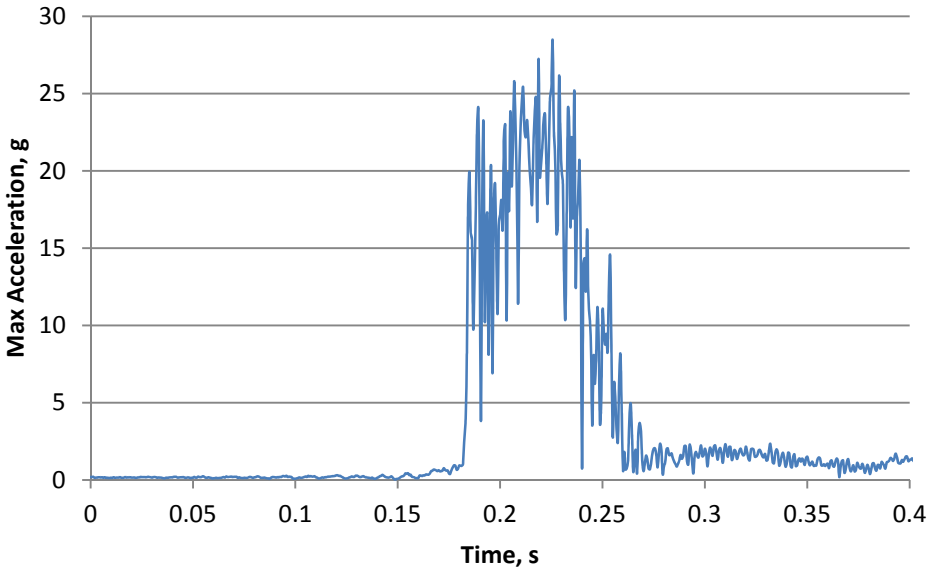

Figure C.18. Maximum acceleration record for Shell 12, Vessel 2, 48 cm

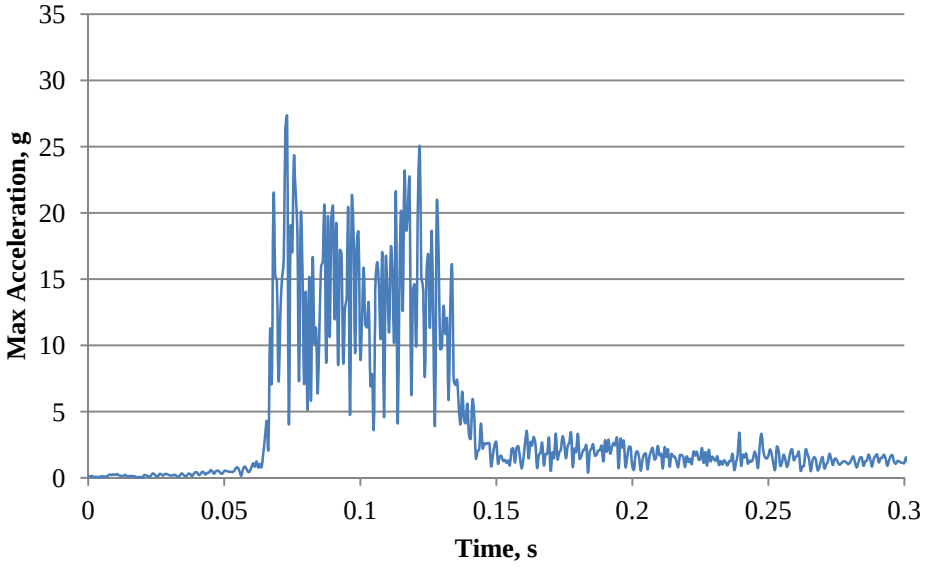

Figure C.19. Maximum acceleration record for Shell 13, Vessel 2, 48 cm

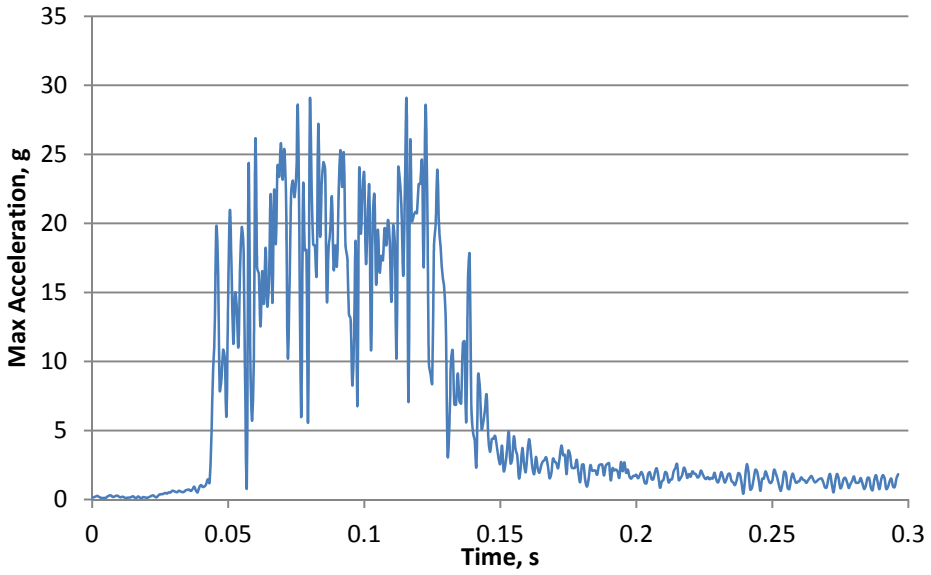

Figure C.20. Maximum acceleration record for Shell 14, Vessel 2, 48 cm

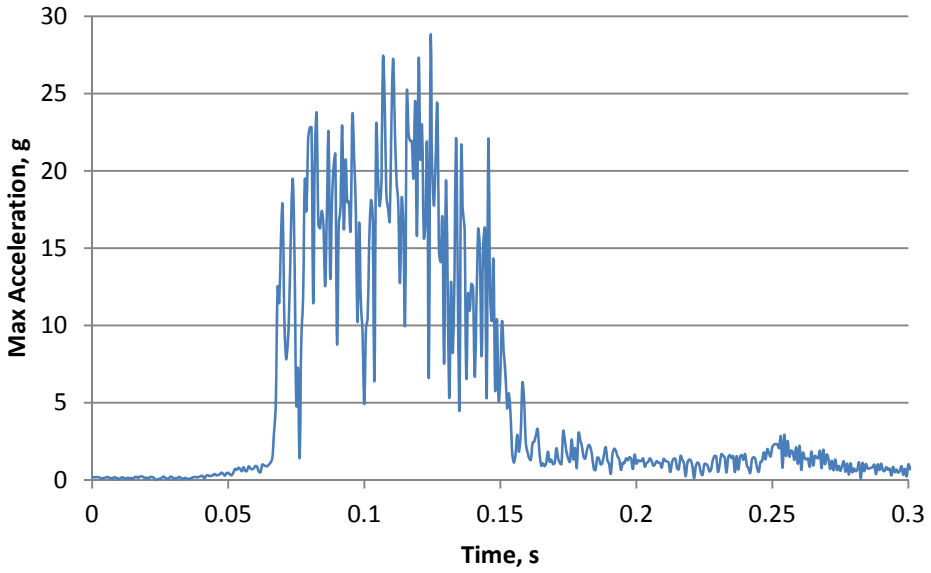

Figure C.21. Maximum acceleration record for Shell 15, Vessel 2, 48 cm

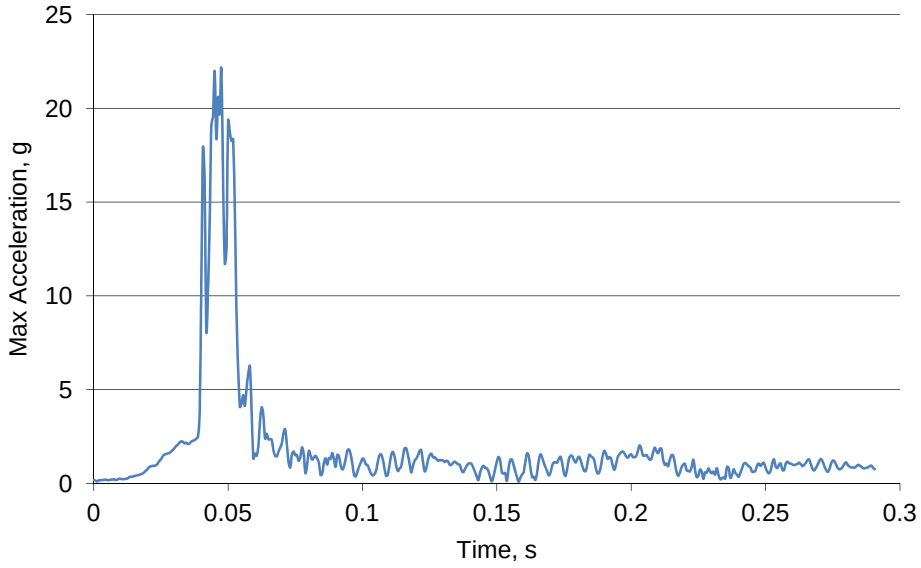

Figure C.22. Maximum acceleration record for Shell 4, Vessel 1, Surface

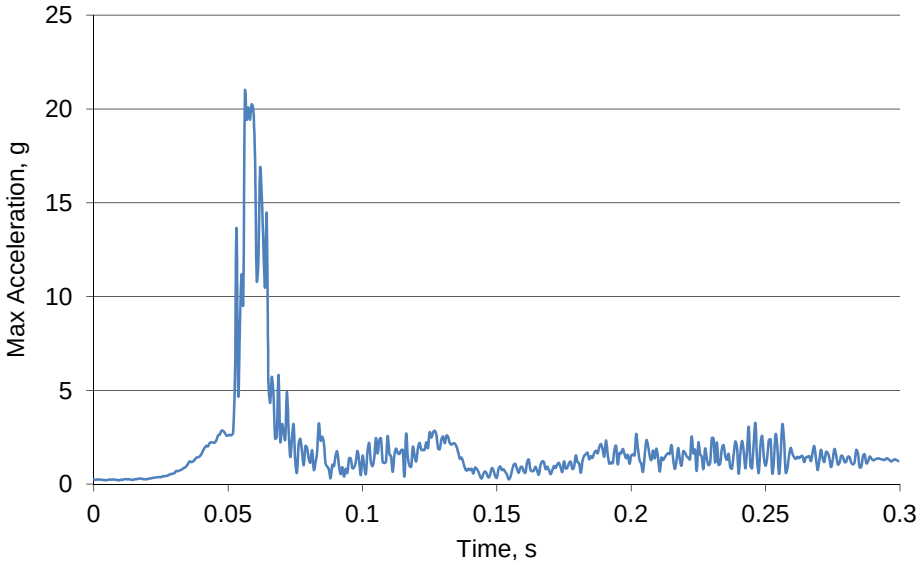

Figure C.23. Maximum acceleration record for Shell 26, Vessel 1, Surface

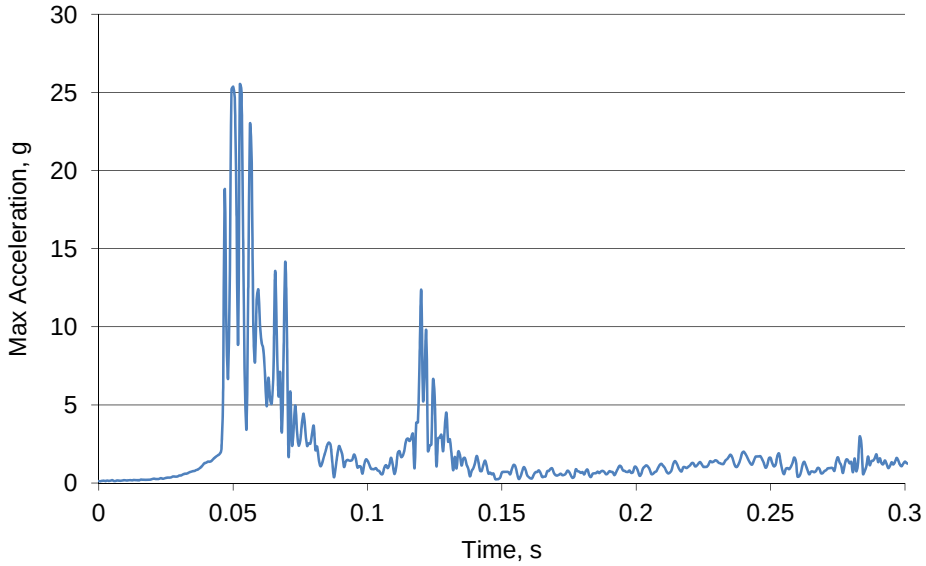

Figure C.24. Maximum acceleration record for Shell 22, Vessel 1, Surface

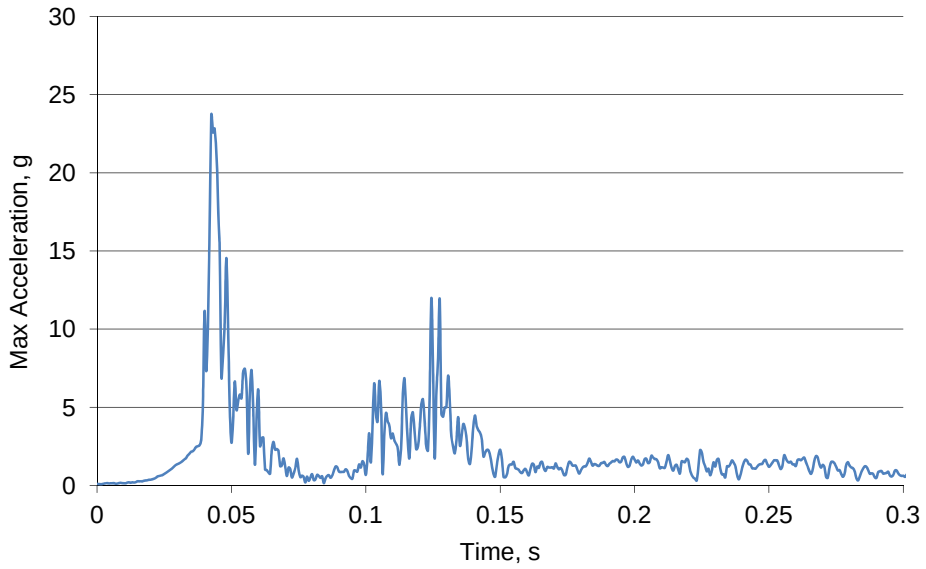

Figure C.25. Maximum acceleration record for Shell 28, Vessel 1, Surface

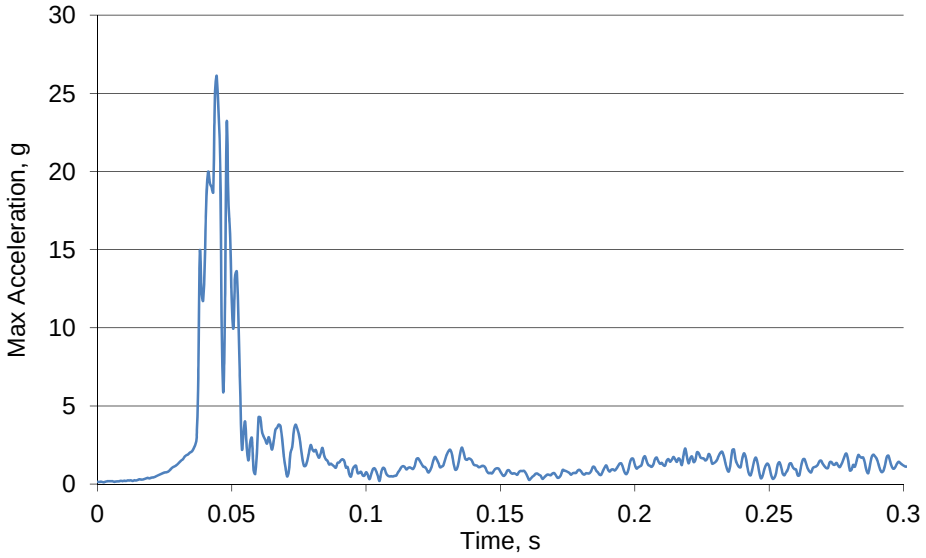

Figure C.26. Maximum acceleration record for Shell 39, Vessel 1, Surface

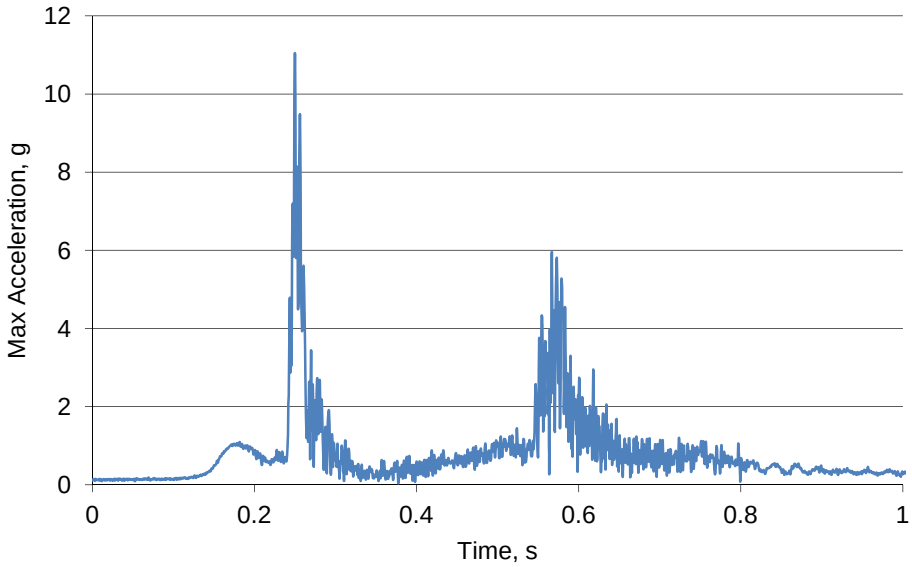

Figure C.27. Maximum acceleration record for Shell 23, Vessel 2, Surface

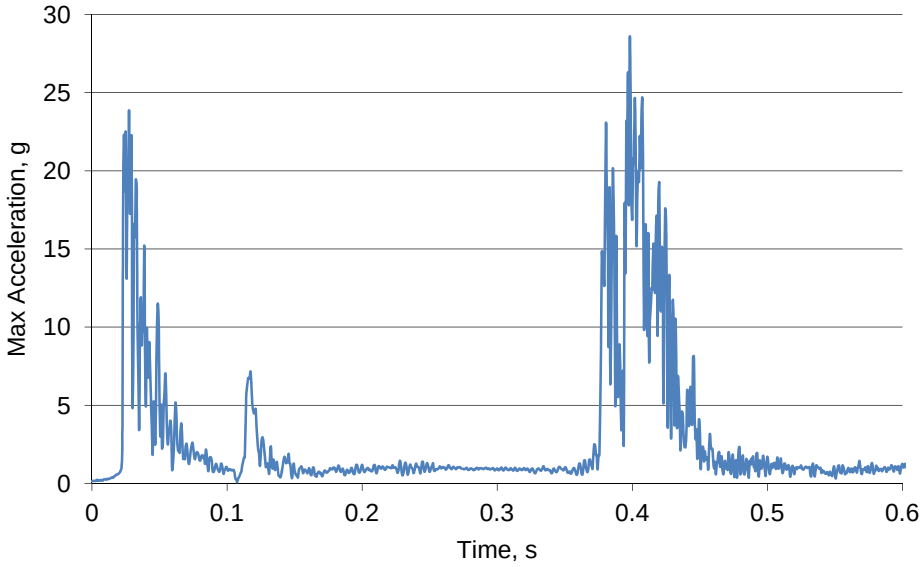

Figure C.28. Maximum acceleration record for Shell 23B, Vessel 2, Surface

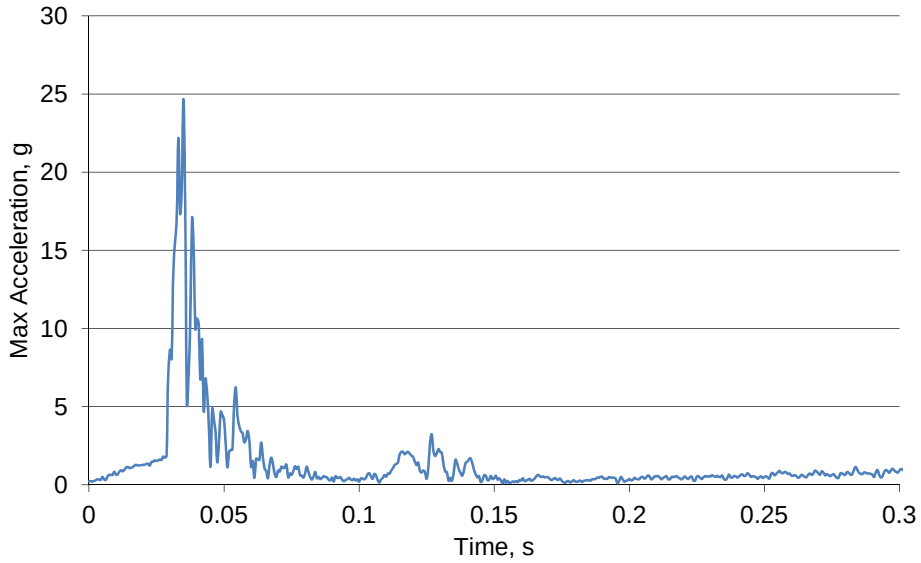

Figure C.29. Maximum acceleration record for Shell 24, Vessel 2, Surface

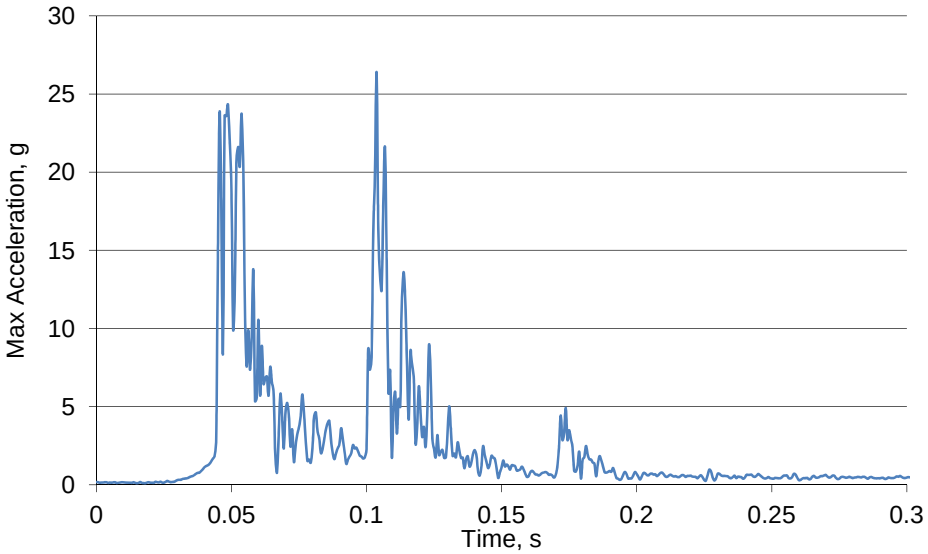

Figure C.30. Maximum acceleration record for Shell 24B, Vessel 2, Surface

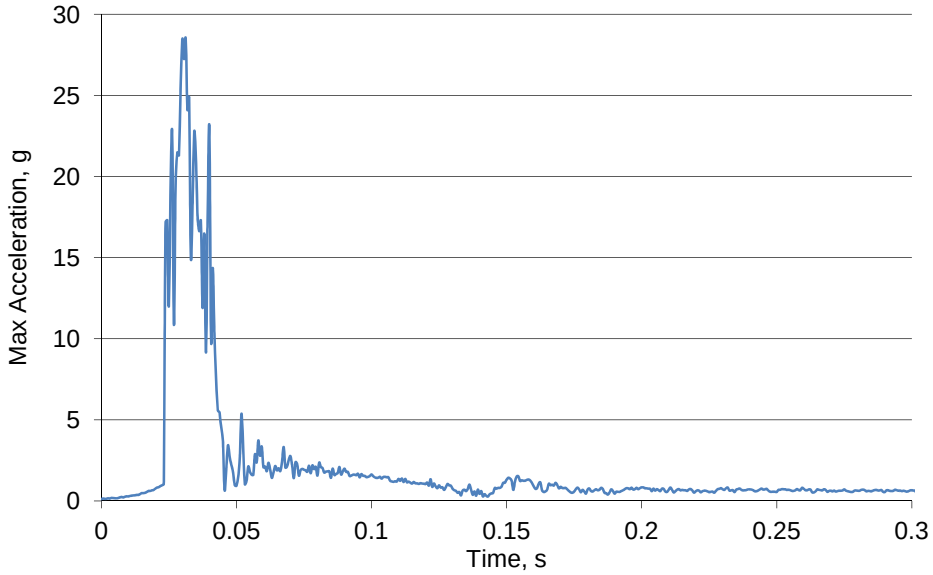

Figure C.31. Maximum acceleration record for Shell 24C, Vessel 2, Surface

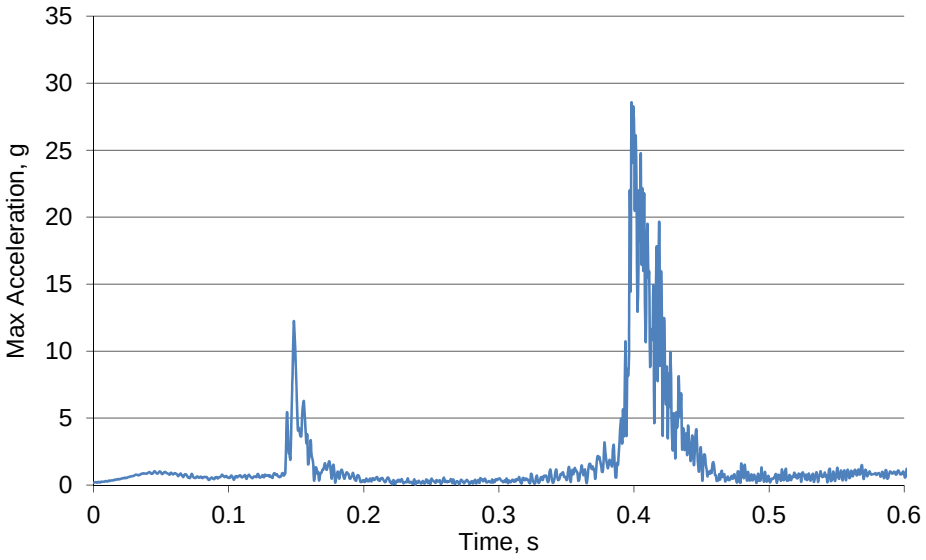

Figure C.32. Maximum acceleration record for Shell 27, Vessel 2, Surface

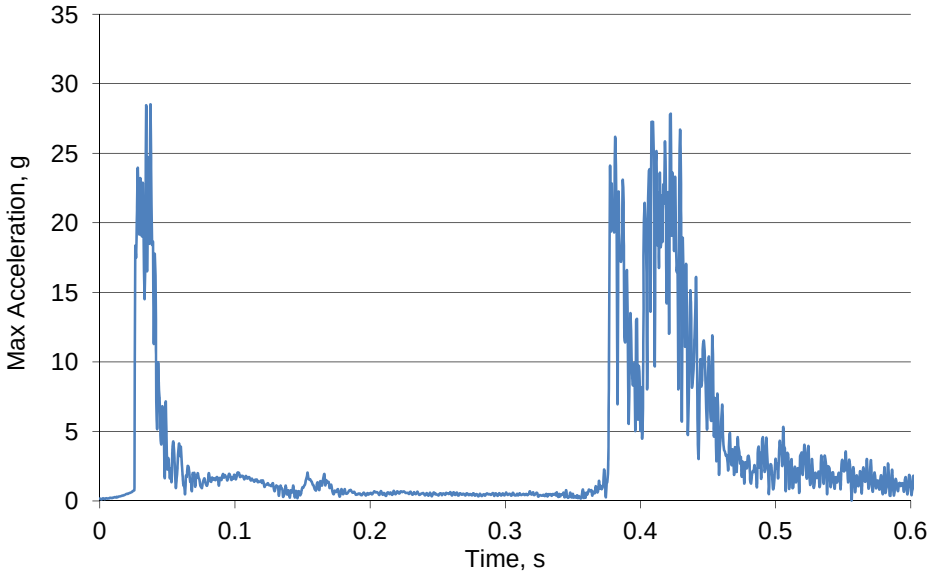

Figure C.33. Maximum acceleration record for Shell 37, Vessel 2, Surface

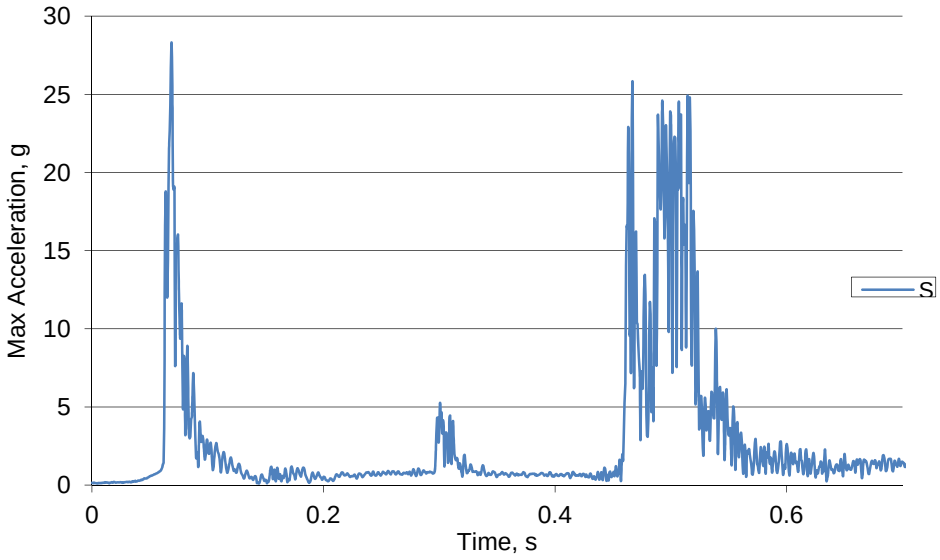

Figure C.34. Maximum acceleration record for Shell 25, Vessel 2, Surface

APPENDIX D

LS-DYNA REDUCED KEYWORD INPUT

```
$# LS-DYNA Keyword file created by LS-PrePost 3.2 - 03Mar2012(09:08)
$# Created on Apr-12-2012 (12:13:26)
*KEYWORD
*TITLE
Turtle model impact
LS-DYNA keyword deck by LS-PrePost
*CONTROL_ALE
$#     dct      nadv      meth      afac      bfac      cfac      dfac      efac
         1         1         1 -1.000000     0.000     0.000     0.000     0.000
$#   start       end     aafac     vfact      prit       ebc      pref   nsidebc
     0.0001.0000E+20  1.000000 1.0000E-6         0         0     0.000         0
$#    ncpl      nbkt    imascl    checkr
         1        50         0     0.000
*CONTROL_TERMINATION
$#  endtim    endcyc     dtmin    endeng    endmas
 40.000000         0     0.000     0.000     0.000
*DATABASE_ELOUT
$#      dt    binary      lcur     ioopt
  1.000000         1         0         1
*DATABASE_GLSTAT
$#      dt    binary      lcur     ioopt
  1.000000         1         0         1
*DATABASE_MATSUM
$#      dt    binary      lcur     ioopt
  1.000000         1         0         1
*DATABASE_NODFOR
$#      dt    binary      lcur     ioopt
  1.000000         1         0         1
*DATABASE_NODOUT
$#      dt    binary      lcur     ioopt      dthf     binhf
  1.000000         1         0         1     0.000         0
*DATABASE_BINARY_D3PLOT
$#      dt      lcdt      beam     npltc    psetid
  0.500000         0         0         0         0
$#   ioopt
         0
*DATABASE_HISTORY_NODE
$#     id1       id2       id3       id4       id5       id6       id7       id8
      2693         0         0         0         0         0         0         0
*DATABASE_HISTORY_SHELL_SET
$#     id1       id2       id3       id4       id5       id6       id7       id8
         1         0         0         0         0         0         0         0
*DATABASE_HISTORY_SOLID_SET
$#     id1       id2       id3       id4       id5       id6       id7       id8
         1         0         0         0         0         0         0         0
*LOAD_NODE_SET
$#    nsid       dof      lcid        sf       cid        m1        m2        m3
         1         2         1  0.900000         0         0         0         0
         1         3         1 -0.435900         0         0         0         0
*PART
$# title
1 Core
$#     pid     secid       mid     eosid      hgid      grav    adpopt      tmid
         1         1         1         0         0         0         0         0
*SECTION_SOLID_TITLE
solid
$#   secid    elform       aet
         1         1         0
```

```
*MAT_SOIL_AND_FOAM_TITLE
foam core
$#     mid        ro         g      bulk        a0        a1        a2        pc
         1 3.2000E-7  0.049000  0.063000  0.012000     0.000     0.000 -0.004000
$#     vcr       ref
     0.000     0.000
$#    eps1      eps2      eps3      eps4      eps5      eps6      eps7      eps8
     0.000 -4.200000 -3.000000 -2.670000 -2.130000 -1.320000 -1.110000 -0.860000
$#    eps9     eps10
 -0.700000 -0.630000
$#      p1        p2        p3        p4        p5        p6        p7        p8
     0.000 5.0000E-4  0.005140  0.005900  0.005500  0.005400  0.005500  0.005900
$#      p9       p10
  0.006600  0.007200
*PART
$# title
2 Body
$#     pid     secid       mid     eosid      hgid      grav    adpopt      tmid
         2         1         2         0         0         0         0         0
*MAT_SOIL_AND_FOAM_TITLE
foam body
$#     mid        ro         g      bulk        a0        a1        a2        pc
         2 1.4000E-6  0.002400 5.6500E-4  0.015000     0.000     0.000 -0.004000
$#     vcr       ref
     0.000     0.000
$#    eps1      eps2      eps3      eps4      eps5      eps6      eps7      eps8
     0.000 -4.200000 -3.000000 -2.670000 -2.130000 -1.320000 -1.110000 -0.860000
$#    eps9     eps10
 -0.700000 -0.630000
$#      p1        p2        p3        p4        p5        p6        p7        p8
     0.000 1.6670E-4  0.001710  0.001970  0.001840  0.001800  0.001850  0.001990
$#      p9       p10
  0.002200  0.002410
*PART
$# title
3 Face
$#     pid     secid       mid     eosid      hgid      grav    adpopt      tmid
         3         2         3         0         0         0         0         0
*SECTION_SHELL_TITLE
face
$#   secid    elform      shrf       nip     propt   qr/irid     icomp     setyp
         2         2  1.000000         2         1         0         0         1
$#      t1        t2        t3        t4      nloc     marea      idof    edgset
  1.000000  1.000000  1.000000  1.000000     0.000     0.000     0.000         0
*MAT_ELASTIC
$#     mid        ro         e        pr        da        db  not used
         3 1.4000E-6  1.157000  0.333000     0.000     0.000         0
*PART
$# title
Water
$#     pid     secid       mid     eosid      hgid      grav    adpopt      tmid
         4         3         4         1         0         0         0         0
*SECTION_SOLID
$#   secid    elform       aet
         3        12         0
*MAT_NULL
$#     mid        ro        pc        mu     terod     cerod        ym        pr
         4 1.0000E-6-1.000E+11     0.000     0.000     0.000     0.000     0.000
*EOS_GRUNEISEN
$#   eosid         c        s1        s2        s3     gamao         a        e0
         1  1.500000     0.000     0.000     0.000     0.000     0.000     0.000
$#      v0
     0.000
*PART
$# title
Air
$#     pid     secid       mid     eosid      hgid      grav    adpopt      tmid
         5         3         4         1         0         0         0         0
*INITIAL_VOID_PART
$#     pid
         5
```

```
*DEFINE_CURVE
$#     lcid      sidr       sfa       sfo      offa      offo    dattyp
         1         0  1.000000  0.040000     0.000     0.000         0
$#               a1                  o1
             0.000               0.000
         1.000000           0.156400
         2.000000           0.309000
         3.000000           0.454000
         4.000000           0.587800
         5.000000           0.707100
         6.000000           0.809000
         7.000000           0.891000
         8.000000           0.951100
         9.000000           0.987700
        10.000000           1.000000
        11.000000           0.987700
        12.000000           0.951100
        13.000000           0.891000
        14.000000           0.809000
        15.000000           0.707100
        16.000000           0.587800
        17.000000           0.454000
        18.000000           0.309000
        19.000000           0.156400
        20.000000           0.000
*SET_NODE_LIST_TITLE
Contact Area
$#     sid       da1       da2       da3       da4    solver
         1     0.000     0.000     0.000     0.000MECH
$#    nid1      nid2      nid3      nid4      nid5      nid6      nid7      nid8
      1170      1135      1078      1012      1013      1079      1136      1171
      1147      1139      1084      1017      1018      1020      1085      1088
      1129      1063      1021       968       944       866       989      1128
      1061      1062       987       988       881       880       781       782
*SET_PART_LIST
$#     sid       da1       da2       da3       da4    solver
         1     0.000     0.000     0.000     0.000MECH
$#    pid1      pid2      pid3      pid4      pid5      pid6      pid7      pid8
         1         2         3         0         0         0         0         0
*SET_PART_LIST
$#     sid       da1       da2       da3       da4    solver
         2     0.000     0.000     0.000     0.000MECH
$#    pid1      pid2      pid3      pid4      pid5      pid6      pid7      pid8
         4         5         0         0         0         0         0         0
*CONSTRAINED_LAGRANGE_IN_SOLID
$#   slave    master     sstyp     mstyp     nquad     ctype     direc     mcoup
         1         2         0         0         0         4         2         1
$#   start       end      pfac      fric    frcmin      norm   normtyp      damp
     0.000     0.000     0.000     0.000  0.500000         0         0     0.000
$#      cq      hmin      hmax     ileak     pleak   lcidpor     nvent  blockage
     0.000     0.000     0.000         0     0.000         0         0         0
$#  iboxid   ipenchk   intforc   ialesof    lagmul    pfacmm      thkf
         0         0         0         0     0.000         0     0.000
```

REFERENCES

Abrate, S. (1997). "Localized impact on sandwich structures with laminated facings." Applied Mechanics Reviews **50**: 69.

Aktay, L., A. F. Johnson and M. Holzapfel (2005). "Prediction of impact damage on sandwich composite panels." Computational Materials Science **32**(3-4): 252-260.

Anderson, T. and E. Madenci (2000). "Experimental investigation of low-velocity impact characteristics of sandwich composites." Composite Structures **50**(3): 239-247.

ASTM Standard D790 (2010). Test Methods for Flexural Properties of Unreinforced and Reinforced Plastics and Electrical Insulating Materials. West Conshohocken, PA, ASTM International.

ASTM Standard D1621 (2010). Test Method for Compressive Properties of Rigid Cellular Plastics. West Conshohocken, PA, ASTM International.

ASTM Standard D3039 (2008). Test Method for Tensile Properties of Polymer Matrix Composite Materials. West Conshohocken, PA, ASTM International.

ASTM Standard D3574 (2011). Test Methods for Flexible Cellular Materials - Slab, Bonded, and Molded Urethane Foams. West Conshohocken, PA, ASTM International.

BoatTEST.com LLC. (2012). "BoatTEST.com." Retrieved June 2, 2012, from www.boattest.com.

Bryant, J. D. (1988). "On the mechanical function of marrow in long bones." Engineering in medicine **17**(2): 55.

Calleson, C. S. and R. K. Frohlich (2007). "Slower boat speeds reduce risks to manatees." Endangered Species Research **3**(3): 295-304.

Carter, D. and W. Hayes (1977). "The compressive behavior of bone as a two-phase porous structure." J Bone Joint Surg Am **59**(7): 954-962.

Conant, T. A., P. H. Dutton, T. Eguchi, S. P. Epperly, C. C. Fahy, M. H. Godfrey, S. L. MacPherson, E. E. Possardt, B. A. Schroeder, J. A. Seminoff, M. L. Snover, C. M. Upite and B. E. Witherington (2009). Loggerhead sea turtle (*Caretta caretta*) 2009 status review under the U.S. Endangered Species Act, Report of the Loggerhead Biological Review Team to the National Marine Fisheries Service**:** 222.

Cristofolini, L. and M. Viceconti (2000). "Mechanical validation of whole bone composite tibia models." Journal of Biomechanics **33**(3): 279-288.

Cristofolini, L., M. Viceconti, A. Cappello and A. Toni (1996). "Mechanical validation of whole bone composite femur models." Journal of Biomechanics **29**(4): 525-535.

Currey, J. D. (2002). Bones : structure and mechanics. Princeton, N.J., Princeton University Press.

Do, I. and J. Day (2005). Overview of ALE Method in LS-DYNA. LSTC.

Dodd, C. K. (1988). Synopsis of the biological data on the loggerhead sea turtle *Caretta caretta* (Linnaeus 1758), U.S. Fish and Wildlife Service. **Biological Report:** 110.

Douglas, A. B., J. Calambokidis, S. Raverty, S. J. Jeffries, D. M. Lambourn and S. A. Norman (2008). "Incidence of ship strikes of large whales in Washington State." Journal of the Marine Biological Association of the UK **88**(06): 1121-1132.

Dumont, E., I. Grosse and G. Slater (2009). "Requirements for comparing the performance of finite element models of biological structures." Journal of theoretical biology **256**(1): 96-103.

Fisher, R. A. (1922). "On the Interpretation of $\chi 2$ from Contingency Tables, and the Calculation of P." Journal of the Royal Statistical Society **85**(1): 87-94.

George, J. C., L. M. Philo, K. Hazard, D. Withrow, G. M. Carroll and R. Suydam (1994). "Frequency of Killer Whale (*Orcinus orcd*) Attacks and Ship Collisions Based on Scarring on Bowhead Whales (*Balaena mysticetus*) of the Bering-Chukchi-Beaufort Seas Stock." Arctic: 247-255.

Gerstein, E. (2002). "Manatees, Bioacoustics and Boats Hearing tests, environmental measurements and acoustic phenomena may together explain why boats and animals collide." American Scientist **90**(2): 154-163.

Gibson, L. J. (1985). "The mechanical behaviour of cancellous bone." Journal of Biomechanics **18**(5): 317-328.

Gibson, L. J. and M. F. Ashby (1999). Cellular solids : structure and properties. Cambridge ; New York, Cambridge University Press.

Gilman, E., D. Kobayashi, T. Swenarton, N. Brothers, P. Dalzell and I. Kinan-Kelly (2007). "Reducing sea turtle interactions in the Hawaii-based longline swordfish fishery." Biological Conservation **139**(1-2): 19-28.

Google. (2012). "Google Maps." Retrieved March 9, 2012, from http://maps.google.com/maps?f=q&hl=en&geocode=&q=Cape%20Fear%20Road%2C%20Bloomingdale%2C%20GA&mrt=all.

Gupta, N. and R. Nagorny (2006). "Tensile properties of glass microballoon-epoxy resin syntactic foams." Journal of Applied Polymer Science **102**(2): 1254-1261.

Hallquist, J. O. (2009). LS-DYNA Keyword User's Manual. Livermore, CA, Livermore Software Technology Corporation.

Hallquist, J. O. (2011). LS-PrePost v3.2. Livermore, CA, Livermore Software Technology Corporation.

Hallquist, J. O. (2012). LS-DYNA v971. Livermore, CA, Livermore Software Technology Corporation.

Hart, K. M., P. Mooreside and L. B. Crowder (2006). "Interpreting the spatio-temporal patterns of sea turtle strandings: going with the flow." Biological Conservation **129**(2): 283-290.

Haubold, E. M., C. Deutsch and C. Fonnesbeck (2006). "Final Biological Status Review of the Florida Manatee (*Trichechus manatus latirostris*)."

Hazel, J. and E. Gyuris (2006). "Vessel-related mortality of sea turtles in Queensland, Australia." Wildlife Research **33**(2): 149-154.

Hazel, J., I. R. Lawler and M. Hamann (2009). "Diving at the shallow end: Green turtle behaviour in near-shore foraging habitat." Journal of Experimental Marine Biology and Ecology **371**(1): 84-92.

Hazel, J., I. R. Lawler, H. Marsh and S. Robson (2007). "Vessel speed increases collision risk for the green turtle *Chelonia mydas*." Endangered Species Research **3**(2): 105-113.

Hodges, J. E. (2008). Evaluation of Turtle Shell Properties and Prototype Biomimetic Shell Fabrication. School of Civil and Environmental Engineering. Savannah, GA, Georgia Institute of Technology. **Master of Science in Civil Engineering**.

Hollister, S. J. (2011). "Bone Structure." Retrieved July 19, 2011, from http://www.engin.umich.edu/class/bme456/bonestructure/bonestructure.htm.

Horgan, T. and M. Gilchrist (2003). "The creation of three-dimensional finite element models for simulating head impact biomechanics." International Journal of Crashworthiness **8**(4): 353-366.

Jiang, D. and D. Shu (2005). "Local displacement of core in two-layer sandwich composite structures subjected to low velocity impact." Composite Structures **71**(1): 53-60.

Johnson, A. and T. Keller (2008). "Mechanical properties of open-cell foam synthetic thoracic vertebrae." Journal of Materials Science: Materials in Medicine **19**(3): 1317-1323.

Jonas, J., J. Burns, E. W. Abel, M. J. Cresswell, J. J. Strain and C. R. Paterson (1993). "A technique for the tensile testing of demineralised bone." Journal of Biomechanics **26**(3): 271-273, 275-276.

Knowlton, A. R. and S. D. Kraus (2001). "Mortality and serious injury of northern right whales (*Eubalaena glacialis*) in the western North Atlantic Ocean." Journal of Cetacean Research and Management (special issue) **2**: 193-208.

Laist, D. W., A. R. Knowlton, J. G. Mead, A. S. Collet and M. Podesta (2001). "Collisions between ships and whales." Marine Mammal Science **17**(1): 35-75.

Laist, D. W. and C. Shaw (2006). "Preliminary evidence that boat speed restrictions reduce deaths of Florida manatees." Marine Mammal Science **22**(2): 472.

Lightsey, J. D., S. A. Rommel, A. M. Costidis and T. D. Pitchford (2006). "Methods used during gross necropsy to determine watercraft-related mortality in the Florida manatee (*Trichechus manatus latirostris*)." Journal of Zoo and Wildlife Medicine **37**(3): 262-275.

Linde, F., P. Nørgaard, I. Hvid, A. Odgaard and K. Søballe (1991). "Mechanical properties of trabecular bone. Dependency on strain rate." Journal of Biomechanics **24**(9): 803-809.

Lowry, R. (2012). "For a 2 x 2 Contingency Table." Retrieved Jan. 26, 2012, from http://faculty.vassar.edu/lowry/tab2x2.html.

Mackerle, J. (2003). "Finite Element Crash Simulations and Impact-Induced Injuries: An Addendum. A Bibliography (1998-2002)." Shock and Vibration Digest **35**(4): 273-280.

Marine Turtle Specialist Group. (1996). "*Caretta caretta*. In: IUCN 2011. IUCN Red List of Threatened Species. Version 2011.1." Retrieved July 17, 2011, from www.iucnredlist.org.

Marmontel, M., S. R. Humphrey and T. J. O'Shea (1997). "Population viability analysis of the Florida manatee (*Trichechus manatus latirostris*), 1976–1991." Conservation Biology **11**(2): 467-481.

Márquez M, R. (1990). Sea turtles of the world : an annotated and illustrated catalogue of sea turtle species known to date. Rome, Food and Agriculture Organization of the United Nations.

Martin, R. (1991). "Determinants of the mechanical properties of bones." Journal of Biomechanics **24**: 79-88.

Martin, R. B. and D. B. Burr (1989). Structure, function, and adaptation of compact bone, Raven Press New York.

Meyers, M. A., P.-Y. Chen, A. Y.-M. Lin and Y. Seki (2008). "Biological materials: Structure and mechanical properties." Progress in Materials Science **53**(1): 1-206.

MSR Electronics GmbH. (2012). "MSR165 Data Sheet." Retrieved June 7, 2012, from http://www.msr.ch/en/product/msr165.php.

National Marine Fisheries Service and U.S. Fish and Wildlife Service (2008). Recovery Plan for the Northwest Atlantic Population of the Loggerhead Sea Turtle (*Caretta caretta*), Second Revision. N. M. F. Service. Silver Spring, MD.

Nemes, J. and K. Simmonds (1992). "Low-velocity impact response of foam-core sandwich composites." Journal of Composite Materials **26**(4): 500.

Nowacek, D. P., M. P. Johnson and P. L. Tyack (2004). "North Atlantic right whales (*Eubalaena glacialis*) ignore ships but respond to alerting stimuli." Proceedings of the Royal Society of London. Series B: Biological Sciences **271**(1536): 227.

Nowacek, S. M., R. S. Wells, E. C. G. Owen, T. R. Speakman, R. O. Flamm and D. P. Nowacek (2004). "Florida manatees, *Trichechus manatus latirostris*, respond to approaching vessels." Biological Conservation **119**(4): 517-523.

Orós, J., A. Torrent, P. Calabuig and S. Déniz (2005). "Diseases and causes of mortality among sea turtles stranded in the Canary Islands, Spain (1998-2001)." Diseases of aquatic organisms **63**(1): 13-24.

Panigada, S., G. Pesante, M. Zanardelli, F. Capoulade, A. Gannier and M. T. Weinrich (2006). "Mediterranean fin whales at risk from fatal ship strikes." Marine Pollution Bulletin **52**(10): 1287-1298.

Patel, P., D. Shepherd and D. Hukins (2008). "Compressive properties of commercially available polyurethane foams as mechanical models for osteoporotic human cancellous bone." BMC Musculoskeletal Disorders **9**(1): 137.

Peterlik, H., P. Roschger, K. Klaushofer and P. Fratzl (2005). "From brittle to ductile fracture of bone." Nature Materials **5**(1): 52-55.

Piekarski, K. (1973). "Analysis of bone as a composite material." International Journal of Engineering Science **11**(6): 557-558, IN551-IN552, 559-565.

Plotkin, P. T., Editor (1995). National Marine Fisheries Service and U. S. Fish and Wildlife Service Status Reviews for Sea Turtles Listed under the Endangered Species Act of 1973. Silver Spring, MD, National Marine Fisheries Service.

Raul, J., C. Deck, R. Willinger and B. Ludes (2008). "Finite-element models of the human head and their applications in forensic practice." International Journal of Legal Medicine **122**(5): 359-366.

Reilly, D. T., A. H. Burstein and V. H. Frankel (1974). "The elastic modulus for bone." Journal of Biomechanics **7**(3): 271-272, IN279-IN212, 273-275.

Rho, J. Y., L. Kuhn-Spearing and P. Zioupos (1998). "Mechanical properties and the hierarchical structure of bone." Med Eng Phys **20**(2): 92-102.

Rieppel, O. (2001). "Turtles as hopeful monsters." BioEssays **23**(11): 987-991.

Sapp, A. (2010). Influence of Small Vessel Operation and Propulsion System on Loggerhead Sea Turtle Injuries. School of Civil and Environmental Engineering. Savannah, GA, Georgia Institute of Technology. **Master of Science in Civil Engineering**.

Sauren, A. and M. Claessens (1993). Finite element modeling of head impact: The second decade.

Scheyer, T. M. (2007). Comparative bone histology of the turtle shell (carapace and plastron) implications for turtle systematics, functional morphology and turtle origins: dissertation. Bonn, Rheinische Friedrich-Wilhelms-Universität, Institut für Paläontologie.

Schubel, P., J. Luo and I. Daniel (2005). "Low velocity impact behavior of composite sandwich panels." Composites Part A: Applied Science and Manufacturing **36**(10): 1389-1396.

Seeman, E. (2008). "Bone quality: the material and structural basis of bone strength." Journal of Bone and Mineral Metabolism **26**(1): 1-8.

Solomon, S., J. Hendrickson and L. Hendrickson (1986). "The structure of the carapace and plastron of juvenile turtles, *Chelonia mydas* (the green turtle) and *Caretta caretta* (the loggerhead turtle)." Journal of Anatomy **145**: 123.

Strobilomyces. (April 19, 2006). "*Caretta caretta* (Loggerhead Sea Turtle)." Retrieved April 3, 2012, from http://commons.wikimedia.org/wiki/File:Caretta_caretta_060417w2.jpg.

Szivek, J. A., J. D. Thompson and J. B. Benjamin (1995). "Characterization of three formulations of a synthetic foam as models for a range of human cancellous bone types." J Appl Biomater **6**(2): 125-128.

Tomás, J., P. Gozalbes, J. A. Raga and B. J. Godley (2008). "Bycatch of loggerhead sea turtles: insights from 14 years of stranding data." Endangered Species Research **5**(2-3): 161-169.

Turner, C. (2006). "Bone strength: current concepts." Annals of the New York Academy of Sciences **1068**(Skeletal Development and Remodeling in Health, Disease, and Aging): 429-446.

Turner, C. and D. Burr (1993). "Basic biomechanical measurements of bone: a tutorial." Bone **14**(4): 595-608.

Venizelos, L. (1993). "Speedboats kill turtles in Laganas Bay, Zakynthos." Marine Turtle Newsletter **63**(15).

Vincent, J. F. V. (1990). Structural biomaterials. Princeton, N.J., Princeton University Press.

Voo, L., S. Kumaresan, F. Pintar, N. Yoganandan and A. Sances (1996). "Finite-element models of the human head." Medical and Biological Engineering and Computing **34**(5): 375-381.

Wegst, U. G. K. and M. F. Ashby (2004). "The mechanical efficiency of natural materials." Philosophical Magazine **84**(21): 2167-2186.

Wells, R. S. and M. D. Scott (1997). "Seasonal incidence of boat strikes on bottlenose dolphins near Sarasota, Florida." Marine Mammal Science **13**(3): 475-480.

Wilke, M., M. Bossley and W. Doak (2005). "Managing human interactions with solitary dolphins." Aquatic Mammals **31**(4): 427.

Willinger, R., B. Diaw and H. Kang (2000). "Finite element modelling of skull fractures caused by direct impact." International Journal of Crashworthiness **5**(3): 249-258.

Work, P. A., A. L. Sapp, D. W. Scott and M. G. Dodd (2010). "Influence of small vessel operation and propulsion system on loggerhead sea turtle injuries." Journal of Experimental Marine Biology and Ecology **393**(1-2): 168-175.

Yan, J. and J. Mecholsky (2007). "How tough is bone? Application of elastic-plastic fracture mechanics to bone." Bone **40**(2): 479-484.

Zar, J. H. (1999). Biostatistical analysis. Upper Saddle River, N.J. :, Prentice Hall.

Žydelis, R., B. P. Wallace, E. L. Gilman and T. B. Werner (2009). "Conservation of marine megafauna through minimization of fisheries bycatch." Conservation Biology **23**(3): 608-616.